Western Australian School of Mines

Department of Metallurgical and Minerals Engineering

Prediction and Influence of Mineral Liberation on Froth Flotation Performance

Jian Zhang

This thesis is presented for the Degree of

Doctor of Philosophy

of

Curtin University

November 2012

Declaration

To the best of my knowledge and belief this thesis contains no material previously published by any other person except where due acknowledgment has been made.

This thesis contains no material which has been accepted for the award of any other degree or diploma in any university.

Signature: Jian Zhang

Date: 01.Nov. 2012

To my parents, wife and daughter

This page is intentionally left blank.

Abstract

In mineral processing, the liberation of valuable mineral is of key importance in achieving high recoveries from downstream separation processes such as froth flotation and gravity concentration. To quantify mineral liberation, information on ore texture of the parent rock as well as properties of comminuted particles is essential. Ore texture provides the information on the distribution of valuable mineral within the gangue matrix in an ore, which is characterized by the mineralogical composition, size and size distribution of grains of each phase and their separation. Ore texture may vary considerably for different ore types and has only been quantified by statistical measures. Texture descriptors that are commonly used by researchers are the two-point probability function, covariance function and linear intercept length distribution. The comminuted particles resulting from the breakage of the parent rock also vary in size, size distribution and mineralogical composition. These properties are generally quantified by statistical measures such as the proximity function, linear intercept length and sectional area distributions.

Current practice of determining mineral liberation in industrial applications is based on the measurements made on polished sections of parent rock and mounted particles using scanning electron microscopy (SEM) based techniques, such as Mineral liberation analyser (MLA) and Quantitative Evaluation of Minerals by Scanning Electron Microscopy (QEM*SEM). However, these techniques have limited use in geometallurgical testing which require quick and cheap techniques that are capable of predicting liberation from ore texture. Predictive liberation models are scarce in the published literature and are also restricted in their use due to the assumptions made on ore texture and particle characteristics.

In this work, predictive liberation models have been developed to address the above shortcomings by first extracting ore texture and particle structure information from SEM images of parent rock and particle polished sections, using convenient and efficient image analysis techniques based on Labview™ software. The ore texture and particle structure has been quantified by direct measurement of the covariance function and the proximity function, respectively, by placing random points on the images. To quantify fully liberated particles, a phase specific line segment function has been introduced and evaluated by placing random line segments. Among the

availability of many useful features for the acquisition, processing and analysis of images, a major advantage of Labview™ software is that it facilitates generating random intercepts which was not possible with conventional SEM-based techniques. In this work, considerable effort was devoted to developing programs that allows the determination of more relevant texture descriptors such as phase specific line segment function described in the text. This software may be used to automate the procedures required to obtain such functions through the development of specific block diagrams.

Using the measured information above, a predictive liberation model to quantify volumetric grade distribution of particles has been developed based on Barbery's work. In addition, using information from measured linear intercept and sectional area distributions, linear (1-D) and areal (2-D) liberation models were also developed. The validity of these models has been tested using data from a high grade sulphide ore and also compared with published models. It is found that the areal and linear grade distributions predicted from the proposed models also agree closely with those measured from particle sections. The fractions of fully liberated particles predicted by the proposed 1-D and 2-D models are much closer to the measured data compared to those predicted by Barbery's and King's models. It was also found that the ore texture assumptions made by Barbery are not valid for the high grade sulphide ore tested and the general applicability of these assumptions is therefore questionable.

In order to determine the influence of mineral liberation on flotation performance, a flotation model that incorporates liberation information explicitly has been developed using a transformation matrix approach. It incorporates a) prediction of the particle grade distribution for size class using the proposed model b) characteristic recoveries of particles in each narrow size/grade class and c) the feed size distribution. The characteristic recoveries were obtained from batch flotation results of individual size fractions and image analysis of feed and products. The validity of this model was tested using a composite feed comprising of a wide size distribution, which is a ground product of a high grade sulphide ore. A good correlation has been found between the recoveries predicted from the proposed transformation matrix model and those determined from batch flotation tests albeit with a bias. This bias may be construed to be due to stereological effects and may be adjusted using a correction

factor. The predicted results have also been found to be superior to those obtained from other published liberation/flotation models.

Acknowledgements

First and foremost, I would like to thank my supervisor Dr. Nimal Subasinghe for his encouragement and introducing me to the area of mineral liberation and flotation modelling. It is hard but wonderful to complete this dissertation, which would not have been possible without his support.

I would express my great gratitude to my parents for their great support. I am especially thankful for the excellent study atmosphere that my wife, Yao, gave me. Special thanks to my daughter, Evelyn, for her sweet smiles.

Thanks to Prof. Eric Grimsey, A/P Richard Browner, A/P Don Ibana, Dr. Marc Steffens and all other WASM staffs and PhD students. The department has been a source of friendship, humour as well as generous advice and multicultural collaboration. Thanks to Mujesira Vukancic for the assistance in preparing chemical reagents and ICP measurements.

I also would like to thank those from the NI (National Instruments) forum for their invaluable assistance in Labview™ programming. I am also indebted to Dr. George M. Leigh for his advice on understanding Barbery's liberation model and suggestions for stereological correction. I am thankful to Elaine Miller, department of Imaging and Applied Physics, for her help with SEM training and operation. Thanks to Dr. Brenton R. Clarke, School of Chemical and Mathematical Sciences, Murdoch University, for explaining the derivation of equations in Barbery's paper and Davy's paper.

I gratefully appreciate the scholarships (APA, CRS, FPA and completion scholarship).

Thanks to Newmont Mining Corporation for their interest in mineral liberation and continued support throughout the project.

Nomenclature

a	Particle shape parameter
A	Area of a particle section
A_i	Area of phase i in a particle section
A_{pp}	Section area of a Poisson polyhedron
$Av(*)$	Average value of a measured quantity
$B(\alpha, \beta)$	Beta function
$C(L)$	Covariance function
$C(x)$	Composite particles with a number fraction in size x
$C_{ij}(L)$	Binary texture covariance function for the binary ore with phase i and phase j
D	Particle size (mesh size)
D_{80}	Diameter of a sphere, in which 80% (by volume) of Poisson polyhedra will fit in
D_{max}	Maximum particle size in a size interval
D_{min}	Minimum particle size in a size interval
$D_{50,d}$	Sieve size of particles at which the liberation in d dimension of the mineral of interest is 50%
E	Relative error
$E(*)$	Mathematical expectation
$E(L)$	Mean intercept length of particle sections
$F(v_c(x))$	Distribution of $v_c(x)$
$F(v_u(x))$	Distribution of $v_u(x)$
$f_0(L)$	Probability density function of linear intercept length distribution of gangue phase
$F_0(L)$	Distribution function of linear intercept length distribution of

	gangue phase
$F_i(L)$	Distribution function of linear intercept length distribution of phase i
$F_i'(L)$	Distribution function of linear intercept length distribution of phase i
$F_i^{(n)}(u)$	The n-fold convolution with itself
$\widehat{f_J}$	Percentage of intercepts in the j-th grade interval
$f_1(L)$	Probability density function of linear intercept length distribution of valuable mineral phase
$F_1(L)$	Distribution function of linear intercept length distribution of valuable mineral phase
$g(A)$	Probability density function of section area distribution of particles
$G(A)$	Cumulative section area distribution of particles
$g(m)$	Volumetric grade distribution of particles
g_l	Apparent linear grade weighted by linear intercept length
g_v	Volumetric grade of particles
g_A^{ij}	Number fraction of particles in size fraction i and areal grade class j
g_L^{ij}	Number fraction of particles in size fraction i and linear grade class j
$h(z)$	Indicating function of ore texture
h_3	Boolean process density
H_p	Particle projected height
H_{pp}	Mean projected height of Poisson polyhedra
$i(L)$	Probability density function of intercept length distribution of particle sections

k	Flotation rate constant
K_f	Flotation rate constant of fast floating component
K_{max}	Maximum flotation rate constant used in Klimpel model
K_s	Flotation rate constant of slow floating component
$k_1(x)$	Flotation rate constant of fully liberated valuable mineral particles of size x
$k_c(x)$	Flotation rate constant of composite particles of size x
k_{max}	Maximum flotation rate constant
$k_u(x)$	Flotation rate constant of occluded mineral particles of size x
K_L^{ij}	Flotation rate constant of jth grade particles in size fraction i by linear grade measurement
K_A^{ij}	Flotation rate constant of jth grade particles in size fraction i by areal grade measurement
L	Length of linear intercept
L_0	Length of gangue grain intercept
$L_0(x)$	Number fraction of fully liberated gangue particles
L_i	Length of phase i in a linear intercept
L_1	Length of valuable mineral grain intercept
$L_1(x)$	Number fraction of fully liberated valuable mineral particles
$\mathcal{L}_0$	Degree of liberation of phase 0 (3-D)
$\mathcal{L}_1$	Degree of liberation of phase 1 (3-D)
$\mathcal{L}_G^{(d)}(D)$	Degree of liberation of grains in particles of size D in space dimension d of Boolean texture with Poisson polyhedra as primary grains
$\mathcal{L}_i^{(d)}(D)$	Degree of liberation of phase i in particles of size D in dimension d

$\mathcal{L}_{po}^{(d)}(D)$	Degree of liberation of pores in particles of size D in space dimension d of Boolean texture with Poisson polyhedra as primary grains
$\mathcal{L}[*]$	Laplace transformation
m	Volumetric grade of a particle
M_A	Mean particle section curvature
M_L	Mean particle intercept curvature
M_P	Mean particle curvature
n	Total number of particles
n_1	First moment of volumetric grade distribution of particles
n_2	Second moment of volumetric grade distribution of particles
$p(D)$	Mass frequency of particles at size D
$p(g_v)$	Volumetric grade distribution density function of particles
$P(g_v)$	Cumulative volumetric grade distribution of particles
$P(g_L\|D)$	Cumulative linear grade distribution in mounted particles of size D
$P(g_L\|g_v, D)$	Linear grade distribution from particles of volumetric grade g_v and size D
$P(g_L\|L)$	Cumulative distribution of linear grades in intercepts of length L
$P(g_L\|L, D)$	Cumulative distribution of linear grades of intercepts of length L from mounted particles of size D
$p(g_v\|D)$	Probability density function of volumetric grade distribution in particles of size D
$P(g_v\|D)$	Cumulative volumetric grade distribution in particles of size D
$P(L)$	Probability that two points with a distance L apart are inside the same particle, also called proximity function
$P(L\|D)$	Cumulative distribution of linear intercept length L from mounted

	particles of size D
$p(L\|D)$	Probability density function for the distribution of linear intercept of length L from mounted particles of size D (=$i(L)$ for King Particles)
$p^i(V)$	Fraction of particles in size fraction i by volume
P_2	Probability that two planes intersect inside a particle
P_3	Probability that three planes intersect inside a particle
p_G	Volumetric concentration of grains in Boolean texture
p_i	Volumetric grade of ore with respect to phase i
p_{po}	Volumetric concentration of pores in Boolean texture
Q	Uniformity measure of particle composition
$Q_{po}(A)$	Probability that a plane section with area A is entirely included in the pores of Boolean texture
$Q_{po}(L)$	Probability that segment L is entirely included in the pores of Boolean texture
$Q_{po}(V_p)$	Probability that a particle of volume V_p is entirely included in the pores of Boolean texture
$Q_{pp}(A)$	Probability that a plane section with area A is entirely included in Poisson polyhedra
$Q_{pp}(L)$	Probability of segment L is entirely included in Poisson polyhedra
$Q_{pp}(V_p)$	Probability that a particle of volume V_p is entirely included in Poisson polyhedra
R	Flotation recovery
R_{gc}	Volumetric fraction of gangue phase recovered from composite particles
R_{gu}	Volumetric fraction of gangue phase recovered from occluded mineral particles

R_{mc}	Volumetric fraction of mineral phase recovered from composite particles
R_{ml}	Volumetric fraction of mineral phase recovered from fully liberated mineral particles
R_{mu}	Volumetric fraction of mineral phase recovered from occluded mineral particles
R_{∞}	Ultimate recovery in Klimpel model
r^{ijk}	The recovery of particles in size fraction i and grade class j reported to the kth concentrate
$r_{L,\infty}^{ij}$	Maximum recovery of particles in size fraction i and grade class j by linear grade measurement
$r_{A,\infty}^{ij}$	Maximum cumulative recovery in size fraction i and grade class j by areal grade measurement
r_{L}^{ijk}	The recovery of particles in size fraction i and grade class j reported to the kth concentrate determined by linear grade measurement
r_{A}^{ijk}	The recovery of particles in size fraction i and grade class j reported to the kth concentrate determined by areal grade measurement
S_p	Particle surface area
S_{vp}	Particle specific surface area
Sv_{01}	Particle specific interface area (per unit volume of particles)
$S_{\widehat{f_J}}$	Standard deviation of $\widehat{f_J}$
t	Flotation time
$U_0(x)$	Number fraction of occluded gangue particles of size x
$U_1(x)$	Number fraction of occluded valuable mineral particles of size x
V	Volume of a particle or total volume of ore sample

$v_c(x), v_c$	Volume fraction of composite particles of size x
V_g	Volume of a grain in Boolean texture
V_i	Volume of phase i in a particle
V_p	Volume of a particle
$v_u(x), v_u$	Volume fraction of occluded particles of size x
X_m	Maximum size of fully liberated mineral particles that can be floated without detachment
z	Parameter for calculating rate constant of free mineral particles
α, β	Parameters for Beta function
$\delta(L)$	Two-point probability function (for mineral phase)(=$\delta^{(11)}(L)$)
$\delta^{(ij)}(L)$	Probability that two points with a distance L apart having one point in phase i and the other point in phase j
θ	Parameter for calculating rate constant of free mineral particles
λ_d	Fineness of texture in d dimensions
Λ_i	Fraction of particles (by volume) that is liberated from phase i (=$\Lambda_i{}^{(3)}(D)$)
$\Lambda_i{}^{(2)}$	Fraction of particles (by section area) that is liberated in phase i
$\Lambda_i{}^{(1)}$	Fraction of particles (by linear intercept) that is liberated in phase i
μ_1	Mean intercept length of valuable mineral grains in the rock
μ_0	Mean intercept length of gangue grains in the rock
$\emptyset$	Fraction of slow-floating component
ρ	Non-dimensional texture fineness parameter, $\rho = \lambda_1 aD$
σ_n	Standard deviation
$\omega^{(0)}(L)$	Phase specific line segment function of the gangue phase
$\omega^{(1)}(L)$	Phase specific line segment function of the valuable mineral phase

$\omega^{(0)}(A)$	Phase specific circular disk segment function of the gangue phase
$\omega^{(1)}(A)$	Phase specific circular disk segment function of the valuable mineral phase

Table of Contents

List of Figures

List of Tables

Abbreviations

MLA	Mineral liberation analyser
QEM*SEM	Quantitative Evaluation of Minerals by Scanning Electron Microscopy
STD	Standard deviation
1-D liberation	Linear grade distribution
2-D liberation	Areal grade distribution
3-D liberation	Volumetric grade distribution
RUIF	Random uniform isotropic fragmentation
CA	Chemical assay

Chapter 1 Introduction

1.1 Overview

The primary objective of most mineral processing operations is to separate the valuable mineral of interest from gangue minerals. Comminution processes such as crushing and grinding are employed to reduce the size of run-of-mine material to liberate the valuable mineral followed by a separation process. The response of separation process depends essentially on the extent of liberation of the valuable mineral. The liberation of valuable mineral is a function of factors such as grain size distribution of the valuable mineral within the host rock, grind size and the fracture pattern of the ore during comminution. Therefore, in order to predict the performance of downstream separation processes, the grade distribution of particles produced by comminution of the ore should be evaluated. Depending on the property being exploited by the separation process, its effectiveness is determined by the properties of particles such as density, mineral content and/or extent of exposure of mineral on the particle surface etc. In order to determine these properties, a predictive model of liberation is required. This project is aimed at developing such a model to characterize the extent of liberation and investigate the dependence of a separation process on the liberation characteristics. While most of the published literature has been focused on the influence of mineral liberation on gravity concentration, flotation has been selected in this work as the downstream separation process.

1.2 Mineral liberation and its influence on flotation

Quantification of mineral liberation has been systematically studied for more than 70 years since Gaudin (1939). He aimed to quantify the extent of fully liberated particles in comminution product. Significant contribution was made by King (1975a) to quantify ore texture using intercept length distributions of mineral and gangue phases. Subsequently, a liberation model based on renewal theory to evaluate the extent of fully liberated particles was developed (King 1979). Schaap (1979) extended King's liberation model to include the information of composite particles. Barbery (1991) used random sets and geometric probability methods to predict the volumetric grade distribution of comminuted particles. The common practice in industry to evaluate liberation is to quantify the distribution of mineral in

comminuted particles using specialized image analysis technique such as Mineral Liberation Analyser (MLA) and Quantitative Evaluation of Minerals by Scanning Electron Microscopy (QEM*SEM). Recent interests have been focused on the incorporation of liberation information in Geometallurgy investigation that aims to evaluate the variability in anticipated separator performance in various zones in the orebody. This is generally measured from drill core samples using cheap and quick measurement methods. In this regard, a reliable predictive liberation model would be of great importance to quantify such separator performance. The main aim of this project is to establish a predictive liberation model to address these concerns and to evaluate the influence of mineral liberation on froth flotation performance.

Flotation models that explicitly incorporate mineral liberation to predict flotation performance are scarce; partly due to the lack of suitable liberation models to accurately predict the grade distribution of feed particles. Schaap (1979) proposed a liberation/flotation model based on King's liberation model to predict the flotation performance of particles generated from a disseminated low grade ores. Previous work on liberation/flotation will be reviewed and developed in this work.

1.3 Assessment of liberation

In order to predict the grade distribution of comminuted particles, the following quantitative information is required: a) the size, shape and association of mineral and gangue grains in the parent rock; b) the nature of breakage of the rock during comminution and c) the size and shape of progeny particles. Generally, the liberation characteristics of ores vary considerably and can be quantified by comparing the mineral grain distribution in the parent rock and comminuted products. The above information may be obtained quantitatively from measurements made on the polished rock and particle sections using microscopic and image analysis techniques.

Commonly used image analysis techniques are based on scanning electron microscopic (SEM) images of polished sections from rock specimens and ground particles. Equipment such as MLA and QEM*SEM has received considerable acceptance in mineral processing industry. Measurement made by MLA and QEM*SEM are time-consuming and expensive. These methods use mounted specimens and generally provide the linear (one dimensional, 1-D) or areal (two dimensional, 2-D) information. However, it is the volumetric (three dimensional, 3-

D) information of particles that is important to quantify mineral processing performance of operations. The information obtained in 1-D and 2-D differs from 3-D information owing to stereological effects. Appropriate stereological correction procedure needs to be implemented on linear and/or areal information to obtain unbiased volumetric information. There have been attempts to quantify stereological bias as reported by researchers (Gay 1994; Gay and Keith 2004; Keith 2000; King and Schneider 1998; Barbery 1991). These methods require further quantitative information to quantify the association of mineral and gangue in the parent rock and progeny particles such as the determination of the transformation kernel in King and Schneider's approach. It is difficult to extract such information using current image analysis techniques without introducing some bias. Therefore, it is necessary to improve the current image analysis techniques to meet the requirements of obtaining liberation information.

Labview™ software with Vision provides a convenient method of image processing and analysis, which is efficient, less time consuming and cheap to operate. It comprises programmed routines in blocks that evaluate specific functions of the image, which may be combined to generate the required information. Once the block diagrams for processing the images are developed, Labview™ software with Vision may also be automated for on-line image processing and analysis purpose. The application of Labview™ software for image analysis in mineral processing to characterize ore texture was initiated by Young (2002). Following methods proposed by King (1979) and Schaap (1979), he measured the linear intercept lengths of both mineral and gangue phases in the rock to quantify liberation characteristics of a binary ore. This technique is to be extended in this thesis to quantify the ore texture and particle structure with more relevant probability functions. Subsequently, the information of ore texture and particle structure obtained will be used in liberation and flotation modelling. The advantages of Labview™ over other image analysis softwares may be a) convenience in its use, as it uses a graphical programming technique as opposed to other programming languages (e.g. C++), b) versatility in measurement (e.g. either in the whole or part of an image) and c) compatibility with other softwares (e.g. MATLAB and Excel) for further analysis.

1.4 Objective and scope of the project

Most published predictive liberation models have been based on measurements made on low grade ores, which generally deviate when applied to high grade ores. Thus, a high grade sulphide ore is selected to test the validity of liberation models and liberation/flotation models developed in this work. The information of ore texture and particle structure is extracted first from SEM images of polished rock and particle sections using image analysis techniques in Labview™ software. This information has been used to test the validity of the assumptions, theorems and published models in relation to ore texture and particle structure. Then, the above information is used to develop liberation models to predict the linear, areal and volumetric grade distributions of particles by applying modification to the work of Barbery (1991). The validity of developed models has been tested by comparing the linear and areal predictions with the measured data. In the absence of measured data, the validity of its volumetric predictions cannot be tested. However, these are compared with the results of Barbery's liberation model in 3-D. A liberation/flotation model to evaluate the flotation performance using transformation matrix approach has also developed based on a) the grade distribution of feed particles predicted using the proposed predictive liberation models, b) the characteristic recoveries of particles in each narrow size/grade class and c) feed size distribution. The validity of this model was tested using the observed data from batch flotation tests, and also compared with the published liberation/flotation models.

1.5 Outline of the thesis

Chapter 2 reviews previous work on liberation modelling and liberation/flotation models. Firstly, features of recent liberation models are discussed, including King's model, Barbery's model and Barbery's model modified by Leigh *et al.*(1996). Then the models used to quantify flotation performance have been reviewed following by the liberation/flotation model developed by Schaap (1979).

Chapter 3 describes a) general experimental procedures used in this project including ore sample preparation, comminution, flotation and chemical assay procedures, and b) development of image processing and analysis procedures/programs using Labview™ software. The beneficial effects of incorporating random lines on the images to extract ore textural and particle structural information from polished rock

and particle sections have been discussed. The measurement methods of estimating linear grade distribution, areal grade distribution and apparent surface composition are also discussed.

Chapter 4 presents the methods of extracting ore textural and particle structural information using Labview™. Firstly, some texture descriptors used for liberation modelling are defined and explained. These include two-point probability function, covariance function, linear intercept length distribution and phase specific line segment function. Similar functions to characterize the structure of progeny particles, for example, linear intercept length distribution, section area distribution and proximity function are also discussed. Then, the measurement methods of these descriptors using Labview™ are illustrated. The measured descriptors are compared with those predicted from published empirical equations. Finally, these descriptors were used to test the validity of the theorems and equations on quantifying the average section area and particle volume such as Gilbert equations (Gilbert 1962) and Crofton theorems (Crofton 1869).

Chapter 5 presents the development of predictive liberation models that follow the concepts proposed by Barbery (1991). These models are based on experimentally determined covariance function, proximity function and phase specific line segment function. The liberation predicted by the proposed liberation models is compared with that predicted from the published liberation models (King's and Barbery's models) and the measured linear and areal grade data.

Chapter 6 describes the influence of mineral liberation on flotation performance. A transformation matrix model which explicitly incorporates the effects of liberation and particle size on the flotation performance is developed. The characteristic recoveries of particles in each narrow size/grade class, liberation and feed size distribution are quantified and presented in terms of individual matrices. The validity of this transformation matrix model to predict flotation performance has been tested using the high grade ore. It is also compared with Schaap's liberation/flotation model to predict the flotation recoveries of particles produced from a high grade sulphide ore.

Chapter 7 presents the conclusion and recommendations for this project.

Chapter 2 Literature review

2.1 Mineral liberation

Liberation of valuable mineral is generally achieved in the comminution circuit which utilizes crushing and grinding process for size reduction. The capital cost of size reduction generally amounts to about 55-75% of the total capital cost of the concentrator and 30-60% of the operational costs (Lynch and Narayanan 1986). Metallurgists strive to predict, control and reduce this cost consistent with anticipated metallurgical performance by reducing over grinding and excessive production of fines. There are a number of comminution models capable of predicting product capacity and particle size distribution in a comminution circuit (Austin and Luckie 1988; Napier-Munn et al. 1996). However, information on the distribution of valuable mineral in the comminuted products cannot be estimated by these models. However, the valuable mineral content in comminuted particles is of key importance in evaluating the performance of downstream separation processes. Therefore it is necessary to quantify the composition of these particles, i.e. volumetric grade distribution, as a function of particle size. This information can be obtained from liberation models, which are based on the information of ore texture and ore breakage.

As stated by King (2001), grinding operations are generally unselective and the fractures introduced in the rock possess no correlation with the mineralogical structure of the ore. As such, comminution operations are generally thought to impose a random fracture mechanism on mineral and gangue matrix of the ore. The size of comminuted particles, their shape and the distribution of mineral phase within them are determined by the fracture pattern. The objective of modelling the mineral liberation process is essentially to determine the volumetric grade distribution of comminuted particles at various grind sizes. Realistic liberation modelling should start by quantifying the mineralogical texture of the ore, which is 3-dimensional in nature. This is a difficult task owing to the irregular shape of mineral grains within the host rock. A practical approach is to reduce the dimensionality of the information sources, i.e. in the absence of 3-D volumetric information (e.g. mineral and gangue association) of the rock, it is estimated from polished sections of the parent rock

either by measuring 2-D (e.g. section areas of mineral grains) or 1-D (e.g. linear intercept lengths from mineral grains) information.

Measurement of ore texture in reduced dimensions and subsequent liberation prediction techniques have been widely discussed by researchers, such as King (2001) and Barbery (1991). Such methods generally use representative sectioned and polished samples of the ore to obtain mineralogical texture information. For particles, this information is obtained from mounted and sectioned specimens. The 1-D liberation information is obtained through linear intercepts of both mineral and gangue phases encountered by random lines traversing the specimens. Measurement of sectional areas of particles gives 2-D liberation information. This 1-D and/or 2-D information may be used to predict the volumetric grade distribution in particles (3-D liberation). The linear grade distribution is relatively easier to obtain than areal grade distribution. However, in general, the grade distribution obtained in 2-D approaches that of 3-D liberation because the full section geometry can be investigated compared to 1-D (Leigh, Lyman, and Gottlieb 1996). There is a stereological bias in the results obtained using 2-D and 1-D measurements compared to the volumetric grade measurements. The stereological bias is dependent on ore texture and structure of particles. In general, a fine-grained ore in which the grains of mineral of interest is much smaller than the complement gangue grains and are well dispersed in the gangue matrix, the bias between 1-D, 2-D, and 3-D liberation would be less than that of a coarsely structured ore (Leigh, Lyman, and Gottlieb 1996). In order to eliminate the bias, stereological correction should be used to transform linear or areal grade distribution to a volumetric grade distribution of the comminuted particles.

Most published liberation models have been developed for binary ores, which contain only two phases: mineral of interest and gangue. It has been suggested that, for multi-component ores, these liberation models can be extended by considering one mineral of interest at a time, while treating all other minerals as gangue. A schematic illustration of a typical cumulative volumetric grade distribution of a comminuted product is shown in Figure 2-1. This plot shows the volumetric fraction of particles having a composition equal to or less than a given grade g_v. The ordinates at the two ends are the fractions of fully liberated mineral and gangue particles denoted by Λ_1 and Λ_0, respectively. The sum of fractions of fully liberated mineral, fully liberated gangue and composite particles should be 1. Liberation

models such as Barbery's model (Barbery 1991) have been developed to describe this curve in terms of ore texture and particle structure information.

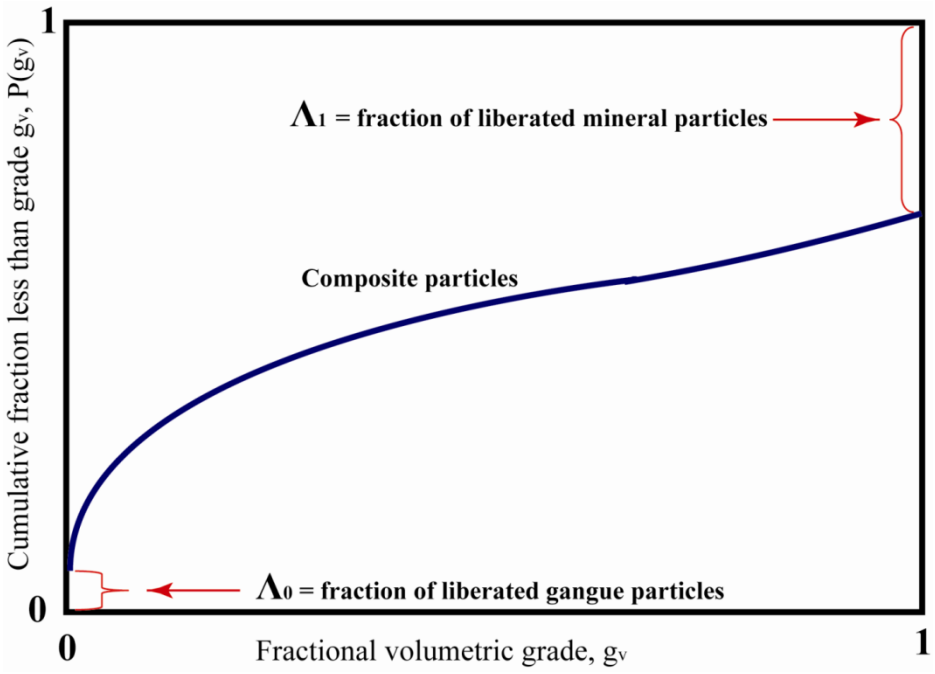

Figure 2-1 Schematic illustration of cumulative volumetric grade distribution of comminuted particles

2.1.1 Brief history of mineral liberation modeling

The pioneering work in mineral liberation modelling was conducted by Gaudin (1939). He proposed a geometric liberation model for binary ores by assuming cubic shaped mineral and gangue grains, and cubic shaped progeny particles of uniform size. The fractions of liberated mineral and gangue particles were determined using the mineral grain size, size of comminuted particles and the ratio of volumetric abundance of the mineral and gangue. The application of this model is restricted due to the assumption of cubic shaped mineral grains and particles independent of mineral-gangue association in the parent rock. In addition, the provision to estimate grade distribution of composite particles has not been explicitly given. Wiegel and Li (1967) extended Gaudin's model by introducing random arrangement of the mineral grains in the progeny particles. Gaudin's liberation model and its extensions are still under investigation by researchers (e.g. (Wiegel 2002, 2010; Hsih, Wen, and Kuan 1995; Wen, Hsih, and Kuan 1996; Owada et al. 2004)). These earlier models have the disadvantage that the grain (and particle) shape and size are subject to strict and impractical assumptions.

Another mathematical model of liberation using integral geometry, was introduced by Bodziony (1965b, 1965a) in the 1960s. He intended to eliminate the assumption of the regular grain (and particle) shape and uniform particle size imposed in Gaudin and Wiegel's liberation models (Lynch 1977). Similar to Bodziony, Davy (1984) extended the geometric probability approach to explain and model the mineral liberation process in terms of a liberation index. It was shown that the distribution of mineral phase in comminuted particles was related to the covariance function that indicates the association of different phases of ore texture and proximity function that quantifies the shape and size of the comminuted particles. She also suggested simulation methods of ore texture such as voronoi tessellation to determine her liberation index. However, this work was more of a theoretical contribution and no practical application was demonstrated. This geometric probability and integral geometry approach for mineral liberation modelling was also adopted and extended by Barbery (1991) as a modelling tool. Barbery's approach will be reviewed in more detail in the later sections.

Andrews and Mika (1975) attempted to quantify liberation at various grind sizes by adopting a population balance approach. Even though their work did not show practical application in the prediction of liberation, it undoubtedly shed light on the interaction of comminution and liberation models. King (2001, 1990) and Schneider (1995) extended Andrews and Mika's work to estimate volumetric grade distribution of particles in continuous grinding circuits and incorporate non-random breakage. The curve that shows the variation of particle size and particle grade during comminution is named after Andrews and Mika as the Andrews and Mika diagram. Herbst *et al.* (1988) also used the population balance method to model the liberation of multi-component ores.

Steiner (1975) proposed a liberation model by assuming particle composition after breakage is a function of interphase surface area, which is conserved for the random breakage of binary ores. This model was re-examined and extended by King (1983). Sutherland *et al.* (1989) attempted to use ore texture information measured by QEM*SEM to explain the processing characteristics of the ore in comminution and separation process in terms of liberation related parameters such as phase specific surface area (PSSA) and effective mean sieve size (EMSS). However, no effective grade distribution of particles at various grind sizes has been predicted by this

procedure. Miller *et al.*(1982) proposed to use cumulative liberation yield (CLY) to express the liberation of mineral phase. CLY is defined as the proportion of valuable mineral appeared in liberated particles plus the portion of valuable mineral in composite particles. CLY contains no information of the other phase (e.g. gangue phase) (Leigh, Lyman, and Gottlieb 1996).

King (1975a; 1979, 1982b) pioneered the use of renewal theory to develop a 1-D liberation model based on linear intercept length distributions of both mineral and gangue phases. He postulated that the alternating mineral and gangue intercepts traversed by a random probe line on a polished section of an ore followed a renewal process. King's initial model was used to estimate the 1-D degree of liberations of both mineral and gangue phases. However, his original work did not quantitatively provide the grade distribution of composite particles. This model was extended by Schaap (1979) to include the quantification of composition for composite particles. King (1994b) subsequently discussed the application of linear stochastic models to quantify liberation and modified his previous model (King 1975a; King 1979, 1982b). This work will be reviewed in the next section. The main feature of published liberation models are summarized in Table 2-1.

Table 2-1 Historical development of mineral liberation models (modified after (Barbery 1991) (p.100))

References	Ore texture	Particle shape	Dimension	Application
(Gaudin 1939)	Cubes, monosized	cubes	3-D	none
(Wiegel 2010, 2006, 2002, 1976, 1975; Wiegel and Li 1967; Wiegel 1964)	Cubes, monosized	cubes	3-D	3-D
(Lai 2003; Owada *et al*. 2004)	Cubes	cubes	3-D	3-D
(King 2001, 1994b, 1983, 1982b, 1979; King 1975a)	Any	any	1-D	1-D,3-D
(Klimpel and Austin 1983; Klimpel 1984)	Sparse mineral phase in gangue matrix	undefined	1-D	2-D, 3-D
(Meloy and Gotoh 1985)	Spheres	spheres	2-D	none
(Austin and Klimpel 1986)	Sparse mineral phase in gangue matrix	undefined	3-D	none
(Leigh, Lyman, and Gottlieb 1996; Barbery 1991; Barbery and Leroux 1988; Barbery et al. 1983; Barbery 1992; Davy 1984)	Any	any	any	any

In this chapter, Barbery's and King's liberation models will be reviewed in detail as they form the basis for the development of present work. They were considered as two main realistic approaches for liberation modelling (Schneider 1995). Other models, which had been critically reviewed by Barbery (1991) will not be discussed in this thesis.

2.1.2 Linear stochastic models

2.1.2.1 King's liberation model

King (1975a) postulated that the relationship between the size distribution of progeny particles and their volumetric grade distribution were both determined by the interaction of the breakage patterns through mineral and gangue phases, which produced the comminuted particles from the parent rock. He assumed the breakage pattern to be random and applied probability theory to quantify the mineral content in the resulting particles. It has also been implicitly assumed that the breakage properties such as hardness of the various mineral phases in the ore are similar and homogeneous. King's model was essentially based on the distribution of linear intercept lengths encountered when a random traverse line intersects a section through the parent rock.

King's linear liberation model was best described in his 1994 paper (King 1994b). The main objective of liberation prediction is to find the variation of cumulative volumetric grade distribution of comminuted particles (it is also called liberation spectrum in other publications), denoted by $P(g_v)$, with the size of particles. Volumetric grade distribution density function, $p(g_v)$, has a well-defined domain $\Re[0,1]$ and two discontinuities at $g_v = 0$ and $g_v = 1$ (Schneider 1995). As shown in Figure 2-1, the grades of composite particles fall in domain $\Re(0,1)$. If the volumetric grade distribution of comminuted particles within a narrow mesh size interval having a mean size D, is denoted by $P(g_v|D)$ and D is taken as the geometric mean of the upper and lower size limit of the mesh size interval, the overall volumetric grade distribution, $P(g_v)$, is obtained by combining the information of volumetric grade distribution from individual size fraction, $P(g_v|D)$. The relationship between $P(g_v|D)$ and $P(g_v)$ is given by

$$P(g_v) = \int_0^\infty P(g_v|D)p(D)dD \qquad \text{Eq. 2-1}$$

$p(D)$ is the particle size distribution (density function) which can be predicted by comminution models or determined by experiments. King assumeed that $P(g_v|D)$ can be approximated from its one dimensional counterpart $P(g_L|D)$, which is defined as the mean fraction of mineral intercepts contained in intercepts of length L from mounted particles of size D. That is, the linear grade distribution of mounted particles of size D. $P(g_L|D)$ can be determined by

$$P(g_L|D) = \int_0^\infty P(g_L|L,D)p(L|D)dL \qquad \text{Eq. 2-2}$$

$p(L|D)$ is the distribution of linear intercept of length L from mounted particles of size D. Its cumulative function, $P(L|D)$, is defined as the cumulative fraction of intercepts less than length L resulting from mounted particles of size D. The cumulative fraction of these intercepts that have a linear grade less than g_L is denoted by $P(g_L|L,D)$. King further assumed that the distribution given by $P(g_L|L,D)$ is independent of particle size D. i.e.

$$P(g_L|L,D) = P(g_L|L) \qquad \text{Eq. 2-3}$$

where $P(g_L|L)$ is the cumulative linear grade distribution of intercepts of length L from all the particles mounted. The validity of this assumption may be tested using image analysis. He showed that $P(g_L|L)$ could be estimated from the measured mean linear intercept lengths of mineral and gangue phases using renewal theory. $P(g_L|D)$ can then be calculated from Eq. 2-2. It is also related to the volumetric grade distribution (density function) of particles of size D, $p(g_v|D)$, by

$$P(g_L|D) = \int_0^1 P(g_L|g_v,D)\, p(g_v|D)dg_v \qquad \text{Eq. 2-4}$$

$P(g_L|g_v,D)$ is the transformation kernel, which allows volumetric grade distribution to be evaluated from the linear grade distribution. The kernel is dependent on the ore texture (which is a measure of mineral and gangue grains as well as their distribution within the ore) and geometrical nature of the particles generated by comminution.

2.1.2.2 Estimation of model parameters

Estimation of $P(L|D)$

King (1979) originally proposed that the cumulative fraction of intercepts less than length L resulting from mounted particles having size D, $P(L|D)$, could be determined by the following relationship proposed by Underwood (1970) for spherical particles,

$$P(L|D) = \frac{L^2}{D^2} \quad \text{Eq. 2-5}$$

In contrast, Finch and Petruk (1984) suggested that $P(L|D)$ could be estimated by

$$P(L|D) = 1 - e^{(-\frac{kL}{D})} \quad \text{Eq. 2-6}$$

where k is a constant that is approximately equal to 2 (2±0.4).

Subsequently, King (1984) recommended using Finlayson equation:

$$P(L|D) = \begin{cases} 1 - \left(1 - \frac{L}{1.2D}\right) e^{-\frac{L}{1.2D}}, & 0 \le L \le 1.2D \\ 1, & L > 1.2D \end{cases} \quad \text{Eq. 2-7}$$

From Eq. 2-7, it can be seen that the maximum intercept length through a particle of mesh size D is less than or equal to $1.2D$. The particles having intercepts that follow such a distribution are generally known as *King Particles*. The density function of the above distribution, which is the distribution of intercept lengths, denoted by $i(L)$, is given by:

$$i(L) = \begin{cases} \frac{1}{aD}(2 - \frac{L}{aD}) e^{(-\frac{L}{aD})}, & 0 \le L < aD \\ 0, & L \ge aD \end{cases} \quad \text{Eq. 2-8}$$

Here, King argued that the linear intercept length distribution in each size fraction is invariant for most ores. Therefore, the denotation of $i(L)$ has been retained for density function of $\frac{L}{D}$ distribution instead of using $p(L|D)$. The validity of Finlayson equation density function (Eq. 2-8) will be tested using the comminuted particles in this project.

Estimation of $P(g_L|L)$

To predict the cumulative linear grade distribution of intercepts of length L, $P(g_L|L)$, using ore texture data, King assumed that the formation of alternating linear

intercepts by a probe line traversing through the mineral (phase **1**) and gangue (phase **0**) phases of the parent rock may be considered as a renewal process. These intercepts include full intercepts through each phase and partial intercepts resulting from the first and the last intersections of the probe line with the rock specimen. In fact, if there are sufficient number of grains that probe line travels through, the effect of partial intercept length can be neglected and the incomplete grains touching the image border can be eliminated using modern image analysis techniques. For the measurements with incomplete intercepts, the cumulative distributions of the full length intercept (denoted by $F_i(L)$) and that for partial intercepts (denoted by $F_i'(L)$) are related through the following equation:

$$F_i{}'(L) = \frac{1}{\mu_i}\int_0^L \big(1 - F_i(x)\big)\,dx \qquad \text{Eq. 2-9}$$

where i denotes the phase (i=1 for mineral and i=0 for gangue). The average intercept length, μ_i is given by

$$\mu_i = \int_0^\infty x\, dF_i(x) \qquad \text{Eq. 2-10}$$

King (1994b, 1979) proposed that the linear grade distribution of intercepts of length L, $P(g_L|L)$, may be calculated by the convolution of the distribution function $F_i(L)$.

Define $F_i{}^{(n)}(u)$ as the n-fold convolution of $F_i(u)$ with itself and $F_i{}^{(0)}(u) = 1$, and let:

$$\Omega_i^{(n)}(u) = F_i^{(n-1)}(u) - 2F_i^{(n)}(u) + F_i^{(n+1)}(u) \qquad \text{Eq. 2-11}$$

When the left edge of the probe line starts in gangue phase, the cumulative grade distribution of intercepts of length L is given by:

$$P(g_L|L, LE = 0) = 1 - \frac{1}{\mu_0}\int_0^{L-g_L L}\left(1 - F_0(u) - \sum_{n=1}^{\infty} F_1^{(n)}(g_L L)\Omega_0^{(n)}(u)\right)du \qquad \text{Eq. 2-12}$$

When the left edge of the probe line starts in mineral phase, the cumulative grade distribution of intercepts of length L is given by:

$$P(g_L|L, LE = 1) = \frac{1}{\mu_1}\int_0^{g_L L}\left(1 - F_1(u) - \sum_{n=1}^{\infty} F_0^{(n)}(1 - g_L L)\Omega_1^{(n)}(u)\right)du \qquad \text{Eq. 2-13}$$

Thus, $P(g_L|L)$ is calculated by

$$P(g_L|L) = Prob(LE = 0|L)P(g_L|L, LE = 0) + Prob(LE = 1|L)P(g_L|L, LE = 1) \quad \text{Eq. 2-14}$$

Under the assumption of random breakage, $P(g_L|L)$ can be expressed by the following equation,

$$P(g_L|L) = p_0 P(g_L|L, LE = 0) + p_1 P(g_L|L, LE = 1) \quad \text{Eq. 2-15}$$

p_0 and p_1 are the volumetric concentration of mineral phase and gangue phase in the parent rock, respectively. LE represents left edge, $LE = i$ denotes the left edge of the probe is in phase i. In Eq. 2-15, it is assumed that the probability of the linear intercept length L of the left edge in phase i is the same as its volumetric concentration p_i, i.e. $Prob(LE = i|L) = Prob(LE = i) = p_i$. The summation of Eq. 2-12 and Eq. 2-13 converges rapidly. In this way, $P(g_L|L)$ can be estimated.

Estimation of the degrees of liberation

The degree of liberation of phase i, $\mathcal{L}_i$, is defined as the ratio of the volume of phase i contained in fully liberated particles to the total volume of phase i in all the particles. King (1994b, 1979) proposed that for particles of size D, the degrees of liberation in 1-D for mineral and gangue phases could be estimated using the following equations:

$$\mathcal{L}_1^{(1)}(D) = 1 - \frac{1}{\mu_1}\int_0^\infty [(1 - P(L|D))(1 - F_1(L)]dL \quad \text{Eq. 2-16}$$

$$\mathcal{L}_0^{(1)}(D) = 1 - \frac{1}{\mu_0}\int_0^\infty [(1 - P(L|D))(1 - F_0(L)]dL \quad \text{Eq. 2-17}$$

where μ_1 and μ_0 are the average intercept lengths for mineral and gangue phases in the parent rock, respectively. $F_1(L)$ and $F_0(L)$ are the cumulative linear intercept length distributions of mineral and gangue phases in the parent rock, respectively.

King found that if both linear intercept distributions of mineral and gangue phases followed negative exponential forms, the calculation of degree of liberation could be greatly simplified, which was the case for low grade ores. This assumption will be tested using measured data in the present work.

2.1.2.3 Schaap's extension

Schaap (1979) extended King's linear stochastic liberation model (King 1975a) and proposed a flotation kinetic model incorporating the liberation characteristics. He classified the comminuted particles resulting from binary ores into five categories: fully liberated mineral particles, fully liberated gangue particles, composite particles, occluded mineral particles and occluded gangue particles. The probability density function of mineral intercept lengths is denoted by $f_1(L)$ and its cumulative distribution function is denoted by $F_1(L)$ with mean μ_1. In the same way, the counterparts for gangue are denoted by $f_0(L), F_0(L)$ and μ_0. Schaap (1979) also retained the following assumptions as in King's liberation model (King 1975a):

a) Alternating intercepts of mineral and gangue phases in the parent rock is a renewal process along the linear probe line;
b) Valuable mineral grains are dispersed randomly in the gangue matrix, and they are independent of the nature of gangue matrix;
c) Linear intercept length distributions of both mineral and gangue phases follow negative exponential distribution form. That is,

$$f_1(L) = \frac{1}{\mu_1} e^{-\frac{L}{\mu_1}} \qquad \text{Eq. 2-18}$$

$$f_0(L) = \frac{1}{\mu_0} e^{-\frac{L}{\mu_0}} \qquad \text{Eq. 2-19}$$

The probability that a randomly selected point on a probe line falls in the mineral phase is given by

$$p_1 = \frac{\mu_1}{\mu_1 + \mu_0} \qquad \text{Eq. 2-20}$$

Similarly, the probability that the point falls in the gangue phase is determined by

$$p_0 = \frac{\mu_0}{\mu_1 + \mu_0} \qquad \text{Eq. 2-21}$$

Schaap (1979) also assumed that a particle of size x, would be formed when two fracture planes intersect the probe line at a distance x apart.

a) When the two fracture planes intersect the same mineral intercept, it is construed as having the same probability of producing a fully liberated mineral particle. This probability is given by

$$L_1(x) = p_1\left[1 - \frac{1}{\mu_1}\int_0^x [1 - F_1(L)]dL\right] \quad \text{Eq. 2-22}$$

Assuming $f_1(L)$ follows a negative exponential functional form (Eq. 2-18), it yields

$$L_1(x) = p_1 e^{-\frac{x}{\mu_1}} \quad \text{Eq. 2-23}$$

b) Similarly, if the two intersections of the fracture planes with the probe line are both in the same gangue intercept, it is considered as the probability of forming a fully liberated gangue particle, which is given by

$$L_0(x) = p_0\left[1 - \frac{1}{\mu_0}\int_0^x [1 - F_0(L)]dL\right] \quad \text{Eq. 2-24}$$

Assuming $f_0(L)$ also follows a negative exponential functional form (Eq. 2-19), it provides a similar equation as Eq. 2-23, which is given by

$$L_0(x) = p_0 e^{-\frac{x}{\mu_0}} \quad \text{Eq. 2-25}$$

c) The number fraction of composite particles, $C(x)$, is estimated from the probability that one fracture plane intersecting with gangue intercept and the other fracture plane intersecting with mineral intercept, which is given by:

$$C(x) = \frac{2\mu_1\mu_0}{{\mu_0}^2 - {\mu_1}^2}\left(e^{-\frac{x}{\mu_0}} - e^{-\frac{x}{\mu_1}}\right) \quad \text{Eq. 2-26}$$

d) The number fraction of occluded mineral particles, $U_1(x)$, is estimated from the probability that two fracture planes both intersect with gangue intercept but an entire mineral intercept existing in between, which is estimated by:

$$U_1(x) = p_0\left[1 - \frac{1}{\mu_0 - \mu_1}(\mu_0 e^{-\frac{x}{\mu_0}} - \mu_1 e^{-\frac{x}{\mu_1}})\right] \quad \text{Eq. 2-27}$$

e) Similarly, the number fraction of occluded gangue particles, $U_0(x)$, is estimated from the probability that two fracture planes both intersect with mineral intercept but an entire gangue intercept lying in between, which is related to $U_1(x)$ by

$$U_0(x) = \frac{\mu_1}{\mu_0} U_1(x) \qquad \text{Eq. 2-28}$$

Schaap (1979) argued that for low grade ores, i.e. $\mu_0 \gg \mu_1$, the number fraction of occluded gangue particles was negligible.

2.1.3 Barbery's liberation models

2.1.3.1 General model assumptions

Barbery's liberation models are based on the random sets and integral geometry, as these theories already have been used in stereology to quantify the stereological bias for microscopic data (Barbery 1987). As assumed by King (1979), Barbery's models were also developed for random breakage, i.e. the breakage of ore is independent of its textural features and the preferential breakage is excluded. In addition to the assumptions that breakage follows Random Uniform Isotropic Fragmentation (RUIF), Barbery (1987) also assumed that the progeny particles were convex in shape. This assumption generally holds for almost all ore types.

2.1.3.2 Quantification of ore texture

The composition of particles generated by comminution is affected by the mineral and gangue grains size, shape and their distribution within the ore. Assuming phase **1** is the mineral of interest and phase **0** is the gangue matrix for a binary ore, the structural relationship of mineral grains and gangue matrix in the parent rock may be quantified by a texture-indicating function, $h(z)$, defined as:

$$h(z) = \begin{cases} 1, & z \in phase\ 1 \\ 0, & z \in phase\ 0 \end{cases} \qquad \text{Eq. 2-29}$$

where z is a randomly selected point within the rock specimen. The expected value of $h(z)$ is the volumetric concentration of phase 1 in the ore, p_1, that is,

$$E\big(h(z)\big) = p_1 \qquad \text{Eq. 2-30}$$

Similar to other researchers such as Davy (1984) and Serra (1982), Barbery (1991) quantified the ore texture using a covariance function between two randomly selected points of distance L apart within the ore, $C(L)$, which is defined as

$$C(L) = E\{[h(z) - p_1][h(z+L) - p_1]\} \quad \text{Eq. 2-31}$$

$C(L)$ has the following properties as shown in Eq. 2-32 (Barbery and Leroux 1988). Sv_{01} is particle specific interface area.

$$C(0) = p_1 p_0$$
$$C(\infty) = 0 \quad \text{Eq. 2-32}$$
$$\frac{dC(0)}{dL} = -\frac{Sv_{01}}{4}$$

Although the boundary values are known, experimental determination of $C(L)$ is still difficult. The proposed estimation method and relevant properties of covariance function will be further discussed in Chapter 4.

2.1.3.3 Quantification of particle structure

Barbery (1991) used the proximity function, $P(L)$, to characterize the structure of comminuted particles. The proximity function is defined as the probability that two random points in the parent rock of a distance L apart fall into the same particle after comminution. The information of particle size and shape is implied in the proximity function (see Chapter 4).

2.1.3.4 Quantification of the fractions of fully liberated particles

Assume the ore is binary, containing phase **1** (mineral of interest or valuable mineral) and its complement phase **0** (the gangue matrix). Two ends in Figure 2-1 represent the fractions of fully liberated mineral (Λ_1) and gangue (Λ_0) particles produced by the comminution process, respectively. The fraction of fully liberated particles (Λ_i) in phase i is related to the degree of liberation of phase i, $\mathcal{L}_i$, by

$$\Lambda_i = p_i \mathcal{L}_i \quad \text{Eq. 2-33}$$

where p_i is the volumetric concentration of phase i in the rock.

2.1.3.5 Characterization of composite particles

The density function of the distribution of volumetric grade m in particles is denoted by $g(m)$, where m varies between 0 and 1. Denote n_1 and n_2 as the first and second moments of volumetric grade distribution $g(m)$ (the same as $p(g_v)$defined earlier by King (1994b)) of comminuted particles, respectively. Barbery (1991) also defined ${n_1}^M$ and ${n_2}^M$ as the first and second moments of volumetric grade distribution for composite particles, respectively. The first moment (n_1) of $g(m)$ can be determined by Eq. 2-34 and it is equivalent to volumetric concentration of phase 1 in the parent rock by assuming random breakage (Barbery 1991) (p.11).

$$n_1 = \int_0^1 mg(m)dm = \frac{E(V_1)}{E(V_p)} = p_1 \qquad \text{Eq. 2-34}$$

Barbery (1991) showed that the mathematical expectation of the product of volume of phase 0 (V_0) and volume of phase 1 (V_1), denoted by $E(V_0V_1)$, could be used to estimate the second moment of $g(m)$, n_2. If the particles are within the same narrow size interval, it may be reasonable to assume that all the particles have very close or equivalent volume. Then, the relationship between the first moment n_1 and the second moment $n_2$of volumetric grade distribution for these particles is given by

$$n_2 = n_1 - \frac{E(V_0V_1)}{E\left({V_p}^2\right)} \qquad \text{Eq. 2-35}$$

$V_p(= V_0+V_1)$ is the volume of a particle comprising a mineral phase of volume V_1 and a gangue phase of volume V_0. Eq. 2-35 has also been confirmed by other researchers (Gay 1994). For particles of the same volume V_p, Barbery and Leroux (1988) showed that

$$E\left(V_1V_p\right) = E\left({V_p}^2\right)\int_0^1 mg(m)dm = p_1E\left({V_p}^2\right) \qquad \text{Eq. 2-36}$$

$$E\left(V_0V_p\right) = E\left({V_p}^2\right)\int_0^1 (1-m)g(m)dm = p_0E\left({V_p}^2\right) \qquad \text{Eq. 2-37}$$

$$E(V_1V_0) = E\left({V_p}^2\right)\int_0^1 m(1-m)g(m)dm = (p_1 - n_2)E\left({V_p}^2\right) \qquad \text{Eq. 2-38}$$

Furthermore, Davy (1984) demonstrated that

$$\frac{E(V_i V_p)}{E(V_p)} = p_i 4\pi \int_0^\infty L^2 P(L) dL \qquad \text{Eq. 2-39}$$

Volume-weighted average volume of particles, $M(V_p)$, is given by Gilbert equation (Gilbert 1962)

$$M(V_p) = \frac{E({V_p}^2)}{E(V_p)} = 4\pi \int_0^\infty L^2 P(L) dL \qquad \text{Eq. 2-40}$$

Of these relationships, Eq. 2-38 may be used to evaluate the grade distribution of composite particles. Since $E({V_1}^2) = n_2 E({V_p}^2)$, it may be rearranged to:

$$E(V_1 V_0) = p_1 E({V_p}^2) - E({V_1}^2) \qquad \text{Eq. 2-41}$$

Dividing Eq. 2-41 by $E(V_p)$ yeilds

$$\frac{E(V_0 V_1)}{E(V_p)} = p_1 \frac{E({V_p}^2)}{E(V_p)} - p_1 \frac{E({V_1}^2)}{E(V_1)} \qquad \text{Eq. 2-42}$$

Similar to Eq. 2-40, the term $\frac{E({V_1}^2)}{E(V_1)}$ may be evaluated in terms of the probability that two random points separated by a distance L apart both belong to the phase 1 in the parent rock and the same particle after comminution, which is given by $P(L)[C(L) + {p_1}^2]$. Then, Barbery and Leroux (1988) showed that

$$\frac{E({V_1}^2)}{E(V_1)} = \frac{4\pi}{p_1} \int_0^\infty L^2 P(L)[C(L) + {p_1}^2] dL \qquad \text{Eq. 2-43}$$

Substituting Eq. 2-40 and Eq. 2-43 into Eq. 2-42 gives

$$\frac{E(V_0 V_1)}{E(V_p)} = 4\pi \int_0^\infty L^2 P(L)\,[p_0 p_1 - C(L)] dL \qquad \text{Eq. 2-44}$$

Eq. 2-44 was derived by Davy (1984) and referred as Davy's equations in this work. Dividing Eq. 2-44 by $\frac{E({V_p}^2)}{E(V_p)}$ from left hand side (LHS) and $4\pi \int_0^\infty L^2 P(L) dL$ from right hand side (RHS) gives

$$\frac{E(V_0V_1)}{E\left(V_p{}^2\right)} = \frac{\int_0^\infty L^2P(L)[p_0p_1 - C(L)]dL}{\int_0^\infty L^2P(L)dL} \qquad \text{Eq. 2-45}$$

Combining Eq. 2-45 and Eq. 2-35, it yields

$$n_2 = n_1 - \frac{\int_0^\infty L^2P(L)[p_0p_1 - C(L)]dL}{\int_0^\infty L^2P(L)dL} \qquad \text{Eq. 2-46}$$

Once the covariance function $C(L)$ that describes the ore texture and the proximity function $P(L)$ that describes the particle structure are evaluated, the second moment of particle volumetric grade distribution may be determined using Eq. 2-46.

Barbery and other researchers (Barbery 1991; Madureira et al. 1988; Barbery and Huyet 1977; Jones and Horton 1979; King 2001; Matos, Goncalves, and Marto 2004; Marto, Gonçalves, and Matos 2004) suggested that the volumetric grade distribution of composite particles may be empirically described using an incomplete Beta distribution. The Beta distribution provides versatile shapes of curve shown in Figure 2-1 with only two parameters. Other researchers (Marto, Gonçalves, and Matos 2004) have shown that the incomplete Beta distribution could also be used to characterize the multiphase particles by considering one mineral phase at a time and the other phases being ascribed into gangue phase. However, Lin *et al.*, (1994) argued that the incomplete Beta distribution function a) tended to smooth out the liberation data and provide a best fit and b) might not reveal the true liberation trend such as jump discontinuities in the liberation data.

The shape of curve for middling particle composition can thus be fitted using the following incomplete Beta distribution.

$$g(m) = \frac{(1 - \Lambda_0 - \Lambda_1)m^{(\alpha-1)}(1-m)^{(\beta-1)}}{B(\alpha,\beta)}, if\ 0 < m < 1 \qquad \text{Eq. 2-47}$$

α and β are the two parameters for the Beta distribution. $B(\alpha,\beta)$ is related to Gamma function $\Gamma(z)$ by

$$B(\alpha,\beta) = \frac{\Gamma(\alpha)\Gamma(\beta)}{\Gamma(\alpha+\beta)} \qquad \text{Eq. 2-48}$$

where $\Gamma(z)$ is defined by

$$\Gamma(z) = \int_0^\infty t^{z-1}e^{-t}dt \qquad \text{Eq. 2-49}$$

For the composite particles, the first and second moments of their volumetric grade distribution are given by Eq. 2-50 and Eq. 2-51 (p.16-17, (Barbery 1991)).

$$n_1{}^M = \frac{n_1 - \Lambda_1}{1 - \Lambda_0 - \Lambda_1} = \frac{\alpha}{\alpha + \beta} \qquad \text{Eq. 2-50}$$

$$n_2{}^M = \frac{n_2 - \Lambda_1}{1 - \Lambda_0 - \Lambda_1} = \frac{\alpha + 1}{\alpha + \beta + 1} \times \frac{\alpha}{\alpha + \beta} \qquad \text{Eq. 2-51}$$

It should be noted that Barbery's original equation for $n_2{}^M$ is incorrect (p.16, equation II.16 (Barbery 1991)).

2.1.3.6 Liberation spectrum

As discussed in the previous sections, the work of Barbery and co-workers (Barbery 1991; Barbery and Huyet 1977) describes the volumetric grade distribution density function for comminuted particles produced from binary ores as

$$g(m) = \begin{cases} \Lambda_0, & m = 0 \\ \dfrac{(1 - \Lambda_0 - \Lambda_1)m^{(\alpha-1)}(1-m)^{(\beta-1)}}{B(\alpha,\beta)}, & m \in (0,1) \\ \Lambda_1, & m = 1 \end{cases} \qquad \text{Eq. 2-52}$$

There are four parameters required to be determined:

a) Fraction of fully liberated mineral particles, Λ_1;
b) Fraction of fully liberated gangue particles, Λ_0;
c) α and β that define the shape of curve of incomplete Beta distribution.

2.1.3.7 Parameter estimation for Barbery's liberation models

Barbery (1991) was unable to estimate the functions ($P(L)$ and $C(L)$) and the degrees of liberation for both mineral and gangue phases ($\mathcal{L}_1, \mathcal{L}_0$) by measurement on ore specimens. He made assumptions of ore texture and particle characteristics to find the analytical solution for his liberation model. Barbery's liberation model was re-derived and modified by Leigh *et al.* (1996) to clarify the model parameter estimation procedure. Barbery's model and that modified by Leigh *et al.* (1996)

(abbreviated as BLL model in this thesis) are discussed below. They both used a) Finlayson equation density function (Eq. 2-8) to estimate their model parameters, b) the same proximity functions (based on the assumption of King Particles), c) the same ore texture assumptions and d) the same functional form (Eq. 2-52) to describe the volumetric grade distribution of particles. The main differences of these two models are due to the model parameter estimation of a) the fractions of fully liberated particles and b) covariance function $C(L)$ for the assumed Poisson polyhedral texture.

In order to characterize the particles, the following information from the particles is required for both models.

a) Linear intercept length distribution, $i(L)$.
   Assuming the comminuted particles possess the same characteristics as King Particles, $i(L)$ is evaluated by Finlayson equation density function (Eq. 2-8).

b) The expected volume of the particles weighted by number, $E(V_p)$.
   For the particles in one narrow size fraction, the average volume of particles weighted by volume (denoted by $M(V_p)$) is close to that weighted by number ($E(V_p)$), i.e. $E(V_p) \approx M(V_p) = \frac{E(V_p{}^2)}{E(V_p)}$. $\frac{E(V_p{}^2)}{E(V_p)}$ may be evaluated through the moments of linear intercept length distribution $i(L)$ by

$$M(V_p) = \frac{E(V_p{}^2)}{E(V_p)} = \frac{\pi}{3}\frac{E(L^4)}{E(L)} \qquad \text{Eq. 2-53}$$

   $E(L)$ is the mean intercept length and $E(L^4)$ is the fourth moment of $i(L)$. The n-th moment of linear intercept length distribution is defined as

$$E(L^n) = \int_0^\infty L^n i(L) dL \qquad \text{Eq. 2-54}$$

   The third and fourth moments of linear grade distribution based on Finlayson equation density function (Eq. 2-8) are given by

$$E(L^3) = (aD)^3 \left(\frac{33}{e} - 12\right) \qquad \text{Eq. 2-55}$$

$$E(L^4) = (aD)^4\left(\frac{196}{e} - 72\right) \quad \text{Eq. 2-56}$$

The derivation of Eq. 2-55 and Eq. 2-56 is given in the appendix A. Substituting Eq. 2-8 into Eq. 2-53 yields

$$E(V_p) \approx \frac{E(V_p{}^2)}{E(V_p)} = 0.2971(aD)^3 \quad \text{Eq. 2-57}$$

c) The expected surface area of particles $E(S_p)$.

$E(S_p)$ is evaluated through the average volume of particles $E(V_p)$ and mean intercept length $E(L)$ by

$$E(S_p) = \frac{4E(V_p)}{E(L)} \quad \text{Eq. 2-58}$$

Substituting Eq. 2-8 into Eq. 2-58 gives

$$E(S_p) = 3.2304(aD)^2 \quad \text{Eq. 2-59}$$

d) The mean projected height $E(H_p)$.

The mean projected height $E(H_p)$ is related to the average area of a section through the particle, $E(A)$, by

$$E(H_p) = \frac{E(V_p)}{E(A)} \quad \text{Eq. 2-60}$$

$E(A)$ cannot be solved analytically from the moments of linear intercept length distribution of King Particles, even though it is related to the moments of linear intercept length distribution and average area of a section weighted by area, $M(A)$, by

$$M(A) = \frac{E(A^2)}{E(A)} = \frac{\pi}{3}\frac{E(L^3)}{E(L)} \quad \text{Eq. 2-61}$$

Barbery (1991) and Leigh *et al.* (1996) used curve fitting of King's experiment data (King 1982a) to evaluate $E(A)$ and found

$$E(A) \approx \frac{175}{648}(aD)^2 \quad \text{Eq. 2-62}$$

Thus, Eq. 2-62 in combination with Eq. 2-57 and Eq. 2-60 yields

$$E(H_p) = 1.1aD \quad \text{Eq. 2-63}$$

Barbery (1991) suggested using Eq. 2-63, while Leigh *et al.* (1996) used the following equation (Eq. 2-64):

$$E(H_p) = aD \quad \text{Eq. 2-64}$$

For BLL model, it also requires two extra parameters, which are the probability that two planes intersect inside a particle (denoted by P_2) and the probability that three planes intersect inside a particle (denoted by P_3). P_2 and P_3 are evaluated by Eq. 2-65 and Eq. 2-66, respectively.

$$P_2 = \pi \frac{E(S_p)}{16[E(H_p)]^2} \quad \text{Eq. 2-65}$$

$$P_3 = \pi \frac{E(V_p)}{8[E(H_p)]^3} \quad \text{Eq. 2-66}$$

Under the assumption of King Particles, substituting Eq. 2-57, Eq. 2-59 and Eq. 2-64 into Eq. 2-65 and Eq. 2-66 yields $P_2 = 0.6343$ and $P_3 = 0.1167$.

Eq. 2-53 and Eq. 2-61 were demonstrated by Crofton (1869) and referred to as Crofton theorems in this thesis. Eq. 2-58 and Eq. 2-60 were presented by Cauchy (1841) and Minkowski (1903), respectively. Note that the Poisson polyhedral and Boolean texture with Poisson polyhedra as primary grains models were called Poisson mosaic model and Boolean texture model by Leigh *et al.* (1996), respectively. For the low grade ore, the difference between two models is insignificant (Leigh, Lyman, and Gottlieb 1996); therefore model selection is not essential to the specific situation.

Estimation of proximity function

Both Barbery (1991) and Leigh *et al.* (1996) used the Finlayson equation density function (Eq. 2-8) proposed by King (1984, 1982a) to estimate proximity function, which is given by

$$P(L) = \begin{cases} 1 - \frac{L}{aD} e^{\left(1-\frac{L}{aD}\right)}, & 0 \le L < aD \\ 0, & L \ge aD \end{cases} \quad \text{Eq. 2-67}$$

where a is a constant between 1.2 and 1.3. Particle size D is determined from geometrical mean of the upper (D_{max}) and lower limits (D_{min}) of size interval. The constant a is dependent on the ratio, D_{max}/D_{min}. Generally, $\sqrt{2}$ series ($\frac{D_{max}}{D_{min}} = \sqrt{2}$) are taken for the practical screening, where a approximately takes the value of 1.2. Barbery suggested a could be estimated from the linear intercept and area measurements on particle sections. For the linear intercept measurement, using Eq. 2-8 and Eq. 2-54, the following two equations can be derived,

$$E(L) = \frac{aD}{e} \quad \text{Eq. 2-68}$$

$$E(L^2) = (aD)^2 \left(\frac{6}{e} - 2\right) \quad \text{Eq. 2-69}$$

Combine Eq. 2-68 and Eq. 2-69, it gives

$$a = \frac{1}{2D(3-e)} \frac{E(L^2)}{E(L)} \quad \text{Eq. 2-70}$$

Similarly, Eq. 2-71 can be derived and used to estimate constant a from the section area measurement.

$$a = \sqrt{\frac{1}{\pi(11-4e)D^2} \frac{E(A^2)}{E(A)}} \quad \text{Eq. 2-71}$$

where L and A are linear intercept and section area of particle sections, respectively. e is Euler's number and lne=1. From the measurement of linear intercepts, Eq. 2-70 may be approximated by the average measured quantities, denoted by $Av(*)$. Eq. 2-70 is then rewritten into Eq. 2-72.

$$a = \frac{Av(L^2)}{D(6-2e)Av(L)} \quad \text{Eq. 2-72}$$

Similarly, replacing $\frac{E(A^2)}{E(A)}$ with the average measured values $\frac{Av(A^2)}{Av(A)}$ in Eq. 2-71, it gives

$$a = \frac{1}{D}\sqrt{\frac{Av(A^2)}{\pi(11-4e)Av(A)}} \qquad \text{Eq. 2-73}$$

Once a is determined from image analysis, proximity function using Eq. 2-67 by assuming King Particles can be obtained.

Estimation of covariance function

Barbery (1991) made assumptions on the ore texture to estimate the covariance function. He proposed two texture models: Poisson polyhedral and Boolean texture (with Poisson polyhedra as primary grains). They both contain two parameters: volumetric grade of mineral (p_1) and fineness of the texture (λ_3).

Poisson polyhedra are generated by random cut of space by planes of uniform density and orientation (Barbery 1992). A plane section through Poisson polyhedral texture results in polygons in the plane and it is shown in Figure 2-2.

Figure 2-2 Illustration of a section of Poisson polyhedra (reproduced from (Leigh, Lyman, and Gottlieb 1996))

The space is divided into cells and flats by isotropic uniform probability Poisson planes with a density (fineness of texture) λ_3. Each flat is drawn randomly with identical probability (=p_1) in phase 1. The corresponding 2-D and 1-D densities (fineness of texture) are denoted by λ_2 and λ_1, respectively. The densities are related by

$$\lambda_1 = 2\lambda_2 = \pi\lambda_3 \qquad \text{Eq. 2-74}$$

λ_1 varies with different texture.

Boolean texture is generated in a different way from that of Poisson polyhedral texture. Firstly, points are selected randomly and isotropically with identical probability, h_3. At each point, a primary Poisson polyhedron plane is implanted. The implantation of primary Poisson polyhedra planes is assumed to be independent of the presence of other grains. A section of Boolean texture is shown in Figure 2-3. The resulting grains and the complement of grains (pores) are not necessarily convex, even though the primary grains are assumed to be convex.

Figure 2-3 Illustration of a section of Boolean texture (reproduced from (Leigh, Lyman, and Gottlieb 1996))

According to Barbery (1991), the covariance function of Poisson polyhedral texture is given by Eq. 2-75, where $Sv_{01} = 4\pi p_1 \lambda_3$. Leigh *et al.* (1996) argued that this equation was incorrect and the corrected equation was Eq. 2-76.

$$C(L) = p_1 p_0 exp\left[-\frac{Sv_{01} L}{4p_1(1-p_1)}\right] \quad \text{Eq. 2-75}$$

$$C(L) = p_0 p_1 e^{-\lambda_1 L} \quad \text{Eq. 2-76}$$

The covariance function for the Boolean textures with Poisson polyhedra as primary grains is given in Eq. 2-77, while Leigh *et al.* (1996) suggested using Eq. 2-78. Note that, these two equations are equivalent by substituting $h_3 = \frac{\pi^4 {\lambda_3}^3}{6} log p_0$ and $\lambda_1 = \pi\lambda_3$ into Eq. 2-77.

$$C(L) = (1-p_1)^2 exp\left[\frac{6h_3}{\pi^4 {\lambda_3}^3} exp(-\pi\lambda_3 L) - 1\right] \quad \text{Eq. 2-77}$$

$$C(L) = {p_0}^2\left[{p_0}^{-e^{-\lambda_1 L}} - 1\right] \quad \text{Eq. 2-78}$$

Estimation of α and β

Parameters of the incomplete Beta distribution, α and β can be estimated from the combination of $\Lambda_0, \Lambda_1, n_1$ and n_2 using Eq. 2-50 and Eq. 2-51. n_1 can be obtained by image analysis. n_2 can be determined using covariance function $C(L)$ and proximity function $P(L)$ by Eq. 2-46. From Eq. 2-50 and Eq. 2-51, α and β may then be given by

$$\alpha = \frac{(n_1 - n_2)(p_1 - \Lambda_1)}{(1 - \Lambda_0 - p_1)(n_2 - \Lambda_1) - (n_1 - n_2)(p_1 - \Lambda_1)} \quad \text{Eq. 2-79}$$

$$\beta = \frac{(n_1 - n_2)(1 - \Lambda_0 - p_1)}{(1 - \Lambda_0 - p_1)(n_2 - \Lambda_1) - (n_1 - n_2)(p_1 - \Lambda_1)} \quad \text{Eq. 2-80}$$

Estimation of fractions of fully liberated particles (Λ_0 and Λ_1)

Barbery (1991) also developed methods for determining (Λ_0 and Λ_1) based on the two texture assumptions (Poisson polyhedral and Boolean texture with Poisson polyhedra as primary grains).

a) Estimation Λ_0 and Λ_1 from Poisson polyhedral texture

For Poisson polyhedral texture, he proposed that a particle was liberated only when it was included in a polyhedron; however, Leigh *et al.* (1996) argued that the particle was liberated when all the polyhedra in the particle were assigned to the same phase. Therefore the equations for fractions of fully liberated particles are different for these two models under the same assumption of Poisson polyhedral texture. The probability of a particle is entirely contained in a polyhedron is given by

$$Q_{pp}(V_p) = exp[-\lambda_3 M_p] \quad \text{Eq. 2-81}$$

M_p is the mean particle curvature. Barbery (1991) proposed that the fraction of fully liberated mineral particles is determined by

$$\Lambda_1 = p_1 Q_{pp}(V_p) \quad \text{Eq. 2-82}$$

For the reduced dimensions (2-D and 1-D), the mean particle section curvature (M_A) and intercept curvature (M_L) are given by $M_A = \pi\sqrt{\pi A}$ and $M_L = \pi L$, respectively. Define $Q_{pp}(A)$ and $Q_{pp}(L)$ as the probabilities of section plane A and segment L are entirely contained in Poisson polyhedra, respectively. Barbery (1991) showed that,

$$Q_{pp}(A) = exp[-\lambda_3 \pi\sqrt{\pi A}] \quad \text{Eq. 2-83}$$

$$Q_{pp}(L) = exp[-\lambda_3 \pi L] \quad \text{Eq. 2-84}$$

Then, the fractions of liberated particles sections and fraction of fully liberated intercepts are given by

$$\Lambda_1^{(1)} = \frac{p_1 \int_0^\infty L\, i(L) Q_{pp}(L) dL}{\int_0^\infty L\, i(L) dL} \quad \text{Eq. 2-85}$$

$$\Lambda_1^{(2)} = \frac{p_1 \int_0^\infty A\, g(A) Q_{pp}(A) dA}{\int_0^\infty A\, g(A) dA} \quad \text{Eq. 2-86}$$

$g(A)$ is particle section area distribution. These two equations are extended later in Chapter 5 to predict the fraction of fully liberated particles in both 1-D and 2-D.

Leigh *et al.* (1996) proposed that the fractions of liberated particles might be determined by the following two equations.

$$\Lambda_1 = e^{-2\rho} \sum_{n=0}^{\infty} \frac{(2\rho)^n}{n!} p_1^{1+n} (1 - p_0 P_2)^{\frac{n(n-1)}{2}} (1 - p_0 P_3)^{\frac{n(n-1)(n-2)}{6}} \quad \text{Eq. 2-87}$$

$$\Lambda_0 = e^{-2\rho} \sum_{n=0}^{\infty} \frac{(2\rho)^n}{n!} p_0^{1+n} (1 - p_1 P_2)^{\frac{n(n-1)}{2}} (1 - p_1 P_3)^{\frac{n(n-1)(n-2)}{6}} \quad \text{Eq. 2-88}$$

where ρ is a non-dimensional parameter and $\rho = \lambda_1 aD$. Because Poisson polyhedral texture is symmetric, which means the mineral grains and gangue grains are both Poisson polyhedra. The method of estimating fraction of fully liberated particles obtained for one phase is the same as that for the other phase, for example, Eq. 2-87 and Eq. 2-88 are essentially the same except for interchanging p_1 and p_0.

b) Estimation Λ_0 and Λ_1 from Boolean texture with Poisson polyhedra as primary grains

Boolean texture with primary Poisson polyhedra grains is asymmetric. If one phase (e.g. grains of Boolean texture) is assigned to the mineral phase, then the gangue phase is the pores. Therefore, the equations for estimating the fractions of liberated particles are different.

According to Barbery (1991), under the assumption of RUIF, the fraction of fully liberated particles resulting from the pores of Boolean texture with Poisson polyhedra as primary grains (in 3-D, denoted by $\Lambda_{po}^{(3)}(D)$) is given by

$$\Lambda_{po}^{(3)}(D) = p_{po} \times exp\left[-h_3\left(\frac{6}{\pi^4 {\lambda_3}^2}8.293D + \frac{3}{4\pi\lambda_3}4.65D^2 + 0.513D^3\right)\right] \quad \text{Eq. 2-89}$$

p_{po} is the volumetric concentration of pores, the counterpart p_G is the volumetric concentration of grains in Boolean texture.

The fraction of fully liberated particles resulting from the grains of Boolean texture with Poisson polyhedra as primary grains is given by

$$\Lambda_G^{(3)}(D) = 1 - exp[ln(1 - p_G)exp(-\lambda_3 M_p)] \quad \text{Eq. 2-90}$$

Note that, the phase of the pores of Boolean texture can be assigned to either valuable mineral or gangue. Similarly, the phase of grains of Boolean texture can also be valuable mineral or gangue. In practice, it is necessary to test which one is better to be assigned to the mineral phase.

Leigh *et al.* (1996) proposed Eq. 2-91 and Eq. 2-92 which are different from Barbery's to estimate the fraction of fully liberated particles by assuming Boolean texture.

$$\Lambda_G^{(3)}(D) = e^{-[\eta_0 + \eta_1\lambda_1 E(H_p) + \eta_2{\lambda_1}^2 E(S_p) + \eta_3{\lambda_1}^3 E(V_p)]} \quad \text{Eq. 2-91}$$

$$\Lambda_{po}^{(3)}(D) = p_1\left[1 + 2\lambda_1 E(H_p) + \frac{\pi{\lambda_1}^2 E(S_p)}{8} + \frac{\pi{\lambda_1}^3 E(V_p)}{6}\right] \quad \text{Eq. 2-92}$$

Mean projected height $E(H_p)$, the expected surface area $E(S_p)$ and the expected particle volume $E(V_p)$ are given by Eq. 2-57, Eq. 2-59 and Eq. 2-64, respectively. Parameters η_0, η_1, η_2 and η_3 are defined by

$$\eta_0 = -\log p_G \quad \text{Eq. 2-93}$$

$$\eta_1 = -\frac{2p_{po}\log p_{po}}{p_G} \quad \text{Eq. 2-94}$$

$$\eta_2 = \frac{p_{po}\log p_{po}}{2p_G}\left[\left(\frac{\pi}{4} + \frac{p_{po}}{p_G}\right)\log p_{po} + 1\right] \quad \text{Eq. 2-95}$$

$$\eta_3 = -\frac{p_{po}\log p_{po}}{p_G}\left[1 + \left(1.9890 + \frac{3p_{po}}{p_G}\right)\log p_{po} + \left(\frac{\pi}{6} + \frac{3\pi p_{po}}{4p_G} + 2\left(\frac{p_{po}}{p_G}\right)^2\right)(\log p_{po})^2\right] \quad \text{Eq. 2-96}$$

In this work, Barbery's model modified by Leigh *et al.* (1996) (BLL model) was used for comparison in Chapter 5.

2.1.3.8 Some relationships of liberation in different dimensions

If $D_{50,d}$ is the sieve size of particles, at which the degree of liberation in d dimension for the mineral of interest is 50%, Barbery (1991) showed some relationships between this size and the degrees of liberation of *sparse phase* in different dimensions. Barbery noted that these relationships were not valid for all cases.

$$\mathcal{L}^{(d)}(D) = exp\left(-\frac{0.693D}{D_{50,d}}\right) \quad \text{Eq. 2-97}$$

$$D_{50,3} = \frac{D_{50,2}}{2} = \frac{D_{50,1}}{4} \quad \text{Eq. 2-98}$$

Eq. 2-98 is equivalent to

$$D_{50,d+i} = \frac{D_{50,d}}{2i} \quad \text{Eq. 2-99}$$

Similarly, for the degrees of liberation in different dimensions have the following relationships:

$$\mathcal{L}^{(1)}(D) = \mathcal{L}^{(3)}\left(\frac{D}{4}\right) \quad \text{Eq. 2-100}$$

$$\mathcal{L}^{(2)}(D) = \mathcal{L}^{(3)}\left(\frac{D}{2}\right) \quad \text{Eq. 2-101}$$

$$\mathcal{L}^{(d+i)}(D) = [\mathcal{L}^{(d)}(D)]^{2i} \quad \text{Eq. 2-102}$$

where i is a natural number. The validity of these simple relationships was questioned by Chiaruttini *et al.* (1999), who showed that the volumetric grades estimated from these relationships were severely underestimated.

2.1.3.9 Estimation of model parameters using King's method

King (1994a) extended the use of Barbery's liberation models by determining some of the required quantities by experimentation. He retained the method of using the incomplete Beta distribution to describe the compositional distribution of unliberated particles (Eq. 2-47). Of the four variables, i.e. n_1, n_2, $\mathcal{L}_1$ and $\mathcal{L}_0$, n_1 was estimated from image analysis, i.e. $n_1 = p_1 = \frac{E(L_1)}{E(L)}$. King and co-workers (King 1994a, 1994c; King and Stirling 1994) suggested that the covariance function could be determined from measured linear intercept length distributions of mineral and gangue phases in the parent rock. Assuming Finlayson equation density function (Eq. 2-8) holds for

$P(L)$, n_2 was estimated by Eq. 2-46. As his measurements were based on intercept lengths, the degrees of liberation,$\mathcal{L}_i^{(1)}(D)$, calculated from these measured intercept length distributions using Eq. 2-16 and Eq. 2-17 were in 1-D. King (1994a) used the relationship proposed by Barbery (1991) (Eq. 2-102) to estimate the degrees of liberation in 3-D, $\mathcal{L}_i^{(3)}(D)$. As it will be shown later in Chapter 4 that the estimation of covariance function from linear intercept length distributions of mineral and gangue phases is difficult. In addition, the validity of Eq. 2-102 for the liberation of specific ore type needs to be tested.

2.1.4 Recent applications of liberation modelling

Schneider (1995) extended the work of King (1990) to determine liberation characteristics of particles in a closed circuit with regrinding using population balance approach proposed by Austin and Luckie (1986). With the use of Andrews-Mika diagram (Andrews and Mika 1975) and under the assumption of random breakage, the quadrivariate breakage function in Austin and Luckie's model was decoupled into two functions: one describes the liberation and the other describes comminution. In this way, the liberation of particles in the closed comminution circuit with regrinding can be estimated.

Yingling (1991) presented stochastic mineral liberation models for multi-component ores. He assumed the sequence of phase transitions had properties of Markov chains and the linear probe through the phases had semi-Markov process, i.e. the probe had a memory of its immediate past history. The whole process of linear probe consists of an imbedded Markov process describing the phase transitions and linear intercept length distribution describing the phases. King (1994b) reviewed and modified Yingling's model in combination with his own random breakage liberation model.

Gay and co-workers (Fandrich, Schneider, and Gay 1998; Gay 1994, 2004b, 2004a; Gay 1999; Gay and Keith 2004; Keith and Gay 2000; Wei and Gay 1999) conducted some important research to incorporate stereological correction in liberation modelling. A liberation model based on a dispersion equation was proposed. The liberation process has been considered as a dispersion process in chemical engineering in their model. The dispersion rate is texture dependent and increases with the decrease of particle size. It becomes 0 for the fully liberated particles, because the fully liberated particles can only provide fully liberated particles with the

same phase. Dispersion rate function was separated into the grade component and size component. Further investigation is required to determine the two components in the liberation modelling using dispersion equation.

Another model proposed by Gay and co-workers is based on the entropy theory. This model considers comminution process to be a probabilistic process, where factors such as grinding machine, grinding time, ore texture and grinding medium affect the size and composition of comminution product. The relationship of size and composition between parent particles and progeny particles is described using a transformation kernel, which is analogous to the stereological correction transformation kernel used by King and Schneider (1998). The transformation kernel is used to determine the probability that a feed particle with certain composition and size will generate the product particles with a particular composition and size. Random breakage pattern is also assumed in this model. The main difficulties of using this entropy liberation model are: a) incorporating non-random breakage pattern to the model; b) the modelling of multi-sized feed to multi-sized product and c) determination of the transformation kernel for different ore types.

Recent attempts to address in liberation modelling are:

a) Direct particle composition measurement in 3-D, which was performed by Miller and co-workers using Cone beam X-ray microtomography (Garcia, Lin, and Miller 2009; Lin and Miller 1996; Miller and Lin 2003; Miller and Lin 1997, 2002, 2004; Miller, Lin, and Cortes 1992; Miller, Lin, and Cortes 1990; Miller *et al.* 2009; Videla, Lin, and Miller 2007).
b) Simulating ore texture and/or breakage pattern such as (Vassiliev, Ledoux, and Gold 2008; Guimarães and Durão 2007; Guimarães and Durão 2003; Stamboliadis 2008).

2.2 Flotation models

2.2.1 Introduction of flotation process

Separation of minerals by flotation has been in existence for over a century. Flotation is a physico-chemical separation process that exploits differences in surface properties (i.e. surface hydrophobicity). The particles in the pulp are conditioned to allow sufficient interaction with collector to render their surface hydrophobic. Then,

the particles are made to contact with air bubbles to allow them to attach air bubbles. This particle/air bubble interaction consists of three steps: collision, attachment and detachment. The interaction depends on the particle size, air bubble size and operating conditions, such as agitation and induction time. The hydrophobic particles attach to air bubbles and rise to form a stable froth layer to be collected in the concentrate.

Flotation process is affected by many factors, such as feed particles size, degree of liberation, mineral surface exposure (i.e. particle surface composition), reagent scheme (and concentrations), residence time distribution, and operational parameters (e.g. agitation, impeller speed, aeration speed) etc. The overall performance of the flotation process is generally measured in terms of recovery and grade of the concentrate.

2.2.2 Flotation modeling

Extensive research is in progress to develop mathematical models of flotation, with the aim of generating a tool to predict the concentrate recovery and grade that can be used in flotation circuit design or optimisation (Runge, Franzidis, and Manlapig 2003). Due to the large quantity of ores treated by froth flotation, any increase in flotation efficiency will be significantly beneficial to the extraction of valuable metal from the ore. With decreasing grades of ores mined and the complex nature of the mineral association in them, the processes involved in flotation are becoming more complex. This requires more detailed flotation models for designing new cells and modifying the present cells for higher throughput (Koh *et al.* 2009). It is often observed that the gap between theoretical flotation performance and actual flotation performance in the plant is significant, indicating the inefficiencies in industrial flotation processes and the potential of improving it (Morizot *et al.* 1997).

Lynch, *et al.* (1981) divided flotation models into three categories: a) empirical models, b) probability models, and c) kinetic models. They argued that empirical models were too specific to the conditions and generally required a trial-and-error feedback approach to optimization. Probability models, however, can be connected to kinetic models with proper constraints (Yuan, Palsson, and Forssberg 1996). In this thesis, a simplistic kinetic model has been chosen to seek the interrelationship

between mineral liberation and flotation behaviour, while keeping the effects due to chemical environment in the pulp constant.

In this work, to simplify the flotation modelling, some operation conditions (such as aeration rate, impeller speed and reagent scheme) are kept constant, while a selected number of impact factors (flotation time, particle size, particle grade, apparent particle surface composition) are investigated. The relationship between flotation time and recovery of particles in each size fraction is used to evaluate their flotation performance.

2.2.3 Kinetic models of flotation

In developing the kinetic models of flotation, flotation cell is considered to be analogous to a chemical reactor, where particles and air bubbles "react" with each other and undergo interaction, attachment and detachment. Generally, the flotation is considered as a first order rate process. The criteria required for mathematical models that can describe the flotation process are:

a) the model should provide a good fit to the observed data;
b) the model parameters should be stable for the statistical analysis.

The flotation rate constant can be used to describe the rapidness of the flotation performance. Flotation rate constant of materials of a given size is considered to be constant throughout the flotation process. However, it is known that the flotation rate constant varies with particle size and composition, because the particles with different size and mineral surface composition do not interact with air bubbles at the same rate and behave differently in flotation cell. Therefore, the flotation rate constant is usually a distribution. There are mainly three methods to quantify the variation of flotation rate constant (Runge, Franzidis, and Manlapig 2003):

a) Empirically derived shape distributions: Generally, the flotation rates of small particles and large particles are low, while the intermediate size particles float well in the cell. The rate constants evaluated by experiments have been described by a known distribution defined by two or three parameters. The empirical distributions used were a) gamma distribution (Imaizumi and Inoue 1963); b) triangular (Harris and Chakravarti 1970); c) rectangular (Huber-

Panu, Ene-Danalache, and Cojocariu 1976); d) sinusoidal (Diao, Fuerstenau, and Hanson 1992) and e) normal (Chander and Polat 1994) distributions.

b) Empirically derived floatability components: The feed is classified into finite number of floatability components. For each component, an individual rate constant is assigned and may be evaluated from experiments. For example, the feed was classified into fast and slow floating components as shown in Kelsall model (Kelsall 1961).

c) Property based floatability component: The feed is divided into classes based on a physical property and each class is considered to have a unique floatability. The physical properties used were a) size (Tomlinson and Fleming 1963; Thorne et al. 1976), b) mineral liberation (Niemi, Ylinen, and Hyötyniemi 1997; Gorain *et al.* 2000; Sutherland 1989; Qi *et al.* 1992; King 1976) and c) chemical surface coverage (Niemi, Ylinen, and Hyötyniemi 1997).

In this work, floatability characteristics due to size, grade and surface exposure of mineral will be investigated.

The first order kinetic models having 2 or 3 model parameters have been widely accepted and used to model batch flotation (Fichera and Chudacek 1992; Çilek 2004). There have been attempts to modify the first order kinetic models to give close agreement with the observed recovery data by introducing more parameters. However, it is often found that the incorporation of more parameters does not generate superior results (Dowling, Klimpel, and Aplan 1986). Of these first order models, the two-parameter model (Eq. 2-103) due to Klimpel (1980) and three-parameter model (Eq. 2-104) due to Kelsall (1961) have been commonly used owing to their simplicity.

Klimpel model is given by

$$R = R_{\infty}[1 - e^{-kt}] \qquad \text{Eq. 2-103}$$

where R_{∞} and k are ultimate recovery and rate constant, respectively. Klimpel model shows that all the floatable particles float at the same rate. However, there are a number of particles that can never be floated. That is, the ultimate recovery is usually less than 100%.

Kelsall model is given by

$$R = (1 - \emptyset)[1 - e^{-K_f t}] + \emptyset[1 - e^{-K_s t}] \quad \text{Eq. 2-104}$$

where $\emptyset$, K_f and K_s are fraction of slow-floating particles, rate constants for fast floating and slow floating particles, respectively. Kelsall model demonstrates that the comminuted particles can be divided into fast floating and slow floating components, floating at different rates.

For Klimpel model, if it is assumed that flotation rate constant follows a rectangular distribution (with a maximum value K_{max}), the kinetic model is given by Eq. 2-105.

$$R = R_\infty \left[1 - \frac{1}{K_{max} t}(1 - e^{-K_{max} t})\right] \quad \text{Eq. 2-105}$$

In the present work, Klimpel model (Eq. 2-103) has been used to analyse the flotation data, since all other factors being constant, any variation in R_∞ and K may be attributed to effects of particle size and liberation.

2.2.4 Influence of mineral liberation on froth flotation performance

2.2.4.1 Flotation of fully liberated and composite particles

During comminution, a majority of the particles produced are composites which comprise mineral and gangue components. For the fully liberated mineral particles, the exposure of mineral on the particle surface is 100% and the flotation rate constant of such particles is generally larger compared to the composite and fully liberated gangue particles at the same size. The fully liberated gangue particles are assumed not to float. These particles are considered as gangue entrainment if they appear in the concentrate. Most liberation related research on the flotation performance of composite particles before 1989 was critically reviewed by Barbery (1991) and the research topics were summarized as:

1. Effect of composite particles on ultimate recovery;
2. The minimum surface exposure of mineral on particle surface or composition of particles to make the particle floatable;
3. The relative flotation rate of composite particles compared to the fully liberated mineral particles of the same size;
4. The effect of particle size on the flotation of composite particles;

5. The relationship between surface composition and volumetric grade of particles.

Gong and co-workers (Qi 1993; Qi et al. 1992) investigated the flotation performance of composite particles produced from Mt. Weld phosphate ore (22% P_2O_5 as mineral and 38% Fe_2O_3 as gangue) by analysing their liberation characteristics using QEM*SEM. It was found that the floatability of a composite particle was related to the mean floatability of each mineral component weighted by its volume fraction within the particle. More recently, similar work was conducted by investigating the surface hydrophobicity of coarse synthetic composite particles of quartz (as mineral) in a lead borate matrix (as gangue) (Wang 2010). The flotation recovery and rate constant of such composite particles were found to increase with the extent of quartz liberation and decrease with particle size. Nonetheless, the above-mentioned 5 problems brought forward by Barbery (1991) have not been solved up to date.

Without considering the variation of shape and density with the grade of particles, the difference of particle structure between the fully liberated mineral and composite particles of the same size lies in a) exposure of mineral on the surface (surface composition) and b) the grade (volumetric composition). Since flotation is a surface-controlled process, particle surface composition seems to be a better parameter than volumetric grade distribution to predict flotation recoveries (Wang 2010). However, the calculation of flotation recovery is based on the volumetric composition of floated particles, not their surface composition. It is therefore important to establish the relationship between surface composition and volumetric composition of the comminuted particles. As suggested by Barbery (1991), the surface composition and volumetric composition of the particles are equivalent under the assumption of pure transgranular breakage. This suggestion is questionable, because it seems to be invalid if there are a large number of occluded particles in the comminution product. Generation of occluded particles is common at coarse grind sizes. As shown in Figure 2-4, gangue grain is occluded in the mineral phase of particle A, while particle C is a fully liberated mineral particle. Particles A and C have almost the same surface composition but contribute differently to the recovery if they are both collected in the concentrate. It may be valid that for the simple texture composite particles such as particle B in Figure 2-4, i.e. no occluded grain (either mineral or gangue) within each

particle, their surface composition and volumetric composition are approximately equivalent. Some published results also revealed there was only insignificant difference between the flotation performance determined based on volumetric composition and surface composition (Runge, Franzidis, and Manlapig 2003; Sutherland 1989; Lastra 2002). Note that, the volumetric composition they used for composition was actually 2-D areal grade determined from image analysis. This relationship will be investigated by the measurements of surface composition and composition of comminuted particles using image analysis in this project.

For the flotation rate of composite particles of grade m, Barbery (1991) proposed that it was proportional to that of fully mineral liberated particles of the same size and the proportionality constant is m. In this sense, m =0 denotes the fully liberated gangue particles, the flotation rate is 0; while for m=1, the fully liberated mineral particles float fastest among all the particles of the same size. This suggestion also needs to be tested by experiments.

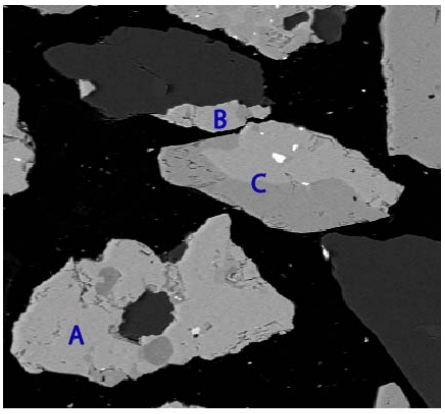

Particle A: Occluded gangue particle.
Particle B: Simple texture binary particle.
Particle C: Fully liberated mineral particle.

Figure 2-4 Illustration of different type of particles after grinding

2.2.4.2 The relationship between mineral liberation and flotation performance

There have been many flotation models that incorporate the influence of grinding information on flotation performance (e.g. (Bazin et al. 1994; McIvor and Finch 1991)). However, none of them explicitly takes surface composition or particle composition into account (Wightman *et al.* 2010). The effect of liberation on the flotation performance was implicitly included in the current flotation models by

lumping it with other factors that influence the flotation performance such as particle size into two or three parameters. There are limited publications that quantify the influence of mineral liberation on flotation performance (e.g. (King 1975b; Kremer and Gurevich 1992; Kremer, Gurevich, and Blekhman 1993; Schaap 1979; Subasinghe 2008)). Some researchers (Sutherland 1989; Steiner 1973; Imaizumi and Inoue 1963) proposed that greater the proportion of hydrophobic mineral in the particles floated, the higher their flotation rate constant was. Furthermore, other researchers (Schaap 1979; Subasinghe 2008) assumed that flotation rate constant for composite particles was proportional to their mineral surface exposure. Mineral liberation information was explicitly included in Schaap's flotation model (Schaap 1979). Subasinghe (2008) modified Schaap's model and attempted to predict the mineral exposure on the particle surface assuming spherically shaped particles. Schaap's liberation/flotation model is discussed below.

2.2.4.3 Schaap's liberation/flotation model

Similar to King's liberation model (King 1979), Schaap (1979) also used renewal theory to evaluate the fractions of fully liberated, composite and occluded particles in the comminution product. Schaap (1979) assigned each type of particles a rate constant, which is a function of particle size and surface exposure. The information required for Schaap's liberation/flotation model is:

a) the fraction of each type of particles;

b) the grade distribution (or average grade) of each type of particles;

c) flotation rate constant of each type of particles;

d) size distribution of feed particles (density function, denoted by $p(x)$) in flotation feed.

Schaap (1979) used the following assumptions for his liberation/flotation model in addition to the assumptions he made for liberation as shown in section 2.1.2.3:

a) The aeration rate does not affect the flotation rate.

b) The flotation is a first-order rate process with the rate constant varying according to their size and liberation properties of the particles.

c) The overall rate constant is a function of particle size and hydrophobic surface

fraction given that the impeller speed, aeration rate, froth depth and conditioning are set as constant.

d) The rate constant is directly proportional to the hydrophobic surface fraction, given that the particle size and other conditions such as agitation speed, aeration rate are kept constant. The rate constants of composite and occluded particles are proportional to the rate constant of fully liberated particles and the proportionality constant is the surface composition of the particles.

Estimation of the fraction of each type of particles

The equations (Eq. 2-23-Eq. 2-28) for estimating the fractions of five types of particles are shown in section 2.1.2.3. As Schaap's liberation/flotation model was established for disseminated low grade ores, the probability of generating occluded gangue particles from these ores is low, i.e. $U_0(x)$=0.

Estimation of the volumetric grade distribution and average grade of each type of particles

For the fully liberated mineral particles, their grade is always 1. For the composite and occluded mineral particles, if their grade distributions are denoted by $v_c(x)$ and $v_u(x)$, respectively, Schaap (1979) showed that:

1. The mean grade of composite particles, $\overline{v_c(x)}$, is determined by

$$\overline{v_c(x)} = \overline{v_c} = \frac{\mu_1\mu_0}{x(\mu_0 - \mu_1)} - \frac{1}{e^{-\left(\frac{x}{\mu_1} - \frac{x}{\mu_0}\right)} - 1} \qquad \text{Eq. 2-106}$$

2. The cumulative grade distribution of composite particles, $F\big(v_c(x)\big)$, is:

$$F\big(v_c(x)\big) = \frac{1 - e^{-v_c\left(\frac{x}{\mu_1} - \frac{x}{\mu_0}\right)}}{1 - e^{-\left(\frac{x}{\mu_1} - \frac{x}{\mu_0}\right)}} \qquad \text{Eq. 2-107}$$

3. The mean grade of occluded mineral particles, $\overline{v_u(x)}$, is given by:

$$\overline{v_u(x)} = \overline{v_u} = \frac{\mu_1}{x} - \frac{1}{e^{\frac{x}{\mu_1}} - 1} \qquad \text{Eq. 2-108}$$

4. The cumulative grade distribution of occluded mineral particles, $F\big(v_u(x)\big)$, is:

$$F\left(v_u(x)\right) = \frac{1 - e^{-v_u \frac{x}{\mu_1}}}{1 - e^{-\frac{x}{\mu_1}}} \qquad \text{Eq. 2-109}$$

Estimation of flotation rate constant of each type of particles

To evaluate the flotation rate constant for the fully liberated mineral particles, Schaap (1979) considered the effect of particle size on the flotation performance: a) a particle should have sufficient momentum to squeeze out of the water film between bubble and particle and b) this probability was dependent on mass of particle. Schaap (1979) also assumed that the small fully liberated mineral particles would be carried up to the froth zone and did not come back until reaches to a maximum size X_m. Above X_m, the particles are instable in the froth zone caused by shaking loose or collision in bubble coalescence and will fall back into pulp phase. However, Schaap (1979) argued that this probability was small due to sufficient opportunity of being captured in the lower levels within the cell. Therefore, Schaap (1979) proposed the following equations (Eq. 2-110 and Eq. 2-111) to predict flotation rate constant of fully liberated mineral particles (θ and z are parameters to be evaluated in the experiment).

For $x \leq X_m$,

$$k_1(x) = k_{max} \frac{1 - e^{-2x/\theta}}{1 + (e^2 - 2)e^{-2x/\theta}} \qquad \text{Eq. 2-110}$$

For $x > X_m$,

$$k_1(x) = k_{max} \frac{1 - e^{-2x/\theta}}{1 + (e^2 - 2)e^{-2x/\theta}} e^{\frac{X_m - x}{z}} \qquad \text{Eq. 2-111}$$

k_{max} is the maximum flotation rate constant.

To determine the flotation rate constant of composite and occluded mineral particles, Schaap (1979) assumed that a) the particle shape was cubic and b) the random cuts were parallel and pass through mineral phase for the occluded mineral particles. He suggested that the occluded mineral particles might also float provided some of hydrophobic surface was at least on one side. Under the assumption of rate constant being directly proportional to fraction of hydrophobic area on particle surface, the rate constants of composite particles (denoted by $k_c(x)$) and occluded mineral particles (denoted by $k_u(x)$) are determined by

$$k_c(x) = (0.25 + 0.5v_c)\, k_1(x) \qquad \text{Eq. 2-112}$$

$$k_u(x) = 0.25v_u\, k_1(x) \qquad \text{Eq. 2-113}$$

Estimation of particle size distribution

Particle size distribution, $p(x)$, was assumed to follow a Weibull distribution.

Prediction of flotation recovery

In terms of the above information, Schaap (1979) proposed that the volume fraction of total mineral in the feed recovered as fully liberated mineral particles (denoted by R_{ml}), composite particles (denoted by R_{mc}), and occluded mineral particles (denoted by R_{mu}), in the size interval x_1 to x_2 during batch flotation time t may be evaluated from:

$$R_{ml} = \int_{x_1}^{x_2} \frac{\mu_1 + \mu_0}{\mu_1}\, L_1(x)\left(1 - e^{-k_1(x)t}\right)p(x)dx \qquad \text{Eq. 2-114}$$

$$R_{mc} = \int_{x_1}^{x_2} \frac{\mu_1 + \mu_0}{\mu_1}\, C(x)v_c(x)\left(1 - e^{-k_c(x)t}\right)p(x)dx \qquad \text{Eq. 2-115}$$

$$R_{mu} = \int_{x_1}^{x_2} \frac{\mu_1 + \mu_0}{\mu_1}\, U_1(x)v_u(x)v_u(x)\left(1 - e^{-k_u(x)t}\right)p(x)dx \qquad \text{Eq. 2-116}$$

Since R_{mc} and R_{mu} involved the random variables $v_c(x)$ and $v_u(x)$, Schaap (1979) used the expectations $E[v_u(x)v_u(x)(1 - e^{-k_u(x)t})]$ and $E[v_c(x)(1 - e^{-k_c(x)t})]$ to evaluate R_{mc} and R_{mu}.

Similarly, the associated gangue recovery from the composite particles and occluded mineral particles are determined by

$$R_{gc} = \int_{x_1}^{x_2} \frac{\mu_1 + \mu_0}{\mu_1}\, C(x)\left(1 - v_c(x)\right)\left(1 - e^{-k_c(x)t}\right)p(x)dx \qquad \text{Eq. 2-117}$$

$$R_{gu} = \int_{x_1}^{x_2} \frac{\mu_1 + \mu_0}{\mu_1}\, U_1(x)v_u(x)\left(1 - v_u(x)\right)\left(1 - e^{-k_u(x)t}\right)p(x)dx \qquad \text{Eq. 2-118}$$

The theoretical recovery is given by the sum of R_{ml}, R_{mc} and R_{mu}.

$$R = R_{ml} + R_{mc} + R_{mu} \quad \text{Eq. 2-119}$$

The main flaws of Schaap's model lie in:

a) The assumption of negative exponential distributions for both mineral intercepts and gangue intercepts is of no general applicability. King (1994c; 1994) argued that linear intercept length distributions of certain ore bodies (e.g. low grade ores) followed negative exponential distribution for mineral phase and the sum of two negative exponential distributions for gangue phase. This assumption needs to be tested prior to using.

b) The assumption of cubic particle shape limits the application of this model. Further extension using spherical particles was discussed by Subasinghe (2008).

In summary, the Schaap's liberation/flotation model is convenient to predict the trend of flotation rate constants and recoveries. Schaap's model will be tested and discussed in Chapter 6.

2.3 Concluding remarks

The difficulty of using King's linear stochastic liberation model lies in the determination of transformation kernel, $P(g_L|g_v, D)$, to convert linear information into volumetric. Some researchers have attempted to establish this kernel through experiments and computer simulation (King and Schneider 1998; Schneider et al. 1991; Chiaruttini, Piga, and Schena 1999; Schena and Chiaruttini 2001). However, this leads to ill-conditioned problems and problems in using numerical methods.

Barbery's model is subject to the four assumptions: RUIF, ore texture, particle shape (Eq. 2-67) and particle convexity. Assumption of RUIF has been widely used in liberation modelling. The limitation of RUIF as suggested by Leigh *et al.* (1996) should be considered in different ways. On one hand, the preferential breakage might result in the large error in predicting particle volumetric grade distribution, and this should be evaluated. On the other hand, if the RUIF is only applied for stereological correction, Barbery's model is acceptable and able to provide accurate results of liberation. For the particle shape assumption (King Particles), validity of Eq. 2-67 for proximity function needs to be tested. Ore texture and particle structure assumption may be eliminated using more powerful image analysis technique. Validity of

particle convexity assumption was discussed in detail by Barbery (1991). This does not seem to be restrictive in mineral processing application.

It should be noted that the predictive liberation models should include the information of ore texture, particle structure and breakage pattern. Currently, limited information of ore texture and particle structure for liberation modelling can be extracted from the polished sections of parent rock and mounted particles using image analysis technique. For example, Barbery (1991) could not determine the covariance function and proximity function directly. Alternatively, he estimated them by assuming specific ore texture and the shape of particles (King Particles). In this thesis, attempts will be made to quantify the ore texture and particle characteristics using an improved image analysis technique.

In summary, the main drawbacks of the published liberation models (King's and Barbery's models) are:

a) Ore texture assumptions. The method of extracting ore textural information has not been established for arbitrary ores. Therefore, some artificial structures are used for liberation modelling, as their texture information is known in advance.

b) Particle structure assumptions. Certain shape of particles needs to be assumed to simplify liberation modelling. For example, King Particles was used in King's and Barbery's liberation models. Assumption of King Particles shape may not be valid for the comminuted particles from various ore types.

c) Assumption of particle convexity. This assumption is not required for King's liberation model; however, it is necessary for Barbery's liberation models.

To investigate the influence of mineral liberation on flotation performance, prediction of flotation recoveries should include liberation characteristics of particles. The current liberation/flotation models (e.g. Schaap's model) are subject to assumptions of particle shape and ore texture. Other flotation models simply incorporate liberation information implicitly together with other factors by two or three parameters. It seems that the flotation performance of comminuted particles in a narrow size interval with known grade distribution should be determined in order to find more information to quantify the influence of mineral liberation on flotation performance.

Chapter 3 Experimental and methods

This chapter discusses the detailed experimental methods and procedures for sample preparation, batch flotation tests, sample analysis and quantification of liberation characteristics using image analysis techniques based on Labview™. In order to test the theories of liberation and their relationship to flotation, samples of a high grade sulphide ore were used. This chapter comprises of three parts:

a) the sample preparation, batch flotation tests, sulphur analysis and chemical assay;
b) the procedure of SEM measurement;
c) the application of Labview™ software to analyse the SEM images from polished rock and mounted particle sections. Development of programs using Labview™ software to evaluate liberation characteristics using image analysis techniques are demonstrated, as there is limited information in the literature regarding the application of this technique in mineral liberation measurement.

3.1 Sample preparation and analysis procedure

The ore selected is a high grade sulphide ore consisting of chalcopyrite, sphalerite, pyhrrotite and pyrite from Western Australia. Chemical assay and sulphur analysis were employed to obtain the grade of chalcopyrite, sphalerite, pyhrrotite and pyrite. The metal element concentrations by mass in the ore are: copper 5.36%, zinc 17.53% and iron 29.02%.

3.1.1 Sample preparation

The ore received from the mine was SAG mill feed material with diameter of 15-25cm. The largest pieces of rock were sawn off and randomly selected largest pieces were kept for microscopy work. The resulting sample with diameter less than 10cm was fed to a Jaw crusher to crush down to 3-5cm. Then, it was crushed using a cone crusher to sizes less than 2cm.

Grinding

Dry grinding was conducted in a 20cm internal diameter batch laboratory rod mill. The crushed product from cone crusher was screened on a 250μm Tyler sieve using

Ro-Tap Shaker. To avoid the production of excessive fines, the oversize sample was stage-ground to -250 μm. After grinding, all the samples were mixed, riffled, collected in plastic bags, sealed and stored in sample storage room to minimize oxidation.

Sieving

To prepare the samples for liberation analysis and batch flotation tests, the comminuted particles (-250μm) were dry-screened on standard Tyler sieves to narrow size fractions using a $\sqrt{2}$ series as suggested by Schneider *et al.* (1991) and Barbery (1991). The material was screened to the following size fractions: -250+212μm, -212+150μm, -150+106μm, -106 +75μm, -75+53μm, -53+38μm and -38μm.

Sample preparation for image analysis

Sample preparation for image analysis is important, because inappropriate sample preparation would lead to the biased image analysis results. Particles are required to be mounted to ensure uniform and isotropic randomness. In practice, the comminuted particles may have various densities, shape, orientation and settling rate in resin. A sufficient number of particles were used to make particle sections for image analysis without over-crowding. The randomly selected rock samples were cut in perpendicular direction to account for any anisotropic effects present in the rock. The detailed procedure of sample preparation for SEM measurement can be found in references (Jones 1987; Jackson, Reid, and Wittenberg 1984). All the polished sections were coated with carbon (20nm) and stored in the vacuumed desiccators to avoid oxidation.

3.1.2 Batch flotation tests

A 3-litre Leeds cell was used for all the batch flotation tests. This cell takes advantage over other flotation cells by maintaining a constant pulp level and the depth of froth (Rofe 1995). The pulp level can be maintained by varying not more than 2-3mm. As far as possible, all operational conditions were maintained constant throughout the testwork.

Kalgoorlie tap water (pH=7.3-7.6, ≈18^{o}C) and flotation reagents were used for all flotation tests. Collector (PAX, from Orica Mining Chemicals), frother (MIBC, from Orica Mining Chemicals) and $CuSO_4$ (CP) were made into 1.0% solution (wt/wt).

PH regulators were made into 1M and 0.1M solutions. The reagents used in the flotation tests were:

Reagents name	Usage	Dosage
Potassium amyl xanthate (PAX)	collector	20g/t
Copper sulphate ($CuSO_4$)	activator	30g/t
Methyl isobutyl carbinol (MIBC)	frother	40g/t
Sodium hydroxide (NaOH)	pH regulator	As required
Hydrochloric acid (HCl)	pH regulator	As required

The following operational parameters were kept constant during batch flotation tests.

Operational parameter	Dosage
Impeller speed	1000rpm
Froth height	2.5cm
Aeration speed	4.1 L/min
pH	8.00 (±0.02)

During the batch flotation test, the following procedure was followed. The feed particles (550-600g) and water were added into the Leeds cell. The cell was checked in advance to exclude air bubble before conditioning. If the air bubbles appear, they can be eliminated by opening a small bleed valve. Then, the pH value of the pulp was adjusted to 8 (±0.02). The pulp was allowed to condition for 7 minutes. The other reagents were added during conditioning by the following order:

Sequence of reagents addition	At time added (min)
pH regulator	0
$CuSO_4$	1
Collector (PAX)	3
Frother (MIBC)	5

At the end of condition time, air was introduced at the rate of 4.1 L/min. The concentrate was collected at 15, 30, 60, 120, 240 and 360s to estimate the flotation kinetics. Plastic trays were used to receive the froth, in which the total mass of concentrate and water was measured for each concentrate. Then, the froth

(concentrate + water) was filtrated using funnels with quantitative filter paper. The filtrate cakes were dried to constant weight in the oven under 50^{o}C. Dried samples were weighed and mass of concentrate at each flotation time interval was obtained. Tailings were removed from the cell, filtered under pressure and dried to constant weight in oven under 50^{o}C. Random samples were taken from well mixed feed, concentrates and tailing for sulphur analysis, chemical analysis and mounting for SEM measurement.

3.1.3 Analytical methods

Sulphur analysis

Sulphur analysis was performed using a LECO IR sulphur analyser. All samples were first ground using a marble mortar and pestle to very fine size to ensure sufficient combustion during analysis. The samples (0.0100-5.0000 grams, according to the sulphur content in the sample) were fed into a combustion chamber in an oxygen atmosphere, where the sulphur can be oxidized into sulphur dioxide (SO_2) under high temperature (1370^{o}C). Moisture and dust are removed and the amount of SO_2 gas is measured by a solid state infrared detector. The sulphur content results were obtained after pre-programmed calibration, linearization and weight compensation. During the measurement, the pump pressure gauge was kept within the range of 8 and 18 psi and furnace temperature were maintained 1370±5^{o}C. The measurement time was 1~10 minutes. Calibration was carried out using standards (silica, S%=0%; zinc sulphide, from LECO, S%=32.46±0.13% and other standards, S%=7.74%, 13.77%). The standards should be changed when analysing samples with different sulphur content (medium sulphur (flotation feed), high sulphur (flotation concentrate), and low sulphur (tailing sample)). Standards were also interspersed through the samples as a check to ensure the machine was operating satisfactorily. All the tests for each sample were repeated at least 6 times. The sulphur content of particles in each size fraction is given in Table 3-1. It should be noted that the oxidation of sulphides in this high grade sulphide ore is unavoidable before being received from the process plant and during crushing and grinding in the lab. Therefore, to calculate the overall sulphides concentration in the ore and particles, the concentrations of metal elements, i.e. Cu, Zn and Fe measured by chemical analysis were considered as more accurate values, while sulphur content was used as a reference.

Chemical assay

Chemical analysis for the metal sulphides in the ore, flotation feeds, concentrates and tailings was performed using an Aqua Regia Digest method in Kalgoorlie Metallurgical Laboratory (KML). Flotation feed, concentrates and tailing of each size fraction were further ground using a marble mortar and pestle, weighed about 5 g for each sample accurate to four decimal places and placed into pre-labelled 500 mL conical flask covered with watch glass. Then, 75 mL concentrated nitric acid (70%) was slowly added into the conical flask. The whole operation was conducted in fume hood. Strong brown fume began to release. Then, the conical flasks were placed on a hot plate (pre-heated to about 140^{o}C) to boil to release the fume. Once the fume disappeared, the conical flasks were cooled down to room temperature and 150mL concentrated hydrochloric acid was added in. In order to decompose elemental sulphur generated from acid digestion, 25mL $HClO_4$ was added into the conical flask immediately after adding Hydrochloric acid. The solution in conical flask was allowed to boil for about 1.5 h until the whole volume of solution is less than 100mL. Finally, the solution was diluted in volumetric flask for ion coupled plasma (ICP) measurement. Measurement of each sample was repeated three times unless there was insufficient sample for the measurement (e.g. insufficient concentrates collected from batch flotation tests). Elemental concentration (C, ppm) is given by the following equation. The Cu, Zn and Fe concentrations of particles in each size fraction by chemical analysis are shown in Table 3-1.

$$C = \frac{volume\ of\ volumetric\ flask\ (mL) \times ICP\ reading\ (ppm) \times Dilution\ factor}{mass\ of\ sample} \qquad \text{Eq. 3-1}$$

Table 3-1 Mass concentrations of Fe, Cu, Zn and S of particles in each size fraction determined by chemical analysis and sulphur analysis

Size fraction (μm)	Fe%	Cu%	Zn%	S%	STD*
Rock	29.02	5.36	17.53	26.63	0.23
-250+212	30.47	5.18	15.32	24.47	0.61
-212+150	30.25	5.02	15.51	26.48	0.70
-150+106	29.62	4.86	16.59	26.48	0.99
-106+75	24.65	5.11	17.92	27.00	0.64
-75+53	18.27	5.90	19.03	28.30	0.78
-53+38	27.92	6.60	19.72	27.33	0.81
-38	27.22	7.20	20.48	27.12	0.63

*STD: standard deviation of sulphur analysis from LECO

X-Ray diffraction (XRD) and X-ray Fluorescence (XRF)

The received ore sample was analysed by XRD and semi-quantitative XRF to obtain the compositional information of the rock. The results of XRD and XRF analysis are given in Table 3-2 and Table 3-3. The XRD spectrum of the rock sample is attached in appendix B.

Table 3-2 Semi-quantitative phase analysis results of the ore sample from XRD

Phase	% (wt)
Chalcopyrite	35
Sphalerite	17
Pyrite	16
Pyrrhotite	16
Quartz	7
Plagioclase feldspar (albite)	7
Galena	1
Bannisterite	1

Table 3-3 Semi-quantitative XRF analysis results of the ore sample

Element	Concentration (%wt)
S	>10
K	0.4
Ca	4.0
Mn	0.08
Fe	>10
Cu	>10
Zn	>10
Pb	0.8
Ag	0.02
Cd	0.02
Sn	0.15
Sb	0.06

The results from XRD and XRF analysis were not adopted for the further liberation and flotation analysis due to their small sample size used during measurement. The chemical analysis results from ICP were used for liberation and flotation analysis, because much more sample were digested by acids compared to that of XRD and XRF.

Density measurement

The average density of each feed was measured using a 50ml pycnometer. From XRD and XRF measurement, it is shown that the ore contains chalcopyrite, sphalerite, pyrite, pyrrhotite, silica and albite. Silica and albite have close densities and they are combined as gangue phase. The density of the feed can also be approximated by calculating the average density in terms of density of each mineral and its weight fraction in the particles. Note that the density of one particular mineral, e.g. pyrite, is not specific. Therefore, average densities for each mineral were used to calculate quantities such as volumetric grade and flotation recoveries (by volume) of the particles and they were tabulated in Table 3-4. In terms of these average densities and composition data provided in Table 3-1 and Table 3-4, the volumetric grade of particles in each size fraction was estimated and tabulated in Table 3-5. The valuable mineral phase comprises of pyrite, sphalerite, chalcopyrite and pyrrhotite. The gangue material other than quartz and albite in the ore is also assumed to have a SG=2.62 and does not contain Cu, Zn or Fe element.

Table 3-4 Specific gravity and composition of each mineral in the ore

Mineral	Formula	SG†	Mw(g/mol)	Fe(%wt)	S(%wt)	Cu(%wt)	Zn(%wt)
Pyrite	FeS_2	5.01	119.98	46.55	53.45	0	0
Sphalerite	$(Zn_{0.95}Fe_{0.05}S)$	4.05	96.98	2.88	33.06	0	64.06
Chalcopyrite	$CuFeS_2$	4.19	183.53	30.43	34.94	34.63	0
Pyrrhotite	$Fe_{0.95}S$	4.61	85.12	62.33	37.67	0	0
Quartz	SiO_2	2.62	60.08	-	-	-	-
Albite	$NaAlSi_3O_8$	2.62	263.02	-	-	-	-

*Data source: http://www.webmineral.com. †Average specific gravity.

Table 3-5 Volumetric grade and specific gravity for each size fraction

Size fraction (μm)	Mass(g)	p_1*	SG†
-250+212	2577.8	0.756	3.90
-212+150	5557.4	0.751	3.90
-150+106	5472.6	0.755	3.93
-106+75	5554.0	0.786	3.90
-75+53	3739.7	0.789	3.93
-53+38	5176.7	0.775	3.98
-38	1379.6	0.714	3.89

*Volumetric grade. † Measured from pycnometer

3.2 SEM measurement of polished rock and particle sections

In this project, scanning electron microscope (SEM) with Back-scattered electrons (BSE) beam was used to perform the measurement on carbon coated polished sections of parent rock and particles in Physics department (Curtin University of Technology). The sulphides together were considered as one mineral phase. For the polished sections, the gray level of Back-scattered electrons (BSE) images is a function of average atomic number of the mineral grains (Lastra 2002). For the SEM imaging of the specimen, the resolution and magnification should be selected to preserve the detailed information of the structures of small particles and also completely include the sectional feature for the largest particles (Neumann and Schneider 2001). At least 6 sequential images were taken for each particle section sample when possible without image overlapping. The magnification ranges from 15 to 400, according to particle size and grain size in the rock. Electron beam energy was set at 20KeV. The scanning speed was maintained at 9 frames per second and a 5 frame averaged image was collected. The images collected were stored in .tif format with a resolution 2048*1536.

During the SEM measurement, all the operational parameters such as magnification for each sample were maintained constant, so that the subsequent image stitching could be performed. Background correction was also performed for all the images to ensure that the background (epoxy resin) is at the same grey level intensity (pixel value=0 for 8 bits image). 62 sections were measured by SEM including 8 mounted

particle sections (1 feed+6 concentrates+1 tailing) for each size fractions (7 size fraction in total) and 6 rock polished sections.

3.3 Image processing and analysis using Labview™ software

Image processing is an image-to-image process, in which an image is transformed into another image without losing useful information. Image analysis being an image-to-data process, allows extracting information from an image. In general, image processing and analysis depends on the following operations (Moen 2006; Delbem et al. 2011):

a) Image acquisition;
b) Image enhancement;
c) Segmentation and colour threshold;
d) Binary image processing;
e) Measurements and analysis.

The general image processing and analysis operations have been described in most image analysis books. In this chapter, image processing and analysis technique based on Labview™ software are introduced and discussed. The method for measuring linear intercept length distribution used by Young (2002) was extended in this thesis. This is a new technique that has not been explored in mineral processing for liberation related analysis. The main features of Labview™ software used in mineral processing lie in:

1. It is graphical programming technique.
2. It provides versatile functions by simple icons. One can also define and create new icons.
3. It provides specific tasks. A block diagram needs to be assembled by dragging, dropping and wiring the relevant icons in order. Image processing and analysis can be done within one block diagram. Special functions such as versatile shapes of *region of interest* (ROI) for image analysis are available. Alternatively, self-defined ROIs can be easily developed.
4. Progress of image processing and analysis can be monitored visually by displaying results in image windows or pop-up windows.
5. Image analysis data may be written to Excel files for further processing.

6. A random generator can be used to generate random points, random lines and other shapes, which are necessary for the image analysis technique used in this work.

The detailed basic image processing and analysis operations using Labview™ software, have been described in Labview™ manual and elsewhere, such as (Johnson and Jennings 2006; Klinger 2003; Relf 2004). An example block diagram (of point counting) is attached in appendix C.

3.3.1 Image processing

Image acquisition

In this thesis, all the images were taken from SEM measurements using backscattered electron (BSE) mode. All the resulting images were digital and stored in duplicate in .tif format.

Colour threshold

The original images obtained from SEM measurement must be transformed into 8 bit images for further processing. The greyscale ranges of mineral and gangue should be determined prior to processing. For example, it is found that RGB (Red, Blue and Green) values for describing the mineral and gangue phases in the images of rock polished sections in this work are:

a) Mineral phase, R=20-255, G=20-255 and B=20-255;
b) Gangue phase, R=0-19, G=0-19 and B=0-19.

After colour thresholding using the above RGB values, the resulting image is binary (8 bit).

Region of interest (ROI)

Region of interest is a selected region for analysis within a given image and it is also called sub-image (Relf 2004). ROI may be the whole image. ROI does not contain image data, but it is a placeholder that retains information of a defined location in the image (Relf 2004). ROI can be, theoretically, any shape. For instance, line segment, rectangle, oval, annulus or other self-defined shapes. In this thesis, different ROIs have been created during image analysis.

Basic operators

Digital images may be transformed into arrays, so that it is easy to perform simple transformation (similar to the basic calculation of the numbers) of images. The simple calculations such as add, subtract and multiply within two images or a image with a constant are allowed in Labview™. Some mixing operation is also permitted. These operations are useful for processing images from the sections of mounted composite particles.

Morphology

Morphology operation is a key step in this project. Basic morphology operations include dilation, erosion, closing and opening. In this section, specific morphology operations such as particle removal, filling particle holes, border rejection, and particle separation are introduced.

Particle removal is used to eliminate unwanted particles. The parameters (upper value and lower value) of this operation can be selected according to the requirements. In this project, those particles of area less than 2 pixels were removed from the image. Particle removal is not only for the real "particle", but also for the small dots (noise) originated from image acquisition.

Filling particle holes is also used to eliminate the noise. The holes on the image border cannot be filled, because it is not possible to determine whether they are holes.

Border rejection is used to discard incomplete particles touching the image border. Biased results (such as grade) may be obtained from incomplete particles. Therefore, incomplete particles need to be discarded before image analysis.

Particle separation is another useful tool. The number of particles touching each other in the section image from a well-prepared mounting sample is very small. However, with samples from the particles at small size, for some reasons (e.g. particle touching during mounting), the two separate particles may be jointed with each other in the image, so that they would have been considered by mistake as one particle during analysis. This may lead to errors for estimating particle size, shape and grade. Hence, it is important to separate the particles correctly before analysis. Normal particle touching problems can be solved using built-in methods of particle separation in Labview™, for example, watershed segmentation and IMAQ

separation. For heavily touched particle sections, separation methods proposed by van den Berg *et al*.(2002), and Wang (2008) were used.

All the morphological operations are also useful for processing rock polished sections. For example, removing small particles and filling the holes are necessary before analysing the images from polished rock sections. The sequence of the operation is essential and critical for image processing. For instance, if there are two particles touching each other and one of them touches the image border, they will cause problems during the operation of particle separation and reject border. If reject border operation was done before separating these two particles, then the two particles will be removed from the image, because they are considered by mistake as one particle and one of this particle happens to touch the image border. If they are separated before border rejection, then the particle does not touch image border can be left for analysis. There are also other important skills such as setting up the selectable region of ROIs. They are noted whenever necessary.

Image stitching

The statistical error can be reduced if appropriate amount of particles are analysed in each image. There are approximately 100~300 particles in each image taken from SEM. In order to obtain a bigger image with more particles, several sequential images taken from SEM measurement were stitched as suggested by Schneider and co-workers (Schneider, Neumann, and King 2003; Neumann and Schneider 2001; Schneider and Neumann 2004). This step was carried out using Microsoft Research Image Composite Editor (ICE). At least 6 sequential images were stitched to form one large image for each section sample of mounted particles. After stitching, the original images and stitched image were stored separately for further analysis. The use of one large image to replace several small images for analysis also saves a lot of image processing time.

The influence of image-stitching on the estimation of volumetric grade of parent rock using various measurement methods (areal grade, point counting and linear grade measurements) are shown in Table 3-6. It can be seen that the grade measured from single small image deviates considerably from the average values obtained all 5 images. Stitched image (5 images, covering the whole section) gives closer average grade of ore to that determined from chemical assay compared to the grade obtained

from individual images. The measurement methods used in Table 3-6 will be introduced in the next section.

Table 3-6 Comparison of measured grade results for parent rock from single images and stitched image using different methods

Image	p_1 (areal)	p_1 (linear-400lines)	p_1 (point counting-10000points)
1	0.856	0.858	0.856
2	0.762	0.749	0.767
3	0.855	0.854	0.856
4	0.860	0.872	0.859
5	0.541	0.534	0.543
Average	0.775	0.773	0.776
Standard deviation	0.137	0.143	0.136
Stitched	0.775	0.773	0.774
Chemical analysis*	0.775		

* The mass concentration was converted into volumetric grade using density of each mineral.

3.3.2 Image analysis

All the images from polished sections of parent rock and mounted particles are analysed to obtain the following information:

a) For rock: volumetric grade of parent rock, linear intercept length distributions of mineral and gangue phases, covariance function, two-point probability function, phase specific line segment function and phase specific circular disk segment function;
b) For particles: linear intercept length distribution, proximity function, linear/areal grade distributions of particles in each size fraction for the feed, concentrates and tailing.

In this section, the methods of estimating volumetric grade of the parent rock, linear intercept lengths, linear grade distribution, areal grade distribution and surface composition of particles from SEM images using Labview™ software are introduced. Measurement methods for other functions will be given in Chapter 4.

Estimation of volumetric grade of parent rock

The direct measurement of volumetric grade distribution of particles using image analysis is not easy, even though there has been the attempt of using cone beam x-ray micro-tomography (e.g. (Miller and Lin 1997)). Common image analysers mainly provide linear intercept lengths and section areas, which may be used to estimate the volumetric grade of parent rock in reduced dimensions (1-D and 2-D). There are mainly three methods available to estimate the volumetric grade of parent rock: point counting, linear grade and areal grade measurements. These measurement methods have been developed using Labview™ in this thesis, where one of the major improvements is the introduction of random points and random lines during analysis. The advantages of the proposed image analysis technique by incorporating random points and random lines over the commonly used image analysis techniques that use grid points and equidistant parallel lines are: a) it is not affected by the orientation of the image (anisotropy); b) the information of small particles or grains may not be missed and c) it offers the feasibility of estimating other probabilistic texture descriptors such as proximity function, which will be shown in Chapter 4. The following schematic illustration in Figure 3-1 shows the process of using 5 random lines for the measurement of linear intercept lengths from SEM image of polished sections of parent rock. The linear intercepts from mineral phase (L_1) and gangue phase (L_0) were recorded and written to an Excel file. The number of random lines used can be set by the program.

Point counting was carried out by placing a desired number of random points on the SEM image from polished sections of parent rock. The number fraction of points falling in mineral phase was taken as the grade of parent rock. Areal grade of the parent rock is taken as the ratio of mineral phase area to the total area of the rock on the SEM image of polished sections of parent rock. Linear grade measurement was carried out by placing a desired number of random lines on the SEM image from polished sections of parent rock. The linear grade is taken as the ratio of the sum of mineral intercept lengths to the total intercept lengths.

From Table 3-6, it can be seen that result of volumetric grade of parent rock measured from these three methods are very close. This also demonstrates the validity of the basic principle from stereology: the average grade estimated from 1-D,

2-D and 3-D should be the same. Hence, all these methods may be used to evaluate the grade of an ore in practice.

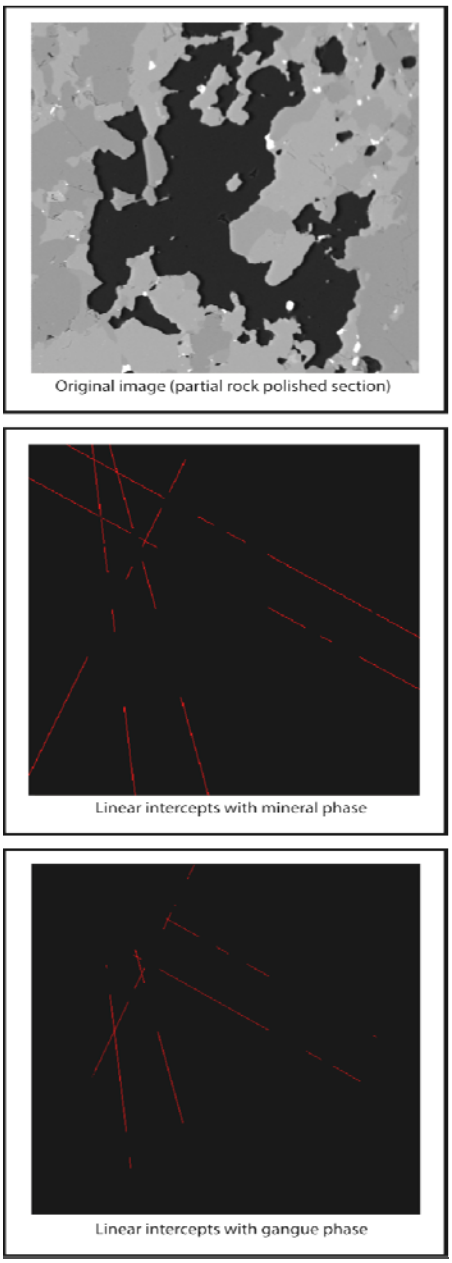

Figure 3-1 Schematic illustration of 5 random lines traversed on the polished rock sections for both mineral phase (gray) and gangue phase (dark)

Linear grade distribution measurement from particle sections

Linear grade distribution measurement is commonly used in the current automatic image analysers, where equidistant horizontal lines were employed to scan the particle sections. In this work, an improved method of measuring the linear grade distribution by employing lines generated by random points both in location and orientation, which would minimize the effect due to anisotropy. The particle sections

were analysed one by one by placing a desired number of such random lines on each particle section. The ratio of mineral intercept lengths to the total intercept lengths is taken as the linear grade of the particle section. By repeating this measurement for all the particle sections, the linear grade distribution of the particle sections can be obtained. The grade in domain [0,1] was subdivided into 12 classes (0, 0.05, 0.15, 0.25, 0.35, 0.45, 0.55, 0.65, 0.75, 0.85, 0.95 and 1). Grade 0 and 1 represent fractions of fully liberated gangue and mineral particles, respectively. In general, this method is superior to the current automatic image analysers by:

a) The use of random lines;
b) The measurement was conducted on each particle section. Each particle was traversed the same number of random lines; therefore, the weight of each particle contributed to the overall grade is the same. The structural information for each particle may not be missed.

The schematic illustration of the linear grade measurement of a particle is illustrated in Figure 3-2. Note that, the number of random lines used in practice is much more than that (2 random lines) illustrated in Figure 3-2. For the particle sections with more than two mineral grains, the sum of mineral intercept lengths is taken rather than one intercept length (see also Figure 3-2).

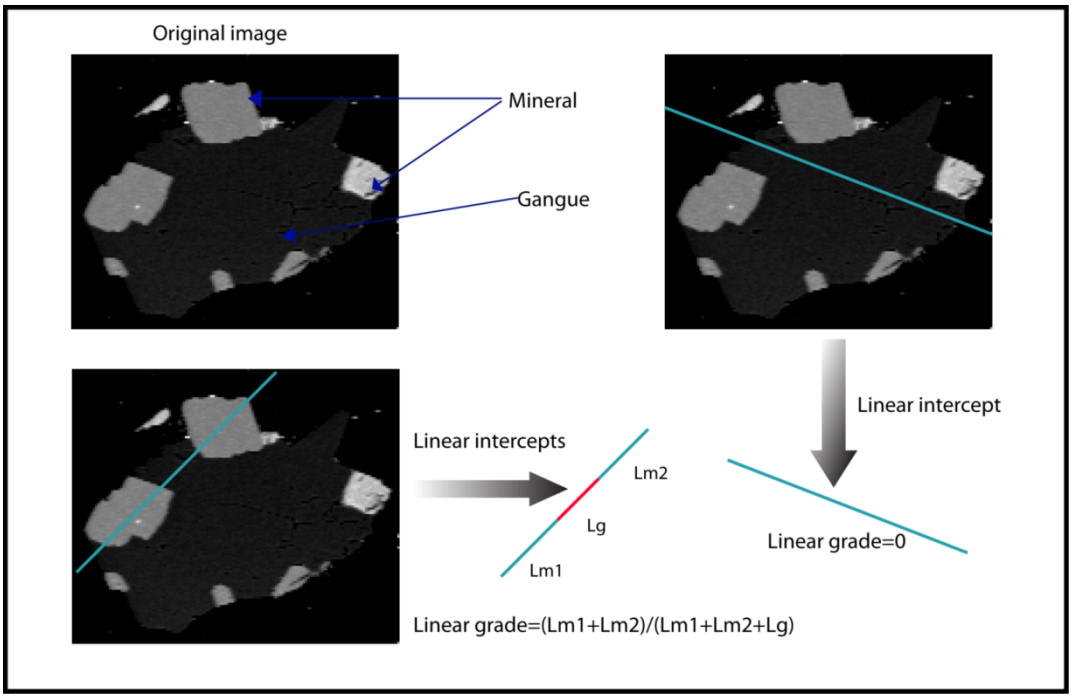

Figure 3-2 Schematic illustration of linear grade measurement on a particle section

Areal grade distribution measurement from particle sections

Areal grade measurement is more straightforward compared to linear grade measurement. The areal grade of each particle was obtained from the ratio of the area of mineral phase to the total section area, i.e. the area of mineral phase + the area of gangue phase in the particle. Similar to the linear grade measurement, areal grade measurement was also performed on each particle section. The schematic illustration of areal grade measurement is shown in Figure 3-3. Note that, areal grade measurement is much quicker than linear grade measurement. For a particle section with more than one mineral (or gangue) grain, the area of mineral phase is taken as the sum of areas of all the mineral (or gangue) grains in the particle. For example, since there are 6 mineral grains in the particle section shown in Figure 3-3, the area of mineral phase used for estimating the areal grade of this particle is the sum of areas of the 6 mineral grains.

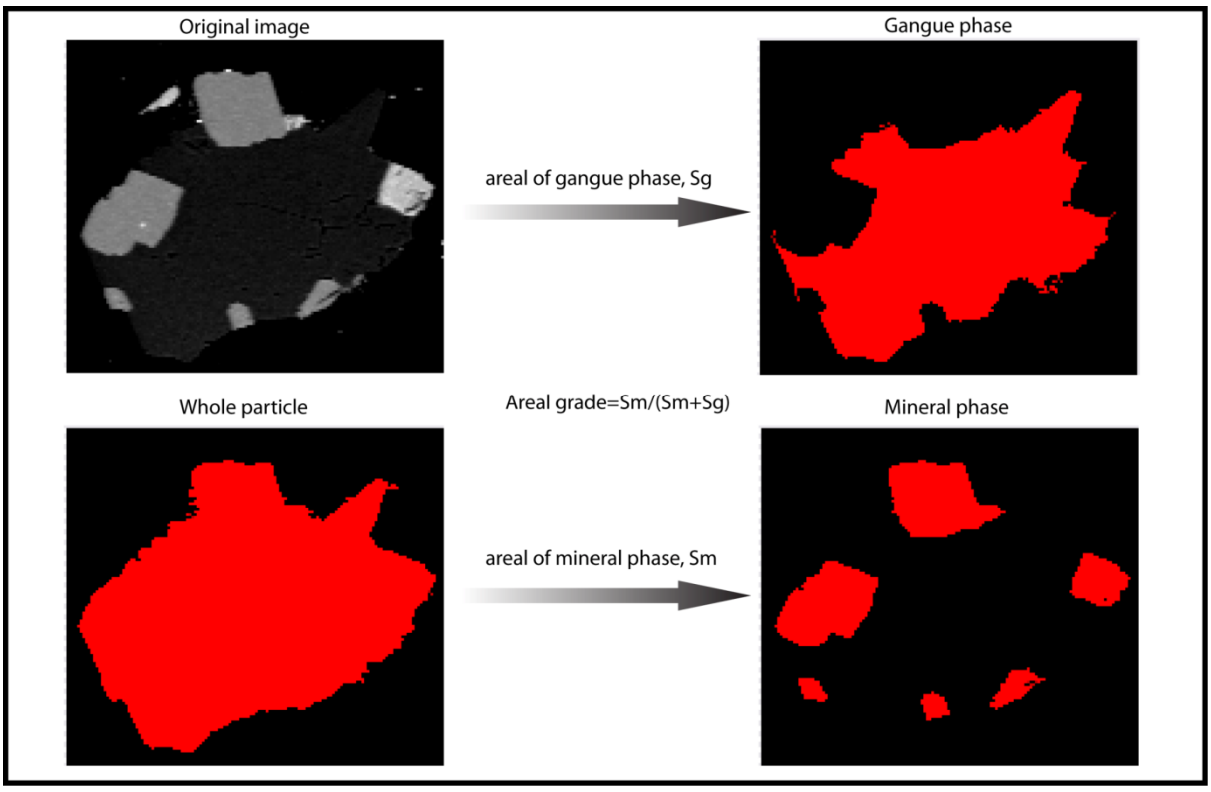

Figure 3-3 Schematic illustration of areal grade measurement implemented on a particle section

Because the areal and linear grade measurements were both performed on each particle section, it is of interest to compare the grade of a particle estimated from

both methods. For linear grade measurement, the number of random lines placed on the particle sections may have an effect on the measured linear grade. This was investigated using a single particle section was selected from a SEM image, shown in Figure 3-4. The particle section under measurement is in the middle of the image. The incomplete particle section at the right bottom corner was left in the image deliberately to test whether the algorithm can eliminate the interference of surrounding incomplete particle section(s). The results are shown in Table 3-7.

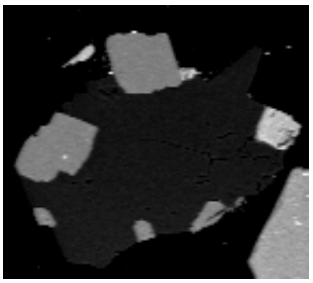

Figure 3-4 A particle section for comparison of areal grade measurement with linear grade measurement (pixel values: 5-54, gangue, dark gray; 55-255, mineral, gray+white)

From Table 3-7, it has been seen that the number of random lines has a significant effect on the measured linear grade. If the number of random lines is small, the measured linear grades vary considerably. This is demonstrated by their standard deviations, which decreases with the increase of number of random lines. Test with 2000 random lines was also run to compare the results with areal grade. More stable results were obtained (see Table 3-7), however it took approximately 30s to complete the measurement for one particle section (compared to several seconds with 50 random lines). In this work, 20 random lines were adopted during linear grade measurement.

Table 3-7 Comparison of areal and linear grades measured from one particle section

Method	N*	Run1	Run2	Run3	Run4	Run5	Run6	Average	STD
Areal	-	-	-	-	-	-	-	0.287	
Linear	10	0.142	0.404	0.211	0.217	0.257	0.240	0.245	0.087
	20	0.219	0.318	0.195	0.262	0.293	0.273	0.260	0.046
	50	0.281	0.295	0.310	0.306	0.237	0.328	0.293	0.032
	100	0.334	0.284	0.298	0.279	0.308	0.286	0.298	0.021
	200	0.274	0.285	0.266	0.318	0.293	0.316	0.292	0.021
	2000	0.287	0.293	0.300	0.299	0.306	0.289	0.296	0.007

* N= Number of random lines; STD=standard deviation.

Apparent surface composition measurement on particle sections

In this thesis, it is assumed that the average mineral exposure on the surface (i.e. surface composition) of a particle section is equivalent to the ratio of mineral pixels to total pixels on the edge of the particle section. That is, the outmost perimeter consisting of mineral phase pixels is divided by the total pixels on the perimeter of the particle section. The algorithm of estimating particle surface composition developed in this thesis is to compute the overall mineral phase pixels and the gangue phase pixels for the silhouette of each particle section. The particle surface composition estimated by this method is referred to as apparent surface composition.

The apparent surface composition were measured by Sutherland (1989) using QEM*SEM through counting the two ends of a line segment intersecting with particle edge during linear grade measurement and it was calculated by the number fraction of mineral ends to the total ends within each particle section. Because the step size of the paralleled scan lines is often much larger than one pixel in commercial image analysers, the approximation of apparent surface composition obtained from QEM*SEM seems to be less accurate.

An improved algorithm was developed in this work by reducing the step size to 1 pixel. The measurement was performed separately on each particle section. Pixel values at the intersection of each line with particle periphery were measured and recorded. The number fraction of pixels corresponding to mineral is taken as the

surface composition of that particle section. The schematic illustration of apparent surface composition measurement is shown in Figure 3-5. Only two end points are considered, e.g. point A and D in Figure 3-5.

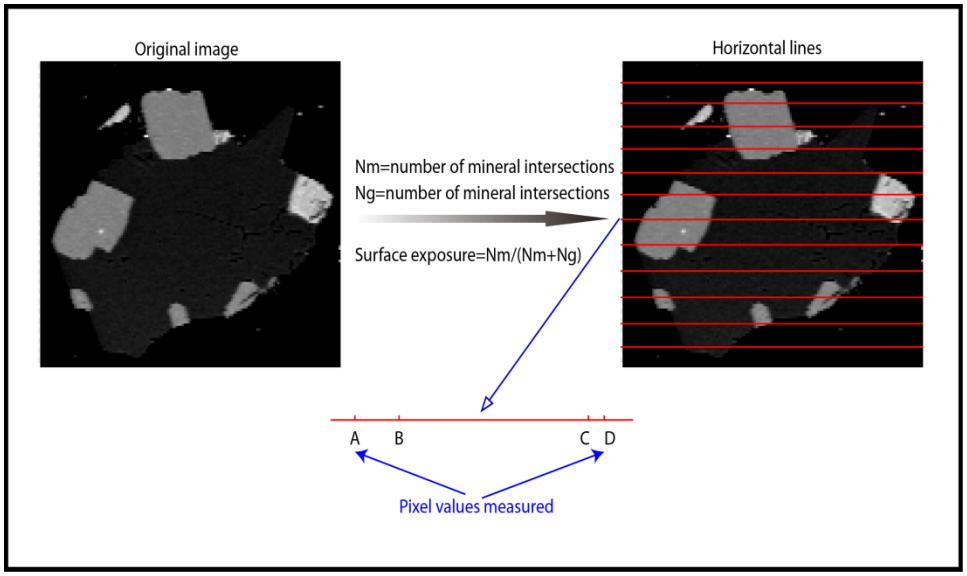

Figure 3-5 Schematic illustration of apparent surface composition measurement on a particle section

Identification of breakage pattern using image analysis

Most liberation models are based on the assumption of random breakage, it is then necessary to determine whether the breakage pattern in practice is random. A simple method is to measure the average mineral content of particles in each narrow size fraction. If the measured mineral contents do not change significantly at various size fractions, the breakage pattern may be considered as random breakage. Table 3-8 shows volumetric grades measured on particles in each narrow size fraction by point-counting algorithm and chemical analysis. Note that the mass concentration of mineral phase obtained by chemical analysis was transformed into volumetric grade using density of each mineral.

Table 3-8 Volumetric grade for each size fraction measured by pointing counting and chemical analysis

Size fraction	p_1								
	Run 1	Run2	Run 3	Run 4	Run 5	Run 6	average	STD	CA*
-250+212μm	0.768	0.767	0.764	0.769	0.767	0.767	0.767	0.00164	0.756
-212+150μm	0.778	0.778	0.776	0.777	0.774	0.777	0.777	0.00157	0.751
-150+106μm	0.780	0.780	0.780	0.778	0.781	0.781	0.780	0.00119	0.755
-106+75μm	0.806	0.804	0.806	0.803	0.806	0.804	0.805	0.00137	0.786
-75+53μm	0.797	0.801	0.800	0.801	0.798	0.800	0.800	0.00162	0.789
-53+38μm	0.783	0.777	0.786	0.783	0.785	0.784	0.783	0.00327	0.775
-38μm	0.710	0.711	0.715	0.710	0.711	0.715	0.712	0.00240	0.714

* CA=chemical assay

From Table 3-8, it may be seen that the average grade of each size fraction does not change significantly; therefore it is reasonable to assume that the ore underwent random breakage in the lab-scale rod mill. In this sense, the experimental data of liberation measurement may be used to compare with the results predicted from published liberation models based on random breakage to test the validity of liberation models.

3.3.3 Operational limitations and errors in image analysis

In practice, errors may occur during image analysis. The possible error sources were (Jones 1987; Barbery 1991): a) misidentification of a mineral due to the resolution, image noise, b) improper particle mounting process, c) effect of composite particles and d) the number of particle to be analysed. They can be categorized into two kinds: error due to observation and image processing by human and statistical error (Lin *et al*. 1987). Error from a) could be reduced to a negligible level by an experienced operator; but b) belongs to the systematic error and is not subject to decrease with the human proficiency. The effects of c) and d) are discussed below.

For image analysis, it is important to determine:

a) The number of random lines required to obtain statistically significant results of the linear grade and linear intercept length distribution measurement from rock polished section;
b) The number of particles required for linear/areal grade distribution measurement to obtain statistically significant results.

For problem a), the method suggested by Jones (1987) can be used to determine the minimum random lines traversed on rock polished sections to obtain statistically significant linear grade. It was shown by Chayes (1956) that the standard deviation σ_n, is determined by the following equation,

$$\sigma_n = \sqrt{\frac{p(1-p)}{N}} \qquad \text{Eq. 3-2}$$

where p = volumetric concentration of mineral phase, and N is the total number of observations (random lines or points). In practice, the acceptable error (e) in most mineral processing is the 95% confidence limit (i.e. $\pm 2\sigma_n$), therefore the absolute error is given by Eq. 3-3.

$$e = \pm 2\sqrt{\frac{p(1-p)}{N}} \qquad \text{Eq. 3-3}$$

The relative error ($E = e/p$) with respect to p, is frequently used as a measure of precision. The number of observations required to obtain a relative error at the 95% confidence level is determined by the following equation.

$$N = \frac{4(1-p)}{pE^2} \qquad \text{Eq. 3-4}$$

The volumetric concentration can be estimated by chemical analysis, and if the limit of relative error is pre-determined, then the minimum number of observations can then be determined using Eq. 3-4.

For problem b), according to Lin *et al.* (1987), the best estimation of the density function (fraction of the total length) in the jth grade interval, $\widehat{f_j}$ and the relative error, $S_{\widehat{f_j}}$, can be determined using the following equations:

$$S_{\widehat{f_j}} = \frac{\widehat{f_j}}{\sqrt{n}} \qquad \text{Eq. 3-5}$$

n is the total number of particles. Obviously, Eq. 3-5 may be used to establish the minimum number of particles required to determine $\widehat{f}_J$.

Chapter 4 Extracting ore texture information using image analysis

As discussed in Chapter 2, the information of ore texture and particle structure is essential to quantify mineral liberation. Some structural information in particles and textural information in ores can be obtained by SEM-based techniques such as MLA and QEM*SEM. Researchers have quantitatively expressed ore texture and particle structure in terms of descriptors such as covariance function, proximity function and linear intercept length distribution. However, measurement of such quantities is difficult in practice and hence models that predict such descriptors have been derived based on assumed ore textures, such as Poisson polyhedral and Boolean textures. Barbery (1991) formulated Eq. 2-46 to estimate the second moment of volumetric grade distribution of valuable mineral in particles under the assumption of random uniform isotropic fragmentation (RUIF). However, he was unable to determine $C(L)$ and $P(L)$ functions directly. Alternatively, he developed models based on assumed mineral/gangue assemblages, such as, Poisson polyhedral and Boolean textures. These textures generally do not describe the spatial distribution of grains within real ores. Hence, application of these models has been limited mainly to ores whose texture is similar to that assumed in the models. In this regard, a reliable method of measuring the textural descriptors is required to be established.

In this chapter, a method is proposed to obtain the ore textural and particle structural information from SEM images of real ore and particle sections using image analysis technique based on Labview^{TM} software. This eliminates the need for any assumption about the texture of the ore. Firstly, the ore texture and particle structure descriptors will be defined and discussed. Then, the measurement methods for these descriptors will be introduced. The conventional texture descriptors, such as linear intercept distribution $i(L)$, covariance function $C(L)$, proximity function $P(L)$ and new descriptors such as phase specific circular disk segment function $\omega^{(i)}(A)$ and phase specific line segment function $\omega^{(i)}(L)$ have been obtained from 2-D images and compared with those from models proposed by King (1982a, 1984) and Barbery (1991). Finally, the published theorems and relationships relating to liberation models are tested and discussed.

4.1 Ore texture descriptors

Mineral ores are heterogeneous material and their properties depend on the properties of individual phases present and the microstructure of the assemblage, which include the mineral phase volume fraction and the spatial distribution of the phases. To quantify the average volumetric fraction of the mineral in the ore is not difficult in practice. However, the information relating to the distribution of valuable mineral within the gangue matrix is complex and is characterised by factors such as the size of the grains, shape of the grains, the distance between grains, etc. It is important to quantify these features in order to obtain the distribution of mineral in comminuted products of an ore. Owing to the complex nature of the variations, researchers have resorted to probabilistic and statistical methods to quantify the above characteristics.

Before introducing the measuring technique for ore texture and particle composition, it is important to clarify the definitions of the texture descriptors used. In this work, the notations used in Barbery's book on liberation (Barbery 1991) have been adopted where appropriate. There are a number of texture descriptors available (Torquato 2002) for the quantification of ore texture but only those that are strongly related to the modelling of mineral liberation will be discussed in this chapter. They are the two-point probability function, covariance function, proximity function, linear intercept length distribution function and new descriptors such as phase specific line segment function and phase specific circular disk segment function, whose properties are discussed below.

4.1.1 Two-point probability function

Two-point probability function $\delta^{(ii)}(L)$, is defined as the probability that two points with a distance L apart are found in phase i. It is essentially a measure of the separation between mineral grains in the parent rock. Under the assumption of *isotropic* texture of the rock, this probability only depends on the distance of the two points. The boundary conditions associated with this function is provided below, which may be used to test the validity of measured $\delta^{(ii)}(L)$.

If the distance between the two placed points is zero, this function equates to the volumetric mineral concentration, p_i, obtained by the point counting procedure. That is,

$$\delta^{(ii)}(0) = p_i \qquad \text{Eq. 4-1}$$

Similarly, if there is no long-range order, the following equation is valid.

$$\lim_{L\to\infty} \delta^{(ii)}(L) = {p_i}^2 \qquad \text{Eq. 4-2}$$

Eq. 4-1 and non-negative property of two-point probability function lead to

$$0 \le \delta^{(ii)}(L) \le p_i \qquad \text{Eq. 4-3}$$

Another necessary condition states that the slope at $L = 0$ is always negative

$$\left.\frac{d\delta^{(ii)}(L)}{dL}\right|_{L=0} < 0 \qquad \text{Eq. 4-4}$$

It is shown that the following relationship is true for binary ores comprising of phases **0** (gangue) and **1** (valuable mineral) (King 1994c).

$$\delta^{(10)}(L) = \delta^{(01)}(L) = p_1 - \delta^{(11)}(L) = p_0 - \delta^{(00)}(L) \qquad \text{Eq. 4-5}$$

The infimum of the two-point probability function should satisfy the inequalities (Jiao 2010):

$$max(0, 2p_i - 1) \le inf\,[\delta^{(ii)}(L)] \le {p_i}^2 \qquad \text{Eq. 4-6}$$

Quintanilla (2008) derived an inequality for $\delta^{(ii)}(L)$,

$$\delta^{(ii)}(L) \ge -\left[\delta^{(ii)}(r) + \delta^{(ii)}(t)\right] + (4{p_i}^2 - p_i) \qquad \text{Eq. 4-7}$$

where $L = t - r$. A similar inequality was derived by Matheron (1993),

$$\delta^{(ii)}(L) \ge \delta^{(ii)}(r) + \delta^{(ii)}(t) - p_i \qquad \text{Eq. 4-8}$$

4.1.2 Covariance function

The covariance function between the mineral phases at points *L* apart, similar to the two-point probability function described above, is also a measure of the size and the separation of mineral (or gangue) grains within the ore. It is defined as

$$C_{ii}(L) = E[(h(z) - p_i)(h(z + L) - p_i)] \qquad \text{Eq. 4-9}$$

where $h(z)$ is indicator function (see also Eq. 2-29), and the subscript i represents the phase under consideration. The values of i take 1 and 0 to represent the mineral and gangue phases of a binary ore, respectively.

For the mineral phase of binary ores, $C_{11}(L)$ is defined by

$$C_{11}(L) = E[(h(z) - p_1)(h(z+L) - p_1)] \quad \text{Eq. 4-10}$$

Similarly, for the gangue phase,

$$C_{00}(L) = E[(g(x) - p_0)(g(x+L) - p_0)] \quad \text{Eq. 4-11}$$

where $g(x)$ is another indicator function defined by

$$g(x) = \begin{cases} 1, & x \in gangue\ phase \\ 0, & x \in mineral\ phase \end{cases} \quad \text{Eq. 4-12}$$

Since $C_{11}(L) = C_{00}(L)$, the subscripts may be dropped from the notation, so that the covariance function is represented by $C(L)$. Therefore, for a binary ore, the covariance function does not change with different phases under consideration and it correlates the physical interaction of the two phases. The general properties of covariance function were presented in section 2.1.3.2.

The relationship between the two-point probability function and covariance function is given by (Torquato 2002):

$$C(L) = \delta^{(ii)}(L) - {p_i}^2 \quad \text{Eq. 4-13}$$

Also,

$$C(L) = p_1 p_0 - \delta^{(01)}(L) = p_1 p_0 - \delta^{(10)}(L) \quad \text{Eq. 4-14}$$

For a binary ore, $C(L)$ has the limiting conditions (Barbery 1991):

$$C(0) = \delta(0) - {p_1}^2 = p_1 - {p_1}^2 = p_1 p_0 \quad \text{Eq. 4-15}$$

and

$$C(\infty) = {p_i}^2 - {p_i}^2 = 0 \quad \text{Eq. 4-16}$$

Eq. 4-16 is obtained using Eq. 4-2.

Barbery (1991), Stoyan (1979) and Laslett *et al.* (1990) suggested a negative exponential form for the covariance function,

$$C(L) = p_1 p_0 e^{(-\frac{L}{k})} \quad \text{Eq. 4-17}$$

where k is a constant dependent on the ore texture.

Barbery (1991) suggested that the covariance function might be measrued using image analyser, but he did not show the detailed estimation procedure. Torquato

(2002) proposed that the covariance function could be measured experimentally by using 3-D image processing technique such as tomography and confocal microscopy. However, these methods are both time-consuming and costly in practice. Instead of the direct measurement of $C(L)$ in 3-D, estimation of $C(L)$ from 2-D images of rock polished sections ($C(L)$ in reduced dimension) can be established. Under the assumption of the isotropy of ore texture, $C(L)$ estimated from 2-D images of the rock polished sections is equivalent to $C(L)$ in 3-D.

4.1.3 Linear intercept length distribution of rock sections

Linear intercepts are referred to as line segments formed by the intersections of a random line with the mineral and gangue phases on the surface of the specimen tested. The linear intercept length distribution is also called linear chord length distribution. Linear intercept length distribution can be measured from both polished sections of the parent rock and mounted particles. The measurement of linear intercept length distributions of mineral and gangue phases is commonly used by conventional image analysers to determine the average intercept length of mineral and gangue phases. Linear intercept length distribution function was used by King and co-workers (King 1975a; King 1979; Schneider *et al.* 1991; King 1994b) for liberation modelling.

4.1.4 Phase specific line segment function

The phase specific line segment (PSLS) function, denoted by $\omega^{(i)}(L)$, is defined as the probability that a line segment of length L is completely included in phase i. It indicates a measure of the size and shape of grains of phase i. The application of this function in liberation modelling will be shown in Chapter 5. Similar to this definition, two-point cluster function was defined by Torquato (2002) as the probability that two points of a distance L are fallen in one cluster. A cluster is equivalent to one single grain (mineral or gangue). Assuming the convex shape of clusters, the PSLS function is equivalent to the two-point cluster function. Because the shape of mineral grains or gangue grains may not be always convex, the PSLS function is used instead of the two-point cluster function. Since PSLS function considers all the points on the line segment connecting the two randomly selected end points (with a distance L) or if there are concave grains of phase i in the rock, the PSLS function of phase i is less

than the two-point cluster function of phase i. The properties of two-point cluster function suggested by Torquato (2002) can also be applied for PSLS function.

The PSLS function is somewhat similar to the two-point probability function; however, PSLS function provides continuous information alongside the line segment, while the two-point probability function only gives the information of two end points. Thus, for the same line segment L, $\delta^{(ii)}(L)$ is always greater than $\omega^{(i)}(L)$. $\omega^{(i)}(L)$ contains topological "connectedness" information (Jiao, Stillinger, and Torquato 2009; Lu and Torquato 1992; Torquato 2002).

The exploration of PSLS function is not as much as the two-point probability function, only several publications provide the estimation of its analytical form (e.g. (Cinlar and Torquato 1995)). However, their determination was based on the assumption of specific structure (e.g. one-dimensional continuum-percolation model of Poisson-distributed rods). For real ores, it is unrealistic to make such assumption of ore texture to obtain the PSLS function due to the complex association of mineral and gangue grains within the ore.

The liberation of mineral phase is to some extent determined by the PSLS function. For example, if a particle is generated only from a single mineral or gangue grain, the particle must be a liberated particle (either mineral or gangue). In contrast, two-point probability function tends to include the average distance of grains in the same phase. Therefore, the PSLS function is more effective than two-point probability function in mineral liberation modelling. In this regard, it is necessary to establish the method to evaluate PSLS function from the real ores.

Except for the direct measurement method that will be established in this chapter, there is an alternative method to determine the PSLS functions for the two phases (0 and 1). The PSLS function for a phase i is related to its linear intercept length distribution of the phase, $f_i(L)$, by

$$f_1(L) = \frac{\mu_1}{p_1}\frac{d^2\omega^{(1)}(L)}{dL^2} \qquad \text{Eq. 4-18}$$

$$f_0(L) = \frac{\mu_0}{p_0}\frac{d^2\omega^{(0)}(L)}{dL^2} \qquad \text{Eq. 4-19}$$

$$\omega^{(1)}(L) = \frac{p_1 \int_L^\infty f_1(u)(u-L)du}{\mu_1} \quad \text{Eq. 4-20}$$

$$\omega^{(0)}(L) = \frac{p_0 \int_L^\infty f_0(u)(u-L)du}{\mu_0} \quad \text{Eq. 4-21}$$

μ_1 and μ_0 are the average linear intercept length for mineral and gangue phases, respectively. $f_1(L)$ and $f_0(L)$ are the linear intercept length distribution density functions of mineral and gangue phases, respectively. Eq. 4-18 and Eq. 4-19 were shown by Barbery (1991) in deriving the general liberation equation for 1-D. Note that Barbery normalized the PSLS function by dividing p_i (i.e. $\frac{\omega^{(i)}(L)}{p_i}$), therefore there are no p_1 and p_0 in Barbery's equations (IV. 27 and 28, p65, (Barbery 1991)). As the linear intercept length measurement is easy to obtain using image analysis from parent rock polished section images, these relationships are useful when the direct measurement of PSLS function is not available.

4.1.5 Phase specific circular disk segment function

Phase specific circular disk segment function $\omega^{(i)}(A)$ is defined as the probability of a random circular disk section with area A is fully contained in phase i. This function being similar to phase specific line segment function $\omega^{(i)}(L)$ also demonstrates the size and shape of grains in phase i.

4.2 Particle structure descriptors

4.2.1 Linear intercept length distribution and section area distribution

For linear intercepts measured on sections of narrowly sized particle with size D, King and co-workers (King 1982a, 1984; Finlayson 1980) proposed Finlayson equation density function (Eq. 2-8) for linear intercept length density distribution, $i(L)$. King (1984) also argued that the above equation was valid when the angularity of particles, defined by $(\frac{4\pi A}{P^2})$ is within 0.60-0.66, where A and P are the cross-sectional area and perimeter of the particles, respectively.

The section area distribution can be determined by image analysis from the particle sections. There is no generic analytical equation for this distribution. Barbery (1991)

performed a curve fitting from King's published section area data (King 1982a) and proposed an empirical equation for King Particles:

$$g(A) = \begin{cases} \dfrac{4}{3D^2}, & 0 \le \dfrac{A}{D^2} < 1/2 \\ \dfrac{8}{3D^2}\left(1 - \dfrac{A}{D^2}\right), & 1/2 \le \dfrac{A}{D^2} \le 1 \\ 0, & otherwise \end{cases} \qquad \text{Eq. 4-22}$$

Eq. 4-22 shall not be used as a general equation for section area distribution for comminuted particles.

4.2.2 Proximity function

The proximity function $P(L)$ represents the probability that given a randomly selected point is in a particle, another randomly selected point at a distance L is also in the same particle (Barbery and Leroux 1988). King and co-workers (King 1994c; King and Stirling 1994) also used this function in their work. Davy (1984) and Leigh, et al. (1996) called this function the "proximity function" and this name is retained in this work. $P(L)$ provides the information of breakage, size and shape of comminuted particles. Under the assumption that particles are convex, the proximity function is equivalent to the probability that a line segment of length L fully resides within one particle. It must be noted that the line joining the two points should not intersect the boundary of the particle, which implies that the particles are convex.

$P(L)$ function has the following boundary conditions and relationships with $i(L)$ (Barbery 1991; Serra 1982; Enns and Ehlers 1978):

$$P(0) = 1 \qquad \text{Eq. 4-23}$$

$$P(\infty) = 0 \qquad \text{Eq. 4-24}$$

$$P(L) = \frac{\int_L^\infty i(u)(u - L)du}{\int_0^\infty u\, i(u)du} \qquad \text{Eq. 4-25}$$

$$i(L) = E(L)\frac{d^2P(L)}{dL^2} \qquad \text{Eq. 4-26}$$

where $E(L)$ is the mean of linear intercept length of particle sections.

Using Finlayson equation density function (Eq. 2-8) for $i(L)$ and integrating Eq. 4-26, Barbery (1991) obtained proximity function expressed by Eq. 2-67.

Other particle structure descriptors such as linear grade distribution and areal grade distribution were discussed in Chapter 3 and will be further discussed in Chapter 5.

4.3 Measurement of ore texture and particle structure descriptors using image analysis technique

These functions were determined by placing random points and line segments on the polished section images and evaluating the probabilities according to the respective equations given above. This technique was implemented on the SEM images of polished sections of parent rock and mounted specimens of particles using the Labview™ graphical programming technique. In this work, all sulphides (appears grey on the image, denoted as phase 1) were considered as valuable mineral and the remaining silica/silicates (black, denoted as phase 0) were considered as gangue. The schematic illustration of each function estimated using image analysis is shown in Figure 4-1.

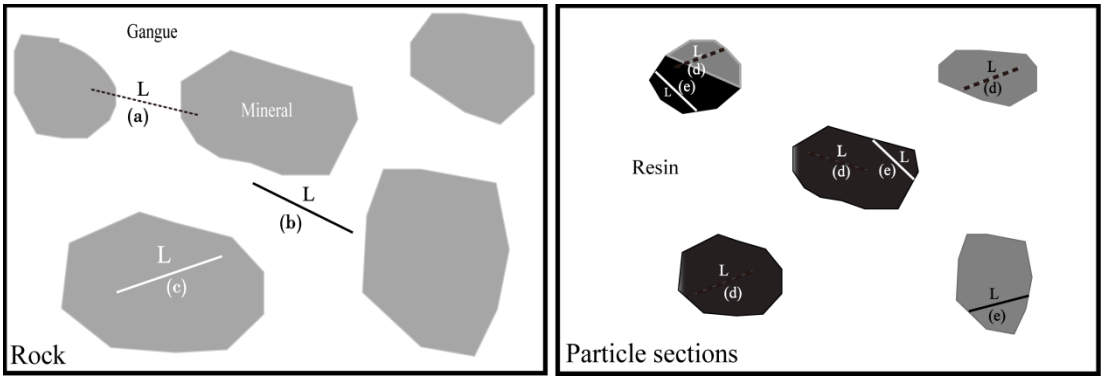

Figure 4-1 Schematic illustration of ore texture and particle structure descriptors (dotted line represents the distance between two end points, solid line represents line segment or linear intercepts)

(a) Two random points at distance L apart to evaluate $\delta^{(ii)}(L)$ on parent rock specimen;

(b) A line segment at length L to evaluate $\omega^{(0)}(L)$ for gangue phase on parent rock specimen;

(c) A line segment at length L to evaluate $\omega^{(1)}(L)$ for valuable mineral phase on parent rock specimen;

(d) Two random points at distance L apart to evaluate $P(L)$ on particle sections;

(e) Linear intercept of length L, $i(L)$ measured from particle sections.

4.3.1 Measurement of two-point probability function, $\delta^{(ii)}(L)$

The two-point probability function could be estimated by randomly placing line segments with certain distance L and then evaluating the probability of two ends falling into one particular phase i (Torquato 2002). The algorithms first required the image to be colour coded and processed so that each phase could be considered one at a time. Then the randomly selected points were placed on the image at given distance L apart and the pixel values read. By repeating the above steps the required probabilities were evaluated. For a given distance L, $\delta^{(ii)}(L)$ is determined by the ratio of number of two points both in phase i to the total number of points.

4.3.2 Measurement of covariance function, $C(L)$

The same procedure was adopted to estimate the covariance function which was also based on two points placed within the image at a distance L apart. After determination of $\delta^{(ii)}(L)$, $C(L)$ was obtained using Eq. 4-13.

4.3.3 Measurement of PSLS function, $\omega^{(i)}(L)$

The PSLS function was estimated by randomly placing line segments of length L on the processed image. The number fraction of these line segments that fall completely within phase i is taken as PSLS for that phase i.

4.3.4 Measurement of phase specific circular disk segment function, $\omega^{(i)}(A)$

The estimation of $\omega^{(i)}(A)$ is similar to that of $\omega^{(i)}(L)$ except for the line segment is replaced by the random circular disks of radius r. The radius r is an integer.

4.3.5 Measurement of proximity function, $P(L)$

$P(L)$ was also measured from the 2D images of particle sections using a procedure similar to that of estimating two-point probability function. Each particle as a whole was considered for this measurement by blanking out only the resin. The difference is that the two-point probability function is measured from the parent rock while the $P(L)$ function is measured from the comminuted particles. Two randomly selected points with a distance L apart were placed on the processed image. By repeating this

step at the given distance L, the proximity function is taken as number fraction of these two points falling completely in one particle.

4.3.6 Measurement of linear intercept length distribution functions, $i(L)$ and $f_i(L)$

Measurement of $f_i(L)$ is carried out by placing random lines (both in position and orientation) across the image using coordinates and orientation angle generated by a random number generator. Particle analysis routines in Labview™ were used to measure the linear intercepts. The number of random lines was changeable by the algorithm. The method of incorporating random lines in the determination of intercept length distribution was introduced in Chapter 3. Figure 4-2 shows a typical procedure of traversing random lines on the image during the measurement. Most of the quantitative measurements on sections reported in the published liberation literature are based on such linear intercept measurements, albeit, using parallel lines.

The measurement of $i(L)$ is similar to that of $f(L)$. Appropriate operations should be taken such as rejecting particles touching image border prior to the measurement.

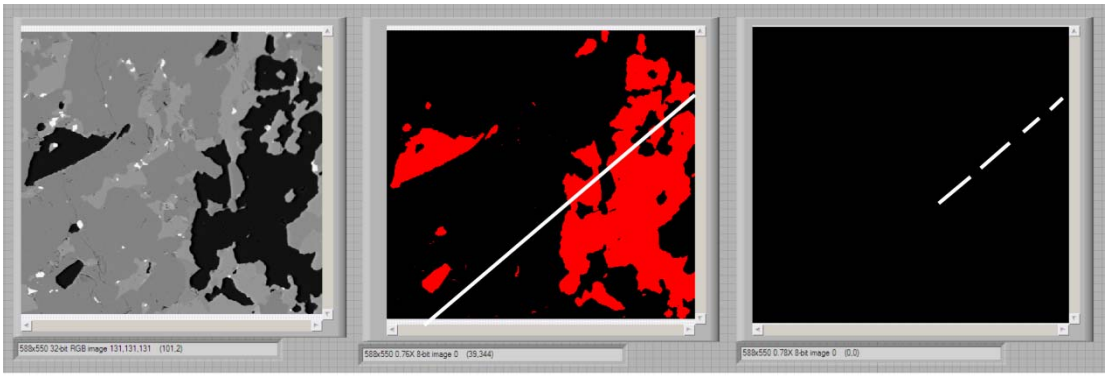

Figure 4-2 Schematic illustration of linear intercept length measurement using Labview™ (one random line)

i) original image of the parent rock (dark is gangue phase and its complement is sulphide minerals)
ii) extracted image of gangue grains
iii) intersection of a random line with gangue grains showing individual intercepts

4.4 Results and discussion

In order to determine the volumetric grade distribution of comminuted particles using Barbery's liberation model (Eq. 2-46), both the covariance function $C(L)$ and the proximity function $P(L)$ must be known. In previous work (Barbery 1991; Barbery and Leroux 1988; Leigh, Lyman, and Gottlieb 1996; King 1994b), these functions were not measured directly. They have described these functions using functional forms derived from assumed structure of ore texture and particles. In this work, the validity of these functions will be tested with the measured data from image analysis.

4.4.1 Covariance function

Because there is direct relationship between the covariance function and two-point probability function (given in Eq. 4-13), only discussion on the covariance function is presented in this section. The experimentally determined values of the covariance function and best fitting results using Eq. 4-17 are shown in Figure 4-3. Based on the measured volumetric mineral grade (p_1) of 0.775, the product of volumetric concentrations of mineral and gangue phases is 0.174, i.e. $p_1 p_0$=0.174. Therefore, the y-intercept of the fitted curve as required by Eq. 4-17 was set at 0.174. Figure 4-3 shows that the observed covariance function generally follows the trend proposed by Stoyan (1979) and Barbery (1991), i.e. negative exponential decay. It also shows that the standard deviations of repeat measurements (error bars) are small, which means the measurement results are very stable.

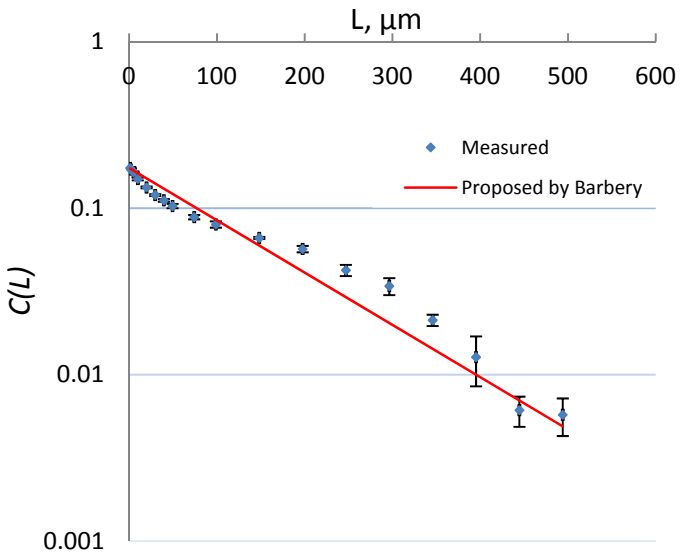

Figure 4-3 Comparison of covariance function measured from image analysis and Eq. 4-17 (proposed by Barbery)

The measured covariance function also fulfils the boundary conditions described previously. Based on the above measurement and using Eq. 4-13, the two-point probability function can be obtained directly by adding the square of volumetric concentration to the covariance function.

It is found that $C(L)$ is well fitted using the sum of two negative exponentials (Eq. 4-27 with R^2=0.9935) for the ore body used in this project.

$$C(L) = 0.131exp\left(-\frac{L}{17.881}\right) + 0.043exp\left(-\frac{L}{201.271}\right) \qquad \text{Eq. 4-27}$$

Comparing Eq. 4-27 with Eq. 4-17 (see also Figure 4-3 and Figure 4-4), it is found that the sum of two negative exponentials gives better fitting results. Therefore, the equation Eq. 4-27 was used in the calculation where covariance function is required in this project.

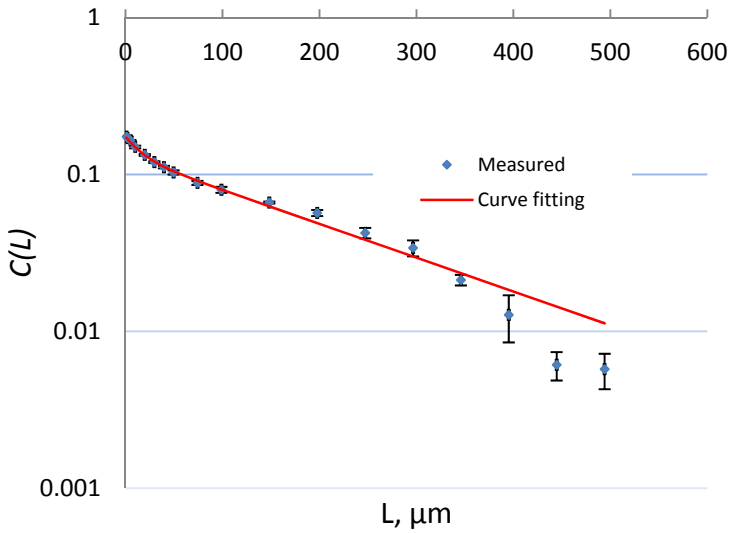

Figure 4-4 Curve fitting of covariance function determined by image analysis

King and co-workers (King 1994c; King and Stirling 1994) proposed a method to determine $C(L)$ through $\delta^{(ii)}(L)$ in terms of linear intercept length distributions of mineral and gangue phases. They showed that, for a binary ore with grade p_i of phase i, the relationship between the two-point probability function and intercept length distributions was given by

$$s\mathcal{L}\left[\frac{\delta^{(ii)}(L)}{p_i}\right] = 1 - \frac{1}{s\mu_i} \times \frac{(1-\mathcal{L}[f_0(L)])(1-\mathcal{L}[f_1(L)])}{1-\mathcal{L}[f_0(L)]\mathcal{L}[f_1(L)]} \qquad \text{Eq. 4-28}$$

The subscript i denotes either phase 1 or phase 0. μ_i is the average intercept length for phase i. $f_1(L)$ and $f_0(L)$ are the linear intercept distributions through mineral and gangue phases, respectively. $\mathcal{L}[*]$ is the Laplace transformation. p_i, $f_1(L)$, $f_0(L)$ and μ_i can be determined by image analysis. However, it requires an analytical form for the linear intercept length distribution functions, i.e. $f_1(L)$ and $f_0(L)$. The error may be introduced during curve fitting to obtain analytical functions of $f_1(L)$ and $f_0(L)$. Consequently, this method is not used in this project.

4.4.2 Linear intercept length distribution

Linear intercept length measurements have been carried out by many researchers to determine its distribution, $i(L)$, even though they have been measured on parallel lines as traversed by computerized microscope stages, and in most cases, equidistant parallel lines have been used. In this work, a set of random lines (both in position and

orientation) have been used to determine the intercept lengths. They were placed on the image using coordinates and orientation angle generated by a random number generator. The results of average intercept length measured from 400 random lines, 400 horizontal lines and 400 vertical lines are compared in Table 4-1. It is shown that the volumetric concentration of mineral phase determined from measurements using horizontal and vertical lines deviate significantly from those determined from chemical assays, implying orientation of lines has a significant effect on the measurements. Comparison of results from the same number of vertical, horizontal and random lines shows that random lines yielded the most accurate results (i.e. calculated p_i is closest to the true value). As such, it may be concluded that the use of random lines are more suitable for the linear intercept length measurements than parallel horizontal or vertical lines, which may offer an economy of measurement.

Intercept length distributions determined from narrowly sized particles are illustrated in Figure 4-5. It shows that the forms of the distributions measured for different size fractions differ, contradicting the assumption of King (1982a, 1984, 1994b, 2001) who assumed that all sizes followed a modified negative exponential distribution. King's empirical functional form (Eq. 2-8) may be true for low grade ores but for high grade ores, such as the ore used in this work, certainly deviates from that assumption. The measured intercept length density distributions of small size fractions, e.g. -53+38μm, seem to follow the negative exponential trend, while for the larger size fractions, for instance, -250+212μm, the density distribution varies considerably from the expected trend. This may imply that the effective grain shape is simplified as the particle size is reduced.

Table 4-1 Comparison of linear intercept length measurement results from random, horizontal and vertical lines

	Average intercept length (pixels)		
	400 random lines	400 horizontal lines	400 vertical lines
mineral	281	319	598
gangue	79	86	84
p_1-linear	0.781	0.787	0.876

Note: p_1 -linear = $\frac{\mu_1}{\mu_1+\mu_0}$ and p_1 is measured by chemical analysis (converted to volumetric concentration using their densities) (p_1=0.775). All the values in pixels are rounded off.

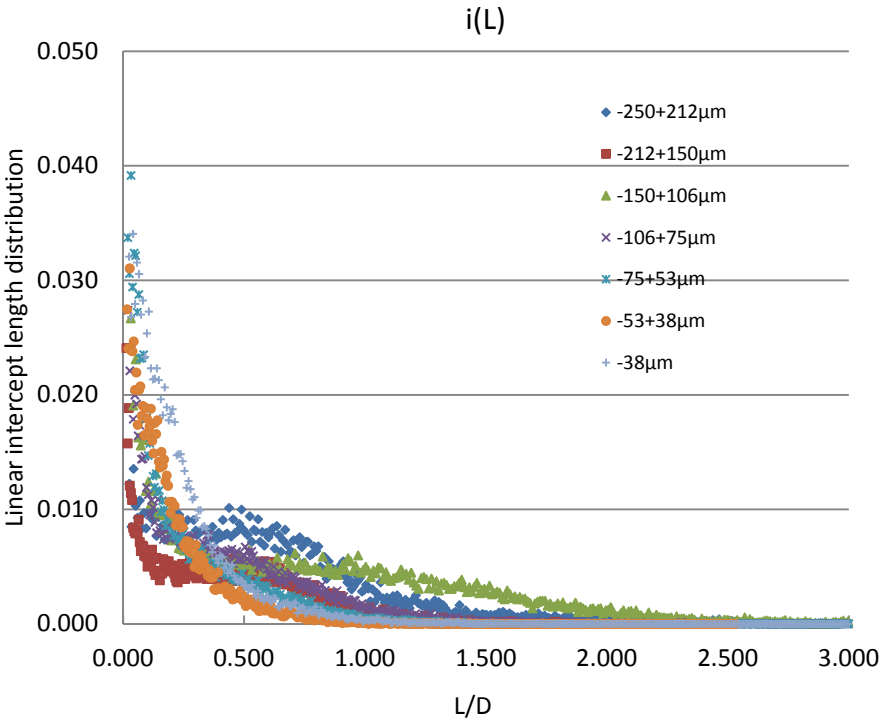

Figure 4-5 Linear intercept length density distribution of particle sections in each narrow size fraction

King (1982a, 1984, 1994b) and Finlayson (1980) have used Eq. 2-8 to describe $i(L)$. As it can be seen from Figure 4-5, the distributions differ considerably from the observed data for different size fractions. It is interesting to note from Figure 4-6 that Eq. 2-8 does not give a good fit with a =1.2 as recommended by King (1982a, 1984, 1994b) and differs greatly from the trends observed. The least square fit of Eq. 2-8 with a =1.07 does not improve the fit either. This has serious implications in deducing the $P(L)$ function from King's $i(L)$ using equation Eq. 4-26.

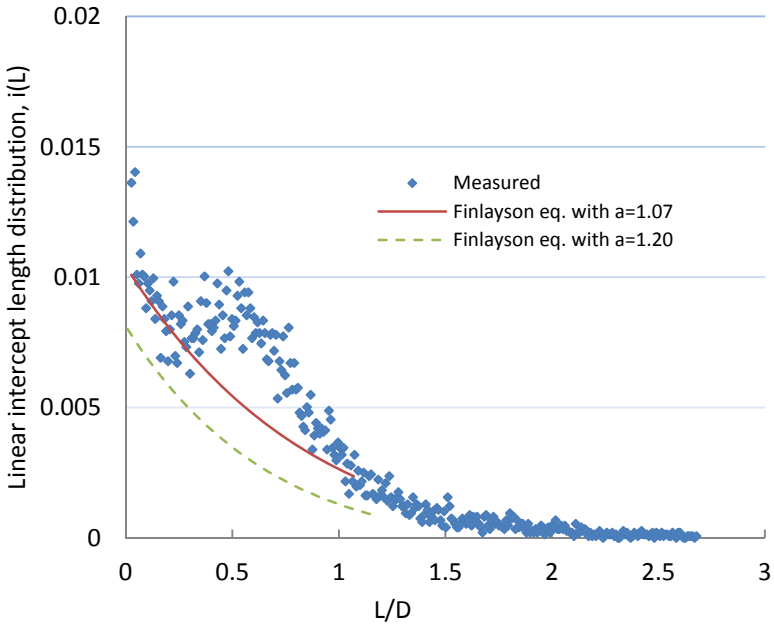

Figure 4-6 Comparison of linear intercept length distribution of the -250+212μm particles determined from image analysis and curve fitting using Eq. 2-8

Figure 4-7 shows the measured mean intercept length versus mean particle sizes D for the various size fractions. The average intercept length for each size fraction is defined as $E(L) = \int_0^\infty L\ i(L)\, dL$. With $i(L)$ given by Eq. 2-8, $E(L) = aD/e$, implying that $E(L)/D = a/e$ is constant. This has been shown as a straight line in Figure 4-7. As can be seen, it deviates considerably from the measured data which implies that Eq. 2-8 does not possess general applicability.

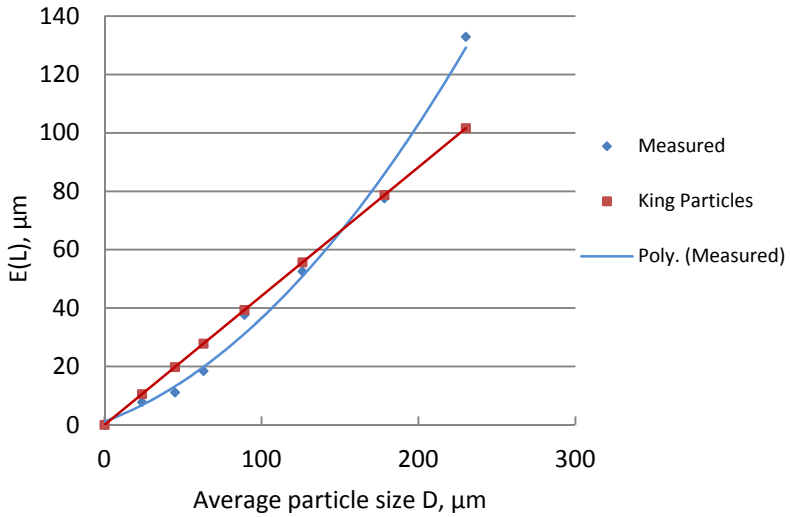

Figure 4-7 Comparison of average intercept lengths for each size fraction i) measured using image analysis and ii) predicted from Finlayson equation density function (Eq. 2-8)

4.4.3 Proximity function

Proximity function has been determined experimentally using the method described above on 2-D SEM images of particle sections for various size fractions and the results are shown in Figure 4-8. Barbery (1991) proposed an analytical function form for $P(L)$ based on the double integration of the Finlayson equation density function $i(L)$ (Eq. 2-8) as in Eq. 2-67. Eq. 2-67 has been used by a few researchers, namely, Barbery (1991) and Leigh *et al.* (1996) to predict liberation. Figure 4-9 shows the measured $P(L)$ function along with Eq. 2-67 with the recommended value of a =1.20 and that with the best fitting value a=1.07 for the -212+150μm particles. It shows that Finlayson equation density function with a=1.07 gives a better fit than that of a=1.20. King (1982a) suggested that for L/D>1.2, $P(L)$=0, implying that the longest intercept length should not be greater than $1.2D$, where D is the average particle size of the size fraction. D is often taken as the geometrical mean of the upper and lower size limits. In practice, the longest intercept length of a particle with size D can be greater than $1.2D$ depending on its shape. Therefore, their equation is not a suitable descriptor for $P(L)$.

Moreover, Eq. 2-67 suggests the distribution of $P(L)$ versus L/D ratio should be a single curve for all the size fractions. This again contradicts the observed data shown in Figure 4-8. As such, the validity and value of Eq. 2-67 is questionable.

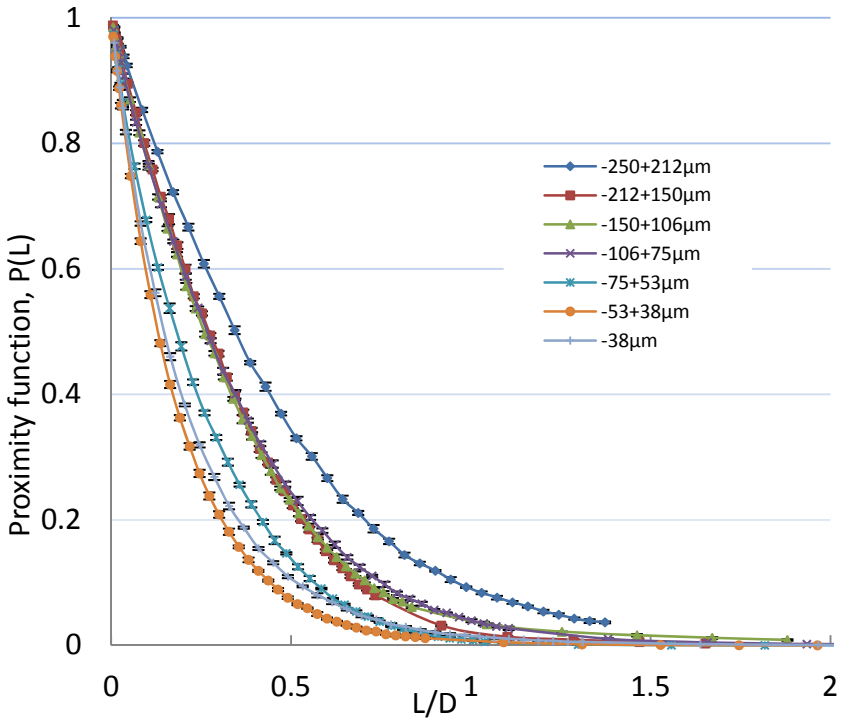

Figure 4-8 Measured proximity functions for various particle size fractions

Alternatively, $P(L)$ may be obtained by numerical integration of the linear intercept distribution $i(L)$ as suggested by Eq. 4-25 or Eq. 4-26. However, numerical integration of Eq. 4-26 is not convenient. To overcome this difficulty, Eq. 4-25 has been modified to yield Eq. 4-29. (See appendix D)

$$P(L) = 1 + \frac{L\int_0^L i(u)du - L - \int_0^L i(u)udu}{E(L)} \qquad \text{Eq. 4-29}$$

Using Eq. 4-29, the calculated proximity function from the measured linear intercept length density distribution is illustrated in Figure 4-10. Figure 4-9 and Figure 4-10 indicate that the direct measurement of $P(L)$ function for size fraction -212+150μm and that calculated by Eq. 4-29 using a numerical integration procedure agree very closely but differs from Eq. 2-67 proposed by Barbery (1991). It must be noted that this procedure did not assume any arbitrarily fitted functional form for $P(L)$ or $i(L)$.

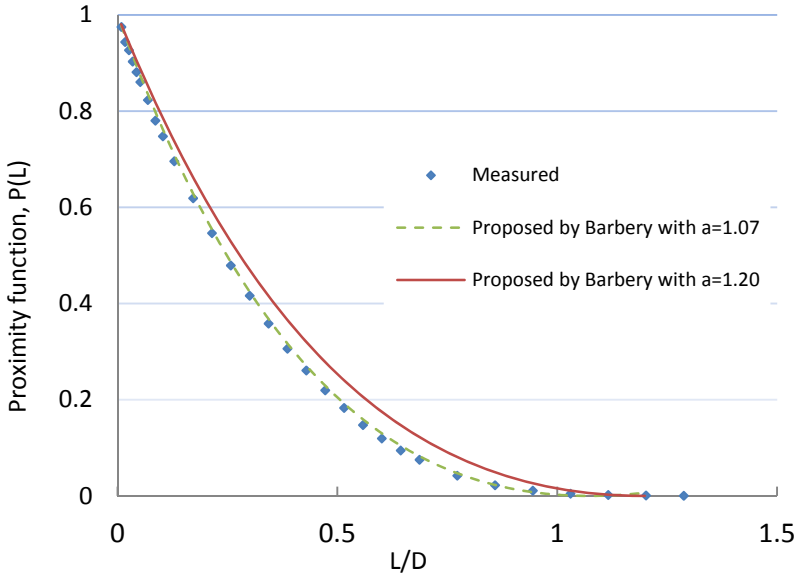

Figure 4-9 Comparison of measured proximity function for -212+150μm particles with published model (Eq. 2-67)

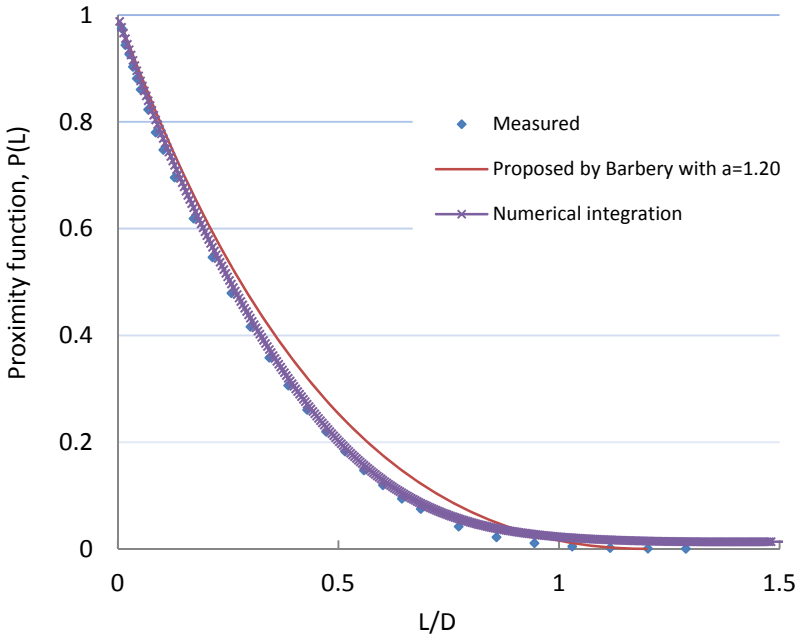

Figure 4-10 Comparison of measured proximity function for -212+150μm particles, proximity function determined by numerical integration from Eq. 4-29 and published model (Eq. 2-67)

Since the proximity function varies with particle size, it is important to investigate the trend of proximity functions as a function of average particle size. This trend may be used to predict proximity functions for other size fractions. In this project, it is

found that the proximity functions are well fitted using a negative exponential form, that is,

$$P(L) = e^{\left(-\frac{L}{AD}\right)} \qquad \text{Eq. 4-30}$$

where constant A is a parameter that defines the shape of the curves as shown in Figure 4-8. From Table 4-2, it is seen that A differs from each narrow size fraction, indicating the failure of using assumption of King Particles to represent the characteristics of the comminuted particle in this project. The calculated A values from Figure 4-8 were plotted against average particle size D and it is shown in Figure 4-11. It follows a polynomial functional form.

Table 4-2 Curve fitting results of proximity functions for various size fractions using negative exponential functions (Eq. 4-30)

Average particle size (μm)	A	R^2
230.22	0.460	0.9958
178.33	0.355	0.9919
126.10	0.347	0.9962
89.16	0.356	0.9972
63.05	0.254	0.9989
44.87	0.189	0.9999

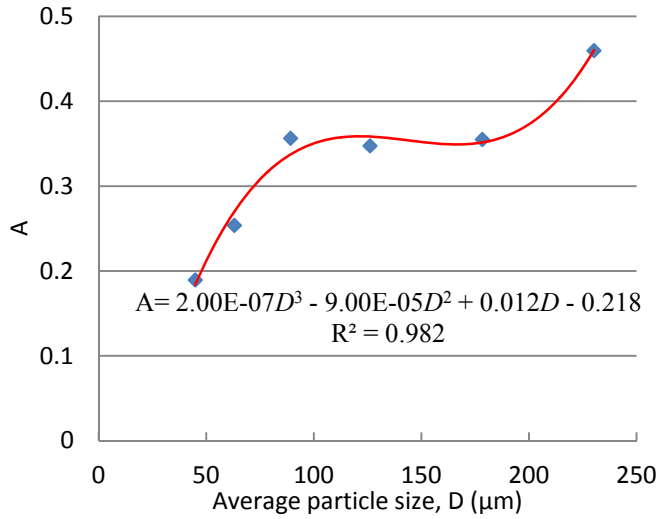

Figure 4-11 Parameter A as a function of average particle size and curve fitting using a polynomial function (cubic) and linear function

4.4.4 Phase specific line segment function

With a similar method to that used for measuring $P(L)$, the PSLS function was also measured for the two phases (0 and 1). The general characteristics of the PSLS function are given here. If the length of the line segment is sufficiently small, i.e. $L \to 0$, the line segment may be considered as a point. In this case, PSLS function is equivalent to the point counting measure of the volumetric concentration of phase i, p_i. Similarly, if the length of a line segment is long enough and no long-range order (it is often the case in real ore texture), the probability of the line segment is wholly included in one grain approaches zero, i.e. Eq. 4-32.

$$\lim_{L\to 0} \omega^{(i)}(L) = p_i \qquad \text{Eq. 4-31}$$

$$\lim_{L\to \infty} \omega^{(i)}(L) = 0 \qquad \text{Eq. 4-32}$$

The measured $\omega^{(i)}(L)$ functions of the mineral and gangue phases are shown in Figure 4-12. For the mineral phase, the function follows a negative exponential decay given by:

$$\omega^{(1)}(L) = 0.775exp\left(-\frac{L}{354.339}\right), \qquad (R^2 = 0.9979) \qquad \text{Eq. 4-33}$$

In contrast, the gangue phase requires a function comprising sum of two negative exponentials, given by:

$$\omega^{(0)}(L) = 0.100exp\left(-\frac{L}{36.229}\right) + 0.125exp\left(-\frac{L}{378.654}\right), (R^2 = 0.9970) \qquad \text{Eq. 4-34}$$

In this project, the ore used is a high grade sulphide ore and the major phase in the ore is the mineral. In practice, the gangue phase will occupy the major phase for most ores. The relationship should then reverse. The PSLS function reflects the size and shape of grains within the phase and may be used to evaluate the extent of fully liberated particles.

Generally, $\omega^{(1)}(L)$ decreases more rapidly with the increase of line segment length L compared to the two-point probability function $\delta^{(11)}(L)$as shown in Figure 4-12. This is because the line segment connected by two points with distance L apart in mineral phase having gangue point(s) in between is excluded in $\omega^{(1)}(L)$.

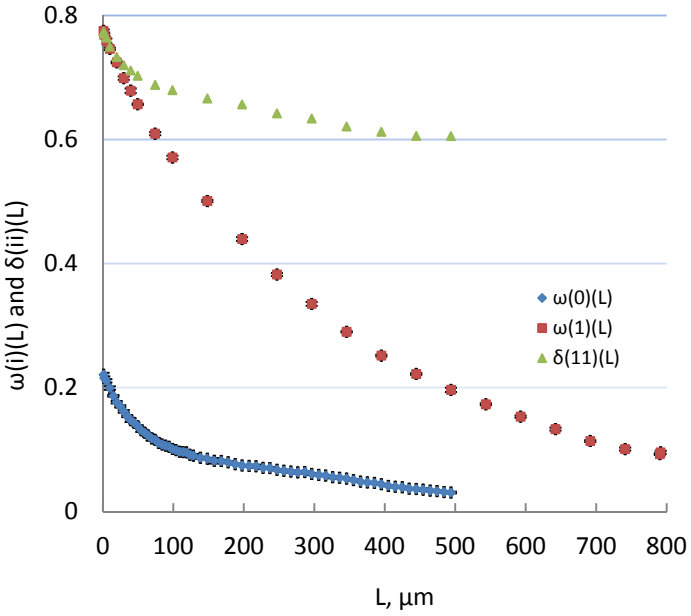

Figure 4-12 PSLS functions of mineral phase ($\omega^{(1)}(L)$) and gangue phase ($\omega^{(0)}(L)$) determined from polished sections of parent rock and comparison with $\delta^{(11)}(L)$

4.4.5 Phase specific circular disk segment function

In this work, random circular disks were used to mask the SEM images taken from polished rock sections. Figure 4-13 shows the measured PSLS function of mineral phase ($g = 1$), $\omega^{(1)}(A)$, and that of gangue phase ($g = 0$), $\omega^{(0)}(A)$, at various disk areas. To avoid large numbers on the x-axis, square root of the disk area, $\sqrt{A}$, was used. $\omega^{(1)}(A)$, is found to be well described using a negative exponential function (Eq. 4-35), whereas $\omega^{(0)}(A)$ is required to be described by a sum of two negative exponential functions (Eq. 4-36).

$$\omega^{(1)}(A) = 0.775exp\left(-\frac{\sqrt{A}}{83.111}\right), (R^2 = 0.9926) \quad \text{Eq. 4-35}$$

$$\omega^{(0)}(A) = 0.118exp\left(-\frac{\sqrt{A}}{164.449}\right) + 0.107exp\left(-\frac{\sqrt{A}}{18.571}\right), (R^2 = 0.9939) \quad \text{Eq. 4-36}$$

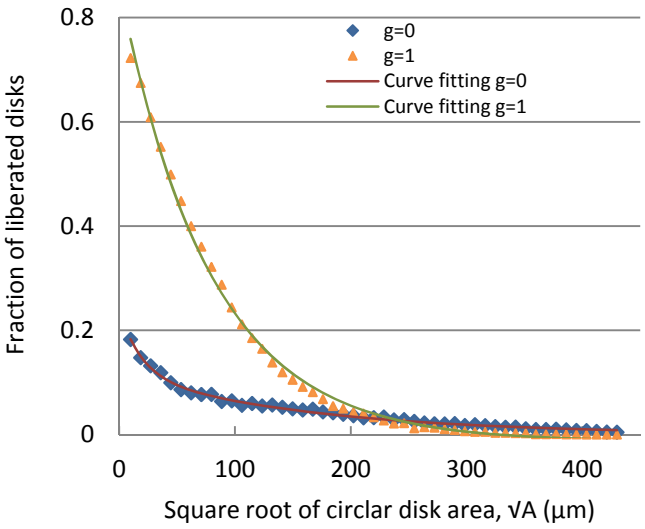

Figure 4-13 Measured phase specific circular disk segment functions of mineral (g=1) and gangue (g=0) phases and curve fitting results

To investigate the influence of shape of the random disks on the measurement results of $\omega^{(i)}(A)$, random square disks were also used. The results are compared with those from random circular disks and shown in Figure 4-14. It is found that the shape of disk (circular and square) does not significantly affect the measured results of the number fractions of fully liberated mineral and gangue disk segments. Therefore, it may be reasonable to use $\omega^{(i)}(A)$ evaluated by using random circular disks to quantify the probability that a section of area A is fully included in one phase in liberation prediction, which will be used in Chapter 5.

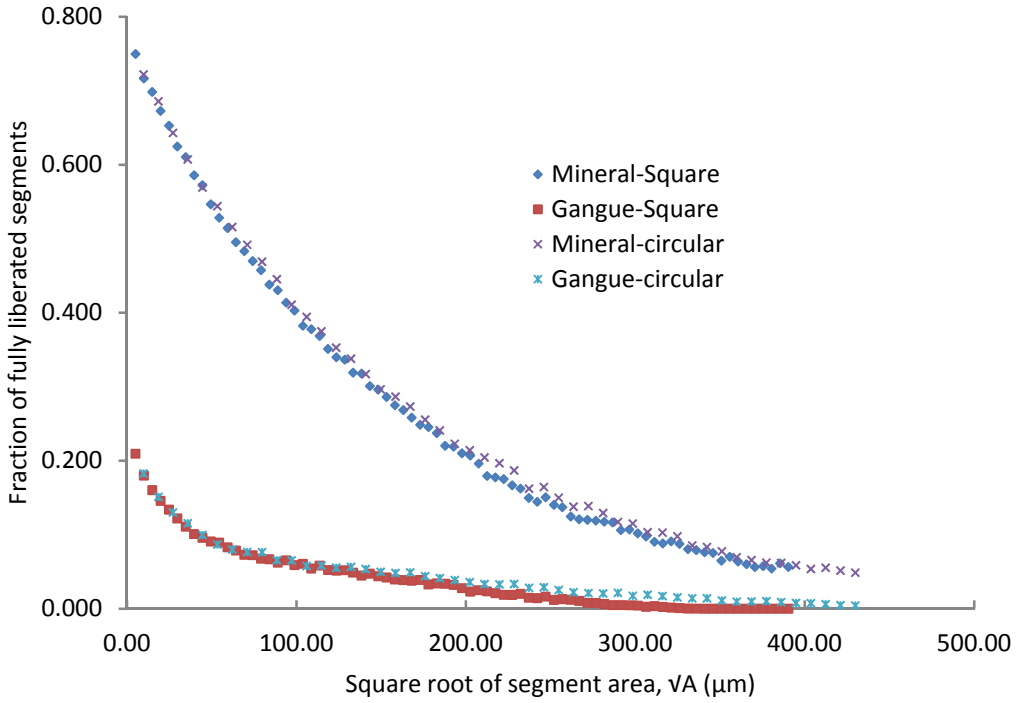

Figure 4-14 Comparison of number fractions of fully liberated mineral and gangue segments determined by random circular and square disks

4.4.6 Re-examination of some published relationships

Image analysis technique based on Labview™ software allows the quantification of ore texture and particle structure using random lines traversed on polished sections of rock and mounted particles. In the published literature, there are theoretical relationships to evaluate the mean intercept length, mean section area and mean volume of particles in terms of linear intercept length distribution and proximity function. These relationships (under the assumption of particle convexity) were derived and used by researchers (Crofton 1869; Gilbert 1962) and shown in Barbery's book (Barbery 1991). Eq. 4-37, Eq. 4-38 and Eq. 4-39 are often called Gilbert equations (Gilbert 1962). Eq. 2-53 and Eq. 2-61 are referred to as Crofton theorems (Crofton 1869). These equations connect the information from 1-D (linear intercept length), 2-D (section area) and 3-D (particle volume) measurements.

$$2\int_0^{\infty} P(L)dL = \frac{E(L^2)}{E(L)} \qquad \text{Eq. 4-37}$$

$$2\pi \int_0^{\infty} LP(L)dL = \frac{E(A^2)}{E(A)} \qquad \text{Eq. 4-38}$$

$$4\pi \int_0^{\infty} L^2P(L)dL = \frac{E(V_p{}^2)}{E(V_p)} \qquad \text{Eq. 4-39}$$

The average volume weighted by volume, denoted by $M(V_p)$, is close to that weighted by number, denoted by $E(V_p)$, given the particles are in the same narrow size interval. That is,

$$M(V_p) = \frac{E(V_p{}^2)}{E(V_p)} \approx \frac{[E(V_p)]^2}{E(V_p)} = E(V_p) \qquad \text{Eq. 4-40}$$

For the linear intercepts and section areas measured from the particle sections in the same narrow size interval, the average linear intercept length weighted by length, $\frac{E(L^2)}{E(L)}$, and average section area weighted by area, $\frac{E(A^2)}{E(A)}$, are larger than their counterparts weighted by number ($E(L)$ and $E(A)$), respectively, as shown in Figure 4-15 and Figure 4-16. It is found that the variation between $\frac{E(L^2)}{E(L)}$ and $E(L)$ increases with average particle size. Similar trend is also found between $\frac{E(A^2)}{E(A)}$ and $E(A)$. It is also found that $\frac{E(L^2)}{E(L)}$ versus $E(L)$ and $\frac{E(A^2)}{E(A)}$ versus $E(A)$ follow linear relationship within the range of average particle size used in this work. Note that, if all the particles within a size interval have the same size and shape, $\frac{E(A^2)}{E(A)}$ and $\frac{E(L^2)}{E(L)}$ from these particles are equivalent to $E(A)$ and $E(L)$, respectively.

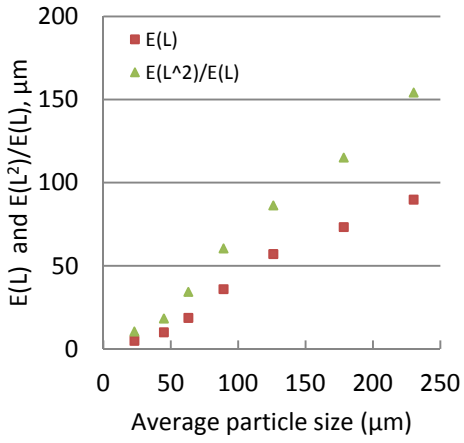

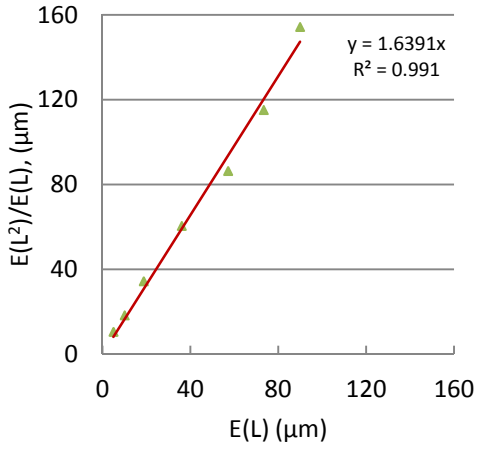

Figure 4-15 Comparison of average intercept length weighted by number ($E(L)$) and by length ($E(L^2)/E(L)$) at various size fractions

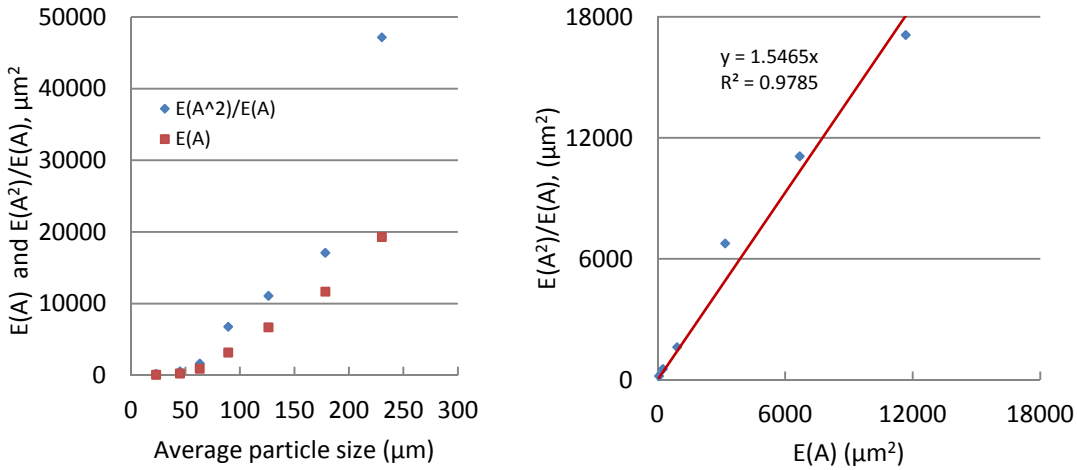

Figure 4-16 Comparison of average section area weighted by area ($E(A^2)/E(A)$) and by number ($E(A)$) at various size fractions

The left hand side of equations (Eq. 4-37, Eq. 4-38 and Eq. 4-39) can be determined from the measured $P(L)$ using numerical methods, while their right hand sides (except for Eq. 4-39) can be estimated from image analysis by linear and area measurements. The validity of Eq. 2-53 and Eq. 2-61 can also be tested using measured linear intercept length distribution. The results calculated are based on micron and shown in Table 4-3, where the units are omitted.

Table 4-3 Testing the validity of Crofton theorems and Gilbert equations using measured intercept length distribution and proximity function

Particle size	I	II	III	IV	V	VI	VII
	LHS of Eq. 4-37	RHS of Eq. 4-37	LHS of Eq. 4-38	RHS of Eq. 4-38	Eq. 2-61	LHS of Eq. 4-39	Eq. 2-53
	$2\int_0^\infty P(L)dL$	$\frac{E(L^2)}{E(L)}$	$2\pi\int_0^\infty LP(L)dL$	$\frac{E(A^2)}{E(A)}$	$\frac{\pi}{3}\frac{E(L^3)}{E(L)}$	$4\pi\int_0^\infty L^2P(L)dL$	$\frac{\pi}{3}\frac{E(L^4)}{E(L)}$
-250+212μm	155.7	154.3	47837.4	47171.6	43323. 6	15861157.0	13076143.6
-212+150μm	120.6	115.2	16344.2	17098.7	16526.1	2505349.4	2546026.5
-150+106μm	85.3	86.4	8923.5	11087.7	9736.5	1070649.5	1256073.4
-106+75μm	60.3	60.5	5131.4	6765.5	4859.6	500458.1	444407.2
-75+53μm	42.6	34.4	1467.1	1624.5	1622.9	74185.4	87862.2
-53+38μm	30.4	18.3	529.0	539.3	487.9	19445.1	15740.0
-38μm	14.4	10.5	173.2	193.87	178.8	3838.8	3904.2

It can be seen that the results calculated from proximity function (columns I and III) are in agreement with those from linear and areal measurements (columns II and IV). Good agreement is also observed from data in the calculated average section areas weighted by area, $M(A)$, using Gilbert equations (Eq. 4-38) (column III) and Crofton theorems (Eq. 2-61) (column V) compared to those from areal measurement (column IV). In addition, the average particle volume weighted by volume, $M(V_p)$, calculated from Gilbert equations (Eq. 4-39) (column VI) and Crofton theorems (Eq. 2-53) (column VII) are very close for each narrow size interval. This suggests both methods can be used to estimate $M(A)$ and $M(V_p)$. Barbery (1991) argued that calculated $M(A)$ and $M(V_p)$ from linear intercept length distribution could be possibly affected by the existence of a small number of very long intercepts.

The calculated $M(V_p)$ values using Gilbert equations (Eq. 4-39) and Crofton theorems (Eq. 2-53) are further compared with the volume of spheres having the geometric mean particle size as diameter. The results are shown in Figure 4-17. It is found that there is a linear relationship between the calculated $M(V_p)$ values using Gilbert equations and Crofton theorems and that of spheres having the mean particle size as their diameter. Because particle volume in (μm^3) is large in number, Figure

4-17 is shown in the logarithmic scale. Therefore, the linear relationship between the calculated $M(V_p)$ values using Gilbert equations and Crofton theorems and the volume of spheres is also in the logarithmic scale.

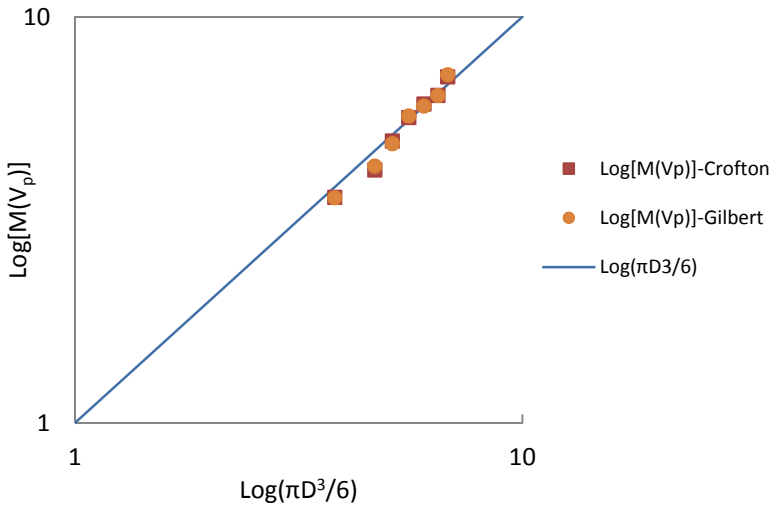

Figure 4-17 Comparison of $M(V_p)$ calculated using Crofton theorems (Eq. 2-53) and Gilbert equations (Eq. 4-39) and volume of spheres having the mean particle size as diameter

4.5 General comments

Labview™ Machine Vision software has been used in the past for the analysis of froth flotation such as (Kaartinen 2009). While Young (2002) and Subasinghe (2008) have used Labview™ software to measure mineral intercept length distributions, there is limited information published on the application of this software in liberation-related analysis. The methods used by Young (2002) and Subasinghe (2008) have been extended in this work to include the measurement of other texture descriptors given above. Versatile algorithms have been developed for this purpose. Most mineral processing engineers are familiar with using MLA or QEM*SEM images and the methods used in this work will enable the extraction of further information from those images. It is expected these methods will be available for mineral processing engineers for routine use to quantify liberation in the future.

4.6 Conclusions

In this chapter, it has been shown that the necessary descriptors of parent rock and comminuted particles for predicting liberation characteristics of an ore can be extracted using the proposed image analysis techniques based on Labview™. In particular, the new texture descriptors such as phase specific circular disk function and PSLS function have been introduced and measured. It is also shown that the empirical equations proposed by King for linear intercept distribution, $i(L)$, are not suitable for the high grade ore used in this work. The proximity function used in Barbery's liberation models can be conveniently obtained by numerical integration of the measured linear intercept length distribution without any assumption on the texture of the ore.

Based on the measured proximity function and linear intercept length distribution, the validity of Gilbert equations and Crofton theorems were tested. It is found that both Gilbert equations and Crofton theorems are valid and may be used to estimate $M(A)$ and $M(V_p)$. It is also found that the average section area weighted by area from each narrow size interval has a linear relationship with the average section area weighted by number. Similar linear relationship is also observed between the average intercept length weighted by length and the intercept length weighted by number from each narrow size interval.

This Labview™-based image analysis technique could be used by mineral processing engineers to extract more useful information of ore texture and particle structure by applying it to images obtained by other techniques such as MLA and QEM*SEM.

Chapter 5 Predicting mineral liberation characteristics of comminuted particles

For most mineral processing operations, prediction of volumetric grade distribution of particles is of significant importance for the determination of down-stream separation processes. On comminution of the parent rock, the resulting volumetric grade distribution of the comminuted particles follows a typical pattern shown in Figure 2-1. Existing liberation models are aimed at describing the above distribution by quantifying the fractions of fully liberated mineral and gangue particles ($\Lambda_1$and Λ_0), and composition of composite particles, $g^c(m)$. Where $g^c(m)$ is the fraction of particles having a mineral grade less than or equal to m. Davy (1984) showed that the composition of composite particles could be quantified by $\frac{E(Z_0Z_1)}{E(Z^2)}$, where Z_1 and Z_0 represent the mineral and gangue contents of a particle, respectively, and $Z = Z_1 + Z_0$. The grade of the particles may be evaluated based on either volumetric, areal or linear measurements. These would defer due to the stereological effect arising from the differences in the nature of samples used for the measurement. i.e. linear and areal measurements are made on polished sections and volumetric grades are determined from particles.

Assuming that the comminuted particles were generated by random breakage and possess convex shapes, Barbery (1991) proposed that the quantity $\frac{E(Z_0Z_1)}{E(Z^2)}$ is related to the first (n_1) and second (n_2) moment of $g(m)$ by

$$n_1 - n_2 = \frac{E(Z_0Z_1)}{E(Z^2)} \qquad \text{Eq. 5-1}$$

Davy (1984) showed that the above quantity $\frac{E(Z_0Z_1)}{E(Z^2)}$, may be evaluated through the covariance function $C(L)$ and proximity function $P(L)$ as defined in Chapter 2. Thus, based on volume,

$$n_1 - n_2 = \frac{E(V_0V_1)}{E(V_p{}^2)} = \frac{\int_0^\infty L^2P(L)[p_0p_1 - C(L)]dL}{\int_0^\infty L^2P(L)dL} \qquad \text{Eq. 5-2}$$

based on section area,

$$n_1 - n_2 = \frac{E(A_0A_1)}{E(A^2)} = \frac{\int_0^\infty LP(L)[p_0p_1 - C(L)]dL}{\int_0^\infty LP(L)dL} \qquad \text{Eq. 5-3}$$

based on linear intercept length,

$$n_1 - n_2 = \frac{E(L_0 L_1)}{E(L^2)} = \frac{\int_0^\infty P(L)[p_0 p_1 - C(L)]dL}{\int_0^\infty P(L)dL} \quad \text{Eq. 5-4}$$

The last two equations were suggested by Leigh et al. (1996). The resulting grade distribution of composite particles $g^c(m)$, was also described empirically using a Beta distribution with parameters α and β.

$$g^c(m) = \frac{m^{(\alpha-1)}(1-m)^{(\beta-1)}}{B(\alpha,\beta)} \quad \text{Eq. 5-5}$$

Together with the fractions of fully liberated mineral (Λ_1) and gangue (Λ_0) particles, this formed a convenient basis for evaluating the grade distribution of comminuted particles in terms of the four parameters α, β, $\Lambda_1$and Λ_0.

5.1 Drawbacks of Barbery's liberation model

The main drawbacks of Barbery's liberation model are:

1. Barbery (1991) used a covariance function $C(L)$ (see section 2.1.3.2) to evaluate the distribution of mineral and gangue grains within the parent rock (ore texture). He proposed an analytical functional form for $C(L)$ assuming that the ore texture follows Poisson polyhedral texture. This $C(L)$ function was given by Eq. 2-76.Where λ_1 is a measure of the fineness of ore texture. While this assumption was adequate for low grade ores; it may not have general validity for the real ores.
2. The proximity function $P(L)$, which characterizes the size and shape of comminuted particles, was assumed to follow a relationship derived from their intercept length distribution (Eq. 2-8) proposed by King (1982a, 1984). Based on this intercept length distribution $i(L)$and Eq. 4-26, Barbery (1991) proposed $P(L)$ was given by Eq. 2-67.

   However, in Chapter 4, it has been shown this analytical function is not of general applicability and deviates considerably from measurements on particle sections.
3. In order to evaluated the fractions of liberated mineral and gangue particles ($\Lambda_1$and Λ_0), Barbery (1991) proposed equations (Eq. 2-82, Eq. 2-85 and Eq. 2-86) based on the above ore texture and particle structure assumptions as described in section 0.

Even though the analytical functions proposed by Barbery (1991) provide a convenient way of estimating the liberation model parameters, they do not comply with those determined from measurements on sections. Therefore, this liberation model does not show general applicability for real ores.

5.2 Quantification of ore texture and particle structure from measurements

One of the major improvements of liberation modelling in this project is that the assumption of ore texture and particle structure was eliminated by obtaining $P(L)$ and $C(L)$ from measurement using image analysis.

5.2.1 Ore texture

The covariance function $C(L)$ which was used by Barbery (1991) to quantify ore texture was measured on the polished sections of parent rock for the high grade ore as described in section 4.3.2. It has been compared with that determined by Barbery's method in Figure 4-3. As can be seen Figure 4-3, the measured distribution deviates considerably from that determined by Barbery's method. The measured distribution may be described by an empirical function:

$$C(L) = 0.131e^{-\frac{L}{17.881}} + 0.043e^{-\frac{L}{201.271}}$$

5.2.2 Particle structure

The proximity function, $P(L)$, which has been used to characterize particle structure was also evaluated by measurement on mounted particle sections using image analysis. As described in section 4.4.3, it was obtained by numerical integration of $i(L)$. The measured $P(L)$ deviates considerably from the one proposed by Barbery (1991) as shown in Figure 4-10. In addition, it can be observed that the proximity function is not unique for each size fraction, which is contradictory to that implied by Barbery's (1991). The measured $P(L)$ functions follow a relationship of the form as given in Eq. 5-6,

$$P(L) = e^{\left(-\frac{L}{AD}\right)} \qquad \text{Eq. 5-6}$$

where constant A varies with the average particle size D according to

$$A = 2.0 \times 10^{-7}D^3 - 9.0 \times 10^{-5}D^2 + 0.012D - 0.218. \qquad \text{Eq. 5-7}$$

5.3 Evaluation of model parameters

5.3.1 The extent of fully liberated mineral and gangue particles

The fractions of fully liberated particles produced by comminution comprising of phase i only are denoted by $\Lambda_i^{(d)}(D)$ (d=1, 2, 3) in 1, 2, 3 dimensions. As described above, Barbery evaluated these in terms of $Q_{pp}(V_p)$, $Q_{pp}(A)$ and $Q_{pp}(L)$ based in an assumed texture of the ore. In this work, an alternative approach is proposed in terms of phase specific line segment function $\omega^{(i)}(L)$ that can be evaluated from measurements on parent rock polished sections. For a particle to be formed that comprises only of a given phase i, the material in the parent rock should be contiguous in that phase i. On a polished section, this would translate to a continuous line segment. Thus, the fraction of fully liberated particles that could be produced by random fracture will be related to the probability of a line segment of length L is fully included in phase i in the parent rock. This probability has been defined as the phase specific line segment function (PSLS) denoted by $\omega^{(i)}(L)$.

Consider a comminuted particle containing mineral phase (volume, V_1) and gangue phase (volume, V_0), the total volume of this particle is denoted by V_p, where $V_p = V_0 + V_1$. As discussed in Chapter 2, Davy (1984) showed that the average volume of composite particles is given by Eq. 2-44. It has been shown from Eq. 4-13 and Eq. 4-14 that $p_1 p_0 - C(L) = \delta^{(10)}(L)$. Substituting this relationship into Eq. 2-44 yields,

$$\frac{E(V_0 V_1)}{E(V_p)} = 4\pi \int_0^\infty L^2 P(L)\, \delta^{(10)}(L) dL \qquad \text{Eq. 5-8}$$

where $\delta^{(10)}(L)$ is the probability that two random points of distance L having one point in mineral phase 1 and the other point in gangue phase 0. To evaluate the fraction of fully liberated mineral particles, the function $\delta^{(10)}(L)$ should be replaced by $\omega^{(1)}(L)$.

Average volume of liberated mineral phase in particles is given by: $4\pi \int_0^\infty L^2 P(L) \omega^{(1)}(L)\, dL$.

Average volume of mineral phase in particles is given by: $p_1 4\pi \int_0^\infty L^2 P(L) dL$.

Thus, the fraction of fully liberated mineral particles, $\Lambda_1^{(3)}(D)$, is given by:

$$\Lambda_1^{(3)}(D) = \frac{\int_0^\infty L^2 P(L)\omega^{(1)}(L)\, dL}{\int_0^\infty L^2 P(L) dL} \quad \text{Eq. 5-9}$$

Similarly, fraction of fully liberated gangue particles is given by

$$\Lambda_0^{(3)}(D) = \frac{\int_0^\infty L^2 P(L)\omega^{(0)}(L)\, dL}{\int_0^\infty L^2 P(L) dL} \quad \text{Eq. 5-10}$$

Similarly, the fractions of fully liberated mineral and gangue particles estimated from section area distribution and linear intercept length distribution are given by the following equations (Eq. 5-11, Eq. 5-12, Eq. 5-13 and Eq. 5-14). These functions retain the same functional form of Barbery's equations (Eq. 2-85 and Eq. 2-86). However, they have advantages over Barbery's equations by: i) without ore texture and particle structure assumption; ii) all the variables are estimated on polished sections of parent rock and particles using image analysis; iii) they can be used in real ores.

For areal (2-D):

$$\Lambda_1^{(2)}(D) = \frac{\int_0^\infty A\, g(A)\, \omega^{(1)}(A) dA}{\int_0^\infty A\, g(A) dA} \quad \text{Eq. 5-11}$$

$$\Lambda_0^{(2)}(D) = \frac{\int_0^\infty A\, g(A)\, \omega^{(0)}(A) dA}{\int_0^\infty A\, g(A) dA} \quad \text{Eq. 5-12}$$

For linear (1-D):

$$\Lambda_1^{(1)}(D) = \frac{\int_0^\infty L\, i(L)\, \omega^{(1)}(L) dL}{\int_0^\infty L\, i(L) dL} \quad \text{Eq. 5-13}$$

$$\Lambda_0^{(1)}(D) = \frac{\int_0^\infty L\, i(L)\, \omega^{(0)}(L) dL}{\int_0^\infty L\, i(L) dL} \quad \text{Eq. 5-14}$$

Note that the fraction of fully liberated particles from phase i is related to the degree of liberation $\mathcal{L}_i(D)$ by

$$\Lambda_i(D) = p_i \times \mathcal{L}_i(D) \quad \text{Eq. 5-15}$$

It is found that PSLS functions for mineral phase and gangue phase determined using image analysis on parent rock polished section can be fitted by the following two equations (i.e. Eq. 4-33 and Eq. 4-34).

$$\omega^{(1)}(L) = 0.775exp\left(-\frac{L}{354.339}\right)$$

$$\omega^{(0)}(L) = 0.100exp\left(-\frac{L}{36.229}\right) + 0.125exp\left(-\frac{L}{378.654}\right)$$

Similarly, phase specific circular disk segment functions of mineral phase and gangue phase are given in the following two equations:

$$\omega^{(1)}(A) = 0.775exp\left(-\frac{\sqrt{A}}{83.111}\right)$$

$$\omega^{(0)}(A) = 0.118exp\left(-\frac{\sqrt{A}}{164.449}\right) + 0.107exp\left(-\frac{\sqrt{A}}{18.571}\right)$$

As the data from image analysis were limited to those obtained from polished sections of the parent rock and particles due to practical limitations, only the linear and areal data have been used for comparison. The measured Λ_i values for linear and areal measurements and those calculated from proposed equations are compared in Figure 5-1 and Figure 5-2. While it can be seen that the measured Λ_i is generally close to the calculated values, indicating the validity of proposed model to estimate Λ_i. It is also found that the deviation between measured and calculated Λ_i values in 2-D is much larger compared to that in 1-D.

In determining the $\omega^{(i)}(A)$ function, a circular mask was placed on the images of parent rock, while for the estimation of $\omega^{(i)}(L)$, a line segment was used as a mask. Because the area covered by the circular mask was much larger than the linear mask, the number of fully liberated sections observed was much lower than that from linear measurement. It appears that the size of 2-D masks has a great influence on this measurement. Using a larger 2-D mask reduces the number of fully liberated sections significantly. This might explain the reason that Λ_1 values in 2-D are mostly underestimated. In the absence of additional data to evaluate the influence of the size and shape of masks on the estimation of $\omega^{(i)}(A)$ function, it is suggested that the Λ_i values calculated from $\omega^{(i)}(L)$ in 1-D is more reliable than those calculated from $\omega^{(i)}(A)$ estimated by using random circular disks in 2-D. In this context, the comparison of liberation prediction in 2-D is omitted in this work.

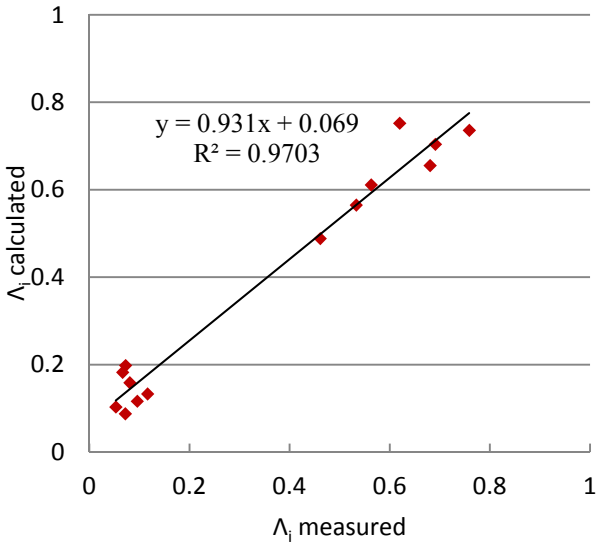

Figure 5-1 Comparison of Λ_i determined from linear grade measurement using image analysis and proposed equations (Eq. 5-13 and Eq. 5-14)

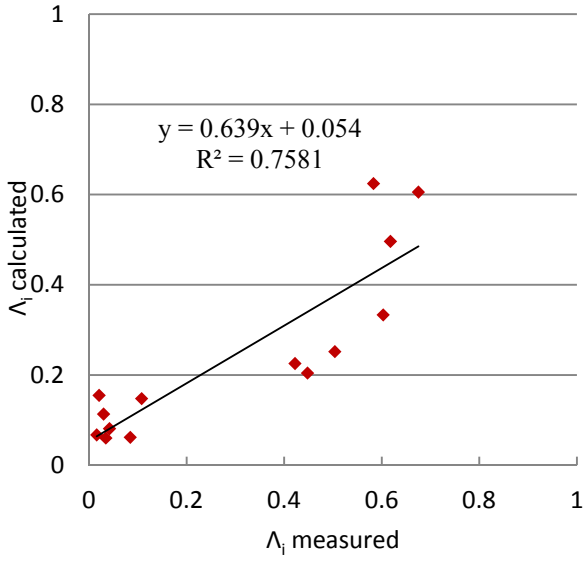

Figure 5-2 Comparison of Λ_i determined from areal grade measurement using image analysis and proposed equations (Eq. 5-11 and Eq. 5-12)

5.3.2 Grade distribution of composite particles

As it has been stated previously, the grade distribution of composite particles may be described by a Beta distribution with parameters α and β (Eq. 5-5). The parameters may be evaluated from the first (n_1) and second (n_2) moments of grade distribution. By using the measured $P(L)$ and $C(L)$ functions, n_1 and n_2 moments of grade

distributions were evaluated using Eq. 5-2, Eq. 5-3 and Eq. 5-4 for volumetric grade, areal grade and linear grade, respectively. The first (${n_1}^M$) and second (${n_2}^M$) moments of grade distribution of composite particles were evaluated by the following relationships:

$${n_1}^M = \frac{n_1 - \Lambda_1}{1 - \Lambda_0 - \Lambda_1} \qquad \text{Eq. 5-16}$$

$${n_2}^M = \frac{n_2 - \Lambda_1}{1 - \Lambda_0 - \Lambda_1} \qquad \text{Eq. 5-17}$$

The best fitting values of α and β, were estimated using the properties of Beta distribution from the following two equations.

$${n_1}^M = \frac{\alpha}{\alpha + \beta} \qquad \text{Eq. 5-18}$$

$${n_2}^M = \frac{\alpha + 1}{\alpha + \beta + 1} \times \frac{\alpha}{\alpha + \beta} \qquad \text{Eq. 5-19}$$

The calculated first and second moments of linear grade distribution of composite particles using proposed liberation model are compared with those from measurement, where the results are shown in Figure 5-3. As can be seen that the ${n_1}^M$ values calculated from proposed 1-D model are in good agreement with those determined from linear grade measurement on particle sections. However, there is a bias between the measured and calculated second moments. This bias between calculated moments and those determined from measurement may be due to deviations in the estimation of $\Lambda_1$and $\Lambda_0$values, experimental error and non-random breakage. As can be seen from Figure 5-3, the calculated ${n_2}^M$ values are linearly related to ${n_2}^M$ measured values.

This implies that the amount of particles that have grades higher and lower than the mean grades are equal but their contribution to the second moment by the higher grade particles outweigh that due to lower grade particles.

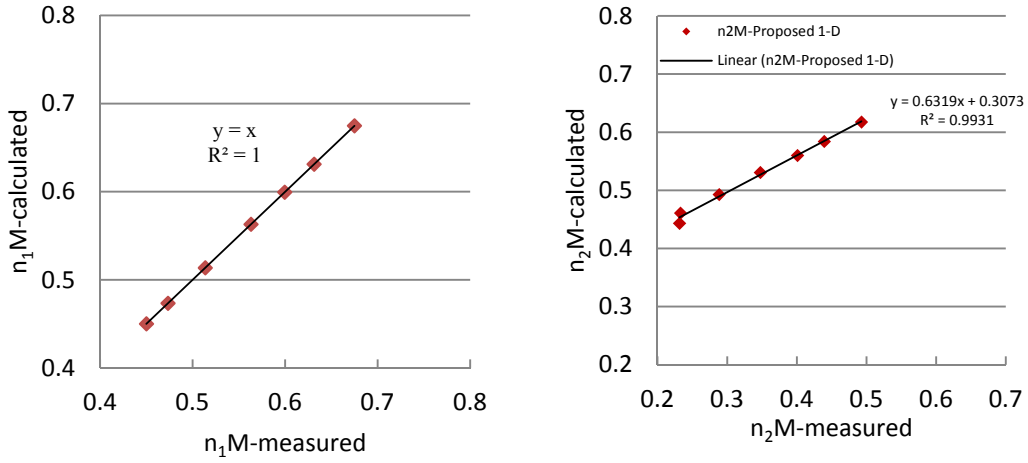

Figure 5-3 Comparison of n_1^M and n_2^M determined from linear grade measurement and calculated from proposed 1-D liberation model for different size fractions

As has been shown in the above section, Λ_i values estimated from the proposed 2-D model deviate considerably from those determined by areal grade measurements. The ${n_1}^M$ and ${n_2}^M$ values determined from Λ_i values estimated from the proposed 2-D model are more prone to error.

5.3.3 Comparison of model parameters determined by measurement

The Λ_i values determined by linear and areal grade measurements are compared in Figure 5-4 for all the size fractions. It was found that a strong linear relationship between Λ_i determined in 1-D and 2-D. The linear relationship demonstrates the stereological bias of grade distribution measurement between linear and areal. The grade distributions determined by linear/areal grade measurements are also fitted using incomplete Beta distribution with four parameters (Λ_0, Λ_1 , α and β) similar to that used by Barbery (1991). The evaluated α and β values are shown in Figure 5-5 for the linear and areal grade measurements on particle sections with various grinding size. It is seen that α and β values for the linear and areal grade distributions follow the similar trend. In addition, deviation between α values of the same size fraction in 2-D and 1-D measurement is slightly larger compared to that of β values. This deviation is owing to the stereological bias between linear (1-D) and areal (2-D) measurements.

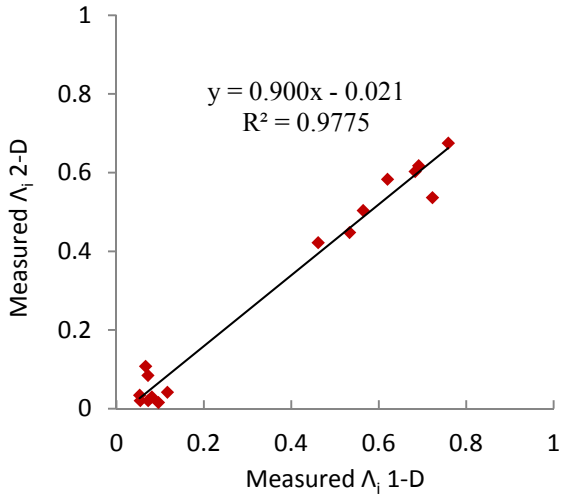

Figure 5-4 Comparison of parameter Λ_i determined from linear and areal grade measurements for all size fractions

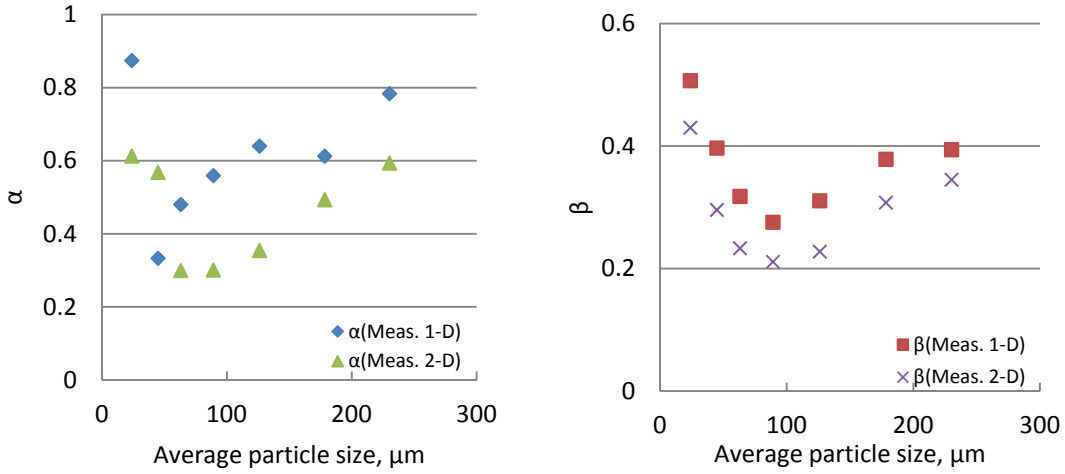

(a) (b)

Figure 5-5 Comparison of α (a) and β (b) determined from linear and areal grade measurements for all size fractions

5.4 Development of improved predictive liberation models in 1-D, 2-D and 3-D

5.4.1 Proposed 3-D model

The main objective of a predictive liberation model is to quantify the volumetric grade distribution of comminuted particles at various grinding sizes. This could be achieved by evaluating the variation of the four parameters (Λ_0, Λ_1 , α and β) of the

model described above with grinding size. The fractions of fully liberated components (Λ_1 and Λ_0) were measured directly through areal and linear measurement. However, in the absence of measured Λ_1 and Λ_0 for 3-D, they are calculated by Eq. 5-9 and Eq. 5-10 based on measured $P(L)$ and $\omega^{(i)}(L)$ functions. Similarly, the parameters of the beta distribution (α and β) were evaluated according to Eq. 5-18 and Eq. 5-19.

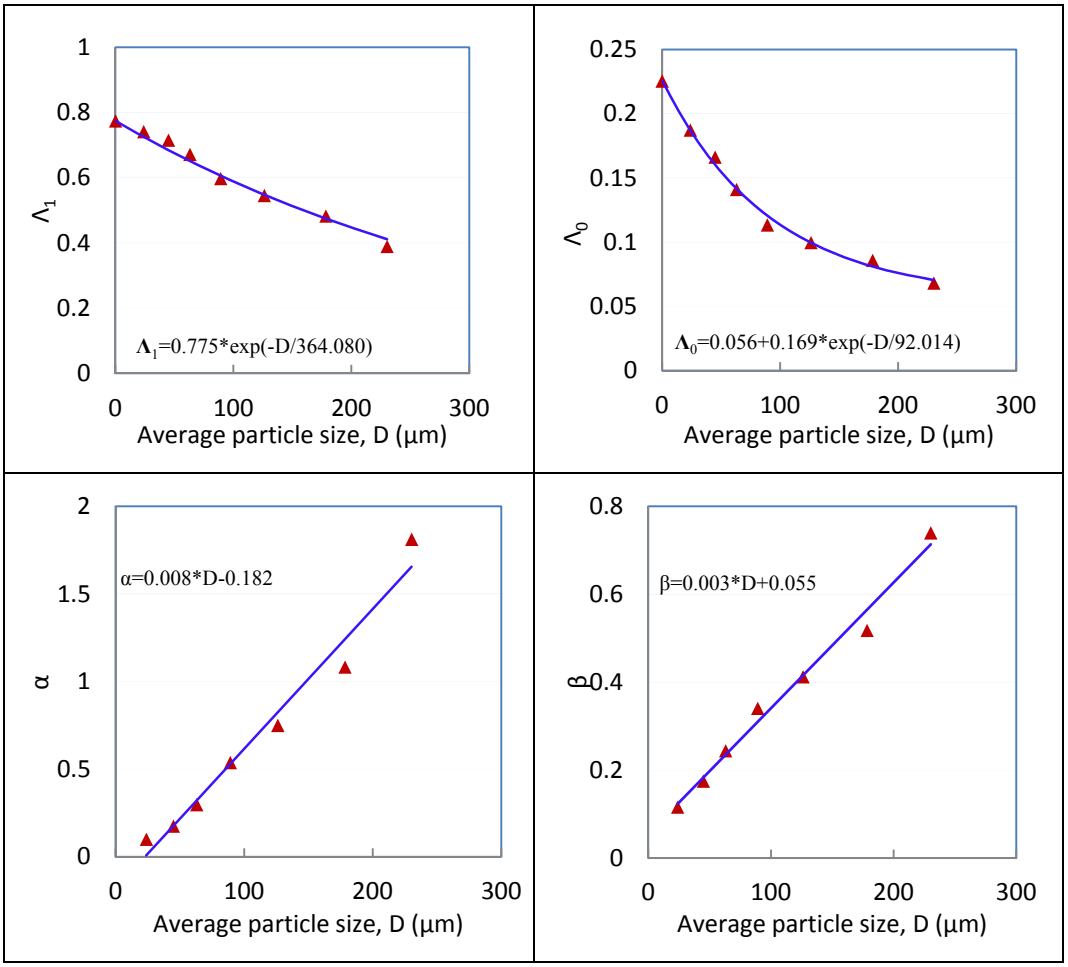

Figure 5-6 Variation of model parameters with average particle size

Figure 5-6 shows the variations of these model parameters with particle size. It is found that the volumetric fractions of liberated mineral and gangue particles can be approximated using negative exponential functions (see Figure 5-6). If average particle size approaches zero (i.e. $D \to 0$), $\Lambda_i^{(3)}(D)$ should be close to p_i. This is confirmed by the fact that the intercept of $\Lambda_i^{(3)}(D)$ against D with y axis approaches p_i.

$$\Lambda_1^{(3)}(D) = 0.775exp\,(-D/364.080) \qquad \text{Eq. 5-20}$$

$$\Lambda_0^{(3)}(D) = 0.056 + 0.169exp\,(-D/92.014) \qquad \text{Eq. 5-21}$$

D is in μm. Similarly, variations of α (or β) with average particle size can be described by linear functions.

$$\alpha = 0.008D - 0.182 \qquad \text{Eq. 5-22}$$

$$\beta = 0.003D + 0.055 \qquad \text{Eq. 5-23}$$

Once these relationships are determined for an ore body, they represent the characteristic features of mineral liberation and may be used to determine the grade distribution of particles at any grind size. Even though the model bears the assumption of random breakage, any deviations from random breakage mechanism through preferential breakage such as grain boundary breakage would be partially accounted for by the use of probability functions $P(L)$, $\omega^{(i)}(L)$ and $C(L)$ measured from the polished sections of the ore.

For the high grade sulphide ore tested, the proposed liberation model may be given by:

$$g(m) = \begin{cases} \Lambda_0^{(3)}(D), & m = 0 \\ \dfrac{\left(1 - \Lambda_0^{(3)}(D) - \Lambda_1^{(3)}(D)\right) m^{(\alpha-1)}(1-m)^{(\beta-1)}}{B(\alpha,\beta)}, & m \in (0,1) \\ \Lambda_1^{(3)}(D), & m = 1 \end{cases} \qquad \text{Eq. 5-24}$$

where $g(m)$ is the density function of the volumetric grade distribution of particles of size D,

$\Lambda_1^{(3)}(D) = 0.775exp\,(-D/364.080)$

$\Lambda_0^{(3)}(D) = 0.056 + 0.169exp\,(-D/92.014)$

$\alpha = 0.008D - 0.182$

$\beta = 0.003D + 0.055$

The corresponding cumulative distribution function $G(m)$ is given by

$$G(m) = \Lambda_0 + (1 - \Lambda_0 - \Lambda_1) I_m(\alpha,\beta) \qquad \text{Eq. 5-25}$$

where $I_m(\alpha,\beta)$ is the incomplete Beta function defined by (King 2001)

$$I_m(\alpha,\beta) = \frac{\int_0^m x^{(\alpha-1)}(1-x)^{(\beta-1)}dx}{B(\alpha,\beta)} \quad \text{Eq. 5-26}$$

Similar to the predictive 3-D liberation model given above, the 2-D and 1-D liberation models may be also derived based on the linear and areal measurement. The variations of four parameters (α, β, $\Lambda_1$and Λ_0) for both 1-D and 2-D model with average particle size are also fitted using similar functional forms to those used for 3-D model.

5.4.2 Proposed 2-D model

The proposed model to predict areal grade distribution density function of particle sections is given by

$$g(m) = \begin{cases} \Lambda_0^{(2)}(D), & m = 0 \\ \dfrac{\left(1-\Lambda_0^{(2)}(D)-\Lambda_1^{(2)}(D)\right)m^{(\alpha-1)}(1-m)^{(\beta-1)}}{B(\alpha,\beta)}, & m \in (0,1) \\ \Lambda_1^{(2)}(D), & m = 1 \end{cases} \quad \text{Eq. 5-27}$$

where

$$\Lambda_1^{(2)}(D) = 0.120 + 0.655exp\,(-D/97.443) \text{ with } (R^2\text{=}0.9179)$$

$$\Lambda_0^{(2)}(D) = 0.053 + 0.172exp\,(-D/56.762) \text{ with } (R^2\text{=}0.9367) \quad \text{Eq. 5-28}$$

$$\alpha = 0.003D - 0.016 \text{ with } (R^2\text{=}0.9799)$$

$$\beta = 0.001D + 0.023\ (R^2\text{=}0.9788) \text{ with } (R^2\text{=}0.9772)$$

5.4.3 Proposed 1-D model

Correspondingly, the proposed model to predict linear grade distribution density function of particle sections is given by

$$g(m) = \begin{cases} \Lambda_0^{(1)}(D), & m = 0 \\ \dfrac{\left(1-\Lambda_0^{(1)}(D)-\Lambda_1^{(1)}(D)\right)m^{(\alpha-1)}(1-m)^{(\beta-1)}}{B(\alpha,\beta)}, & m \in (0,1) \\ \Lambda_1^{(1)}(D), & m = 1 \end{cases} \quad \text{Eq. 5-29}$$

where

$\Lambda_1^{(1)}(D) = 0.775exp\,(-D/540.761)$ with (R^2=0.9776)

$\Lambda_0^{(1)}(D) = 0.064 + 0.161exp\,(-D/117.154)$ with (R^2=0.9707) Eq. 5-30

$\alpha = 0.008D - 0.182$ with (R^2=0.9709)

$\beta = 0.003D + 0.055$ with (R^2=0.9855)

5.5 Application of proposed models

Recently, there has been a growing interest in geometallurgical testing to evaluate the variability and spatial distribution of processing characteristics of ore bodies. This information is normally obtained from testing of drill core samples using rapid tests to evaluate a range of ore characteristics such as hardness, floatability, grades etc. In this context, a model that predicts the grade distribution of comminuted particles is of great interest.

In order to test the validity of the proposed models for such application, the measured grade distribution obtained from a comminuted product comprising of particles with a wide size distribution (composite sample) is compared with that obtained from prediction. The prediction was made based on the grade distribution of individual size fractions and combined according to the volumetric size distribution. The size distribution of the composite sample is given in Table 5-1. The model parameters for the proposed models used to evaluate the grade distributions in both 1-D and 2-D and those fitted to the measured data are given in Table 5-2.

Table 5-1 Particle size distribution (volumetric fraction) of the composite feed

Size fraction (μm)	Volume frequency
-250+212	0.086
-212+150	0.189
-150+106	0.186
-106+75	0.189
-75+53	0.127
-53+38	0.176
-38	0.047

Table 5-2 Summary of model parameters for proposed liberation models and estimated from measured grade distributions

Particle size		Calculated		Measured	
		Proposed 2-D model	Proposed 1-D model	Areal	Linear
-250+212μm	Λ_1	0.226	0.488	0.422	0.461
	Λ_0	0.062	0.088	0.084	0.072
	α	5.859	3.289	0.594	0.784
	β	1.746	1.585	0.345	0.394
-212+150μm	Λ_1	0.204	0.565	0.448	0.533
	Λ_0	0.060	0.103	0.034	0.053
	α	2.208	2.958	0.494	0.613
	β	0.640	1.728	0.308	0.378
-150+106μm	Λ_1	0.252	0.611	0.504	0.564
	Λ_0	0.067	0.116	0.016	0.096
	α	1.632	2.863	0.354	0.640
	β	0.494	1.913	0.228	0.311
-106+75μm	Λ_1	0.333	0.655	0.603	0.683
	Λ_0	0.081	0.133	0.042	0.116
	α	1.448	3.963	0.301	0.559
	β	0.474	3.076	0.211	0.276
-75+53μm	Λ_1	0.496	0.704	0.618	0.691
	Λ_0	0.113	0.159	0.030	0.081
	α	1.350	4.693	0.300	0.480
	β	0.544	4.445	0.233	0.318
-53+38μm	Λ_1	0.605	0.736	0.675	0.759
	Λ_0	0.148	0.182	0.108	0.066
	α	1.489	12.657	0.568	0.333
	β	0.685	14.086	0.296	0.397
-38μm	Λ_1	0.624	0.752	0.583	0.620
	Λ_0	0.155	0.198	0.021	0.072
	α	0.629	3.386	0.613	0.874
	β	0.296	4.140	0.430	0.507

The results obtained from linear model (Eq. 5-29) with parameters given by Eq. 5-30 are shown in Figure 5-7. It is found that the calculated linear grade distributions for the composite sample are somewhat higher than those determined by measurement. This deviation may have arisen from measurement errors, sample preparation errors and systematic errors. For practical purposes, this deviation may be accounted for by

using a correction factor. As it has been explained in section 5.3.1, Λ_i values were considerably underestimated by using $\omega^{(i)}(A)$ function determined from random circular masks. Accordingly, the grade distribution of composite particles estimated from the underestimated Λ_i values has a considerable bias as shown in Figure 5-2.

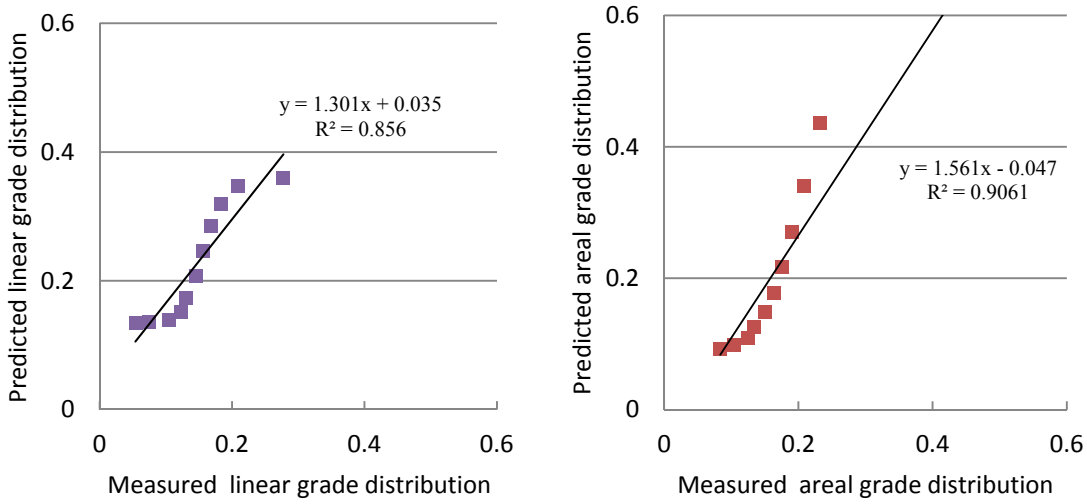

(a) (b)

Figure 5-7 Comparison of linear grade distribution (a) and areal grade distribution (b) of composite feed sample calculated from proposed model and measured on particle sections

5.6 Discussion

In this work, both linear and areal grade measurements were made on polished sections of particles. The necessary probability functions, i.e. $C(L)$, $P(L)$ and $\omega^{(i)}(L)$ were also evaluated from image analysis technique. These functions were then used to estimate the fractions of fully liberated particles (Λ_1 and Λ_0) and grade distribution of composite particles at various grinding sizes. These data have been used to test the validity of some published models that have been used to estimate the fractions of fully liberated particles and also compare their performance with the proposed predictive models. These are discussed below. As the fractions of fully liberated particles estimated from Eq. 5-11 and Eq. 5-12 using the $\omega^{(i)}(A)$ function determined by random circular masks deviated considerably from those measured on particle sections, the proposed 1-D liberation model based on $\omega^{(i)}(L)$ is selected for comparison with other published 1-D liberation models instead of proposed 2-D models.

5.6.1 Estimation of fractions of fully liberated particles in 1-D

As it has been described in Chapter 2, there have been attempts to quantify the fractions of fully liberated particles. Of these methods, the methods proposed by King and Barbery will be compared with the measured and proposed model. i.e. King's 1-D model calculates the degree of liberation $\mathcal{L}_1^{(1)}(D)$ and $\mathcal{L}_0^{(1)}(D)$ as

$$\mathcal{L}_1^{(1)}(D) = 1 - \frac{1}{\mu_1}\int_0^{\infty}[(1 - P(L|D))(1 - F_1(L)]dL \qquad \text{Eq. 5-31}$$

$$\mathcal{L}_0^{(1)}(D) = 1 - \frac{1}{\mu_0}\int_0^{\infty}[(1 - P(L|D))(1 - F_0(L)]dL \qquad \text{Eq. 5-32}$$

This degree of liberation $\mathcal{L}_i^{(1)}(D)$ is related to the fraction of fully liberated particles $\Lambda_i^{(1)}(D)$ through

$$\Lambda_i^{(1)}(D) = \mathcal{L}_i^{(1)}(D) \times p_i$$

i =1 for mineral and 0 for gangue, where

Barbery's 1-D model estimates the fraction of fully liberated particles by

$$\Lambda_1^{(1)} = \frac{p_1 \int_0^{\infty} L\, i(L) Q_{pp}(L) dL}{\int_0^{\infty} L\, i(L) dL} \qquad \text{Eq. 5-33}$$

Following the procedure described by Barbery, the fineness of Poisson polyhedral texture, λ_1, is estimated as 0.006 for this ore body. $\Lambda_i^{(1)}(D)$ values predicted from Barbery's 1-D, King's 1-D and proposed 1-D models (Eq. 5-30) are also compared with those measured from particle sections using image analysis. The results are shown in Figure 5-8. It is seen that King's 1-D liberation model overestimates both $\Lambda_0^{(1)}(D)$ and $\Lambda_1^{(1)}(D)$. Barbery's and the proposed 1-D models predict closer $\Lambda_i^{(1)}(D)$ to the measured values compared to that from King's 1-D model. It is also found that the prediction of $\Lambda_i^{(1)}(D)$ from the proposed 1-D model is better than that predicted by Barbery's 1-D model. It should be noted that the measurement of $\Lambda_0^{(1)}(D)$ at finer sizes (<75μm) may be influenced by the errors generated during sample preparation and image analysis. At larger sizes (>75μm), $\Lambda_0^{(1)}(D)$ values from linear grade

measurement generally follow the same trend as that of the calculated $\Lambda_0^{(1)}(D)$ by proposed 1-D model.

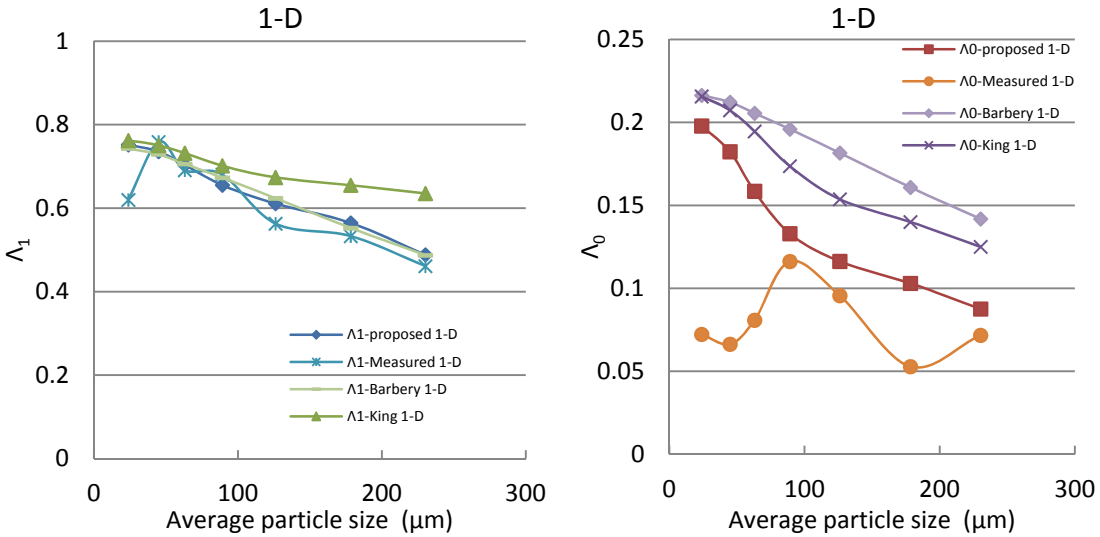

Figure 5-8 Comparison of $\Lambda_1^{(1)}(D)$ and $\Lambda_0^{(1)}(D)$ calculated from Barbery's (Eq. 5-33), King's (Eq. 5-31 and Eq. 5-32) and the proposed models (Eq. 5-13 and Eq. 5-14) and measured from particle sections

From the above analysis, it is found that the proposed liberation model for 1-D provides closest prediction of $\Lambda_i^{(1)}(D)$ to the measured ones. This indicates the proposed models can be used in the 1-D liberation prediction in practice.

5.6.2 Comparison of the proposed model with Barbery's model in 3-D

The calculated volumetric grade distribution for each size fraction using proposed liberation model above has been compared with that using Barbery's liberation model as modified by Leigh *et al.* (1996) (Barbery's model), which assumes Poisson polyhedral texture. Figure 5-9 shows the comparison of the grades for -250+212μm fraction. It is found the proposed 3-D model shows close liberation prediction to that determined from Barbery's model. The only significant difference between the two volumetric grade distributions is Barbery's model yields lower fraction of fully liberated mineral particles compared to the proposed model. This trend was also observed for all other size fractions as shown in Figure 5-10.

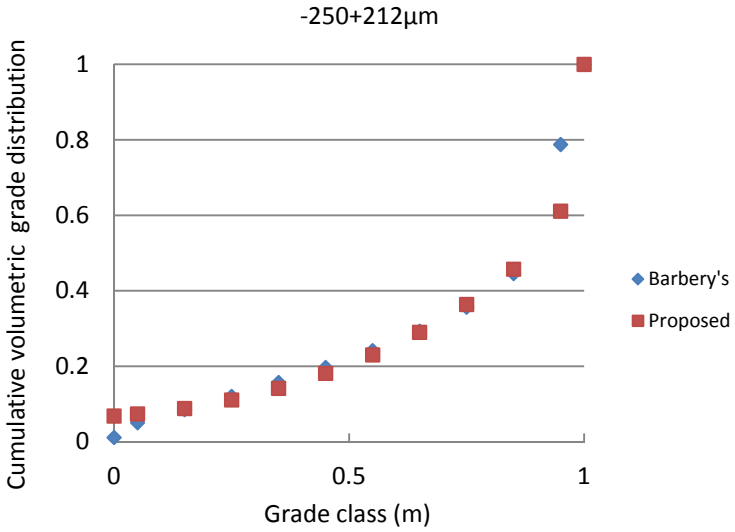

Figure 5-9 Comparison of cumulative volumetric grade distribution for -250+212μm particles predicted using Barbery's model and proposed 3-D model

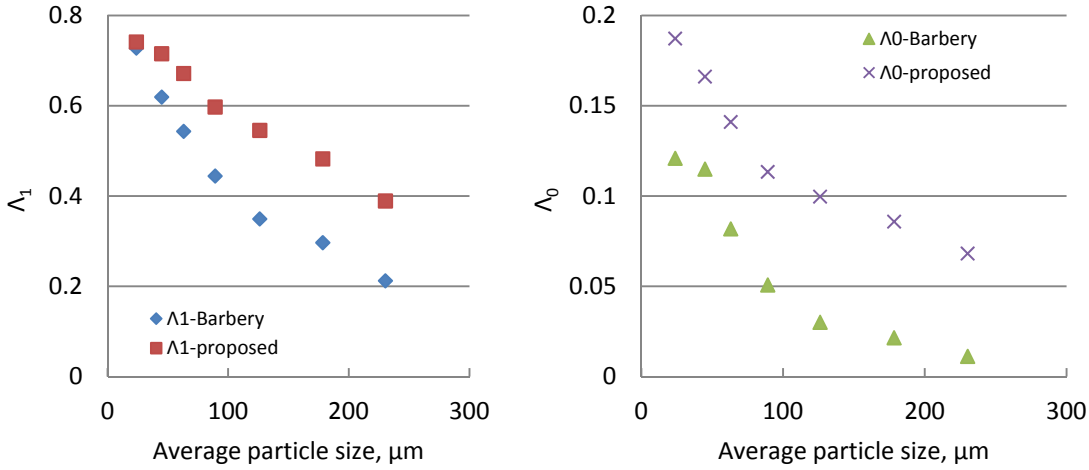

Figure 5-10 Variation of the estimated model parameters Λ_1 and Λ_0 of Barbery's model and proposed model with particle size

Because of the deviation of Λ_i observed in Figure 5-10, it is important to test the validity of volumetric grade distributions calculated from Barbery's model and the proposed model by comparing the calculated average volumetric grades based on these models and that from chemical assay for each size fraction. As shown in Figure 5-11, the average grades determined from the two liberation models are generally close to p_1(=0.775, determined from parent rock) in spite of slight deviations for larger size fractions. Results from chemical assay show a deviation of average

volumetric grades at various mean particle sizes from p_1. The good agreement of the average volumetric grade of particles at larger size fractions (>106 μm) indicates that the breakage follows a random pattern. However, data deviate from this assumption at smaller size fractions (<106 μm). This may be partly due to non-random breakage (e.g. grain boundary breakage) and/or measurement error (e.g. sample aggregation) at fines sizes.

Even though similar volumetric grade distributions have been calculated from both models, Barbery's model may not have general applicability due to the assumption of ore texture and particle structure, while the proposed liberation model can be used in general case.

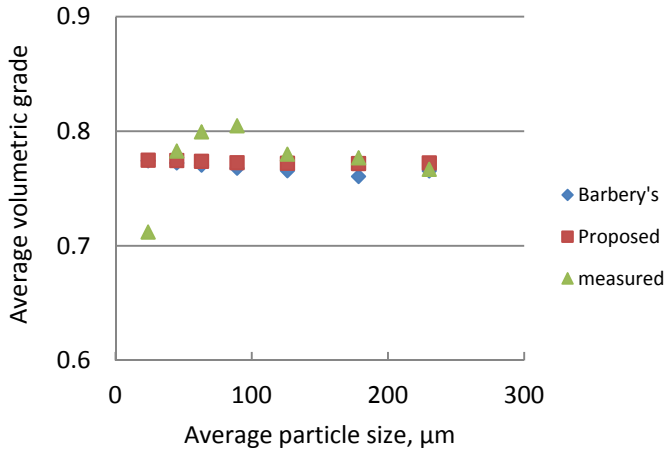

Figure 5-11 Comparison of average grades of comminuted particles determined from Barbery's model, proposed model and chemical assay

5.7 Conclusion

In this chapter, predictive liberation models have been proposed that describe the grade distributions of comminuted particles in the three dimensions following a procedure similar to that of Barbery. The major difference between the two approaches lies in the estimation of fractions of fully liberated particles. The proposed models do not require any assumptions of ore texture and particle structure. As the required probability functions have been evaluated from the measurement, the covariance function $C(L)$ and proximity function $P(L)$ and PSLS function $\omega^{(i)}(L)$ required for proposed liberation model can be estimated directly using the image analysis technique based on Labview™ software. The proposed 1-D model predictions ($\Lambda_i{}^{(1)}(D)$ values) are the closest to those measured from particle sections

in comparison to other published models in 1-D. Proposed 3-D liberation model predicts similar grade distributions to that from Barbery's model, albeit slightly higher $\Lambda_i^{(3)}(D)$ values.

A strong linear relationship was observed between $\Lambda_i^{(1)}(D)$and $\Lambda_i^{(2)}(D)$ determined from measurement, which indicates the stereological bias between 1-D and 2-D measurement on the same sectional image of particles. Similar relationship with 3-D parameters is expected to hold; however, future work is required to test this relationship.

It has been shown that the proposed predictive liberation models for mineral liberation may be useful for the geometallurgical application.

Chapter 6 Influence of mineral liberation on flotation performance

In Chapter 5, a method of evaluating the grade distribution of flotation feeds (i.e. comminuted particles) using the proposed liberation models was discussed. This chapter is aimed at investigating the influence of mineral liberation on flotation performance of comminuted particles. In commonly used flotation models, such as Klimpel model, the influence of impact factors (e.g. particle size and grade distribution, mineral surface exposure on particle surfaces) on flotation performance are generally lumped into two or three parameters, and the effect of mineral liberation is not explicitly quantified. A transformation matrix approach which incorporates the extent of liberation has been proposed in this work to predict flotation performance.

To evaluate the effect of mineral liberation on flotation performance, narrowly sized feeds were floated and the resulting recoveries along with the liberation characteristics of the feed and products were measured. The model used in this work is based on the size by size variation of the above information, which has been presented using matrices. The validity of the model was tested using data obtained from a high grade sulphide ore.

6.1 Evaluation of flotation performance

As described in Chapter 2, flotation performance is affected by many factors, such as degree of liberation of feed particles, surface exposure of mineral on particle surface, reagent scheme, etc. In this work, the parameters such as reagent scheme and dosage, and the operational parameters such as agitation speed, aeration rate, pulp density were kept constant except for the feed size which incorporates variations in liberation. Therefore, any variation in flotation recoveries observed may be ascribed to the effects of size, mineral surface exposure and the grade distribution of the feed particles.

Batch flotation tests were carried out using samples of each size fraction and the concentrates were collected at 15, 30, 60, 120, 240 and 360 seconds (cumulative). The flotation recoveries of total sulphides (mineral phase) were measured by

chemical assay. Observed flotation recoveries of total sulphides based on volume for narrowly sized feeds are shown in Figure 6-1.

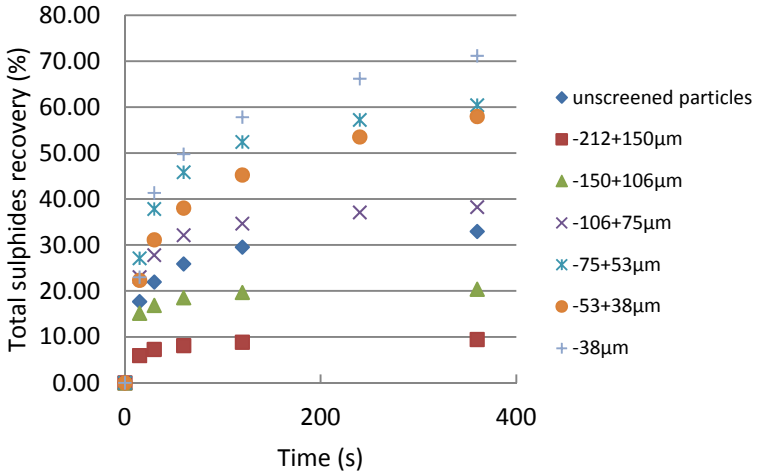

Figure 6-1 Total sulphides recoveries of each narrow particle size fraction as a function of flotation time

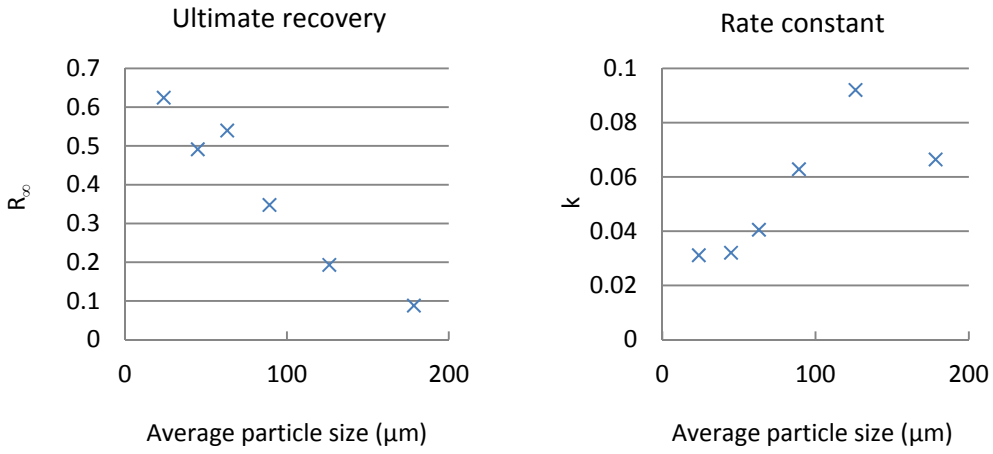

Figure 6-2 Ultimate recoveries (R_∞) and rate constants (k) fitted using Klimpel model from results in Figure 6-1

As expected, the recoveries of total sulphides generally follow the first order kinetic relationship described by Klimpel model (Eq. 2-103). The recovery at very fine sizes i.e. below -38μm is somewhat higher and may be attributed to entrainment of fine mineral particles (Johnson 2005). The resulting rate constants are shown in Figure 6-2. As expected, it shows that the rate constant is high at intermediate size and decreases at large and very fine sizes.

6.2 Liberation characteristics of floated particles

6.2.1 Measurement of grade distribution of particles using image analysis

Scanning electron microscopic (SEM) images of the feed and flotation products were analysed using Labview™ image analysis software. The linear grade, areal grade (see section 3.3.2) and mineral surface exposure (apparent surface composition) were measured for each particle size fraction. Randomly placed lines on the SEM images of particle sections are used in linear grade measurement. Linear grade distribution is obtained from the ratio of total mineral intercept length to total intercept length within each particle in the sample. Areal grade distribution is estimated as the ratio of mineral section area to total section area of each particle in the sample. Figure 6-3 and Figure 6-4 show the typical cumulative grade distributions estimated from flotation feed and concentrates by linear and areal grade measurements. For clarity, the grade distribution data of concentrates collected from 120-360s are not shown. It is seen that the proportions of fully liberated mineral particles in the concentrates are higher than that in the feeds. The grade distributions of particles in concentrates obtained at different time intervals change progressively, implying that the floatability characteristics of particles have changed with flotation time. Also, the proportions of composite particles collected in the concentrates generally increase with flotation time. As expected, it can be seen that the fully liberated mineral particles float faster than composite particles in a given size fraction.

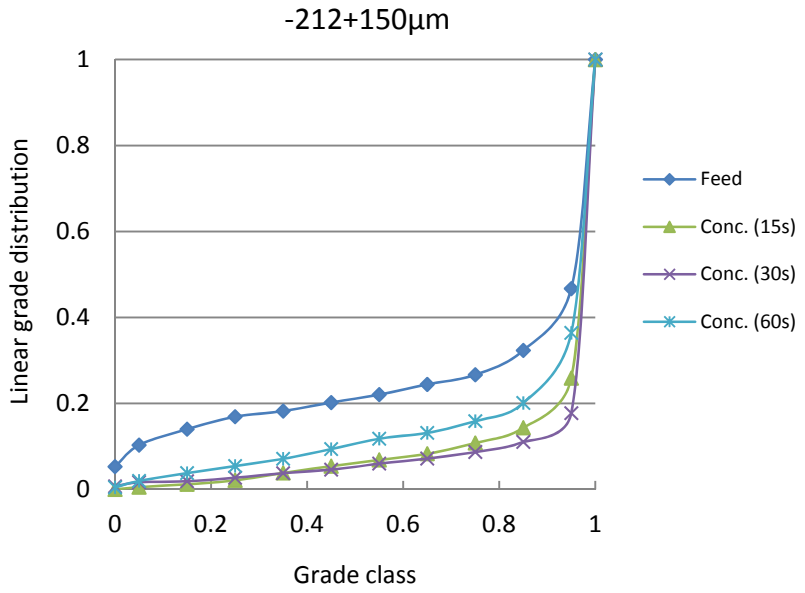

Figure 6-3 Comparison of linear grade distributions measured from feed and concentrates (15, 30 and 60 seconds) of -212+150*µm* particles

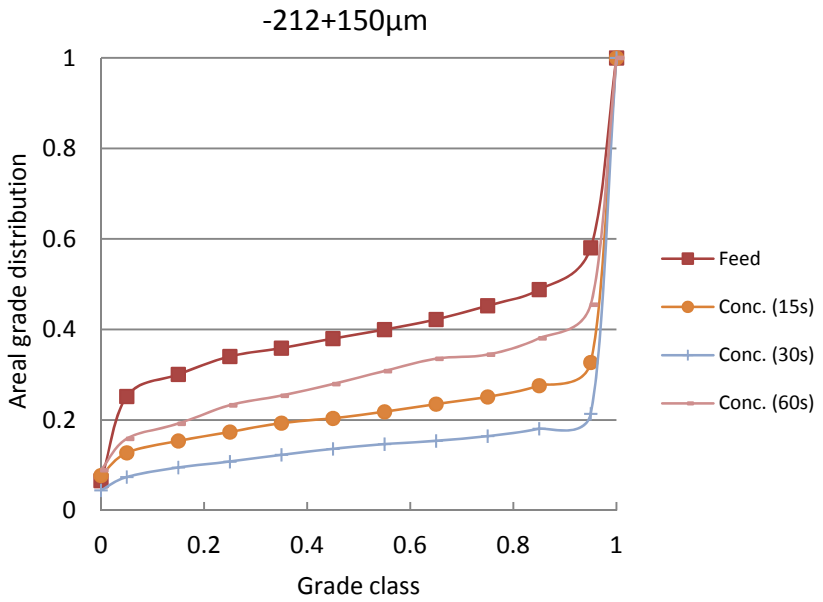

Figure 6-4 Comparison of areal grade distributions measured from feed and concentrates (15, 30 and 60 seconds) of -212+150*µm* particles

6.2.2 Surface exposure of mineral

Assuming that the particles were randomly oriented in the mounting, the extent of apparent mineral exposure on the surface of particles was estimated as the fractional perimeter covered by mineral on each particle in the mounted specimen. In the absence of information in 3-D, it is reasonable to assume that this quantity represents the apparent particle surface composition. The apparent surface composition was

compared with the linear and areal grade distribution and is shown in Figure 6-5 and Figure 6-6, respectively. It is found that there is a linear relationship between apparent surface composition and linear grade distribution/areal grade distribution. This indicates that the surface composition is highly correlated with linear grade distribution and/or areal grade distribution. This is also in good agreement with the conclusions from other researchers (e.g. (Lastra 2002)). Therefore, since the effect of surface composition on flotation performance is implicitly included in linear/areal grade distribution of floated particles, it is not included as an independent variable in the model development.

It should be noted that in this work, the linear grade measurement was made on particle sections using random lines (see section 3.3.2), which is different from that made by conventional image analysers that use equidistant parallel lines. This procedure is more statistically relevant and an improvement on the measuring system. The results differ from those obtained by non-random lines.

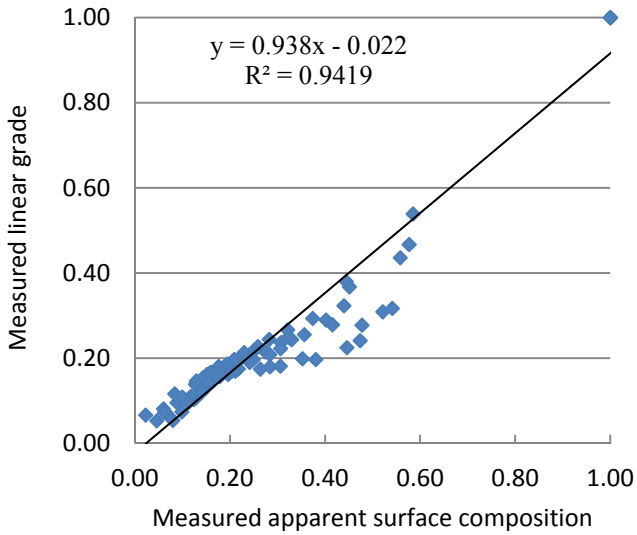

Figure 6-5 Comparison of measured apparent surface composition and linear grade for the comminuted particles (feed)

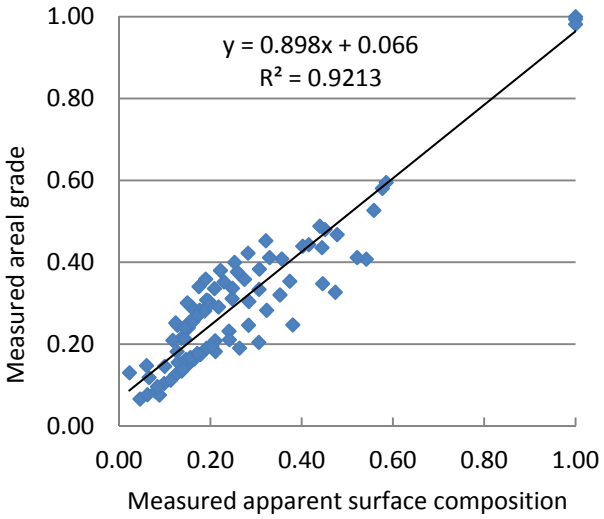

Figure 6-6 Comparison of measured apparent surface composition and areal grade for the comminuted particles (feed)

6.3 Flotation recovery of particles in each grade/size class

The areal/linear grade distributions of flotation products (concentrates and tailings) from batch flotation tests at different flotation times were measured and compared with the areal/linear grade distributions of the corresponding feed using **image analysis**. The grade distributions were evaluated using 12 grade classes comprising fully liberated mineral, fully liberated gangue and composites with 10 grade intervals between 0 and 1.

The recovery of materials in a given size fraction i and grade class j in the kth concentrate is given by r^{ijk} as

$$r^{ijk} = \left(\frac{f^{ijk}}{f^{ij0}}\right)\left(\frac{V^{ik}}{V^{i0}}\right) \qquad \text{Eq. 6-1}$$

where f^{ijk} is the number fractions of particles of size fraction i and grade class j in the kth concentrate and f^{ij0} is that in the feed. These can be measured by image analysis. V^{ik} is the volume (fraction) of the particles in size fraction i reported to the kth concentrate and V^{i0} is that in the feed. These can be measured by experiments.

The fractions f^{ijk} may be evaluated using either section area (2-D) or linear intercept lengths (1-D). Area measurements are denoted by subscript A, while that for linear measurements is L. i=1 represents top size fraction -212+150μm. j=1 for

fully liberated gangue particles, j=12 for fully liberated mineral particles and j=2 for grade class 0-0.1 etc. k represents concentrate number (k =1 for 15 seconds and k=0 denotes the feed particles).

For practical applications, the information of r^{ijk} needs to be established through test work. Once established, r^{ijk} may be treated as characteristic feature of the given ore/reagent system.

6.3.1 Flotation recoveries based on areal grade measurement

The recovery of particles in each size/grade class has been estimated from the areal grade measurement of flotation feed, concentrates and tailing for particles in each size fraction. A typical plot of r_A^{ijk} versus flotation time for -212+150μm particles is shown in Figure 6-7. Similar figures to Figure 6-7 for other size fractions were also obtained. As expected, it can be seen that the flotation recoveries of all size/grade classes approximate first order kinetics. Similar observations could be made for recoveries of particles in other size fractions too.

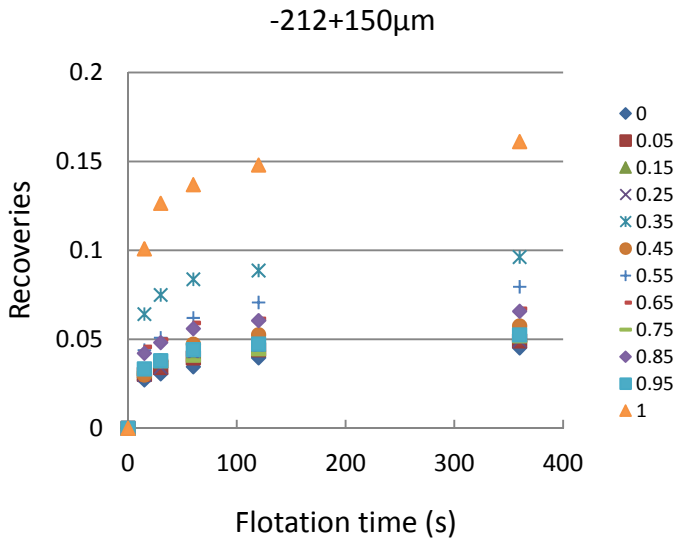

Figure 6-7 r_A^{ijk} vs. flotation time for various grade classes in -212+150μm fraction (based on areal grade measurement)

6.3.2 Flotation recoveries based on linear grade measurement

Similar to the analysis based on areal grade distribution given above, the recovery of particles in each size/grade class was also estimated from linear grade measurement. A typical plot of r_L^{ijk} versus flotation time (also for the -212+150μm particles) is

shown in Figure 6-8. It can be seen that Figure 6-8 is similar to Figure 6-7, which was based on areal grade measurement. However, it also showed considerable difference in the flotation recoveries of the same grade class particles evaluated from the areal and linear measurements (see Figure 6-9). This may be due to the experimental and image analysis errors originated from the low fractions of composite particles.

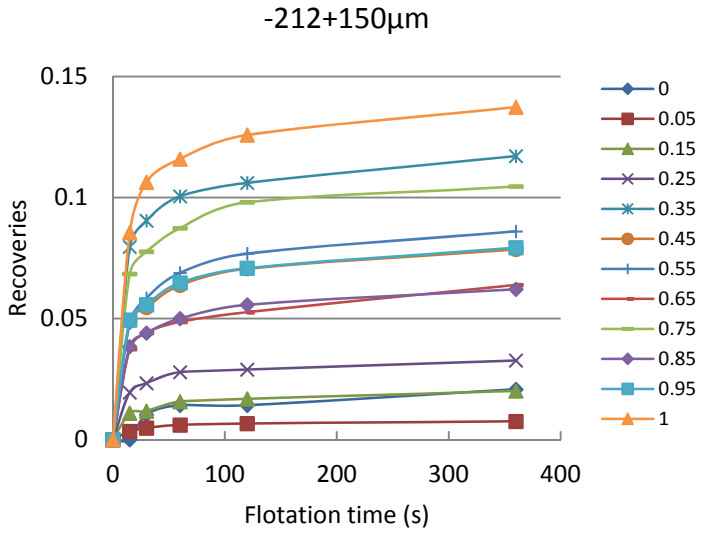

Figure 6-8 r_L^{ijk} vs. flotation time for various grade classes in -212+150μm fraction (based on linear grade measurement)

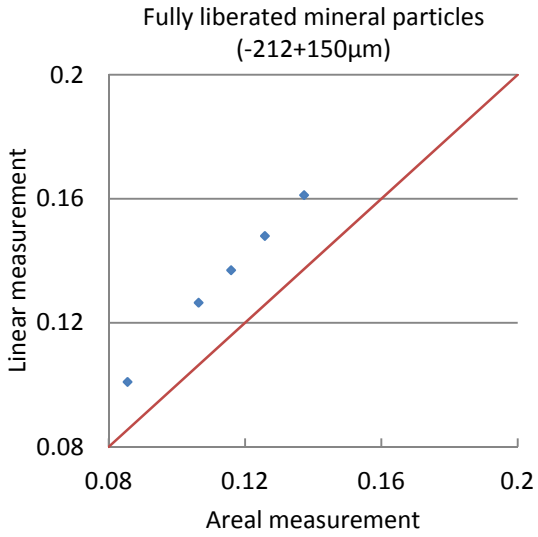

Figure 6-9 Comparison of r_A^{ijk} and r_L^{ijk} in the same grade class (g=1, fully liberated mineral particles) and size fraction (-212+150μm) at different flotation times obtained from areal and linear measurements

6.3.3 Evaluation of Klimpel model parameters

In each size fraction i and grade class j, it is reasonable to assume that all the particles have the same probability of being floated and collected in the concentrates. Therefore, their flotation rate may be considered as constant. To investigate the trends in the recoveries determined for each size/grade class in sections 6.3.1 and 6.3.2, Klimpel model was fitted to the recovery data calculated using both linear and areal measurements. The model used to describe the recovery of particles in each size/grade class is given by:

For areal grade measurement,

$$r_A^{ijk} = r_{A,\infty}^{ij}\left(1 - e^{-K_A^{ij}t}\right) \qquad \text{Eq. 6-2}$$

For linear grade measurement,

$$r_L^{ijk} = r_{L,\infty}^{ij}\left(1 - e^{-K_L^{ij}t}\right) \qquad \text{Eq. 6-3}$$

where

$r_{A,\infty}^{ij}$ and $r_{L,\infty}^{ij}$ are the ultimate recoveries based on areal and linear grade measurements, respectively;

K_A^{ij} and K_L^{ij} are the rate constants based on areal and linear grade measurements, respectively;

r_A^{ijk} and r_L^{ijk} are the cumulative recoveries based on areal and linear grade measurements, respectively.

The best fitting values of the rate constant and ultimate recovery parameters are given in Table 6-1 and Table 6-2 for areal and linear grade measurements, respectively.

Table 6-1 Determined Klimpel parameters R_∞ and k (s^{-1}) of particles in each size/grade class based on areal grade measurement

	-212+150μm		-150+106μm		-106+75μm		-75+53μm		-53+38μm		-38μm	
g	R_∞	K	R_∞	K	R_∞	K	R_∞	K	R_∞	K	R_∞	K
0.00	0.039	0.067	0.074	0.061	0.100	0.015	0.084	0.035	0.119	0.005	0.180	0.028
0.05	0.044	0.068	0.079	0.071	0.209	0.020	0.094	0.030	0.147	0.011	0.351	0.024
0.15	0.047	0.070	0.084	0.063	0.194	0.012	0.135	0.067	0.203	0.018	0.343	0.021
0.25	0.045	0.063	0.087	0.100	0.154	0.021	0.073	0.020	0.209	0.076	0.301	0.020
0.35	0.089	0.078	0.078	0.084	0.150	0.012	0.089	0.064	0.224	0.042	0.294	0.024
0.45	0.053	0.047	0.081	0.112	0.193	0.017	0.139	0.087	0.260	0.068	0.282	0.022
0.55	0.073	0.046	0.123	0.099	0.134	0.016	0.126	0.048	0.513	0.108	0.395	0.024
0.65	0.062	0.079	0.113	0.095	0.218	0.029	0.044	0.007	0.458	0.083	0.275	0.021
0.75	0.043	0.076	0.076	0.122	0.105	0.017	0.089	0.127	0.177	0.071	0.248	0.025
0.85	0.060	0.071	0.080	0.103	0.112	0.022	0.049	0.052	0.274	0.088	0.216	0.021
0.95	0.048	0.068	0.090	0.128	0.067	0.029	0.086	0.085	0.219	0.038	0.263	0.030
1.00	0.149	0.070	0.286	0.100	0.427	0.076	0.719	0.036	0.538	0.028	1.000	0.033

Table 6-2 Determined Klimpel parameters R_∞ and k (s^{-1}) of particles in each size/grade class based on linear grade measurement

	-212+150μm		-150+106μm		-106+75μm		-75+53μm		-53+38μm		-38μm	
g	R_∞	K	R_∞	K	R_∞	K	R_∞	K	R_∞	K	R_∞	K
0.00	0.020	0.016	0.023	0.149	0.006	0.063	0.043	0.145	0.050	0.002	0.223	0.036
0.05	0.007	0.046	0.020	0.058	0.044	0.027	0.076	0.141	0.050	0.004	0.279	0.045
0.15	0.018	0.044	0.086	0.058	0.173	0.030	0.106	0.037	0.088	0.005	0.325	0.020
0.25	0.030	0.059	0.164	0.053	0.258	0.021	0.327	0.015	0.319	0.013	0.364	0.022
0.35	0.107	0.080	0.091	0.096	0.408	0.022	0.294	0.030	0.241	0.013	0.521	0.020
0.45	0.071	0.062	0.185	0.112	0.210	0.029	0.275	0.015	1.000	0.157	0.797	0.017
0.55	0.079	0.052	0.157	0.114	0.234	0.034	0.184	0.007	0.355	0.025	0.547	0.021
0.65	0.055	0.063	0.198	0.109	0.317	0.027	0.242	0.030	0.465	0.077	0.834	0.024
0.75	0.097	0.069	0.162	0.084	0.225	0.036	0.081	0.051	0.364	0.081	0.458	0.022
0.85	0.056	0.063	0.144	0.097	0.221	0.031	0.119	0.068	0.223	0.083	0.595	0.020
0.95	0.072	0.063	0.080	0.071	0.127	0.027	0.088	0.038	0.188	0.074	0.521	0.024
1.00	0.127	0.068	0.269	0.098	0.416	0.070	0.666	0.037	0.578	0.028	0.622	0.030

It is seen that the ultimate recovery of fully liberated mineral particles within each size fraction is always the largest compared to that of the other grade classes. At the coarse size fractions (e.g. -212+150μm), the ultimate recoveries for all the grade classes are close; while at the fine particle size fractions (e.g. -53+38μm), the variation of ultimate recoveries determined from different grade classes is

significant. In the same grade class of all size fractions, the ultimate recoveries generally increase with the decrease of particle size.

The best fitting values of rate constant and ultimate recovery of each size/grade class based on linear/areal grade measurements are compared and shown in Figure 6-10. It can be seen that there is a considerable scatter in the data. There is no general trend of the rate constant and ultimate recovery determined for each size/grade class, in particular for composite particles, as shown in Figure 6-11. This indicates that the Klimpel's first order model may not be suitable for describing the recovery of particles in each size/grade class.

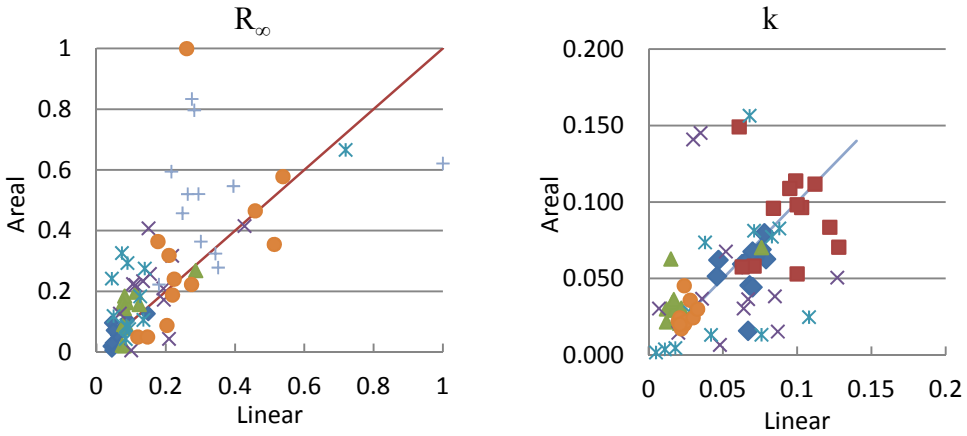

Figure 6-10 Comparison of ultimate recoveries r_{∞}^{ij} (R_{∞}) and rate constants K^{ij} (K,s^{-1}) determined from curve fitting using Klimpel model based on linear/areal grade measurements on the flotation products

This variation of the rate constant and ultimate recovery of each size/grade class determined from different measurement methods may be due to:

(1) Sample size: The sample mass of concentrates used in particle mounting is generally small leading to sampling error. Segregation effects due to small particles during mounting may also result in errors. Because most of the comminuted particles are liberated or nearly liberated; the fractions of middling particles are low. The middling particles are subdivided into 10 classes according to their grade. The sample size of particles that fall in each grade class is much lower and measurements on such middling particles may have contributed to errors.

(2) Model fit: Errors may be generated from the Klimpel model fitting of the recoveries data obtained from image analysis.

(3) Image analysis: The field of observation during SEM measurement is limited; hence biased results may be produced from the images taken. This can be overcome by taking more images during SEM measurement.

(4) Stereological bias: Similar to that introduced in linear/areal grade measurements of comminuted particle during liberation analysis, stereological bias exists during the measurement of the flotation products using image analysis.

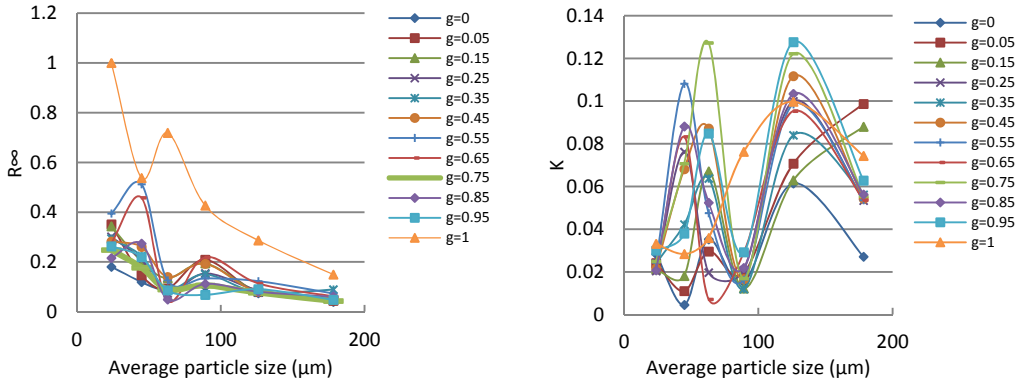

Figure 6-11 Variation of ultimate recoveries r_{∞}^{ij} (R_{∞}) and rate constants K^{ij} (k) of each grade class (determined from curve fitting of recoveries using Klimpel model based on linear grade measurement) with average particle size

For the above reasons, it is not possible to identify any trends for the variation of Klimpel model parameters determined from various size/grade classes. Hence, the evaluated r_L^{ijk} and r_A^{ijk} values could be used directly by eliminating the need for model fitting. This could be achieved by using a transformation matrix approach that incorporates liberation and flotation effects separately in terms of matrices.

6.4 Development of Liberation/flotation model- Transformation matrix approach

6.4.1 Model development

Based on the assumption that within each narrow size/grade class, the flotation characteristics of the particles are constant, a transformation matrix model is developed to incorporate liberation information to predict flotation performance. Similar to the probability flotation models that separate the effects such as particle-bubble collision, adhesion, detachment on the recoveries (Lynch *et al.* 1981), the

effects of liberation and flotation are incorporated separately and quantified in this model by defining individual matrices. The other parameters such as operation parameters and reagent scheme are kept constant during flotation tests.

The effects due to various factors have been quantified and presented as matrices. They are:

a) Liberation information of flotation feed (g^{ij}) which describes the grade of particles in size fraction i and grade class j. g^{ij} can be obtained from the predictive liberation models developed in section 5.4 on using proposed liberation models. Note that g^{ij} is similar to f^{ij0} but differs in that g^{ij} is predicted using liberation models, while f^{ij0} is measured using image analysis.
b) Recoveries of each grade/size class (r^{ijk}) which provides the flotation characteristics of particles. r^{ijk} can be determined from batch flotation tests and image analysis (see section 6.3). If the flotation operational parameters and reagent scheme are kept constant, r^{ijk} should be constant.
c) Particle size distribution of the comminuted particles weighted by volume ($p^i(V)$). $p^i(V)$ can be calculated from the particle size distribution obtained from experiments.

Thus, the predictive transformation model to evaluate the cumulative recovery of size i material comprising all grade classes in the kth concentrate (R^{ik}) may be given by:

$$[R^{ik}]_{n\times 1} = [T_k]_{n\times n} \times [p^i(V)]_{n\times 1} \qquad \text{Eq. 6-4}$$

The elements T_k^{il} in square transformation matrix, $[T_k]_{n\times n}$, is defined as

$$T_k^{il} = \begin{cases} \sum_{j=1}^{m} (r^{ijk} \times g^{ji}), & for\ i = l, i = 1\ to\ n, j = 1\ to\ m \\ 0, & for\ i \neq l, i = 1\ to\ n, l = 1\ to\ n \end{cases} \qquad \text{Eq. 6-5}$$

where

k is the concentrate class.

m is the total number of grade classes used.

r^{ijk} is the recovery of particles in each size/grade class reporting to kth concentrate. It can be estimated from both linear measurement (denoted by r_L^{ijk}) and areal measurement (denoted by r_A^{ijk}).

g^{ji} is the transpose of grade distribution of flotation feeds, g^{ij}. g^{ji} can be predicted both in 2-D (denoted by g_A^{ji}) and 1-D (denoted by g_L^{ji}).

i, j and k denote the size, grade and concentrate class, respectively.

n is the total number of size fractions used.

$p^i(V)$ is the volume fraction of particles in size fraction i. $[p^i(V)\,]_{n\times 1}$ is a $n \times 1$ column matrix where n is the total number of size fractions.

R^{ik} is the recovery of particles in size fraction i reporting to the kth concentrate.

Having evaluated R^{ik} , the overall cumulative recovery of the composite feed in kth concentrate, R^k, may be obtained by summing up the individual contributions from all size fractions.

$$R^k = \sum_{i=1}^{n} R^{ik} \qquad \text{Eq. 6-6}$$

R^k values are compared with batch flotation results to test the validity of the transformation matrix model below.

6.4.2 Testing the validity of the transformation matrix model

The validity of the proposed transformation matrix model to predict the flotation performance was tested using a high grade sulphide ore. The feed comprised of a wide size distribution (-212μm). In order to obtain model parameters, the feed was screened to narrow size intervals and each fraction was batch floated under identical reagent condition as described in section 3.1.2. The recoveries of individual size/grade classes at various flotation times, r^{ijk}, was evaluated as described in section 6.3 in terms of both linear and areal grade measurements. The liberation characteristics of the ore at the respective grinding sizes g^{ji} were predicted from the proposed predictive liberation models as shown in section 5.4. The above information was used in the prediction of flotation performance of a composite feed that has a known wide size distribution $p^i(V)$ using the model (Eq. 6-4 and Eq. 6-5).

Figure 6-12 shows the comparison of predicted recoveries (R^{ik}) of particles in each size fraction i that were collected at different flotation times and those measured from batch flotation tests (observed recoveries). It shows that the predictions agree with the observed values. This implies that by identifying the liberation and flotation characteristics of an ore at various grinding sizes, the flotation of a composite feed may be predicted accurately. This would be a useful technique that can be applied in geometallurgical testing of new ore bodies for downstream separation using flotation.

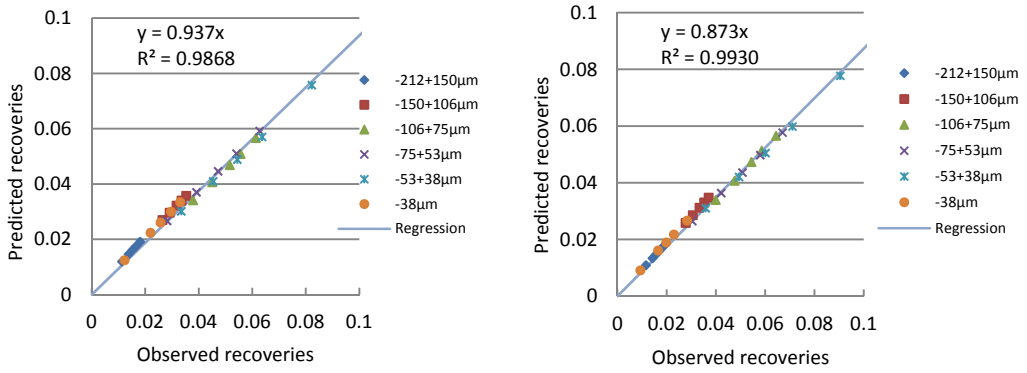

(a) Areal (2-D) (b) Linear (1-D)

Figure 6-12 Observed vs. predicted flotation recoveries of particles in each size fraction at different flotation times (15, 30, 60, 120 and 240s) based on (a) 2-D and (b) 1-D information

(The predicted recoveries were summed over the grade classes)

The predicted recoveries of the composite feed particles at various flotation times, R^k, were compared with observed data obtained from experiments and are shown in Figure 6-13. A strong linear relationship between the predicted and observed results indicates the validity of the model. There is however a bias in the prediction (i.e. predicted results are slightly lower in both areal and linear cases). This may be attributed to the stereological bias in predicting volumetric data from areal and linear measurements. The slope of the line in these plots indirectly quantifies this stereological bias. Thus, in practice, a correction factor may be assigned to the flotation performance prediction upon using the transformation matrix model. It is also found from Figure 6-13 that the bias in results is similar for the predictions based on both linear and areal measurements. Note that the composite feed comprised of 6 size fractions.

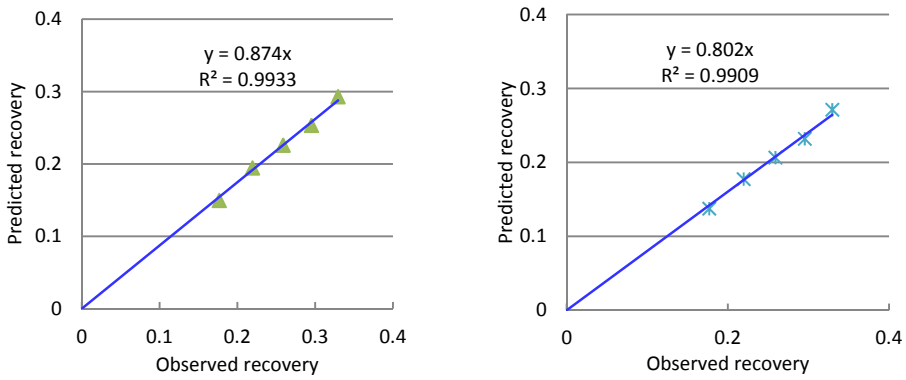

(a) Areal (2-D) (b) Linear (1-D)

Figure 6-13 Observed versus predicted cumulative recoveries of the composite feed at different flotation times (15, 30, 60, 120 and 240s) based on (a) 2-D and (b) 1-D information

(The predicted recoveries were summed over the grade and size classes)

It may be postulated that the bias between the predicted and observed recoveries may be due to:

a) The stereological bias. The use of image analysis based areal/linear grade measurement to estimate the matrix $[r^{ijk}]_{\mathrm{n\times m}}$ instead of volumetric grade measurements requires a stereological correction. The extent of this correction is reflected in the slope of the line (slope=1 indicates no bias).

b) Experimental error. As matrix $[r^{ijk}]_{\mathrm{n\times m}}$ is constructed using data from image analysis on the particle sections, sufficient number of particles is required to obtain statistically significant results. The sampling errors of preparing the feed particles and operation error during flotation test may be incorporated in the model.

c) Errors from g^{ji} predicted by the proposed liberation models. As shown in Chapter 5, there is similar bias between the grade distributions of the comminuted particles predicted from the proposed liberation models (in both 1-D and 2-D) and observed values from measurements.

6.4.3 Comparison of the transformation matrix model with published models

Schaap (1979) proposed a method of predicting flotation performance based on liberation characteristics for the disseminated low grade ores. The liberation

characteristics of the ores were predicted by extending King's liberation model that was based on renewal theory (King 1975a). Schaap's model was discussed in Chapter 2 and its main limitations are:

a) Ore texture assumption. The linear intercept length distribution density functions of both mineral and gangue phases are assumed to follow negative exponential functional form.
b) The comminuted particles are assumed to have cubic shape.
c) The proportions of each type of particles are predicted based on 1-D information.

In order to use Schaap's model for flotation prediction, the linear intercept length distributions for both mineral and gangue phases need to be assumed to follow negative exponential functional form. Based on the image analysis on the parent rock specimen, the average intercept lengths of mineral and gangue phases are estimated to be μ_1 =277.63μm and μ_0 =78.05μm using Eq. 6-7 and Eq. 6-8 for mineral and gangue phases, respectively. However, the observed data did not fit negative exponential distributions as assumed (see Figure 6-14 and Figure 6-15).

$$F_1(x) = 1 - e^{-\frac{x}{\mu_1}} \qquad \text{Eq. 6-7}$$

$$F_0(x) = 1 - e^{-\frac{x}{\mu_0}} \qquad \text{Eq. 6-8}$$

where x is the length of intercept.

Note that, x axis has been scaled using an arbitrary parameter φ by $x = \frac{L}{\varphi}$ for convenience. In this work, the values of φ were selected as 800μm and 300μm for mineral and gangue phases, respectively. It is found that the deviation between Schaap's cumulative linear intercept length distribution of mineral phase is larger than that of gangue phase. Note that the ore body in this project is high grade sulphide ore (p_1=0.775), which is different from the disseminated low grade ores used by Schaap.

To calculate the flotation recoveries of the composite feed particles using Schaap's model, the following parameters and quantities were determined:

(1) Parameters θ and z (see Eq. 2-110 and Eq. 2-111). As discussed in Chapter 2, the best fitting values of θ and z were determined from the experiments and image analysis.

(2) R_{ml}, R_{mc}, R_{mu}, R_{gc} and R_{gu} were estimated by numerical integration using equations (Eq. 2-114-Eq. 2-118) as suggested by Schaap.

(3) The total recovery is calculated by the sum of R_{ml}, R_{mc}, R_{mu}, R_{gc} and R_{gu}.

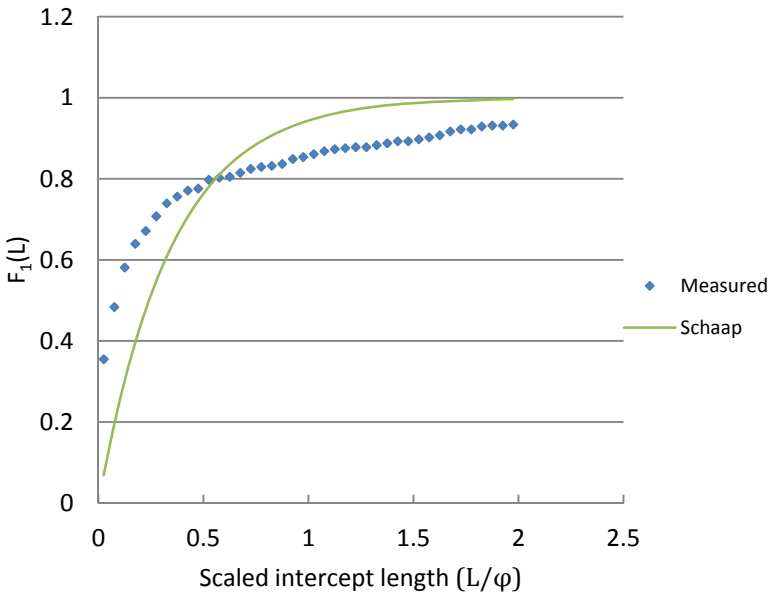

Figure 6-14 Cumulative intercept length distributions for mineral phase determined from experiment ($\boldsymbol{\varphi}$=800μm) and Schaap's model

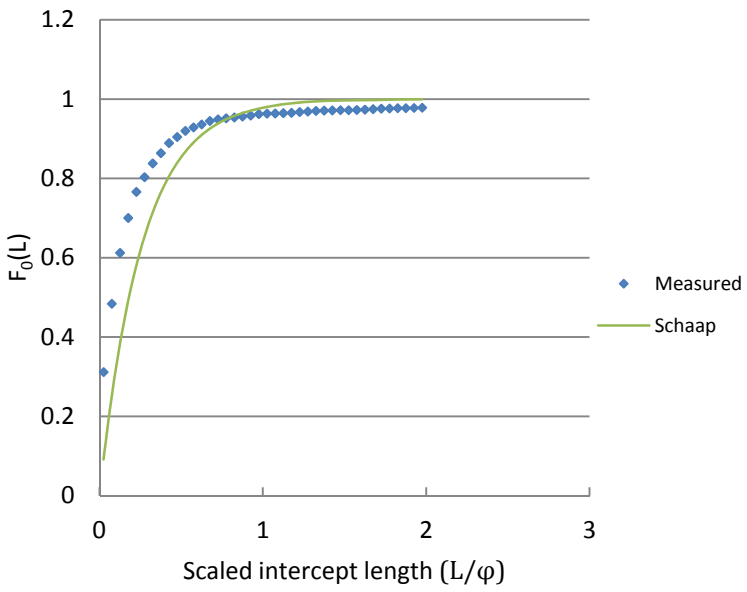

Figure 6-15 Cumulative intercept length distributions for gangue phase determined from experiment ($\boldsymbol{\varphi}$=300μm) and Schaap's model

The best fitting values of the parameters were found to be: $k_{max} = 0.000573s^{-1}$, θ=45.52μm, X_m=20.05μm and z=30.00 μm. The value of k_{max} is low compared to the rate constants determined from Klimpel model. The predicted recoveries of the composite feed particles and those determined from experiments are compared in Figure 6-16 and Figure 6-17. Figure 6-16 shows the comparison of the observed and predicted recoveries of particles in each size fraction i at different flotation times, R^{ik}. Figure 6-17 presents the comparison of the observed and predicted overall recoveries for all size fractions at different flotation times, R^k, respectively. It is found that the flotation recoveries R^k during 15-120s were notably underestimated using Schaap's model. It is also seen from Figure 6-16 that the predicted R^{ik}values deviate significantly from the observed recoveries. Figure 6-16 and Figure 6-17 also reveal that Schaap's model does not predict recoveries of comminuted particles produced from high grade ores accurately. The deviation of observed data from model prediction may be due to the high grade nature of the ore and the intercept length distributions not following negative exponential trends.

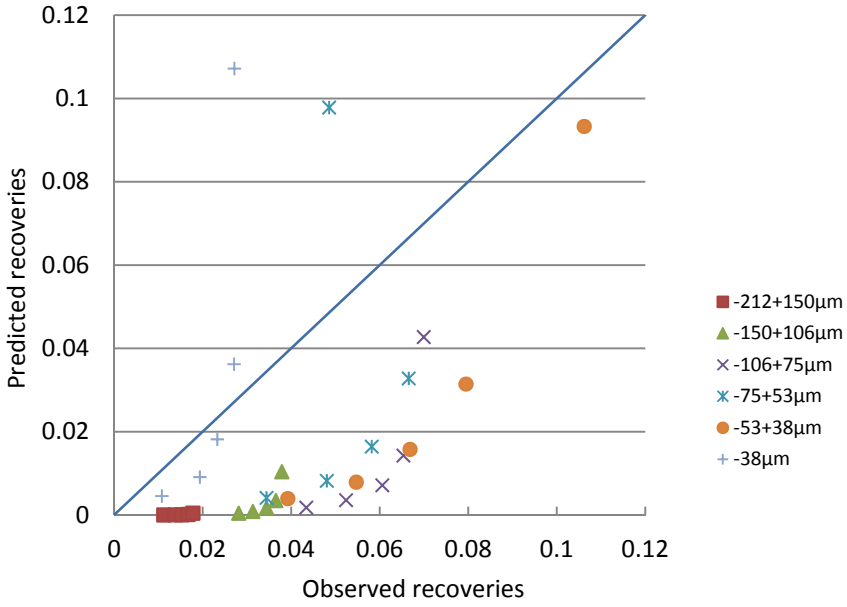

Figure 6-16 Comparison of flotation recoveries of particles in each size fraction ***i*** at different flotation times (15, 30, 60, 120 and 240s) determined from experiments (observed) and predicted from Schaap's model (predicted)

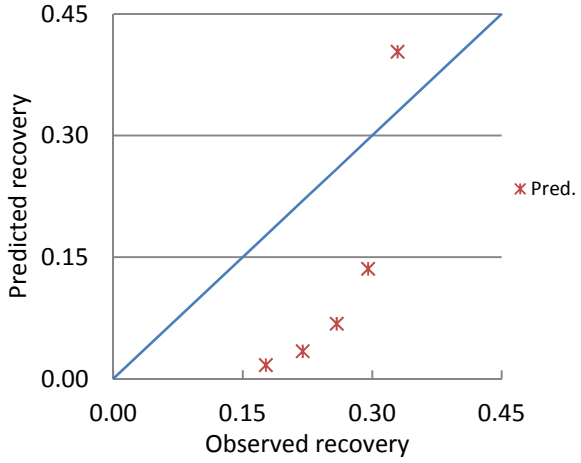

Figure 6-17 Comparison of flotation recoveries of the composite feed particles at different flotation times (15, 30, 60, 120 and 240s) determined from experiments (observed) and predicted from Schaap's model (predicted)

6.5 Discussion and conclusion

In this chapter, a transformation matrix model (Eq. 6-4) to predict flotation performance has been developed. The required model parameters are 1) flotation recoveries r^{ijk} in each size/grade class at different flotation times; 2) grade

distribution of feed particles g^{ji} and 3) size distribution of feed particles $p^i(V)$. r^{ijk} were estimated from batch flotation tests and image analysis technique. g^{ji} were predicted from the proposed liberation models (Eq. 5-27 and Eq. 5-29) based on the information of ore texture and particle structure extracted from the rock and comminuted particles. $p^i(V)$ is the feed size distribution. A characteristic feature of this model is that the impact factors that affect flotation performance have been decoupled. The effect of mineral liberation and particle size on the flotation performance are included in g^{ji} and $p^i(V)$, respectively. The effects of other factors such as flotation reagent scheme and operational parameters (e.g. aeration speed) are quantified in terms of r^{ijk}. However, it was observed that there was a bias in the model predictions when compared the observed data, which may be attributed to stereological factors. This bias may be quantified and corrected by applying a correction factor.

The model parameters evaluated from the observed data for the Klimpel first order model showed considerable variability as the liberation/flotation characteristics are combined. As such, it was not possible to determine any trends in their variation with particle size. Thus, the proposed model is an improvement over the Klimpel model for predictive purposes.

Of the liberation/flotation models published, Schaap's model gives a convenient way of relating the influence of liberation on flotation performance. However, due to inherent assumptions in the model, it was found to be unsuitable for the high grade ore tested.

Chapter 7 Conclusions and recommendations

In order to determine the influence of mineral liberation on flotation performance, it is required to quantify the texture of the ore, the structure and liberation characteristics of the flotation feed and product particles. This thesis describes

a) the development of a methodology to measure ore texture of the parent rock and extent of liberation of comminuted particles;
b) the development of predictive liberation models to quantify the grade distribution of comminuted particles;
c) the comparison of liberation characteristics of feed and floated particles;
d) the development of a model to predict the flotation performance of an ore based on liberation and flotation characteristics of particles in the narrow size/grade classes in the feed.

7.1 Development of measurement technique for extracting information of ore texture and particle structure

The ore texture and particle structure properties were determined through analysing SEM images of the polished sections of the rock and mounted particles. The analysis included the measurement of relevant statistical quantities of the ore texture and particle structure using image analysis software. For this purpose, image analysis techniques were developed using Labview™ software with Vision as described in Chapter 3 and 4. It provides a cheaper and more effective alternative to mineral liberation analyser (MLA) and QEM*SEM techniques that are commonly used in the mining industry.

7.2 Evaluation of liberation characteristics

- Labview™ image analysis software programs were developed to extract the information of ore texture and particle structure information. The ore texture descriptors of the parent rock were:
  a) covariance function
  b) two-point probability function
  c) linear intercept distribution of each phase
  d) phase specific line segment (PSLS) function of each phase.

The structure descriptors of particles were

a) linear intercept length distribution

b) section area distribution

c) proximity function

d) linear/areal grade distribution

In particular, the PSLS function has been introduced to quantify the probability of the particles being fully liberated from the comminution of the parent rock.

- Using the functions evaluated from the image analysis technique, the validity of ore texture and particle structure assumptions in some published liberation models were tested. It is found that:

  a) Finlayson equation density function (Eq. 2-8) used by King does not describe accurately the structure of particles produced from the high grade ore used in this project.

  b) Proximity function (Eq. 2-67) derived from Finlayson equation density function (Eq. 2-8) also failed to describe the structure of comminuted particles in this project.

  c) Covariance function used by Barbery (Eq. 4-17), were found not suitable for the quantification of the texture of the high grade ore used in this work.

7.3 Predictive liberation model

- Predictive liberation models (Eq. 5-24, Eq. 5-27 and Eq. 5-29) that describe the grade distributions of comminuted particles in the three dimensions were developed without assumption of ore texture and particle structure based on a procedure similar to that of Barbery. The models are based on phase specific line segment function $\omega^{(i)}(L)$, proximity function $P(L)$ and covariance function $C(L)$. These functions were evaluated directly from image analysis on the polished sections of parent rock and mounted particles. The grade distribution of comminuted particles was quantified by four parameters (α, β, $\Lambda_1$and Λ_0) from which α , β determine the shape and Λ_1, Λ_0 provide the two ends of the grade distribution curve as shown in Figure 2-1.

- The validity of the proposed liberation models in 1-D, 2-D and 3-D was tested using the high grade sulphide ore. It has been shown in section 5.6 that the areal and linear grade distributions predicted from the proposed models agree closely to those measured from particle sections.
- The proposed predictive liberation models were also compared with other published liberation models. The fractions of fully liberated particles both in 1-D and 2-D predicted by the proposed models are much closer to the measured data than those predicted by Barbery's and King's models. The volumetric fractions of fully liberated particles predicted by the proposed liberation model are slightly higher that those by Barbery's model.

7.4 Liberation/flotation model

- A transformation matrix model (Eq. 6-4) which incorporates the information of mineral liberation, flotation characteristics and particle size in terms of individual matrices was developed to predict the flotation performance. The flotation characteristics r^{ijk} have been quantified through a matrix representing recovery in each size and grade class. r^{ijk} values were estimated from batch flotation tests and image analysis on the flotation feed and products. Liberation characteristics of the feed, g^{ji} was calculated from the proposed predictive liberation models (Eq. 5-27 and Eq. 5-29), while particle size $p^i(V)$ was determined directly from experiments. Once r^{ijk} is established for a given ore/reagent system, it may be used in geometallurgical test work to predict the expected plant performance at the plant design stage.
- This proposed transformation matrix model was tested using a composite feed comprising of a wide size distribution, which is a ground product from the high grade sulphide ore. The recoveries predicted from the proposed transformation matrix model agree well with those from experiments by a linear relationship. The deviation between the predicted and observed recoveries can be quantified using a correction factor.
- The proposed transformation matrix model was compared with other published liberation/flotation models. Schaap's model, originally established for disseminated low grade ores, does not provide good prediction of flotation recoveries as that from the proposed transformation matrix model.

7.5 Recommendations for future work

Following the investigations described in this thesis, several research directions may be suggested for future study:

- Verification of volumetric grade distribution of comminuted particles predicted by the proposed predictive liberation model with that measured from particles using other ore types (low grade sulphide and also non-sulphide ores) to test the general applicability of the models.
- Extension of the proposed predictive liberation models to multi-component ores.
- Extension of the proposed predictive liberation models by considering grain boundary breakage and/or preferential breakage.
- Extension of the transformation matrix model based on volumetric grade (3-D) to predict flotation performance. Due to the limitation of image analysis, only the linear (1-D) and areal (2-D) measurements were used to establish the characteristic recoveries r^{ijk} of particles. Stereological bias may exist in the transformation matrix model during flotation prediction. Stereological correction may be applied to convert the results from 1-D and 2-D measurements into those in 3-D.

References

Every reasonable effort has been made to acknowledge the owners of copyright material. I would be pleased to hear from any copyright owner who has been omitted or incorrectly acknowledged.

Andrews, J. R. G., and T. S. Mika. 1975. *Proceedings of 11th International Mineral Processing Congress*, *Comminution of a heterogeneous material: development of a model for liberation phenomena*. Cagliari:

Austin, L. G., and R. R. Klimpel. 1986. *SME-AIME Annual Meeting*, *A First Study of Liberation Combined with Breakage Kinetics in a Mill*. New Orleans, Louisiana: SME

Austin, L. G., and P. T. Luckie. 1986. *New Orleans, Louisiana*, *An Assessment of the Problems of Quantifying Mineral Liberation*. Warrendale, PA: The Metallurgical Society of AIME

Austin, L. G., and P. T. Luckie. 1988. The Problems of Quantifying Mineral Liberation: A review. *Particle and Particle Systems Characterization* 5 (3): 122-129.

Barbery, G. 1987. Random sets and integral geometry in comminution and liberation of minerals. *Minerals and Metallurgical Processing* 4 (2): 96-102.

Barbery, G. 1991. *Mineral Liberation-measurement, simulation and practical use in mineral processing*. Quebec.

Barbery, G. 1992. Liberation 1, 2, 3: Theoretical analysis of the effect of space dimension on mineral liberation by size reduction. *Minerals Engineering* 5 (2): 123-141.

Barbery, G., R. Bloise, C. Gateau, and C. Reinhart. 1983. *Proceedings of the First International Congress on Applied Mineralogy, ICAM 81*, *Mineral Liberation Measurements and Their Interpretation*. Johannesburg: Geological Society of South Africa

Barbery, G., and G. Huyet. 1977. Mineral liberation analysis: theoretical study and computer simulation. In *Paper presented at the 106th American Institute of Mining, Metallurgical, and Petroleum Engineers (AIME) Annual Meeting*. Atlanta, Georgia, USA.

Barbery, G., and D. Leroux. 1988. Prediction of particle composition distribution after fragmentation of heterogeneous materials. *International Journal of Mineral Processing* 22 (1-4): 9-24.

Bazin, C., R. Grant, M. Cooper, and R. Tessier. 1994. A method to predict metallurgical performances as a function of fineness of grind. *Minerals Engineering* 7 (10): 1243-1251.

Bodziony, J. 1965a. On the Liberation of Mineral Grains. *Bull. Acad. Polonaise des Sciences, Serie des Sciences Techniques* 13: 513-517.

--------. 1965b. On the possibility of application of integral geometry methods in certain problems of liberation of mineral grains. *Bull. Acad. Polon. Sci* 13: 459-467.

Cauchy, A. 1841. Note sur divers théorèmes relatifs à la rectification des courbes et à la quadrature des surfaces. *C. R. Acad. Sci. Paris* 13: 1060-1063.

Chander, S., and M. Polat. 1994. *Proceedings of the Fourth Meeting of the Southern Hemisphere on Mineral Technology*, *In quest of a more realistic flotation kinetics model*. Concepcion, Chile: University of Concepción

Chayes, F. 1956. *Petrographic Modal Analysis*. New York: John Wiley & Sons.

Chiaruttini, C., L. Piga, and G. Schena. 1999. An assessment of the efficiency of a stereological correction for recovering the volumetric grade of particles from measures on polished sections. *International Journal of Mineral Processing* 57 (4): 303-322.

Çilek, E. C. 2004. Estimation of flotation kinetic parameters by considering interactions of the operating variables. *Minerals Engineering* 17 (1): 81-85.

Cinlar, E., and S. Torquato. 1995. Exact determination of the two-point cluster function for one-dimensional continuum percolation. *Journal of Statistical Physics* 78 (3): 827-839.

Crofton, M. W. 1869. Sur quelques théoremes de calcul intégral. *Comptes Rendus de l'Académie des Sciences* 68: 1469-1470.

Davy, P. 1984. Probability models for liberation. *Journal of Applied Probability* 21 (2): 260-269.

Delbem, I. D., R. Galery, P. R. G. Brandão, and A. E. C. Peres. 2011. *2nd International Seminar on Geology the Mining Industry*, *A 2D mineral liberation analysis and phase recognition system for mineral characterisation*. Antofagasta, Chile: Gecamin

Diao, J., D. W. Fuerstenau, and J. S. Hanson. 1992. *SME-AIME Annual Meeting*, *Kinetics of coal flotation. Reprint Number 92-200*. Phoenix, Arizona: SME

Dowling, E. C. J., R. R. Klimpel, and F. F. Aplan. 1986. *The Reinhardt Schuhmann International Symposium on Innovative Technology and Reactor Design in Extraction Metallurgy*, *Use of kinetic models to analyze industrial flotation circuits*. Colorado, USA: TMS

Enns, E. G., and P. F. Ehlers. 1978. Random Paths through a Convex Region. *Journal of Applied Probability* 15 (1): 144-152.

Fandrich, R. G., C. L. Schneider, and S. L. Gay. 1998. Two stereological correction methods: Allocation method and kernel transformation method. *Minerals Engineering* 11 (8): 707-715.

Fichera, M. A., and M. W. Chudacek. 1992. Batch cell flotation models -- A review. *Minerals Engineering* 5 (1): 41-55.

Finch, J. A., and W. Petruk. 1984. Testing a solution to the King liberation model. *International Journal of Mineral Processing* 12 (4): 305-311.

Finlayson, R. M. 1980. The study and simulation of the behaviour of individual minerals in a grinding circuit, University of Natal

Garcia, D., C. L. Lin, and J. D. Miller. 2009. Quantitative analysis of grain boundary fracture in the breakage of single multiphase particles using X-ray microtomography procedures. *Minerals Engineering* 22 (3): 236-243.

Gaudin, A. M. 1939. *Principles of Mineral Dressing*. New York: McGraw-Hill.

Gay, S. L. 1994. Liberation modelling using particle sections, Department of Mining, Minerals and Materials Engineering, University of Queensland, Brisbane, Australia

Gay, S. L. 1999. Numerical verification of a non-preferential-breakage liberation model. *International Journal of Mineral Processing* 57 (2): 125-134.

Gay, S. L. 2004a. A liberation model for comminution based on probability theory. *Minerals Engineering* 17 (4): 525-534.

--------. 2004b. Simple texture-based liberation modelling of ores. *Minerals Engineering* 17 (11-12): 1209-1216.

Gay, S. L., and J. M. Keith. 2004. Geometric probability based stereological corrections. *Australian and New Zealand Industrial and Applied Mathematics Journal* 45 (E): C618-C631.

Gilbert, E. N. 1962. Random Subdivisions of Space into Crystals. *The Annals of Mathematical Statistics* 33 (2): 958-972.

Gorain, B. K., J. P. Franzidis, K. Ward, N. W. Johnson, and E. V. Manlapig. 2000. Modeling of the Mount Isa rougherscavenger copper flotation circuit using size-by-liberation data. *Minerals and Metallurgical Processing* 17 (3): 173-180.

Guimarães, C., and F. Durão. 2003. 2D simulation model of mineral particles yielded by discriminatory size reduction. *Minerals Engineering* 16 (12): 1339-1348.

Guimarães, C., and F. Durão. 2007. Application of a cellular automata based simulation model of size reduction in mineral processing. *Minerals Engineering* 20 (6): 541-551.

Harris, C. C., and A. Chakravarti. 1970. Semi-batch froth flotation kinetics: species distribution analysis. *Transactions of American Institute of Mining, Metallurgical, and Petroleum Engineers* 247: 162-172.

Herbst, J., K. Rajamani, C. Lin, and J. Miller. 1988. Development of a multicomponent-multisize liberation model. *Minerals Engineering* 1 (2): 97-111.

Hsih, C. S., S. B. Wen, and C. C. Kuan. 1995. An exposure model for valuable components in comminuted particles. *International Journal of Mineral Processing* 43 (3-4): 145-165.

Huber-Panu, I., E. Ene-Danalache, and D. G. Cojocariu. 1976. *Mathematical models of batch and continuous flotation*. Edited by M. C. Fuerstenau. 2 vols. Vol. 2, *Flotation: A. M. Gaudin Memorial*. New York: American Institute of Mining, Metallurgical, and Petroleum Engineers.

Imaizumi, T., and T. Inoue. 1963. *Proceedings of Sixth International Mineral Processing Congress*, *Kinetic considerations of froth flotation*. Cannes: Pergamon

Jackson, B. R., A. F. Reid, and J. C. Wittenberg. 1984. *Proceedings of the Australian Institute of Mining and Metallurgy*, *Technical note-rapid production of high quality polished sections for automated image analysis of minerals*.

Jiao, Y. 2010. Characterization of the Structure of Heterogeneous Materials and Particle Packings, Department of Mechanical and Aerospace Engineering, Princeton University

Jiao, Y., F. H. Stillinger, and S. Torquato. 2009. A superior descriptor of random textures and its predictive capacity. *Proceedings of the National Academy of Sciences* 106 (42): 17634-17639.

Johnson, G. W., and R. Jennings. 2006. *LabVIEW graphical programming*. Fourth ed. New York: McGraw-Hill Professional.

Johnson, N. W. 2005. *Centenary of Flotation Symposium*, *A review of the entrainment mechanism and its modelling in industrial flotation processes*. Brisbane, Australia: Australasian Institute of Mining and Metallurgy (AusIMM)

Jones, M. P. 1987. *Applied mineralogy: a quantitative approach*. London: Graham & Trotman, Limited.

Jones, M. P., and R. Horton. 1979. *Proceeding of the XIth Commonwealth Mining and Metallurgy Congress*, *Recent developments in the stereological assessment of composite (middling) particles by linear measurements*. Hongkong: Institution of Mining and Metallurgy: London

Kaartinen, J. 2009. Machine Vision in Measurement and Control of Mineral Concentration Process, Control Engineering, Helsinki University of Technology, Helsinki

Keith, J. M. 2000. A stereological correction for multiphase particles, JKMRC, University of Queensland, Brisbane

Keith, J. M., and S. L. Gay. 2000. Estimating volume distributions using maximum entropy. *Image Analysis and Stereology* 19: 195-198.

Kelsall, D. F. 1961. Application of probability in the assessment of flotation systems. *Transactions of the Institution of Mining and Metallurgy* 70 (3): 191-204.

King, R. P. 1975a. A quantitative model for mineral libertaion. *Journal of the South African Institute of Mining and Metallurgy* 76 (Special issue, Oct.): 170-172.

King, R. P. 1975b. Simulation of flotation plants. *Transactions of the Society of Mining Engineers of the American Institute of Mining and Metallurgical Engineers* 258 (4): 286-293.

--------. 1976. *The use of simulation in the design and modification of flotation plants*. Edited by M. C. Fuerstenau. Vol. 2, *Flotation: A Gaudin Memorial Volume*. New York: American Institute of Mining, Metallurgical, and Petroleum Engineers.

--------. 1979. A model for the quantitative estimation of mineral liberation by grinding. *International Journal of Mineral Processing* 6 (3): 207-220.

--------. 1982a. Determination of the distribution of size of irregularly shaped particles from measurements on sections or projected areas. *Powder Technology* 32 (1): 87-100.

--------. 1982b. *Proceedings of XIV International Mineral Processing Congress*, *The prediction of mineral liberation from mineralogical texture*. Toronto: Canadian Institute of Mining and Metallurgy

--------. 1983. *Proceedings of the First International Congress on Applied Mineralogy, ICAM 81*, *Stereological methods for the prediction and measurement of mineral liberation*. Johannesburg: Geological Society of South Africa

--------. 1984. Measurement of particle size distribution by image analyser. *Powder Technology* 39 (2): 279-289.

--------. 1990. *Proceedings of the 7th European Symposium on Comminution*, *Calculation of the liberation spectrum in products produced in continuous milling circuits*. Ljubljana: Fakulteta za Naravoslovje in Tehnologijo-Vtozd montanistika

--------. 1994a. Comminution and liberation of minerals. *Minerals Engineering* 7 (2-3): 129-140.

--------. 1994b. Linear stochastic models for mineral liberation. *Powder Technology* 81 (3): 217-234.

--------. 1994c. Quantitative characterization of mineralogical texture by image analysis. In *Process Mineralogy XII: Applications to Environment, Precious Metals, Mineral Beneficiation, Pyrometallurgy, Coal and Refractories*, ed. W. Petruk and A. R. Rule, 189-200. Reno: The Minerals, Metals & Materials Society.

--------. 2001. *Modeling and Simulation of Mineral Processing Systems*. Boston: Butterworth-Heinemann.

King, R. P., and C. L. Schneider. 1998. Stereological correction of linear grade distributions for mineral liberation. *Powder Technology* 98 (1): 21-37.

King, R. P., and P. A. Stirling. 1994. Linear intercept analysis of mineralogical texture. In *Process Mineralogy XII: Applications to Environment, Precious Metals, Mineral Beneficiation, Pyrometallurgy, Coal and Refractories*, ed. W. Petruk and A. R. Rule, 201-211. Reno: The Minerals, Metals & Materials Society.

Klimpel, R. R. 1980. Selection of chemical reagents for flotation. In *Mineral Processing Plant Design*, ed. A. Mular and R. Bhappu, 907–934. New York: AIME.

--------. 1984. Applications of a model for the analysis of liberation from a binary system. *Powder Technology* 39 (1): 117-128.

Klimpel, R. R., and L. G. Austin. 1983. A preliminary model of liberation from a binary system. *Powder Technology* 34 (1): 121-130.

Klinger, T. 2003. *Image processing with LabVIEW and IMAQ Vision*. Upper Saddle River, NJ: Prentice Hall.

Koh, P. T. L., F. P. Hao, L. K. Smith, T. T. Chau, and W. J. Bruckard. 2009. The effect of particle shape and hydrophobicity in flotation. *International Journal of Mineral Processing* 93 (2): 128-134.

Kremer, Y. B., and L. S. Gurevich. 1992. *Proceedings of the First International Conference on Modern Process Mineralogy and Mineral Processing*, *Physico-kinetic join modelling of mineral liberation and flotation*. Beijing, China: International Academic Publishers Beijing, China

Kremer, Y. B., L. S. Gurevich, and L. I. Blekhman. 1993. *XVIII International Mineral Processing Congress*, *Simulation of grinding and mineral liberation processes in industrial circuits: a non-linear model*. Sydney, Australia: Australasian Institute of Mining and Metallurgy

Lai, C. W. 2003. Effects of grain boundary fracturing on particle size distributions and grade variations in comminuted ores. Doctoral Dissertation Department of Resources Engineering, National Cheng Kung University, Tainan, China

Laslett, G. M., D. N. Sutherland, P. Gottlieb, and N. R. Allen. 1990. Graphical assessment of a random breakage model for mineral liberation. *Powder Technology* 60 (2): 83-97.

Lastra, R. 2002. Comparison of liberation determinations by particle area percentage and exposed particle perimeter percentage in a flotation concentrator. *Minerals & Metallurgical Processing* 19 (4): 203-208.

Leigh, G. M., G. J. Lyman, and P. Gottlieb. 1996. Stereological estimates of liberation from mineral section measurements: A rederivation of Barbery's formulae with extensions. *Powder Technology* 87 (2): 141-152.

Lin, C. L., and J. D. Miller. 1996. Cone beam X-ray microtomography for three-dimensional liberation analysis in the 21st century. *International Journal of Mineral Processing* 47 (1-2): 61-73.

Lin, C. L., J. D. Miller, J. A. Herbst, and K. Rajamani. 1987. Comparison of Methods for the Measurement of Linear Grade Distributions in Liberation Analysis. *Particle and Particle Systems Characterization* 4 (1-4): 78-82.

Lin, D., C. O. Gomez, and J. A. Finch. 1994. Test of Barbery's liberation correction procedure. *Transactions of the Institution of Mining and Metallurgy. Section C. Mineral Processing and Extractive Metallurgy* 103: C91-C96.

Lu, B., and S. Torquato. 1992. Lineal-path function for random heterogeneous materials. *Physical Review A* 45 (2): 922-929.

Lynch, A. J. 1977. *Mineral Crushing and Grinding Circuits. Their simulation, optimization, design and control.* Edited by D. W. Fuerstenau. Vol. 1, *Developments in Mineral Processing*. Amsterdam: Elsevier Scientific Publishing Company.

Lynch, A. J., N. W. Johnson, E. V. Manlapig, and C. G. Thome. 1981. Mineral and Coal Flotation Circuits: Their Simulation and Control. In *Development in Mineral Processing*, ed. D. W. Fuerstenau, 291. New York: Elsevier.

Lynch, A. J., and S. S. Narayanan. 1986. Simulation-the design tool for the future. In *Mineral Processing at a Crossroads: Problems and Prospects*, ed. B. A. Wills and R. W. Barley, 89-116. Dordrecht, the Netherlands: Martinus Nijhoff Publishers in cooperation with North Atlantic Treaty Organization, Scientific Affairs Division.

Madureira, C. M. N., M. R. M. Leite, A. A. T. Cavalheiro, and J. Silva. 1988. *Proceedings of the XVI International Mineral Processing Congress.*, *Size, Grade and Liberation: A Stochastic Approach to the Fundamental Problem of Mineral Processing*. Stockholm, Sweden: Elsevier

Marto, M. H., J. H. Gonçalves, and M. J. Matos. 2004. Mathematical Description of the Composition Distribution of Comminuted Polyphase Materials. *Materials Science Forum* 455 - 456: 866-870.

Matheron, G. 1993. Une conjecture sur covariance d'un ensemble aleatoire. *Cahiers de Géostatistique* 107: 107-113.

Matos, M. J., J. H. Goncalves, and M. H. Marto. 2004. Testing incomplete Beta function to describe composition of real unliberated particles. *Mineral Processing and Extractive Metallurgy* 113 (2): 121-128.

McIvor, R. E., and J. A. Finch. 1991. A guide to interfacing of plant grinding and flotation operations. *Minerals Engineering* 4 (1): 9-23.

Meloy, T. P., and K. Gotoh. 1985. Liberation in a homogeneous two-phase ore. *International Journal of Mineral Processing* 14 (1): 45-55.

Miller, J. D., and C. L. Lin. 1997. Direct three-dimensional liberation analysis by cone beam x-ray microtomography. In *Comminution Practices*, ed. S. K. Kawatra, 85-91. Littleton, CO: Society for Mining, Metallurgy, and Exploration.

--------. 2002. Cone beam X-ray microtomography - a new facility for three-dimensional analysis of multiphase materials. *Minerals and Metallurgical Processing* 19 (2): 65-71.

Miller, J. D., and C. L. Lin. 2003. *XXII International Mineral Processing Congress*, *3D analysis of particulates in mineral processing systems by cone beam X-ray microtomography*. Cape Town, South Africa: South African Institute of Mining & Metallurgy (SAIMM)

Miller, J. D., and C. L. Lin. 2004. Three dimensional analysis of particulates in mineral processing systems by cone beam X-ray microtomography. *Minerals and Metallurgical Processing* 21 (3): 113-124.

Miller, J. D., C. L. Lin, and A. Cortes. 1992. Applications of X-ray computed tomography in particulate systems. *Kona* 10: 88-95.

Miller, J. D., C. L. Lin, and A. B. Cortes. 1990. A Review of X-Ray Computed Tomography and Its Applications in Mineral Processing. *Mineral Processing and Extractive Metallurgy Review: An International Journal* 7 (1): 1-18.

Miller, J. D., C. L. Lin, L. Hupka, and M. I. Al-Wakeel. 2009. Liberation-limited grade/recovery curves from X-ray micro CT analysis of feed material for the evaluation of separation efficiency. *International Journal of Mineral Processing* 93 (1): 48-53.

Miller, P. R., A. F. Reid, and M. A. Zuiderwyk. 1982. *XIV International Mineral Processing Congress*, *QEM*SEM image analysis in the determination of modal assays, mineral associations and mineral liberation*. Toronto, Canada:

Minkowski, H. 1903. Volumen und Oberfläche. *Mathematische Annalen* 57 (4): 447-495.

Moen, K. 2006. Quantitative measurements of mineral microstructure, Department of Geology and Mineral Resources Engineering, Norwegian University of Science and Technology

Morizot, G., P. Conil, M. V. Durance, and F. Gourram Badri. 1997. Liberation and its role in flotation-based flowsheet development. *International Journal of Mineral Processing* 51 (1-4): 39-49.

Napier-Munn, T. J., S. Morrell, R. D. Morrison, and T. Kojovic. 1996. *Mineral Comminution Circuits. Their operation and optimisation*. Edited by T. J. Napier-Munn, *JKMRC Monograph Series in Mining and Mineral Processing*. Brisbane: Julius Kruttschnitt Mineral Research Centre, The University of Queensland.

Neumann, R., and C. L. Schneider. 2001. Prediction of monazite liberation from the silexitic rare earth ore of Catalão I. *Minerals Engineering* 14 (12): 1601-1607.

Niemi, A. J., R. Ylinen, and H. Hyötyniemi. 1997. On characterization of pulp and froth in cells of flotation plant. *International Journal of Mineral Processing* 51 (1-4): 51-65.

Owada, S., T. Ohmiya, R. Oda, and M. Ito. 2004. *Global Symposium On Recycling, Waste Treatment And Clean Technology*, *Creating New Liberation Model Considering Preferential Breakage at Phase Boundaries*. Madrid, Spain: The Minerals, Metals & Materials Society

Polyanin, A. D., and A. V. Manzhirov. 2007. *Handbook of mathematics for engineers and scientists*. Boca Raton: Chapman & Hall/CRC, Taylor and Francis Group.

Qi, G. W. 1993. Use of the QEM*SEM analysis in flotation testwork on a phosphate ore containing monazite. *International Journal of Mineral Processing* 37 (1-2): 89-108.

Qi, G. W., A. Parentich, L. H. Little, and L. J. Warren. 1992. A QEM*SEM study of the flotation of composite particles. *International Journal of Mineral Processing* 34 (1-2): 71-82.

Quintanilla, J. A. 2008. Necessary and sufficient conditions for the two-point phase probability function of two-phase random media. *Proceedings of the Royal Society A: Mathematical, Physical and Engineering Science* 464 (2095): 1761-1779.

Relf, C. G. 2004. *Image acquisition and processing with LabVIEW*. Boca Raton: CRC Press.

Rofe, A. 1995. Flotation of gold bearing pyrite and tellurides in north Kalgurli ores., Department of Minerals Engineering and Extractive Metallurgy, Western Australian School of Mines, Curtin University of Technology, Kalgoorlie

Runge, K. C., J. P. Franzidis, and E. V. Manlapig. 2003. *Proceedings of the XXII International Mineral Processing Congress A study of the flotation characteristics of different mineralogical classes in different streams of an industrial circuit* Cape Town, South Africa: South African Institute of Mining and Metallurgy

Schaap, W. 1979. Illustrated liberation-flotation recovery model for a disseminated mineral in low-grade ore. *Transactions of the Institution of Mining and Metallurgy. Section C, Mineral processing and extractive metallurgy* 88: C220-228.

Schena, G., and C. Chiaruttini. 2001. Reconstruction capability of the kernel-based stereological inversion applied to particle separation techniques. *Computers & Geosciences* 27 (10): 1217-1230.

Schneider, C. L. 1995. Measurement and Calculation of Liberation in Continuous Milling Circuits, Department of Metallurgical Engineering University of Utah, Salt Lake City

Schneider, C. L., C. L. Lin, R. P. King, and J. D. Miller. 1991. Improved transformation technique for the prediction of liberation by a random fracture model. *Powder Technology* 67 (1): 103-111.

Schneider, C. L., and R. Neumann. 2004. *8th International Congress on Applied mineralogy*, *Experimental verification of the three-phase linear grade distribution prediction method by direct measurement*. Sao paulo: ICAM

Schneider, C. L., R. Neumann, and R. P. King. 2003. *Proceedings of XXII International Mineral Processing Congress*, *Prediction of Liberation from Unbroken 3-phase Texture-a case study on a coal sample*. CapeTown, South Africa: South African Institute of Mining and Metallurgy

Serra, J. P. 1982. *Image analysis and mathematical morphology*. Vol. 1. London: Academic Press.

Stamboliadis, E. T. 2008. The evolution of a mineral liberation model by the repetition of a simple random breakage pattern. *Minerals Engineering* 21 (3): 213-223.

Steiner, H. J. 1973. *Proceeding of X International Mineral Processing Congress*, *Kinetic aspects of the flotation behaviour of locked particles*. London: Institution of Mining and Metallurgy

--------. 1975. *Proceeding of XI International Mineral Processing Congress*, *Liberation kinetics in grinding operations*. Cagliari, Rome: Università, Istituto di arte mineraria e preparazione dei minerali

Stoyan, D. 1979. On the accuracy of lineal analysis. *Biometrical Journal* 21 (5): 439-449.

Subasinghe, G. K. N. 2008. *Proceedings of XXIV International Mineral Processing Congress*, *The Prediction of Flotation Characteristics of a Disseminated Ore Using Ore Texture Data*. Beijing, China: Science Press

Sutherland, D. N. 1989. Batch flotation behaviour of composite particles. *Minerals Engineering* 2 (3): 351-367.

Sutherland, D. N., G. W. Wilkie, and C. R. Johnson. 1989. *Mineralogy-Petrology Symposium Simple prediction of processing characteristics of an ore using QEM*SEM*. Sydney: Australian Institute of Mining and Metallurgy

Thorne, G. C., E. V. Manlapig, J. S. Hall, and A. J. Lynch. 1976. *Modelling of industry sulphide flotation circuit*. Edited by M. C. Fuerstenau. Vol. 2, *Flotation: A Gaudin Memorial Volume*. New York: American Institute of Mining, Metallurgical, and Petroleum Engineers.

Tomlinson, H. S., and M. G. Fleming. 1963. *Proceedings of VI International Mineral Processing Congress*, *Flotation rate studies*. Cannes, France Pergamon Press

Torquato, S. 2002. *Random heterogeneous materials: microstructure and macroscopic properties*. Edited by S. S. Antman, J. E. Marsden, L. Sirovich and S. Wiggins, *Interdisciplinary Applied Mathematics*. New York: Springer-Verlag.

Underwood, E. E. 1970. *Quantitative stereology*: Addison-Wesley Publishing Company.

van den Berg, E. H., A. G. C. A. Meesters, J. A. M. Kenter, and W. Schlager. 2002. Automated separation of touching grains in digital images of thin sections. *Computers & Geosciences* 28 (2): 179-190.

Vassiliev, P. V., H. Ledoux, and C. Gold. 2008. Modeling Ore Texture and Mineral Liberation Using 3D Voronoi Diagrams. In *Proceedings of the International Conference on Numerical Geometry, Grid Generation and Scientific Computing*, edited by V. A. Garanzha, Y. G. Evtushenko, B. K. Soni and N. P. Weatherhill. Moscow. Russian Academy of Sciences.

Videla, A. R., C. L. Lin, and J. D. Miller. 2007. 3D characterization of individual multiphase particles in packed particle beds by X-ray microtomography (XMT). *International Journal of Mineral Processing* 84 (1-4): 321-326.

Wang, W. 2008. Rock Particle Image Segmentation and Systems. In *Pattern Recognition Techniques, Technology and Applications*, ed. P. Y. Yin, 197-226. InTech.

Wang, W. 2010. The flotation of coarse composite particles Ian Wark Research Institute, University of South Australia, Adelaide

Wei, X., and S. Gay. 1999. Liberation modelling using a dispersion equation. *Minerals Engineering* 12 (2): 219-227.

Wen, S. B., C. S. Hsih, and C. C. Kuan. 1996. The application of a mineral exposure model in a gold leaching operation. *International Journal of Mineral Processing* 46 (3-4): 215-230.

Wiegel, R. L. 1964. *Proceedings of VIIth International Mineral Processing Congress.*, *A quantitative approach to mineral liberation*. New York: Preprints volume Gordon and Breach

--------. 1975. Liberation in Magnetic Iron Formation. *Trans SME, AIME* 258: 247-256.

--------. 1976. Integrated size-reduction-mineral liberation model. *Trans SME, AIME* 260: 147-152.

--------. 2002. Size reduction/mineral liberation simulation for a magnetic taconite concentrator. *Minerals & Metallurgical Processing* 19 (3): 113-122.

--------. 2006. The Rationale behind the Development of One Model Describing the Size Reduction/Liberation of Ores. In *Advances in Comminution*, ed. K. S. Kawatra, 225-242. Littleton, CO.: Society for Mining and Engineering.

--------. 2010. Comparison of volumetric and section area particle compositions using the Gaudin random mineral liberation model *Minerals & Metallurgical Processing* 27 (1): 24-33.

Wiegel, R. L., and K. Li. 1967. A random model for mineral liberation by size reduction. *Trans SME, AIME* 238: 179-189.

Wightman, E., C. Evans, D. Bradshaw, and E. Manlapig. 2010. *XXV International Mineral Processing Congress*, *Predicting flotation response from liberation information*. Brisbane, Australia: Australasian Institute of Mining and Metallurgy

Yingling, J. C. 1991. Liberation model for multi-component ores. *Minerals and Metallurgical Processing* 8 (2): 65-72.

Young, D. 2002. Influence of Mineral Liberation on the Flotation Characteristics of a Disseminated Ore, Extractive Metallurgy, Murdoch University, Perth, West Australia

Yuan, X. M., B. I. Palsson, and K. S. E. Forssberg. 1996. Statistical interpretation of flotation kinetics for a complex sulphide ore. *Minerals Engineering* 9 (4): 429-442.

Publications based on this work

Based on Chapter 4:

Zhang, J. and N. Subasinghe. 2012. Extracting ore texture information using image analysis. *Mineral Processing and Extractive Metallurgy (IMM Transactions section C)* 121(3), 123-130

Zhang, J. and N. Subasinghe. 2012. Testing the validity of ore texture descriptors used in mineral liberation modelling. *XXVI International Mineral Processing Congress* 6069-6086. New Delhi, India: The Indian Institute of Mineral Engineers.

Based on Chapter 5:

Zhang, J. and N. Subasinghe. Prediction of mineral liberation characteristics of comminuted particles of high grade ores. (submitted)

Appendices

A. Derivation of $E(L^n)$ based on assumption of King Particles.

$$E(L^n) = \int_0^{\infty} L^n i(L) dL$$

where $(L) = \begin{cases} \frac{1}{aD}(2 - \frac{L}{aD})e^{(-\frac{L}{aD})}, & 0 \le L < aD \\ 0, & L \ge aD \end{cases}$.

First of all, an integration formula is introduced here (Polyanin and Manzhirov 2007) (p. 283. Ch. 7).

$$\int P_n(x)e^{ax}dx = e^{ax}\left[\frac{P_n(x)}{a} - \frac{P_n{}'(x)}{a^2} + \cdots + (-1)\frac{P_n{}^n(x)}{a^{n+1}}\right] + C$$

a and C are constants. $P_n(x)$ is a polynomial. It is straightforward that:

$$E(L^n) = \int_0^{\infty} L^n i(L) dL = \int_0^{aD} L^n \frac{1}{aD}(2 - \frac{L}{aD})e^{(-\frac{L}{aD})}dL$$

Changing the variable of integration with $\frac{L}{aD} = x$, then $L = aDx$ and it gives,

$$E(L^n) = \int_0^1 (aDx)^n \frac{1}{aD}(2 - x)e^{(-x)}d(aDx) = (aD)^n \int_0^1 x^n(2 - x)e^{-x}dx$$

Let $T_n(x) = \int_0^1 x^n e^{-x}dx$, we have:

$$E(L^n) = (aD)^n\ (2T_n(x) - T_{n+1}(x))$$

In particular, substituting $n = 1$ into the above equation and using equation $\int P_n(x)e^{ax}dx = e^{ax}\left[\frac{P_n(x)}{a} - \frac{P_n{}'(x)}{a^2} + \cdots + (-1)\frac{P_n{}^n(x)}{a^{n+1}}\right] + C$, it yields the following relationships:

$$E(L) = aD/e$$

$$E(L^2) = (aD)^2(\frac{6}{e} - 2)$$

$$E(L^3) = (aD)^3(\frac{33}{e} - 12)$$

$$E(L^4) = (aD)^4(\frac{196}{e} - 72)$$

In this way, the average particle volume for King Particles can be obtained.

$$V_p = \frac{\pi}{3}\frac{E(L^4)}{E(L)} = 0.2971(aD)^3$$

B. XRD spectrum of the rock

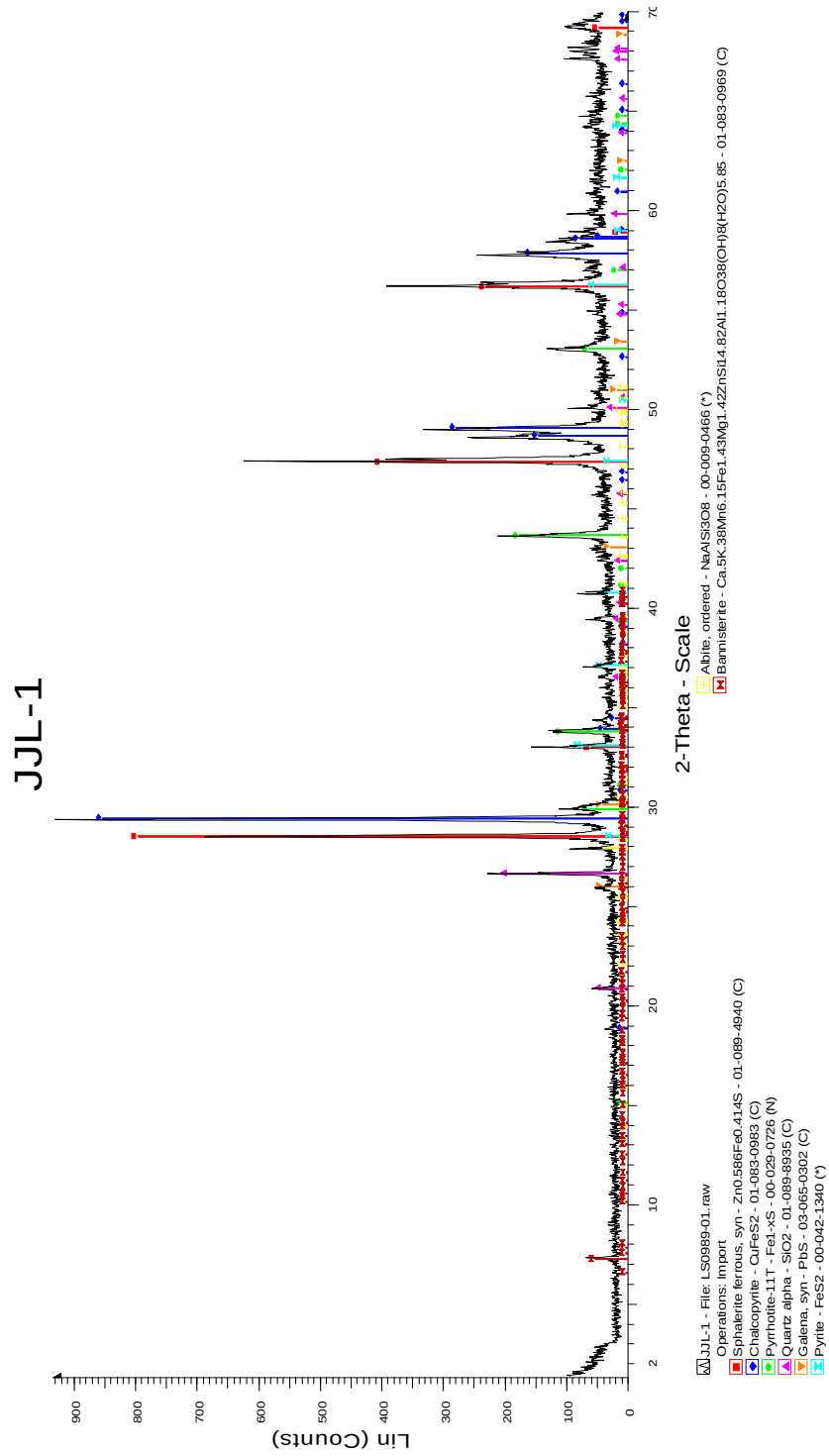

C. Sample block diagram using Labview™ software (block diagram for Point counting)

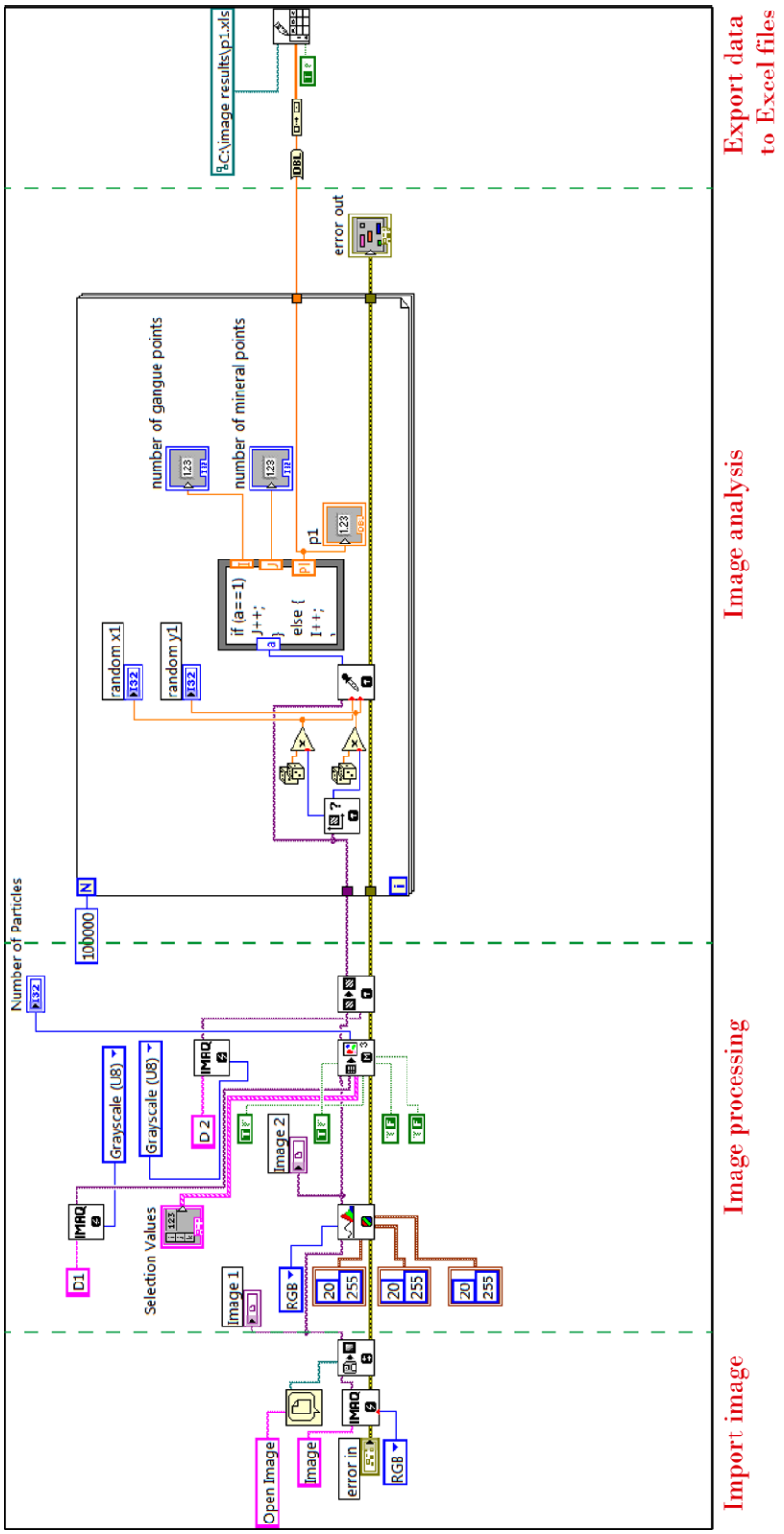

D. Derivation of $P(L) = 1 + \frac{L\int_0^L i(u)du - L - \int_0^L i(u)udu}{E(L)}$

Replacing $\int_0^\infty u\, i(u)du$ with the mean intercept length, $E(L)$ and rewriting $P(L) = \frac{\int_L^\infty i(u)(u-L)du}{\int_0^\infty u\, i(u)du}$ into Eq. 0-1.

$$E(L)P(L) = \int_L^\infty i(u)(u-L)du \qquad \text{Eq. 0-1}$$

Changing the limit of integration of Eq. 0-1 yields

$$E(L)P(L) + \int_0^L i(u)(u-L)du = \int_0^\infty i(u)(u-L)du \qquad \text{Eq. 0-2}$$

The right hand side of Eq. 0-1 can be simplified into $\int_0^\infty i(u)udu + L\int_0^\infty i(u)du$, where the former is $E(L)$ and the latter is L.

Similarly,

$$\int_0^L i(u)(u-L)du = \int_0^L i(u)udu - L\int_0^L i(u)du$$

Thus, after transformation, Eq. 4-29, $P(L) = 1 + \frac{L\int_0^L i(u)du - L - \int_0^L i(u)udu}{E(L)}$, is immediately obtained.

E. Chemical and sulphur analysis results of flotation concentrates and tailings

Sample	Fe(%wt)	Cu(%wt)	Zn(%wt)	S (%wt)	STD of S analysis
Composite feed-C1	32.11	9.11	16.70	44.35	0.97
Composite feed-C2	28.73	9.90	22.04	41.37	1.80
Composite feed-C3	27.99	9.23	24.16	40.61	1.85
Composite feed-C4	27.12	7.94	25.42	43.80	0.49
Composite feed-C5	26.32	6.49	25.38	41.59	0.30
Composite feed-T	28.21	3.85	16.04	25.98	0.98
-250+212µm-C	35.74	4.30	9.71	44.02	2.79
-212+150µm-C1	37.86	2.55	8.81	41.60	1.10
-212+150µm-C2	37.57	3.43	10.11	40.80	0.86
-212+150µm-C3	36.70	4.12	11.29	41.67	0.52
-212+150µm-C4	36.63	4.19	11.03	39.92	0.39
-212+150µm-C5	36.68	4.47	11.57	25.94	1.01
-212+150µm-T	30.42	5.02	16.58	40.27	0.82
-150+106µm-C1	38.28	4.35	9.64	36.96	1.01
-150+106µm-C2	34.15	7.10	15.49	35.21	0.67
-150+106µm-C3	32.56	7.48	17.24	30.81	1.76
-150+106µm-C4	31.73	6.95	17.21	30.31	0.22
-150+106µm-C5	31.57	6.49	16.47	25.47	0.79
-150+106µm-T	31.00	4.77	18.70	41.69	0.42
-106+75µm-C1	36.35	7.13	13.70	35.68	0.40
-106+75µm-C2	31.22	9.71	21.40	34.96	0.89
-106+75µm-C3	29.77	9.23	22.76	32.69	1.42
-106+75µm-C4	28.15	8.56	23.41	33.56	0.88
-106+75µm-C5	27.94	8.36	24.20	33.62	0.97
-106+75µm-T	29.17	3.45	18.39	25.50	0.45
-75+53µm-C1	35.00	8.66	16.19	37.69	1.01
-75+53µm-C2	28.93	11.27	21.29	35.16	1.03

(Continued)

Sample	Fe(%wt)	Cu(%wt)	Zn(%wt)	S (%wt)	STD of S analysis
-75+53µm-C3	27.28	10.49	24.40	33.39	1.18
-75+53µm-C4	26.34	8.76	25.97	30.24	1.42
-75+53µm-C5	25.96	7.10	26.85	29.40	1.91
-75+53µm-C6	26.66	5.58	26.12	27.90	0.24
-75+53µm-T	27.80	1.79	15.94	23.12	0.97
-53+38µm-C1	29.86	11.59	15.50	33.15	1.05
-53+38µm-C2	29.17	12.74	17.26	33.59	0.63
-53+38µm-C3	27.23	12.63	18.83	33.50	0.39
-53+38µm-C4	27.03	10.49	22.27	32.34	0.36
-53+38µm-C5	26.40	8.95	24.74	29.86	0.78
-53+38µm-C6	26.24	7.14	26.04	29.66	0.88
-53+38µm-T	26.91	1.93	18.10	24.30	0.94
-38µm-C1	27.42	11.27	19.05	30.89	0.64
-38µm-C2	26.80	12.30	20.50	31.48	0.68
-38µm-C3	26.18	12.61	21.30	31.60	1.23
-38µm-C4	26.01	10.58	24.53	30.63	0.30
-38µm-C5	25.58	8.86	24.83	29.85	1.02
-38µm-C6	25.90	6.18	24.60	27.60	1.25
-38µm-T	27.10	1.66	16.13	21.99	0.74

*C=concentrate; T=tailing

F. Flotation results of the sulphide ore in each size fraction

	Mass (g)								
Feed size	Flotation time	15s	30s	60s	120s	240s	360s		
	Feed	C1	C2	C3	C4	C5	C6	T	Loss
Composite feed*	1500.0	237.6	54.7	49.9	46.8	27.0	18.8	1010.6	54.6
-250+212μm*	1461.6	11.2	4.0	4.9	5.1	5.4	3.0	1405.1	22.9
-212+150μm*	1739.9	107.0	23.5	13.9	12.7	9.7	5.9	1537.0	30.2
-150+106μm*	1573.4	233.9	24.4	23.4	16.3	10.7	4.7	1222.8	37.2
-106+75μm†	955.1	202.7	38.8	35.3	21.1	20.2	9.6	606.3	21.1
-75+53μm†	1192.1	286.6	110.2	81.1	68.1	50.5	34.7	546.0	14.9
-53+38μm†	1045.2	212.8	80.8	63.9	65.3	74.8	40.7	491.0	15.9
-38μm†	952.6	190.2	147.0	66.9	63.0	67.4	42.0	362.1	14.0

*Flotation tests were replicated 3 times and the concentrates in each concentrate class (e.g. C1) were combined.

† Flotation tests were replicated twice and the concentrates in each concentrate class (e.g. C1) were combined.

G. Sulphides recoveries estimated by volume (%)

	Recovery (%)					
Time(s)	15	30	60	120	240	360
Composite feed	17.68	21.95	25.89	29.53	*	32.94
-212+150µm	5.93	7.29	8.10	8.85	*	9.42
-150+106µm	15.14	16.86	18.52	19.66	*	20.38
-106+75µm	23.02	27.78	32.12	34.65	37.09	38.24
-75+53µm	27.10	37.84	45.83	52.42	57.21	60.42
-53+38µm	22.31	31.12	38.03	45.22	53.50	57.96
-38µm	22.99	41.33	49.75	57.81	66.18	71.16

*The concentrates collected at 240s and 360s were combined together for chemical analysis.

H. Measured linear and areal grade distributions of particles in each size fraction

Linear grade distribution (density):

Grade class	Composite feed	-250+212µm	-212+150µm	-150+106µm	-106+75µm	-75+53µm	-53+38µm	-38µm
0	0.054	0.072	0.053	0.096	0.116	0.081	0.066	0.072
0-0.1	0.020	0.034	0.050	0.037	0.022	0.029	0.042	0.024
0.1-0.2	0.031	0.040	0.037	0.020	0.015	0.038	0.038	0.024
0.2-0.3	0.017	0.016	0.029	0.009	0.008	0.006	0.008	0.023
0.3-0.4	0.009	0.034	0.013	0.021	0.005	0.008	0.008	0.015
0.4-0.5	0.015	0.019	0.020	0.014	0.007	0.005	0.001	0.012
0.5-0.6	0.010	0.022	0.018	0.016	0.007	0.007	0.005	0.021
0.6-0.7	0.011	0.019	0.024	0.014	0.006	0.005	0.005	0.018
0.7-0.8	0.016	0.034	0.022	0.016	0.012	0.019	0.007	0.041
0.8-0.9	0.024	0.078	0.057	0.035	0.024	0.026	0.016	0.044
0.9-1	0.069	0.171	0.144	0.157	0.095	0.084	0.044	0.087
1	0.723	0.461	0.533	0.563	0.680	0.691	0.759	0.620

Areal grade distribution (density):

Grade class	Composite feed	-250+212µm	-212+150µm	-150+106µm	-106+75µm	-75+53µm	-53+38µm	-38µm
0	0.021	0.084	0.034	0.016	0.042	0.030	0.108	0.021
0-0.1	0.093	0.061	0.087	0.102	0.099	0.095	0.038	0.093
0.1-0.2	0.028	0.046	0.034	0.042	0.018	0.036	0.009	0.028
0.2-0.3	0.026	0.018	0.033	0.018	0.012	0.010	0.007	0.026
0.3-0.4	0.011	0.020	0.018	0.010	0.006	0.005	0.005	0.011
0.4-0.5	0.018	0.026	0.021	0.010	0.006	0.005	0.007	0.018
0.5-0.6	0.016	0.020	0.015	0.014	0.004	0.006	0.007	0.016
0.6-0.7	0.035	0.026	0.023	0.003	0.010	0.005	0.008	0.035
0.7-0.8	0.036	0.028	0.023	0.018	0.011	0.018	0.014	0.036
0.8-0.9	0.071	0.056	0.060	0.046	0.034	0.036	0.043	0.071
0.9-1	0.129	0.192	0.204	0.217	0.155	0.139	0.080	0.082
1	0.536	0.422	0.448	0.504	0.603	0.618	0.675	0.583

I. Measured apparent surface composition of particles in each size fraction

Apparent surface composition (density):

Grade class	Composite feed	-250+212µm	-212+150µm	-150+106µm	-106+75µm	-75+53µm	-53+38µm	-38µm
0	0.080	0.065	0.046	0.088	0.084	0.060	0.022	0.062
0-0.1	0.019	0.062	0.078	0.048	0.043	0.057	0.077	0.051
0.1-0.2	0.025	0.029	0.026	0.019	0.016	0.027	0.030	0.027
0.2-0.3	0.013	0.039	0.026	0.010	0.009	0.016	0.017	0.016
0.3-0.4	0.013	0.052	0.015	0.027	0.008	0.011	0.010	0.015
0.4-0.5	0.014	0.026	0.032	0.017	0.013	0.016	0.021	0.032
0.5-0.6	0.014	0.033	0.031	0.021	0.004	0.030	0.034	0.038
0.6-0.7	0.013	0.049	0.030	0.029	0.018	0.067	0.053	0.042
0.7-0.8	0.019	0.046	0.039	0.071	0.053	0.068	0.042	0.040
0.8-0.9	0.030	0.049	0.118	0.086	0.059	0.094	0.074	0.051
0.9-1	0.237	0.134	0.137	0.143	0.235	0.076	0.093	0.071
1	0.522	0.415	0.423	0.444	0.462	0.480	0.529	0.563

J. Sample of measured data of two-point probability function, $\delta^{(ii)}(L)$

L(μm)	$\delta^{(11)}(L)$	$\delta^{(00)}(L)$	L(μm)	$\delta^{(11)}(L)$	$\delta^{(00)}(L)$
4.94	0.763	0.180	207.48	0.654	0.092
9.88	0.747	0.170	212.42	0.647	0.100
14.82	0.734	0.175	217.36	0.648	0.098
19.76	0.732	0.155	222.30	0.649	0.100
24.70	0.727	0.154	227.24	0.645	0.095
29.64	0.718	0.148	232.18	0.643	0.091
34.58	0.714	0.141	237.12	0.638	0.095
39.52	0.716	0.145	242.06	0.635	0.094
44.46	0.712	0.137	247.00	0.653	0.093
49.40	0.700	0.141	251.94	0.638	0.087
54.34	0.705	0.128	256.88	0.640	0.085
59.28	0.700	0.125	261.82	0.643	0.084
64.22	0.692	0.113	266.76	0.637	0.090
69.16	0.692	0.125	271.70	0.640	0.088
74.10	0.692	0.126	276.64	0.635	0.084
79.04	0.677	0.121	281.58	0.636	0.087
83.98	0.680	0.116	286.52	0.637	0.085
88.92	0.679	0.115	291.46	0.639	0.086
93.86	0.680	0.119	296.40	0.639	0.085
98.80	0.681	0.113	301.34	0.631	0.082
103.74	0.678	0.108	306.28	0.630	0.085
108.68	0.675	0.110	311.22	0.627	0.086
113.62	0.680	0.111	316.16	0.636	0.083
118.56	0.669	0.110	321.10	0.638	0.085
123.50	0.675	0.105	326.04	0.619	0.081
128.44	0.664	0.106	330.98	0.627	0.081
133.38	0.673	0.107	335.92	0.627	0.079
138.32	0.673	0.107	340.86	0.627	0.081
143.26	0.669	0.104	345.80	0.621	0.079
148.20	0.670	0.102	350.74	0.616	0.080
153.14	0.669	0.102	355.68	0.627	0.075
158.08	0.660	0.105	360.62	0.611	0.075
163.02	0.663	0.103	365.56	0.618	0.079
167.96	0.663	0.100	370.50	0.613	0.076
172.90	0.662	0.107	375.44	0.616	0.077
177.84	0.658	0.103	380.38	0.605	0.080
182.78	0.658	0.107	385.32	0.611	0.074
187.72	0.659	0.100	390.26	0.614	0.077
192.66	0.657	0.097	395.20	0.606	0.069
197.60	0.642	0.097	400.14	0.612	0.071
202.54	0.652	0.093	405.08	0.607	0.074

(Continued)

L(μm)	$\delta^{(11)}(L)$	$\delta^{(00)}(L)$	L(μm)	$\delta^{(11)}(L)$	$\delta^{(00)}(L)$
410.02	0.610	0.067	454.48	0.603	0.062
414.96	0.602	0.070	459.42	0.606	0.061
419.90	0.614	0.070	464.36	0.608	0.061
424.84	0.616	0.073	469.30	0.603	0.064
429.78	0.610	0.066	474.24	0.593	0.063
434.72	0.608	0.066	479.18	0.599	0.063
439.66	0.611	0.067	484.12	0.619	0.059
444.60	0.606	0.067	489.06	0.598	0.062
449.54	0.609	0.060	494.00	0.607	0.058

K. Sample of measured data of proximity function, $P(L)$, for each size fraction

L(μm)	$P(L)$			
	Composite feed	**-250+212μm**	**-212+150μm**	**-150+106μm**
4.94	0.908	0.952	0.937	0.914
9.88	0.828	0.907	0.879	0.842
14.82	0.754	0.867	0.828	0.768
19.76	0.681	0.824	0.772	0.692
24.70	0.617	0.790	0.721	0.622
29.64	0.556	0.751	0.670	0.563
34.58	0.500	0.712	0.625	0.505
39.52	0.445	0.682	0.580	0.446
44.46	0.397	0.648	0.537	0.390
49.40	0.355	0.613	0.491	0.346
54.34	0.317	0.584	0.456	0.304
59.28	0.277	0.554	0.419	0.261
64.22	0.250	0.526	0.379	0.224
69.16	0.223	0.495	0.342	0.190
74.10	0.197	0.471	0.315	0.165
79.04	0.175	0.444	0.283	0.139
83.98	0.153	0.419	0.251	0.114
88.92	0.136	0.395	0.228	0.093
93.86	0.120	0.371	0.199	0.080
98.80	0.105	0.349	0.178	0.065
103.74	0.092	0.330	0.157	0.054
108.68	0.083	0.309	0.135	0.043
113.62	0.070	0.290	0.122	0.034
118.56	0.062	0.272	0.104	0.028
123.50	0.055	0.254	0.087	0.024
128.44	0.048	0.238	0.075	0.019
133.38	0.040	0.224	0.066	0.016
138.32	0.038	0.205	0.055	0.012
143.26	0.033	0.192	0.044	0.011
148.20	0.028	0.181	0.040	0.008
153.14	0.025	0.168	0.033	0.007
158.08	0.021	0.156	0.027	0.006
163.02	0.017	0.146	0.022	0.004
167.96	0.016	0.135	0.019	0.004
172.90	0.013	0.130	0.015	0.003
177.84	0.011	0.120	0.013	0.003
182.78	0.010	0.113	0.010	0.002
187.72	0.009	0.104	0.008	0.002
192.66	0.007	0.097	0.006	0.001

(Continued)

L(μm)	$P(L)$			
	Composite feed	**-250+212μm**	**-212+150μm**	**-150+106μm**
197.60	0.007	0.093	0.005	0.001
202.54	0.006	0.088	0.004	0.001
207.48	0.005	0.079	0.004	0.001
212.42	0.004	0.077	0.002	0.001
217.36	0.004	0.071	0.002	0.001
222.30	0.003	0.068	0.002	0
227.24	0.003	0.065	0.001	0
232.18	0.003	0.060	0.001	0
237.12	0.002	0.056	0.001	0
242.06	0.002	0.056	0.001	0
247.00	0.001	0.052	0.001	0
251.94	0.002	0.051	0	0
256.88	0.001	0.047	0	0
261.82	0.001	0.044	0	0
266.76	0.001	0.041	0	0
271.70	0.001	0.041	0	0
276.64	0.001	0.040	0	0
281.58	0.001	0.036	0	0
286.52	0.001	0.034	0	0
291.46	0.001	0.033	0	0
296.40	0	0.031	0	0
301.34	0	0.031	0	0
306.28	0	0.029	0	0
311.22	0.001	0.029	0	0
316.16	0	0.027	0	0
321.10	0	0.028	0	0
326.04	0	0.026	0	0
330.98	0	0.024	0	0
335.92	0	0.023	0	0
340.86	0	0.023	0	0
345.80	0	0.022	0	0
350.74	0	0.021	0	0
355.68	0	0.021	0	0
360.62	0	0.019	0	0
365.56	0	0.019	0	0
370.50	0	0.018	0	0
375.44	0	0.017	0	0
380.38	0	0.017	0	0
385.32	0	0.015	0	0
390.26	0	0.016	0	0
395.20	0	0.015	0	0

(Continued)

L(μm)	$P(L)$			
	Composite feed	**-250+212μm**	**-212+150μm**	**-150+106μm**
400.14	0	0.014	0	0
405.08	0	0.013	0	0
410.02	0	0.012	0	0
414.96	0	0.011	0	0
419.90	0	0.012	0	0
424.84	0	0.011	0	0
429.78	0	0.010	0	0
434.72	0	0.010	0	0
439.66	0	0.009	0	0
444.60	0	0.008	0	0
449.54	0	0.007	0	0
454.48	0	0.007	0	0
459.42	0	0.007	0	0
464.36	0	0.007	0	0
469.30	0	0.006	0	0
474.24	0	0.005	0	0
479.18	0	0.006	0	0
484.12	0	0.005	0	0
489.06	0	0.004	0	0
494.00	0	0.004	0	0

L(μm)	-106+75μm	L(μm)	-75+53μm	L(μm)	-53+38μm	L(μm)	-38μm
	$P(L)$		$P(L)$		$P(L)$		$P(L)$
3.08	0.920	2.05	0.897	1.22	0.887	0.61	0.889
6.16	0.848	4.09	0.810	2.45	0.785	1.22	0.793
9.24	0.788	6.14	0.730	3.67	0.699	1.83	0.706
12.32	0.725	8.19	0.651	4.90	0.617	2.44	0.625
15.40	0.663	10.23	0.586	6.12	0.545	3.05	0.555
18.48	0.601	12.28	0.523	7.35	0.477	3.66	0.490
21.56	0.550	14.32	0.464	8.57	0.414	4.28	0.429
24.64	0.502	16.37	0.409	9.79	0.359	4.89	0.382
27.72	0.455	18.42	0.360	11.02	0.315	5.50	0.340
30.80	0.408	20.46	0.317	12.24	0.272	6.11	0.301
33.88	0.365	22.51	0.276	13.47	0.240	6.72	0.267
36.96	0.330	24.56	0.241	14.69	0.207	7.33	0.239
40.04	0.294	26.60	0.211	15.92	0.179	7.94	0.210
43.12	0.261	28.65	0.183	17.14	0.156	8.55	0.189
46.20	0.232	30.69	0.158	18.36	0.136	9.16	0.170
49.28	0.204	32.74	0.133	19.59	0.117	9.77	0.154
52.36	0.179	34.79	0.115	20.81	0.103	10.38	0.137
55.44	0.157	36.83	0.096	22.04	0.089	10.99	0.122
58.52	0.137	38.88	0.079	23.26	0.076	11.60	0.109
61.60	0.123	40.93	0.067	24.49	0.064	12.22	0.095
64.68	0.105	42.97	0.056	25.71	0.056	12.83	0.088
67.76	0.094	45.02	0.049	26.93	0.051	13.44	0.078
70.84	0.080	47.06	0.039	28.16	0.041	14.05	0.068
73.92	0.069	49.11	0.031	29.38	0.036	14.66	0.063
77.00	0.061	51.16	0.026	30.61	0.032	15.27	0.052
80.08	0.052	53.20	0.022	31.83	0.027	15.88	0.049
83.16	0.044	55.25	0.017	33.05	0.025	16.49	0.045
86.24	0.040	57.30	0.014	34.28	0.022	17.10	0.039
89.32	0.034	59.34	0.011	35.50	0.019	17.71	0.035
92.40	0.031	61.39	0.009	36.73	0.017	18.32	0.030
95.48	0.024	63.43	0.007	37.95	0.015	18.93	0.028
98.56	0.022	65.48	0.006	39.18	0.012	19.54	0.024
101.64	0.020	67.53	0.004	40.40	0.011	20.15	0.022
104.72	0.017	69.57	0.003	41.62	0.009	20.77	0.021
107.80	0.015	71.62	0.003	42.85	0.008	21.38	0.018
110.88	0.013	73.67	0.002	44.07	0.009	21.99	0.017
113.96	0.011	75.71	0.002	45.30	0.007	22.60	0.014
117.04	0.010	77.76	0.002	46.52	0.006	23.21	0.014

(Continued)

L(μm)	-106+75μm	L(μm)	-75+53μm	L(μm)	-53+38μm	L(μm)	-38μm
	$P(L)$		$P(L)$		$P(L)$		$P(L)$
120.12	0.009	79.80	0.001	47.75	0.005	23.82	0.012
123.20	0.008	81.85	0.001	48.97	0.005	24.43	0.011
126.28	0.007	83.90	0	50.19	0.004	25.04	0.009
129.36	0.006	85.94	0.001	51.42	0.004	25.65	0.009
132.44	0.006	87.99	0	52.64	0.003	26.26	0.008
135.52	0.005	90.04	0	53.87	0.003	26.87	0.007
138.60	0.004	92.08	0	55.09	0.003	27.48	0.006
141.68	0.004	94.13	0	56.32	0.003	28.09	0.006
144.76	0.003	96.17	0	57.54	0.003	28.71	0.006
147.84	0.003	98.22	0	58.76	0.002	29.32	0.004
150.92	0.002	100.27	0	59.99	0.002	29.93	0.004
154.00	0.002	102.31	0	61.21	0.002	30.54	0.004
157.08	0.002	104.36	0	62.44	0.001	31.15	0.003
160.16	0.002	106.41	0	63.66	0.002	31.76	0.003
163.24	0.002	108.45	0	64.89	0.001	32.37	0.003
166.32	0.001	110.50	0	66.11	0.001	32.98	0.003
169.40	0.001	112.54	0	67.33	0.001	33.59	0.002
172.48	0.001	114.59	0	68.56	0.001	34.20	0.002
175.56	0.001	116.64	0	69.78	0.001	34.81	0.002
178.64	0.001	118.68	0	71.01	0.001	35.42	0.002
181.72	0.001	120.73	0	72.23	0.001	36.03	0.001
184.80	0.001	122.78	0	73.46	0.001	36.65	0.002
187.88	0	124.82	0	74.68	0.001	37.26	0.001
190.96	0	126.87	0	75.90	0.001	37.87	0.001
194.04	0	128.91	0	77.13	0.001	38.48	0.001
197.12	0	130.96	0	78.35	0	39.09	0.001
200.20	0	133.01	0	79.58	0	39.70	0.001
203.28	0	135.05	0	80.80	0	40.31	0.001
206.36	0	137.10	0	82.02	0	40.92	0.001
209.44	0	139.15	0	83.25	0	41.53	0.001
212.52	0	141.19	0	84.47	0	42.14	0.001
215.60	0	143.24	0	85.70	0	42.75	0.001
218.68	0	145.28	0	86.92	0	43.36	0.001
221.76	0	147.33	0	88.15	0	43.97	0.001
224.84	0	149.38	0	89.37	0	44.58	0.001
227.92	0	151.42	0	90.59	0	45.20	0.001
231.00	0	153.47	0	91.82	0	45.81	0
234.08	0	155.52	0	93.04	0	46.42	0

(Continued)

L(μm)	-106+75μm	L(μm)	-75+53μm	L(μm)	-53+38μm	L(μm)	-38μm
	$P(L)$		$P(L)$		$P(L)$		$P(L)$
237.16	0	157.56	0	94.27	0	47.03	0
240.24	0	159.61	0	95.49	0	47.64	0
243.32	0	161.65	0	96.72	0	48.25	0
246.40	0	163.70	0	97.94	0	48.86	0
249.48	0	165.75	0	99.16	0	49.47	0
252.56	0	167.79	0	100.39	0	50.08	0

L. Sample of measured data of $\omega^{(i)}(L)$ and $\omega^{(i)}(A)$

L(μm)	Line			Square			Circular	
	$\omega^{(1)}(L)$	$\omega^{(0)}(L)$	$\sqrt{A}$ (μm)	$\omega^{(1)}(A)$	$\omega^{(0)}(A)$	$\sqrt{A}$ (μm)	$\omega^{(1)}(A)$	$\omega^{(0)}(A)$
4.94	0.762	0.175	4.94	0.750	0.210	9.73	0.722	0.183
9.88	0.747	0.168	9.88	0.717	0.180	18.46	0.686	0.151
14.82	0.735	0.161	14.82	0.698	0.160	27.04	0.643	0.130
19.76	0.718	0.156	19.76	0.673	0.146	35.80	0.607	0.116
24.70	0.715	0.148	24.70	0.653	0.134	44.46	0.569	0.100
29.64	0.700	0.143	29.64	0.625	0.122	53.29	0.544	0.087
34.58	0.694	0.133	34.58	0.610	0.111	62.02	0.516	0.080
39.52	0.678	0.122	39.52	0.586	0.101	70.87	0.492	0.077
44.46	0.676	0.124	44.46	0.572	0.096	79.61	0.469	0.076
49.40	0.665	0.122	49.40	0.547	0.091	88.40	0.445	0.066
54.34	0.644	0.114	54.34	0.528	0.089	97.09	0.411	0.065
59.28	0.637	0.111	59.28	0.514	0.083	105.94	0.394	0.058
64.22	0.626	0.107	64.22	0.495	0.079	114.66	0.375	0.058
69.16	0.613	0.103	69.16	0.483	0.073	123.39	0.353	0.055
74.10	0.613	0.103	74.10	0.470	0.072	132.12	0.338	0.057
79.04	0.599	0.100	79.04	0.458	0.068	140.84	0.317	0.054
83.98	0.591	0.096	83.98	0.438	0.067	149.65	0.296	0.050
88.92	0.599	0.097	88.92	0.430	0.062	158.39	0.287	0.048
93.86	0.583	0.091	93.86	0.414	0.065	167.11	0.273	0.049
98.80	0.578	0.088	98.80	0.403	0.059	175.88	0.256	0.044
103.74	0.560	0.094	103.74	0.382	0.061	184.60	0.241	0.041
108.68	0.561	0.094	108.68	0.378	0.054	193.41	0.223	0.039
113.62	0.542	0.088	113.62	0.369	0.058	202.21	0.214	0.036
118.56	0.540	0.091	118.56	0.351	0.052	210.94	0.204	0.033

(Continued)

L(μm)	Line			Square			Circular	
	$\omega^{(1)}(L)$	$\omega^{(0)}(L)$	$\sqrt{A}$ (μm)	$\omega^{(1)}(A)$	$\omega^{(0)}(A)$	$\sqrt{A}$ (μm)	$\omega^{(1)}(A)$	$\omega^{(0)}(A)$
123.50	0.537	0.087	123.50	0.340	0.051	219.73	0.197	0.033
128.44	0.535	0.082	128.44	0.337	0.052	228.45	0.187	0.033
133.38	0.525	0.079	133.38	0.319	0.049	237.22	0.162	0.028
138.32	0.514	0.081	138.32	0.318	0.045	245.99	0.165	0.029
143.26	0.515	0.083	143.26	0.301	0.047	254.72	0.150	0.025
148.20	0.491	0.079	148.20	0.296	0.044	263.50	0.138	0.022
153.14	0.486	0.077	153.14	0.286	0.042	272.23	0.139	0.021
158.08	0.487	0.078	158.08	0.275	0.040	280.98	0.129	0.021
163.02	0.486	0.074	163.02	0.269	0.039	289.69	0.117	0.021
167.96	0.472	0.078	167.96	0.258	0.038	298.48	0.115	0.017
172.90	0.469	0.075	172.90	0.249	0.039	307.22	0.103	0.019
177.84	0.472	0.072	177.84	0.245	0.033	316.01	0.103	0.017
182.78	0.460	0.071	182.78	0.237	0.034	324.78	0.098	0.015
187.72	0.457	0.071	187.72	0.220	0.034	333.52	0.086	0.014
192.66	0.442	0.070	192.66	0.219	0.032	342.26	0.083	0.014
197.60	0.437	0.075	197.60	0.210	0.028	351.06	0.078	0.011
202.54	0.429	0.070	202.54	0.207	0.023	359.80	0.070	0.010
207.48	0.424	0.071	207.48	0.196	0.025	368.57	0.066	0.010
212.42	0.422	0.066	212.42	0.179	0.024	377.29	0.062	0.010
217.36	0.420	0.061	217.36	0.178	0.021	386.04	0.062	0.009
222.30	0.413	0.069	222.30	0.175	0.019	394.79	0.059	0.008
227.24	0.407	0.065	227.24	0.167	0.019	403.55	0.054	0.007
232.18	0.406	0.067	232.18	0.162	0.020	412.29	0.055	0.006
237.12	0.400	0.064	237.12	0.150	0.015	421.06	0.052	0.005
242.06	0.391	0.066	242.06	0.145	0.014	429.80	0.049	0.004
247.00	0.382	0.066	247.00	0.151	0.016			

(Continued)

L(μm)	Line			Square			Circular	
	$\omega^{(1)}(L)$	$\omega^{(0)}(L)$	$\sqrt{A}$ (μm)	$\omega^{(1)}(A)$	$\omega^{(0)}(A)$	$\sqrt{A}$ (μm)	$\omega^{(1)}(A)$	$\omega^{(0)}(A)$
251.94	0.375	0.063	251.94	0.140	0.012			
256.88	0.378	0.067	256.88	0.137	0.013			
261.82	0.362	0.067	261.82	0.125	0.012			
266.76	0.355	0.064	266.76	0.121	0.011			
271.70	0.363	0.064	271.70	0.120	0.008			
276.64	0.357	0.059	276.64	0.119	0.008			
281.58	0.344	0.060	281.58	0.118	0.006			
286.52	0.346	0.064	286.52	0.117	0.005			
291.46	0.336	0.058	291.46	0.106	0.005			
296.40	0.334	0.056	296.40	0.107	0.005			
301.34	0.321	0.057	301.34	0.102	0.004			
306.28	0.324	0.055	306.28	0.098	0.003			
311.22	0.317	0.057	311.22	0.091	0.004			
316.16	0.316	0.055	316.16	0.088	0.002			
321.10	0.312	0.052	321.10	0.091	0.002			
326.04	0.307	0.056	326.04	0.088	0.001			
330.98	0.295	0.057	330.98	0.081	0.000			
335.92	0.303	0.054	335.92	0.079	0.000			
340.86	0.306	0.053	340.86	0.076	0			
345.80	0.291	0.051	345.80	0.075	0			
350.74	0.283	0.049	350.74	0.065	0			
355.68	0.285	0.052	355.68	0.070	0			
360.62	0.276	0.047	360.62	0.064	0			
365.56	0.266	0.048	365.56	0.060	0			
370.50	0.274	0.050	370.50	0.056	0			
375.44	0.263	0.048	375.44	0.058	0			

(Continued, for $\omega^{(i)}(L)$ only)

L(μm)	Line		L(μm)	Line		L(μm)	Line	
	$\boldsymbol{\omega^{(1)}(L)}$	$\boldsymbol{\omega^{(0)}(L)}$		$\boldsymbol{\omega^{(1)}(L)}$	$\boldsymbol{\omega^{(0)}(L)}$		$\boldsymbol{\omega^{(1)}(L)}$	$\boldsymbol{\omega^{(0)}(L)}$
380.38	0.267	0.045	484.12	0.203	0.030	627.38	0.135	0.020
385.32	0.259	0.048	489.06	0.197	0.031	632.32	0.142	0.018
390.26	0.248	0.043	494.00	0.196	0.029	637.26	0.130	0.018
395.20	0.246	0.042	498.94	0.205	0.026	642.20	0.136	0.020
400.14	0.253	0.041	503.88	0.194	0.029	647.14	0.138	0.019
405.08	0.245	0.042	548.34	0.165	0.029	691.60	0.110	0.015
410.02	0.240	0.039	553.28	0.166	0.024	696.54	0.113	0.017
414.96	0.251	0.037	558.22	0.169	0.022	701.48	0.115	0.014
419.90	0.240	0.040	563.16	0.167	0.024	706.42	0.108	0.013
424.84	0.243	0.038	568.10	0.163	0.027	711.36	0.107	0.014
429.78	0.229	0.040	573.04	0.163	0.024	716.30	0.110	0.016
434.72	0.221	0.036	577.98	0.160	0.026	721.24	0.104	0.016
439.66	0.223	0.037	582.92	0.163	0.025	726.18	0.106	0.014
444.60	0.229	0.033	587.86	0.159	0.022	731.12	0.103	0.013
449.54	0.214	0.035	592.80	0.151	0.025	736.06	0.101	0.015
454.48	0.212	0.035	597.74	0.151	0.023	741.00	0.099	0.014
459.42	0.208	0.033	602.68	0.147	0.023			
464.36	0.217	0.032	607.62	0.153	0.021			
469.30	0.203	0.031	612.56	0.142	0.021			
474.24	0.214	0.033	617.50	0.147	0.023			
479.18	0.205	0.034	622.44	0.143	0.020			
508.82	0.186	0.032	652.08	0.128	0.019			
513.76	0.194	0.029	657.02	0.122	0.020			
518.70	0.182	0.030	661.96	0.127	0.018			
523.64	0.185	0.027	666.90	0.124	0.018			
528.58	0.180	0.025	671.84	0.123	0.015			
533.52	0.180	0.025	676.78	0.121	0.017			
538.46	0.175	0.025	681.72	0.117	0.017			
543.40	0.166	0.026	686.66	0.116	0.015			

M. Sample of measured data of linear intercept length distribution $i(L)$ for each size fraction

L/D	-250+212µm	L/D	-212+150µm	L/D	-150+106µm
0.026	0.012	0.014	0.024	0.031	0.027
0.034	0.008	0.018	0.016	0.042	0.019
0.043	0.014	0.023	0.019	0.052	0.023
0.052	0.010	0.028	0.012	0.063	0.016
0.060	0.009	0.032	0.011	0.073	0.016
0.069	0.011	0.037	0.011	0.084	0.016
0.077	0.008	0.041	0.008	0.094	0.012
0.086	0.010	0.046	0.008	0.104	0.012
0.094	0.008	0.050	0.008	0.115	0.010
0.103	0.010	0.055	0.008	0.125	0.012
0.112	0.010	0.060	0.008	0.136	0.013
0.120	0.009	0.064	0.009	0.146	0.010
0.129	0.010	0.069	0.007	0.157	0.010
0.137	0.008	0.073	0.006	0.167	0.008
0.146	0.009	0.078	0.007	0.178	0.009
0.155	0.008	0.083	0.007	0.188	0.009
0.163	0.009	0.087	0.006	0.198	0.007
0.172	0.007	0.092	0.006	0.209	0.008
0.180	0.008	0.096	0.006	0.219	0.007
0.189	0.008	0.101	0.005	0.230	0.007
0.197	0.008	0.106	0.006	0.240	0.007
0.206	0.010	0.110	0.005	0.251	0.006
0.215	0.010	0.115	0.005	0.261	0.007
0.223	0.009	0.119	0.006	0.272	0.006
0.232	0.010	0.124	0.006	0.282	0.007
0.240	0.007	0.129	0.005	0.292	0.007
0.249	0.008	0.133	0.004	0.303	0.006
0.257	0.007	0.138	0.006	0.313	0.006
0.266	0.009	0.142	0.005	0.324	0.006
0.275	0.008	0.147	0.005	0.334	0.006
0.283	0.007	0.151	0.004	0.345	0.005
0.292	0.009	0.156	0.005	0.355	0.006
0.300	0.008	0.161	0.004	0.366	0.006
0.309	0.008	0.165	0.006	0.376	0.005
0.318	0.006	0.170	0.005	0.386	0.006
0.326	0.008	0.174	0.005	0.397	0.006
0.335	0.007	0.179	0.005	0.407	0.005
0.343	0.007	0.184	0.005	0.418	0.006
0.352	0.008	0.188	0.005	0.428	0.006
0.360	0.007	0.193	0.005	0.439	0.005

(Continued)

L/D	-250+212µm	L/D	-212+150µm	L/D	-150+106µm
0.369	0.008	0.197	0.005	0.449	0.005
0.378	0.008	0.202	0.005	0.460	0.005
0.386	0.007	0.207	0.005	0.470	0.005
0.395	0.008	0.211	0.004	0.480	0.006
0.403	0.008	0.216	0.004	0.491	0.005
0.412	0.009	0.220	0.004	0.501	0.005
0.421	0.008	0.225	0.004	0.512	0.005
0.429	0.008	0.230	0.005	0.522	0.006
0.438	0.010	0.234	0.005	0.533	0.005
0.446	0.008	0.239	0.004	0.543	0.005
0.455	0.009	0.243	0.005	0.554	0.006
0.463	0.008	0.248	0.004	0.564	0.005
0.472	0.008	0.252	0.005	0.574	0.005
0.481	0.009	0.257	0.004	0.585	0.005
0.489	0.010	0.262	0.005	0.595	0.005
0.498	0.008	0.266	0.004	0.606	0.005
0.506	0.008	0.271	0.005	0.616	0.005
0.515	0.008	0.275	0.005	0.627	0.005
0.524	0.009	0.280	0.004	0.637	0.006
0.532	0.007	0.285	0.005	0.648	0.005
0.541	0.008	0.289	0.004	0.658	0.005
0.549	0.008	0.294	0.005	0.668	0.005
0.558	0.009	0.298	0.005	0.679	0.006
0.566	0.007	0.303	0.004	0.689	0.005
0.575	0.008	0.308	0.004	0.700	0.005
0.584	0.007	0.312	0.004	0.710	0.006
0.592	0.008	0.317	0.005	0.721	0.005
0.601	0.008	0.321	0.005	0.731	0.005
0.609	0.008	0.326	0.004	0.742	0.005
0.618	0.008	0.330	0.005	0.752	0.005
0.627	0.007	0.335	0.004	0.762	0.005
0.635	0.009	0.340	0.004	0.773	0.005
0.644	0.008	0.344	0.004	0.783	0.005
0.652	0.006	0.349	0.005	0.794	0.005
0.661	0.007	0.353	0.004	0.804	0.005
0.669	0.008	0.358	0.004	0.815	0.005
0.678	0.007	0.363	0.004	0.825	0.006
0.687	0.006	0.367	0.004	0.836	0.005
0.695	0.006	0.372	0.004	0.846	0.005
0.704	0.007	0.376	0.005	0.856	0.005
0.712	0.006	0.381	0.004	0.867	0.004
0.721	0.007	0.386	0.006	0.877	0.005

(Continued)

L/D	-250+212µm	L/D	-212+150µm	L/D	-150+106µm
0.730	0.008	0.390	0.005	0.888	0.004
0.738	0.007	0.395	0.004	0.898	0.005
0.747	0.005	0.399	0.005	0.909	0.005
0.755	0.007	0.404	0.005	0.919	0.005
0.764	0.007	0.409	0.005	0.930	0.006
0.772	0.006	0.413	0.004	0.940	0.005
0.781	0.006	0.418	0.005	0.950	0.005
0.790	0.007	0.422	0.005	0.961	0.005
0.798	0.006	0.427	0.004	0.971	0.006
0.807	0.007	0.431	0.005	0.982	0.004
0.815	0.005	0.436	0.004	0.992	0.005
0.824	0.005	0.441	0.005	1.003	0.005
0.833	0.006	0.445	0.005	1.013	0.005
0.841	0.004	0.450	0.006	1.024	0.004
0.850	0.005	0.454	0.004	1.034	0.005
0.858	0.005	0.459	0.004	1.044	0.004
0.867	0.005	0.464	0.005	1.055	0.005
0.875	0.005	0.468	0.005	1.065	0.005
0.884	0.004	0.473	0.004	1.076	0.004
0.893	0.005	0.477	0.004	1.086	0.005
0.901	0.005	0.482	0.005	1.097	0.004
0.910	0.005	0.487	0.005	1.107	0.004
0.918	0.004	0.491	0.005	1.118	0.004
0.927	0.004	0.496	0.005	1.128	0.004
0.936	0.004	0.500	0.004	1.138	0.004
0.944	0.003	0.505	0.004	1.149	0.005
0.953	0.003	0.509	0.004	1.159	0.004
0.961	0.004	0.514	0.005	1.170	0.004
0.970	0.004	0.519	0.004	1.180	0.004
0.978	0.004	0.523	0.005	1.191	0.004
0.987	0.003	0.528	0.005	1.201	0.004
0.996	0.003	0.532	0.005	1.212	0.003
1.004	0.003	0.537	0.005	1.222	0.003
1.013	0.003	0.542	0.004	1.232	0.004
1.021	0.002	0.546	0.005	1.243	0.004
1.030	0.003	0.551	0.004	1.253	0.004
1.039	0.002	0.555	0.004	1.264	0.003
1.047	0.003	0.560	0.004	1.274	0.004
1.056	0.002	0.565	0.005	1.285	0.003
1.064	0.004	0.569	0.004	1.295	0.004
1.073	0.002	0.574	0.005	1.306	0.003
1.081	0.002	0.578	0.005	1.316	0.004

(Continued)

L/D	-250+212µm	L/D	-212+150µm	L/D	-150+106µm
1.090	0.002	0.583	0.005	1.326	0.004
1.099	0.002	0.588	0.004	1.337	0.003
1.107	0.002	0.592	0.004	1.347	0.003
1.116	0.002	0.597	0.005	1.358	0.003
1.124	0.002	0.601	0.004	1.368	0.003
1.133	0.003	0.606	0.005	1.379	0.003
1.142	0.002	0.610	0.004	1.389	0.004
1.150	0.002	0.615	0.004	1.400	0.004
1.159	0.001	0.620	0.004	1.410	0.003
1.167	0.002	0.624	0.005	1.420	0.003
1.176	0.001	0.629	0.004	1.431	0.003
1.184	0.001	0.633	0.004	1.441	0.003
1.193	0.002	0.638	0.004	1.452	0.003
1.202	0.002	0.643	0.004	1.462	0.004
1.210	0.003	0.647	0.005	1.473	0.003
1.219	0.002	0.652	0.004	1.483	0.003
1.227	0.002	0.656	0.003	1.494	0.003
1.236	0.002	0.661	0.004	1.504	0.003
1.245	0.002	0.666	0.004	1.514	0.003
1.253	0.002	0.670	0.004	1.525	0.003
1.262	0.001	0.675	0.004	1.535	0.003
1.270	0.002	0.679	0.004	1.546	0.003
1.279	0.001	0.684	0.003	1.556	0.003
1.287	0.002	0.688	0.004	1.567	0.002
1.296	0.001	0.693	0.004	1.577	0.002
1.305	0.002	0.698	0.003	1.588	0.003
1.313	0.001	0.702	0.004	1.598	0.003
1.322	0.002	0.707	0.003	1.608	0.002
1.330	0.001	0.711	0.003	1.619	0.002
1.339	0.001	0.716	0.003	1.629	0.002
1.348	0.001	0.721	0.004	1.640	0.002
1.356	0.001	0.725	0.003	1.650	0.002
1.365	0.001	0.730	0.003	1.661	0.002
1.373	0.001	0.734	0.003	1.671	0.002
1.382	0.001	0.739	0.003	1.682	0.002
1.390	0.002	0.744	0.003	1.692	0.001
1.399	0.001	0.748	0.003	1.702	0.002
1.408	0.001	0.753	0.004	1.713	0.002
1.416	0.001	0.757	0.003	1.723	0.002
1.425	0.001	0.762	0.003	1.734	0.002
1.433	0.000	0.767	0.003	1.744	0.002
1.442	0.001	0.771	0.003	1.755	0.002

(Continued)

L/D	-250+212µm	L/D	-212+150µm	L/D	-150+106µm
1.451	0.001	0.776	0.003	1.765	0.002
1.459	0.001	0.780	0.003	1.776	0.002
1.468	0.001	0.785	0.002	1.786	0.002
1.476	0.001	0.789	0.003	1.796	0.002
1.485	0.001	0.794	0.003	1.807	0.002
1.493	0.001	0.799	0.002	1.817	0.002
1.502	0.001	0.803	0.003	1.828	0.001
1.511	0.000	0.808	0.002	1.838	0.001
1.519	0.001	0.812	0.002	1.849	0.002
1.528	0.000	0.817	0.003	1.859	0.001
1.536	0.001	0.822	0.002	1.870	0.002
1.545	0.001	0.826	0.002	1.880	0.001
1.554	0.001	0.831	0.002	1.890	0.002
1.562	0.001	0.835	0.002	1.901	0.001
1.571	0.001	0.840	0.002	1.911	0.001
1.579	0.001	0.845	0.002	1.922	0.001
1.588	0.000	0.849	0.003	1.932	0.001
1.596	0.001	0.854	0.002	1.943	0.001
1.605	0.001	0.858	0.002	1.953	0.001
1.614	0.001	0.863	0.002	1.964	0.001
1.622	0.001	0.867	0.003	1.974	0.001
1.631	0.001	0.872	0.002	1.984	0.001
1.639	0.000	0.877	0.002	1.995	0.001
1.648	0.001	0.881	0.002	2.005	0.001
1.657	0.001	0.886	0.001	2.016	0.001
1.665	0.001	0.890	0.002	2.026	0.001
1.674	0.001	0.895	0.002	2.037	0.001
1.682	0.000	0.900	0.002	2.047	0.001
1.691	0.001	0.904	0.002	2.058	0.001
1.699	0.001	0.909	0.001	2.068	0.001
1.708	0.000	0.913	0.002	2.078	0.001
1.717	0.001	0.918	0.001	2.089	0.001
1.725	0.001	0.923	0.002	2.099	0.001
1.734	0.001	0.927	0.002	2.110	0.001
1.742	0.001	0.932	0.001	2.120	0.001
1.751	0.000	0.936	0.001	2.131	0.001
1.760	0.001	0.941	0.002	2.141	0.001
1.768	0.000	0.946	0.001	2.152	0.001
1.777	0.000	0.950	0.001	2.162	0.001
1.785	0.001	0.955	0.001	2.172	0.001
1.794	0.000	0.959	0.001	2.183	0.001
1.802	0.000	0.964	0.001	2.193	0.001

(Continued)

L/D	-250+212µm	L/D	-212+150µm	L/D	-150+106µm
1.811	0.000	0.968	0.001	2.204	0.001
1.820	0.001	0.973	0.001	2.214	0.001
1.828	0.001	0.978	0.001	2.225	0.001
1.837	0.001	0.982	0.001	2.235	0.001
1.845	0.001	0.987	0.001	2.246	0.001
1.854	0.000	0.991	0.001	2.256	0.001
1.863	0.000	0.996	0.001	2.266	0.001
1.871	0.000	1.001	0.001	2.277	0.000
1.880	0.001	1.005	0.001	2.287	0.001
1.888	0.000	1.010	0.001	2.298	0.000
1.897	0.000	1.014	0.001	2.308	0.000
1.905	0.000	1.019	0.001	2.319	0.000
1.914	0.000	1.024	0.001	2.329	0.000
1.923	0.000	1.028	0.001	2.340	0.000
1.931	0.000	1.033	0.001	2.350	0.001
1.940	0.000	1.037	0.001	2.360	0.000
1.948	0.000	1.042	0.001	2.371	0.000
1.957	0.000	1.047	0.000	2.381	0.000
1.966	0.001	1.051	0.001	2.392	0.000
1.974	0.000	1.056	0.001	2.402	0.000
1.983	0.001	1.060	0.000	2.413	0.000
1.991	0.000	1.065	0.001	2.423	0.000
2.000	0.000	1.069	0.001	2.434	0.000
2.008	0.000	1.074	0.001	2.444	0.000
2.017	0.000	1.079	0.001	2.454	0.000
2.026	0.000	1.083	0.001	2.465	0.000
2.034	0.000	1.088	0.001	2.475	0.000
2.043	0.000	1.092	0.001	2.486	0.000
2.051	0.000	1.097	0.001	2.496	0.000
2.060	0.000	1.102	0.001	2.507	0.000
2.069	0.000	1.106	0.001	2.517	0.000
2.077	0.000	1.111	0.000	2.528	0.000
2.086	0.000	1.115	0.001	2.538	0.000
2.094	0.000	1.120	0.000	2.548	0.000
2.103	0.000	1.125	0.000	2.559	0.000
2.111	0.000	1.129	0.000	2.569	0.001
2.120	0.000	1.134	0.000	2.580	0.000
2.129	0.000	1.138	0.000	2.590	0.000
2.137	0.000	1.143	0.000	2.601	0.000
2.146	0.000	1.147	0.001	2.611	0.000
2.154	0.000	1.152	0.001	2.622	0.000
2.163	0.000	1.157	0.001	2.632	0.000

(Continued)

L/D	-250+212µm	L/D	-212+150µm	L/D	-150+106µm
2.172	0.000	1.161	0.000	2.642	0.000
2.180	0.000	1.166	0.000	2.653	0.000
2.189	0.000	1.170	0.001	2.663	0.000
2.197	0.000	1.175	0.000	2.674	0.000
2.206	0.000	1.180	0.000	2.684	0.000
2.214	0.000	1.184	0.000	2.695	0.000
2.223	0.000	1.189	0.000	2.705	0.000
2.232	0.000	1.193	0.000	2.716	0.000
2.240	0.000	1.198	0.000	2.726	0.000
2.249	0.000	1.203	0.000	2.736	0.000
2.257	0.000	1.207	0.000	2.747	0.000
2.266	0.000	1.212	0.000	2.757	0.000
2.275	0.000	1.216	0.000	2.768	0.000
2.283	0.000	1.221	0.001	2.778	0.000
2.292	0.000	1.226	0.000	2.789	0.000
2.300	0.000	1.230	0.000	2.799	0.000
2.309	0.000	1.235	0.000	2.810	0.000
2.317	0.000	1.239	0.000	2.820	0.000
2.326	0.000	1.244	0.000	2.830	0.000
2.335	0.000	1.248	0.001	2.841	0.000
2.343	0.000	1.253	0.000	2.851	0.000

For other size fractions:

L/D	-106+75µm	L/D	-75+53µm	L/D	-53+38µm	L/D	-38µm
0.021	0.027	0.019	0.034	0.016	0.027	0.025	0.032
0.028	0.022	0.026	0.031	0.022	0.024	0.033	0.027
0.035	0.024	0.032	0.039	0.027	0.031	0.041	0.034
0.041	0.018	0.039	0.029	0.033	0.024	0.049	0.028
0.048	0.020	0.045	0.032	0.038	0.024	0.057	0.032
0.055	0.019	0.052	0.032	0.044	0.025	0.066	0.031
0.062	0.016	0.058	0.027	0.049	0.020	0.074	0.027
0.069	0.017	0.065	0.029	0.055	0.022	0.082	0.028
0.076	0.014	0.071	0.023	0.060	0.017	0.090	0.023
0.083	0.014	0.078	0.023	0.065	0.020	0.098	0.025
0.090	0.015	0.084	0.024	0.071	0.021	0.106	0.027
0.097	0.012	0.091	0.018	0.076	0.018	0.115	0.022
0.104	0.011	0.097	0.018	0.082	0.019	0.123	0.021
0.111	0.010	0.104	0.015	0.087	0.016	0.131	0.021
0.117	0.011	0.110	0.016	0.093	0.019	0.139	0.022
0.124	0.010	0.117	0.016	0.098	0.018	0.147	0.021
0.131	0.009	0.123	0.013	0.104	0.017	0.156	0.020
0.138	0.008	0.130	0.012	0.109	0.017	0.164	0.018
0.145	0.011	0.136	0.013	0.115	0.019	0.172	0.021
0.152	0.008	0.143	0.012	0.120	0.016	0.180	0.019
0.159	0.008	0.149	0.012	0.125	0.015	0.188	0.018
0.166	0.007	0.156	0.010	0.131	0.018	0.197	0.018
0.173	0.008	0.162	0.011	0.136	0.017	0.205	0.019
0.180	0.008	0.169	0.010	0.142	0.018	0.213	0.018
0.187	0.009	0.175	0.009	0.147	0.014	0.221	0.015
0.193	0.007	0.182	0.009	0.153	0.014	0.229	0.015
0.200	0.008	0.188	0.010	0.158	0.015	0.238	0.015
0.207	0.008	0.195	0.010	0.164	0.014	0.246	0.014
0.214	0.008	0.201	0.008	0.169	0.014	0.254	0.013
0.221	0.008	0.208	0.008	0.175	0.012	0.262	0.012
0.228	0.008	0.214	0.008	0.180	0.013	0.270	0.012
0.235	0.007	0.221	0.009	0.186	0.012	0.278	0.012
0.242	0.007	0.227	0.008	0.191	0.011	0.287	0.011
0.249	0.007	0.234	0.007	0.196	0.010	0.295	0.011
0.256	0.008	0.240	0.007	0.202	0.011	0.303	0.009
0.263	0.007	0.247	0.008	0.207	0.010	0.311	0.010
0.269	0.007	0.253	0.007	0.213	0.010	0.319	0.010
0.276	0.007	0.260	0.006	0.218	0.009	0.328	0.008
0.283	0.007	0.266	0.007	0.224	0.009	0.336	0.009
0.290	0.008	0.273	0.006	0.229	0.009	0.344	0.008

(Continued)

L/D	-106+75µm	L/D	-75+53µm	L/D	-53+38µm	L/D	-38µm
0.297	0.007	0.279	0.006	0.235	0.009	0.352	0.008
0.304	0.006	0.286	0.006	0.240	0.008	0.360	0.007
0.311	0.006	0.292	0.006	0.246	0.008	0.369	0.006
0.318	0.007	0.299	0.006	0.251	0.007	0.377	0.007
0.325	0.006	0.305	0.006	0.256	0.007	0.385	0.006
0.332	0.007	0.312	0.007	0.262	0.007	0.393	0.005
0.339	0.007	0.318	0.006	0.267	0.007	0.401	0.006
0.345	0.008	0.325	0.006	0.273	0.007	0.410	0.006
0.352	0.008	0.331	0.005	0.278	0.006	0.418	0.005
0.359	0.007	0.338	0.006	0.284	0.006	0.426	0.005
0.366	0.007	0.344	0.005	0.289	0.006	0.434	0.004
0.373	0.006	0.351	0.005	0.295	0.005	0.442	0.005
0.380	0.006	0.357	0.005	0.300	0.007	0.450	0.005
0.387	0.006	0.364	0.004	0.306	0.006	0.459	0.004
0.394	0.006	0.370	0.005	0.311	0.006	0.467	0.004
0.401	0.006	0.376	0.005	0.316	0.005	0.475	0.004
0.408	0.006	0.383	0.004	0.322	0.006	0.483	0.004
0.415	0.006	0.389	0.005	0.327	0.005	0.491	0.004
0.421	0.006	0.396	0.004	0.333	0.005	0.500	0.003
0.428	0.006	0.402	0.006	0.338	0.005	0.508	0.003
0.435	0.006	0.409	0.005	0.344	0.005	0.516	0.003
0.442	0.005	0.415	0.004	0.349	0.004	0.524	0.003
0.449	0.007	0.422	0.005	0.355	0.005	0.532	0.003
0.456	0.005	0.428	0.004	0.360	0.004	0.541	0.003
0.463	0.006	0.435	0.005	0.366	0.004	0.549	0.002
0.470	0.006	0.441	0.005	0.371	0.004	0.557	0.003
0.477	0.006	0.448	0.004	0.376	0.003	0.565	0.002
0.484	0.006	0.454	0.004	0.382	0.003	0.573	0.002
0.491	0.006	0.461	0.004	0.387	0.003	0.582	0.002
0.497	0.006	0.467	0.004	0.393	0.005	0.590	0.002
0.504	0.007	0.474	0.004	0.398	0.003	0.598	0.002
0.511	0.006	0.480	0.004	0.404	0.003	0.606	0.002
0.518	0.006	0.487	0.004	0.409	0.003	0.614	0.002
0.525	0.006	0.493	0.004	0.415	0.003	0.622	0.002
0.532	0.006	0.500	0.004	0.420	0.003	0.631	0.002
0.539	0.006	0.506	0.004	0.426	0.003	0.639	0.001
0.546	0.006	0.513	0.003	0.431	0.003	0.647	0.001
0.553	0.005	0.519	0.004	0.436	0.003	0.655	0.002
0.560	0.005	0.526	0.003	0.442	0.003	0.663	0.002
0.567	0.005	0.532	0.003	0.447	0.003	0.672	0.002
0.573	0.005	0.539	0.003	0.453	0.002	0.680	0.002
0.580	0.005	0.545	0.004	0.458	0.002	0.688	0.002

(Continued)

L/D	-106+75µm	L/D	-75+53µm	L/D	-53+38µm	L/D	-38µm
0.587	0.006	0.552	0.003	0.464	0.003	0.696	0.002
0.594	0.005	0.558	0.004	0.469	0.002	0.704	0.002
0.601	0.004	0.565	0.003	0.475	0.002	0.713	0.002
0.608	0.004	0.571	0.003	0.480	0.003	0.721	0.001
0.615	0.004	0.578	0.003	0.486	0.003	0.729	0.001
0.622	0.005	0.584	0.003	0.491	0.002	0.737	0.001
0.629	0.004	0.591	0.003	0.496	0.002	0.745	0.001
0.636	0.004	0.597	0.003	0.502	0.002	0.754	0.001
0.643	0.005	0.604	0.002	0.507	0.002	0.762	0.001
0.649	0.004	0.610	0.003	0.513	0.002	0.770	0.001
0.656	0.004	0.617	0.003	0.518	0.002	0.778	0.001
0.663	0.004	0.623	0.003	0.524	0.002	0.786	0.001
0.670	0.004	0.630	0.003	0.529	0.002	0.794	0.001
0.677	0.004	0.636	0.003	0.535	0.002	0.803	0.001
0.684	0.004	0.643	0.002	0.540	0.002	0.811	0.001
0.691	0.004	0.649	0.003	0.546	0.001	0.819	0.001
0.698	0.004	0.656	0.002	0.551	0.002	0.827	0.001
0.705	0.004	0.662	0.002	0.557	0.002	0.835	0.001
0.712	0.004	0.669	0.002	0.562	0.001	0.844	0.001
0.719	0.004	0.675	0.002	0.567	0.002	0.852	0.001
0.725	0.003	0.682	0.002	0.573	0.001	0.860	0.001
0.732	0.003	0.688	0.002	0.578	0.002	0.868	0.001
0.739	0.004	0.695	0.002	0.584	0.002	0.876	0.001
0.746	0.004	0.701	0.002	0.589	0.001	0.885	0.001
0.753	0.003	0.708	0.002	0.595	0.002	0.893	0.001
0.760	0.004	0.714	0.002	0.600	0.001	0.901	0.001
0.767	0.003	0.721	0.002	0.606	0.001	0.909	0.001
0.774	0.003	0.727	0.002	0.611	0.002	0.917	0.000
0.781	0.003	0.733	0.002	0.617	0.001	0.926	0.000
0.788	0.003	0.740	0.002	0.622	0.001	0.934	0.000
0.795	0.003	0.746	0.002	0.627	0.001	0.942	0.001
0.801	0.003	0.753	0.002	0.633	0.001	0.950	0.000
0.808	0.003	0.759	0.002	0.638	0.001	0.958	0.000
0.815	0.003	0.766	0.002	0.644	0.001	0.966	0.000
0.822	0.003	0.772	0.001	0.649	0.001	0.975	0.000
0.829	0.003	0.779	0.002	0.655	0.001	0.983	0.000
0.836	0.003	0.785	0.002	0.660	0.001	0.991	0.000
0.843	0.002	0.792	0.001	0.666	0.001	0.999	0.000
0.850	0.002	0.798	0.001	0.671	0.001	1.007	0.000
0.857	0.003	0.805	0.001	0.677	0.001	1.016	0.000
0.864	0.002	0.811	0.001	0.682	0.001	1.024	0.000
0.871	0.002	0.818	0.002	0.687	0.001	1.032	0.000

(Continued)

L/D	-106+75µm	L/D	-75+53µm	L/D	-53+38µm	L/D	-38µm
0.877	0.002	0.824	0.001	0.693	0.001	1.040	0.000
0.884	0.003	0.831	0.001	0.698	0.001	1.048	0.000
0.891	0.002	0.837	0.001	0.704	0.001	1.057	0.000
0.898	0.002	0.844	0.001	0.709	0.001	1.065	0.000
0.905	0.002	0.850	0.001	0.715	0.001	1.073	0.000
0.912	0.002	0.857	0.001	0.720	0.001	1.081	0.000
0.919	0.002	0.863	0.001	0.726	0.001	1.089	0.000
0.926	0.002	0.870	0.001	0.731	0.001	1.098	0.000
0.933	0.002	0.876	0.001	0.737	0.001	1.106	0.000
0.940	0.002	0.883	0.001	0.742	0.001	1.114	0.000
0.946	0.001	0.889	0.001	0.747	0.001	1.122	0.000
0.953	0.002	0.896	0.001	0.753	0.001	1.130	0.000
0.960	0.002	0.902	0.001	0.758	0.000	1.138	0.000
0.967	0.001	0.909	0.001	0.764	0.000	1.147	0.000
0.974	0.002	0.915	0.001	0.769	0.001	1.155	0.000
0.981	0.001	0.922	0.001	0.775	0.000	1.163	0.000
0.988	0.002	0.928	0.001	0.780	0.000	1.171	0.000
0.995	0.001	0.935	0.001	0.786	0.001	1.179	0.000
1.002	0.001	0.941	0.001	0.791	0.000	1.188	0.000
1.009	0.001	0.948	0.001	0.797	0.000	1.196	0.000
1.016	0.001	0.954	0.001	0.802	0.000	1.204	0.000
1.022	0.001	0.961	0.000	0.807	0.001	1.212	0.000
1.029	0.001	0.967	0.000	0.813	0.000	1.220	0.000
1.036	0.001	0.974	0.001	0.818	0.000	1.229	0.000
1.043	0.001	0.980	0.001	0.824	0.000	1.237	0.000
1.050	0.001	0.987	0.001	0.829	0.000	1.245	0.000
1.057	0.001	0.993	0.000	0.835	0.000	1.253	0.000
1.064	0.001	1.000	0.000	0.840	0.000	1.261	0.000
1.071	0.001	1.006	0.000	0.846	0.000	1.270	0.000
1.078	0.001	1.013	0.001	0.851	0.000	1.278	0.000
1.085	0.001	1.019	0.000	0.857	0.000	1.286	0.000
1.092	0.001	1.026	0.000	0.862	0.000	1.294	0.000
1.098	0.001	1.032	0.000	0.867	0.000	1.302	0.000
1.105	0.001	1.039	0.000	0.873	0.000	1.310	0.000
1.112	0.001	1.045	0.000	0.878	0.000	1.319	0.000
1.119	0.001	1.052	0.000	0.884	0.000	1.327	0.000
1.126	0.001	1.058	0.001	0.889	0.000	1.335	0.000
1.133	0.001	1.065	0.000	0.895	0.000	1.343	0.000
1.140	0.001	1.071	0.000	0.900	0.000	1.351	0.000
1.147	0.000	1.078	0.000	0.906	0.000	1.360	0.000
1.154	0.001	1.084	0.000	0.911	0.000	1.368	0.000
1.161	0.001	1.091	0.000	0.917	0.000	1.376	0.000

(Continued)

L/D	-106+75µm	L/D	-75+53µm	L/D	-53+38µm	L/D	-38µm
1.168	0.001	1.097	0.000	0.922	0.000	1.384	0.000
1.174	0.001	1.103	0.000	0.928	0.000	1.392	0.000
1.181	0.001	1.110	0.000	0.933	0.000	1.401	0.000
1.188	0.001	1.116	0.000	0.938	0.000	1.409	0.000
1.195	0.001	1.123	0.000	0.944	0.000	1.417	0.000
1.202	0.001	1.129	0.000	0.949	0.000	1.425	0.000
1.209	0.001	1.136	0.000	0.955	0.000	1.433	0.000
1.216	0.001	1.142	0.000	0.960	0.000	1.442	0.000
1.223	0.001	1.149	0.000	0.966	0.000	1.450	0.000
1.230	0.001	1.155	0.000	0.971	0.000	1.458	0.000
1.237	0.000	1.162	0.000	0.977	0.000	1.466	0.000
1.244	0.001	1.168	0.000	0.982	0.000	1.474	0.000
1.250	0.001	1.175	0.000	0.988	0.000	1.482	0.000
1.257	0.000	1.181	0.000	0.993	0.000	1.491	0.000
1.264	0.001	1.188	0.000	0.998	0.000	1.499	0.000
1.271	0.001	1.194	0.000	1.004	0.000	1.507	0.000
1.278	0.000	1.201	0.000	1.009	0.000	1.515	0.000
1.285	0.001	1.207	0.000	1.015	0.000	1.523	0.000
1.292	0.000	1.214	0.000	1.020	0.000	1.532	0.000
1.299	0.000	1.220	0.000	1.026	0.000	1.540	0.000
1.306	0.000	1.227	0.000	1.031	0.000	1.548	0.000
1.313	0.000	1.233	0.000	1.037	0.000	1.556	0.000
1.320	0.000	1.240	0.000	1.042	0.000	1.564	0.000
1.326	0.001	1.246	0.000	1.048	0.000	1.573	0.000
1.333	0.000	1.253	0.000	1.053	0.000	1.581	0.000
1.340	0.000	1.259	0.000	1.058	0.000	1.589	0.000

N. Characteristic flotation recoveries of particles (r_L^{ijk}) determined from linear grade measurements

15s: (k=1)

	i	*i*=1	*i*=2	*i*=3	*i*=4	*i*=5	*i*=6
j	Grade	-212+150µm	-150+106µm	-106+75µm	-75+53µm	-53+38µm	-38µm
j=1	0	0.000	0.020	0.004	0.039	0.000	0.103
j=2	0.05	0.003	0.013	0.017	0.068	0.002	0.146
j=3	0.15	0.011	0.054	0.082	0.063	0.016	0.083
j=4	0.25	0.019	0.099	0.079	0.125	0.109	0.130
j=5	0.35	0.080	0.073	0.132	0.164	0.073	0.170
j=6	0.45	0.049	0.153	0.101	0.080	0.870	0.223
j=7	0.55	0.048	0.131	0.113	0.000	0.186	0.165
j=8	0.65	0.037	0.164	0.130	0.080	0.342	0.298
j=9	0.75	0.068	0.122	0.113	0.042	0.283	0.157
j=10	0.85	0.038	0.114	0.102	0.084	0.168	0.166
j=11	0.95	0.049	0.057	0.050	0.045	0.138	0.167
j=12	1	0.086	0.216	0.290	0.321	0.247	0.226

30s: (k=2)

	i	*i*=1	*i*=2	*i*=3	*i*=4	*i*=5	*i*=6
j	Grade	-212+150µm	-150+106µm	-106+75µm	-75+53µm	-53+38µm	-38µm
j=1	0	0.010	0.022	0.005	0.039	0.000	0.150
j=2	0.05	0.005	0.015	0.022	0.069	0.004	0.212
j=3	0.15	0.012	0.068	0.102	0.072	0.019	0.168
j=4	0.25	0.023	0.125	0.120	0.141	0.140	0.198
j=5	0.35	0.090	0.079	0.210	0.182	0.104	0.253
j=6	0.45	0.055	0.170	0.117	0.132	1.169	0.344
j=7	0.55	0.058	0.144	0.153	0.022	0.197	0.276
j=8	0.65	0.044	0.177	0.169	0.163	0.395	0.456
j=9	0.75	0.078	0.139	0.148	0.069	0.298	0.230
j=10	0.85	0.044	0.128	0.133	0.095	0.192	0.292
j=11	0.95	0.056	0.064	0.070	0.063	0.154	0.298
j=12	1	0.106	0.237	0.342	0.449	0.345	0.415

60s: (k=3)

	i	*i*=1	*i*=2	*i*=3	*i*=4	*i*=5	*i*=6
j	Grade	-212+150µm	-150+106µm	-106+75µm	-75+53µm	-53+38µm	-38µm
j=1	0	0.014	0.022	0.005	0.039	0.000	0.180
j=2	0.05	0.006	0.018	0.036	0.069	0.004	0.237
j=3	0.15	0.016	0.078	0.129	0.073	0.021	0.227
j=4	0.25	0.028	0.146	0.180	0.141	0.158	0.254
j=5	0.35	0.101	0.088	0.283	0.188	0.108	0.362
j=6	0.45	0.064	0.179	0.160	0.132	1.280	0.527
j=7	0.55	0.069	0.152	0.180	0.048	0.213	0.380
j=8	0.65	0.049	0.188	0.247	0.191	0.403	0.615
j=9	0.75	0.087	0.150	0.176	0.071	0.309	0.327
j=10	0.85	0.050	0.135	0.165	0.106	0.192	0.417
j=11	0.95	0.065	0.070	0.097	0.067	0.158	0.385
j=12	1	0.116	0.259	0.387	0.546	0.425	0.478

120s: (k=4)

	i	*i*=1	*i*=2	*i*=3	*i*=4	*i*=5	*i*=6
j	Grade	-212+150µm	-150+106µm	-106+75µm	-75+53µm	-53+38µm	-38µm
j=1	0	0.014	0.022	0.006	0.039	0.000	0.215
j=2	0.05	0.007	0.021	0.041	0.071	0.006	0.257
j=3	0.15	0.017	0.085	0.161	0.089	0.029	0.265
j=4	0.25	0.029	0.163	0.229	0.266	0.221	0.290
j=5	0.35	0.106	0.091	0.353	0.270	0.184	0.414
j=6	0.45	0.071	0.186	0.193	0.226	2.334	0.618
j=7	0.55	0.077	0.158	0.224	0.121	0.321	0.455
j=8	0.65	0.053	0.201	0.296	0.229	0.425	0.721
j=9	0.75	0.098	0.165	0.222	0.078	0.346	0.388
j=10	0.85	0.056	0.147	0.216	0.111	0.206	0.493
j=11	0.95	0.071	0.082	0.118	0.075	0.165	0.450
j=12	1	0.126	0.271	0.410	0.623	0.502	0.551

360s: (k=5)

	i	*i*=1	*i*=2	*i*=3	*i*=4	*i*=5	*i*=6
j	Grade	-212+150μm	-150+106μm	-106+75μm	-75+53μm	-53+38μm	-38μm
j=1	0	0.021	0.022	0.007	0.053	0.042	0.233
j=2	0.05	0.008	0.022	0.044	0.087	0.052	0.311
j=3	0.15	0.020	0.093	0.186	0.121	0.079	0.357
j=4	0.25	0.033	0.174	0.263	0.326	0.343	0.400
j=5	0.35	0.117	0.098	0.428	0.316	0.257	0.568
j=6	0.45	0.079	0.194	0.226	0.276	3.280	0.850
j=7	0.55	0.086	0.166	0.252	0.161	0.395	0.581
j=8	0.65	0.064	0.212	0.329	0.251	0.564	0.892
j=9	0.75	0.105	0.173	0.238	0.086	0.446	0.488
j=10	0.85	0.062	0.153	0.230	0.130	0.271	0.632
j=11	0.95	0.079	0.087	0.132	0.100	0.234	0.562
j=12	1	0.137	0.285	0.450	0.716	0.628	0.673

O. Characteristic flotation recoveries of particles (r_A^{ijk}) determined from areal grade measurements

15s: (k=1)

	i	*i*=1	*i*=2	*i*=3	*i*=4	*i*=5	*i*=6
j	Grade	-212+150µm	-150+106µm	-106+75µm	-75+53µm	-53+38µm	-38µm
j=1	0	0.027	0.049	0.030	0.050	0.020	0.071
j=2	0.05	0.030	0.056	0.081	0.045	0.050	0.113
j=3	0.15	0.032	0.055	0.052	0.097	0.087	0.095
j=4	0.25	0.030	0.070	0.065	0.024	0.157	0.095
j=5	0.35	0.064	0.060	0.036	0.059	0.143	0.105
j=6	0.45	0.030	0.068	0.057	0.104	0.190	0.084
j=7	0.55	0.044	0.099	0.047	0.074	0.428	0.124
j=8	0.65	0.046	0.090	0.107	0.000	0.357	0.093
j=9	0.75	0.031	0.067	0.025	0.079	0.128	0.097
j=10	0.85	0.042	0.065	0.043	0.027	0.214	0.061
j=11	0.95	0.033	0.079	0.030	0.066	0.118	0.101
j=12	1	0.101	0.231	0.308	0.339	0.232	0.383

30s: (k=2)

	i	*i*=1	*i*=2	*i*=3	*i*=4	*i*=5	*i*=6
j	Grade	-212+150µm	-150+106µm	-106+75µm	-75+53µm	-53+38µm	-38µm
j=1	0	0.031	0.059	0.043	0.055	0.028	0.110
j=2	0.05	0.034	0.065	0.101	0.060	0.061	0.201
j=3	0.15	0.038	0.067	0.075	0.108	0.106	0.183
j=4	0.25	0.034	0.077	0.081	0.042	0.171	0.149
j=5	0.35	0.075	0.065	0.059	0.074	0.155	0.156
j=6	0.45	0.038	0.072	0.090	0.126	0.206	0.149
j=7	0.55	0.051	0.108	0.070	0.094	0.457	0.231
j=8	0.65	0.050	0.100	0.128	0.014	0.381	0.128
j=9	0.75	0.036	0.068	0.050	0.079	0.143	0.133
j=10	0.85	0.048	0.072	0.061	0.042	0.234	0.110
j=11	0.95	0.038	0.083	0.040	0.075	0.158	0.166
j=12	1	0.127	0.253	0.360	0.479	0.323	0.696

60s: (k=3)

	i	*i*=1	*i*=2	*i*=3	*i*=4	*i*=5	*i*=6
j	Grade	-212+150µm	-150+106µm	-106+75µm	-75+53µm	-53+38µm	-38µm
j=1	0	0.035	0.068	0.061	0.057	0.030	0.140
j=2	0.05	0.040	0.073	0.135	0.065	0.067	0.258
j=3	0.15	0.043	0.076	0.100	0.109	0.116	0.242
j=4	0.25	0.042	0.082	0.099	0.045	0.171	0.207
j=5	0.35	0.084	0.071	0.076	0.077	0.164	0.216
j=6	0.45	0.047	0.076	0.117	0.126	0.212	0.200
j=7	0.55	0.062	0.113	0.073	0.102	0.457	0.288
j=8	0.65	0.059	0.106	0.159	0.014	0.381	0.198
j=9	0.75	0.038	0.072	0.067	0.079	0.150	0.186
j=10	0.85	0.056	0.076	0.074	0.042	0.234	0.153
j=11	0.95	0.044	0.086	0.051	0.077	0.163	0.206
j=12	1	0.137	0.276	0.405	0.586	0.398	0.798

120s: (k=4)

	i	*i*=1	*i*=2	*i*=3	*i*=4	*i*=5	*i*=6
j	Grade	-212+150µm	-150+106µm	-106+75µm	-75+53µm	-53+38µm	-38µm
j=1	0	0.040	0.074	0.071	0.072	0.042	0.157
j=2	0.05	0.044	0.079	0.164	0.081	0.089	0.299
j=3	0.15	0.047	0.083	0.129	0.127	0.151	0.286
j=4	0.25	0.045	0.089	0.118	0.056	0.191	0.251
j=5	0.35	0.089	0.080	0.100	0.089	0.164	0.257
j=6	0.45	0.053	0.083	0.145	0.131	0.237	0.238
j=7	0.55	0.071	0.126	0.096	0.111	0.486	0.336
j=8	0.65	0.062	0.117	0.190	0.021	0.429	0.230
j=9	0.75	0.042	0.078	0.082	0.090	0.165	0.211
j=10	0.85	0.061	0.082	0.089	0.046	0.247	0.181
j=11	0.95	0.047	0.092	0.059	0.081	0.167	0.235
j=12	1	0.148	0.289	0.429	0.670	0.469	0.918

360s: (k=5)

	i	*i*=1	*i*=2	*i*=3	*i*=4	*i*=5	*i*=6
j	Grade	-212+150µm	-150+106µm	-106+75µm	-75+53µm	-53+38µm	-38µm
j=1	0	0.045	0.080	0.106	0.096	0.106	0.199
j=2	0.05	0.049	0.085	0.226	0.102	0.164	0.380
j=3	0.15	0.052	0.091	0.200	0.153	0.239	0.367
j=4	0.25	0.049	0.096	0.172	0.078	0.258	0.320
j=5	0.35	0.096	0.084	0.154	0.095	0.282	0.317
j=6	0.45	0.058	0.088	0.204	0.153	0.310	0.302
j=7	0.55	0.080	0.134	0.146	0.142	0.602	0.429
j=8	0.65	0.067	0.121	0.246	0.041	0.580	0.294
j=9	0.75	0.049	0.082	0.111	0.098	0.214	0.270
j=10	0.85	0.066	0.086	0.124	0.053	0.347	0.228
j=11	0.95	0.053	0.095	0.074	0.097	0.299	0.285
j=12	1	0.161	0.304	0.450	0.772	0.582	1.000